The Development of a Tissue-Engineered Skin Composite Utilising a Biodegradable Polyurethane Scaffold in a Novel Bioreactor for the Treatment of Extensive, Full-Thickness Burns

Bronwyn Dearman B.Sc. (Hons)
Student ID: a1059011

Skin Engineering Laboratory, Adult Burns Centre
Royal Adelaide Hospital

&

Adelaide Medical School
Faculty of Health and Medical Science
University of Adelaide

THE UNIVERSITY of ADELAIDE

A thesis submitted to the University of Adelaide
For the degree of Doctor of Philosophy

May 2022

Table of Contents

DECLARATION

I certify that this work contains no material which has been accepted for the award of any other degree or diploma in my name, in any university or other tertiary institution and, to the best of my knowledge and belief, contains no material previously published or written by another person, except where due reference has been made in the text. In addition, I certify that no part of this work will, in the future, be used in a submission in my name, for any other degree or diploma in any university or other tertiary institution without the prior approval of the University of Adelaide and where applicable, any partner institution responsible for the joint award of this degree. The author acknowledges that copyright of published works contained within the thesis resides with the copyright holder(s) of those works.

I give permission for the digital version of my thesis to be made available on the web, via the University's digital research repository, the Library Search and also through web search engines, unless permission has been granted by the University to restrict access for a period of time.

May 2022

ACKNOWLEDGEMENTS

First and foremost, to my supervisors – Professor John Greenwood AM, you have been with me on this journey since the beginning, through the highs and the lows and enabled our success with the first human use of CCS. I am eternally grateful for your faith in me and your continuous support. Professor Toby Coates AO, the degree of knowledge and experience you have shared with continual encouragement has been instrumental throughout my career. Emeritus Professor Steven Boyce, your scientific leadership, invaluable feedback and wealth of expertise has been inspiring. Thank you for the late-night/early morning Zoom sessions and chats. Meeting the Boyce skin laboratory team in Cincinnati, USA, was a highlight at the onset of my research.

To you all – my team of professors, I extend my deepest thanks and gratitude for your support, guidance and never waning confidence in me. It has been an honour to work with you.

Mr Julian Burton OAM, your support, positivity, trust and belief has been uplifting. I cannot express how much this has meant over the years. To the RAH Burns team and the patients, especially GO, an integral part of my thesis, this journey has been a privilege, and I thank you for permitting me to share it.

I extend my sincere gratitude to SAHMRI LARIF and all the technicians, "Technicians are the gears that move research forward" thank you all. A special mention to Loren, Dan, Rob, Chris, Paul, Sam, Sue and Chris C.

To the many people who have had major influences throughout the years of my candidature, especially to Amy Li for maintaining the laboratory's inventory system and all the hours of culturing assistance, I appreciate you always being there. Thank you to the Centre for Clinical and Experimental Transplantation members, particularly Julie, Jodie, and Daniella, for the advice and assistance with many aspects of the experimental studies. The Adelaide histology facility, Jim Manavis and Sofie Kogoj, for all those problem-solving histology conversations. I would also like to acknowledge Kristian Stefani for his talented design skills and Liesl Ross for her formatting expertise.

Monika Kutyna, as we have navigated through our PhD paths together, you have given me valuable advice and strength. I truly cherish your friendship.

To my family, my ever-enduring husband – Peter and our beautiful daughter – Ella, my mother and father, words cannot express my heartfelt thanks for your patience and never-ending loving support to overcome other life challenges throughout this journey, and not to forget my brother, Brad for the forever "…. are you there yet!"

ABBREVIATIONS

AA	Antibiotics Antimycotic
AG	Autograft
ALI	Air-liquid interface
bFGF	Human Fibroblast Growth Factor
BM	Basement membrane
BPE	Bovine pituitary extract
BTM	Biodegradable temporising matrix
BSC	Biological safety cabinet
CCS	Composite cultured skin
CEA	Cultured epithelial autograft
CFU	Colony forming unit
C-GAG	Collagen-glycosamino-glycan
CM	Coating matrix
DAB	3,3,'-diaminobenzidine
DAPI	4',6-diamidino-2-phenylindole
DAWE	Australian Government Department of Agriculture, Water and the Environment
DEJ	Dermal-epidermal junction
dKGM	Defined keratinocyte growth medium
DM	Dilution Medium
DMEM	Dulbecco's Modified Eagle Medium
DMEM-F12	Dulbecco's Modified Eagle Medium: Nutrient Mixture F-12
ECM	Extracellular matrix
EDC	1-Ethyl-3-(3- dimethylaminopropyl) carbodiimide hydrochloride
ESS	Engineered skin substitute
FACS	Fluorescence activated cell sorting
FBS	Foetal bovine serum
GMP	Good manufacturing practice
GS	Goat serum
FDA	Food and Drug Administration
HAc	Acetic acid
HBSS	Hank's balanced salt solution
H&E	Haematoxylin and eosin
H_2O_2	Hydrogen peroxide
HCl	Hydrochloric acid

HMDS	Hexamethyldisilazane
HSA	Human serum albumin
hFbs	Human dermal fibroblasts
hFFP	Human fresh frozen plasma
hKs	Human keratinocytes
ID	Internal diameter
IHC	Immunohistochemical staining
iHFbs	Irradiated human dermal fibroblasts
ITS	Insulin-Transferrin-Selenium
KGF	Human Keratinocyte Growth Factor
LA	Linoleic Acid
LBL	Layer-by layer
L-AA-2P	Ascorbic Acid-2-Phosphate
LSGS	Low serum growth supplement
MM	Maturation media
MT	Masson's trichrome
MTS	3-(4,5-dimethylthiazol-2-yl)-5-(3-carboxymethoxyphenyl)-2-(4-sulfophenyl)-2H-tetrazolium
MVD	Microvessel density
OCT	Optimal cutting temperature embedding medium
PAS	Periodic acid-Schiff
PBS	Phosphate buffered solution
pFbs	Porcine dermal fibroblasts
pFFP	Porcine fresh frozen plasma
pKs	Porcine keratinocytes
PSR	Picrosirius red stain
PUR	Polyurethane
PVA	Polyvinyl alcohol
QA	Quality assurance
RPM	Revolutions per minute
RO	Reverse osmosis
ROM	Range of motion
RT	Room temperature

SAHMRI	South Australian Health and Medical Research Institute
SBTI	Trypsin inhibitor from Glycine max (soybean)
SD	Standard deviation
SEL	Skin Engineering Laboratory
SEL-Fbs	Skin Engineering Laboratory Fibroblast growth medium
SEL-KGM	Skin Engineering Laboratory Keratinocyte growth medium
SEM	Scanning electron microscopy
SOP	Standard operation procedure
$SrCl_2$	Strontium chloride hexahydrate
SS	Skin substitute
STSG	Split-thickness skin graft
TBSA	Total body surface area
TE	Tissue-Engineering/ed
TEM	Transmission electron microscopy
TGA	Therapeutic Goods Administration
UCDM1	University of Cincinnati Dermatology Medium 1
µg/µL/µm/µM	microgram/ microliter/ micrometre/ micromolar
VE	ViscoElastic/ity

PUBLICATIONS ARISING FROM THIS THESIS

Review

1. Dearman BL, Boyce ST, Greenwood JE. Advances in skin tissue bioengineering and the challenges of clinical translation. Front Surg. 2021;8:640879. DOI: 10.3389/fsurg.2021.640879.

Original Articles

2. Greenwood JE, Damkat-Thomas L, Schmitt B, Dearman B. Successful proof of the 'two stage strategy' for major burn wound repair. Burns Open. 2020;4(3):121-31. DOI: 10.1016/j.burnso.2020.06.003.
3. Dearman BL, Greenwood JE. Scale-up of a Composite Cultured Skin using a novel Bioreactor Device in a Porcine Wound Model. J Burn Care Res. 2021 Feb 26. DOI: 10.1093/jbcr/irab034.
4. Dearman B and Greenwood J. Treatment of a 95% total body surface burns patient with a novel polyurethane-based composite cultured skin. eCM Periodical. 2020; Collection 1 (TERMIS EU **Abstracts**):187.
5. Dearman B and Greenwood J. A novel polyurethane-based composite cultured skin and a bespoke bioreactor in a porcine wound. eCM Periodical. 2020; Collection 1 (TERMIS EU **Abstracts**):315.
6. Dearman BL, Boyce ST, Greenwood JE. Comparison of Biopolymer Scaffolds for the Fabrication of Skin Substitutes in a Porcine Wound Model. Wound Repair and Regeneration, 2022. Submitted.
7. Dearman BL and Greenwood JE. Long-term follow-up of a major burn treated using a composite cultured skin: Case report. Burns Open, 2022;6(4):156-63. DOI: 10.1016/j.burnso.2022.07.002.

ABSTRACT

The fabrication of a laboratory derived skin substitute that promotes epidermal and dermal elements are alternatives that are becoming more widely studied in the field of tissue engineering. Areas of particular interest include significant tissue injuries where skin autograft paucity and donor sites are of concern. The introduction of these products has the potential to reduce the number of surgeries, pain, and scarring for patients with large Total Body Surface Area (TBSA) skin wounds, such as extensive, deep burns. The changes in burn care over the last two decades has seen the percentage of survival burn increase, requiring the need to seek alternative tissue sources. With this in mind, a two stage strategy has been developed to assist with this challenge.

The first stage, a biodegradable temporising matrix (BTM) was developed to temporise the wound, followed by the second stage of definitive wound coverage with a laboratory fabricated skin composite, composite cultured skin (CCS). The CCS has been used in pilot animal studies in small wounds (8cm x 8cm) [1, 2], but the concern with large burns is small pieces may leave a patchwork quilt appearance. The primary aim of this thesis is to reduce the need for skin autograft by upscaling the CCS using a bespoke bioreactor system to enable the production of large pieces (25cm x 25cm) for the use in extensive full-thickness burn patients.

To assess the CCS, optimisation methods investigating culture techniques to refine and reduce the use of animal products for clinical use were employed. The development of a novel bioreactor was concurrently designed to fabricate large pieces 25cm x 25cm and tested in animal model which led to the first use of this polyurethane derived composite in man, enabling a long-term follow-up of this patient. Further investigations were warranted to overcome pore size of this polymer in later iterations of this dermal template and a hybrid collagen/polyurethane were designed and tested with *in vitro* and *in vivo* results showing the potential of a combinational product to overcome the inherent collagen contraction and polyurethane pore size.

This thesis provides a translational clinical research story from bench to bedside, it shows the clinical challenges and provides insights into the fabrication of biopolymers for the construction of skin substitutes and their potential use in full-thickness extensive wounds.

CHAPTER 1:
Introduction and Review

1.1 Thesis Overview

Surviving significant burn injury is, inevitably, life-changing. The trauma of extensive skin loss (wounding) and the outcomes subsequent on treatment and healing, are emotionally and physically scarring for life. Although burn injury of such extent is relatively uncommon globally, the socioeconomic impact and burden on healthcare systems and economies is significant. As burn size increases, the area of available uninjured skin decreases, and tissue engineered solutions are desirable if survival is to be functionally and aesthetically acceptable in the long-term.

This thesis explores the development of an autologous skin substitute utilising a novel polyurethane scaffold, and its subsequent expansion to clinical applicability using a bespoke bioreactor system, with the overarching aim of translating concept to clinical practice (Figure 1.0). **Chapter 1** discusses the anatomy of skin to appreciate its native structure and multiple functions, followed by the mechanisms of wound healing to convey the complex issues presented by large wounds. A brief historical background follows to describe milestones in the field of skin tissue engineering with reference to burn injury management. Concluding this chapter is a published **review** paper, which summarises the challenges of major burn injury and the issues facing skin substitute development (*Frontiers of Surgery*). **Chapter 2** consists of a second manuscript, published in *Journal of Burn Care and Research* which describes the 'scale-up' issues inherent in using an in-house designed bioreactor for the composite cultured skin (CCS) growth in a porcine model. The autologous CCSs fabricated were 24.5cm x 24.5cm and were transplanted successfully on the flanks of three pigs. In **Chapter 3**, this technology progresses from bench to bedside in a world first, when it was used clinically to save life, and provide independent living outcomes, for a patient who suffered 95% full-thickness burns. The results were published in the *Burns Open* journal in 2020. **Chapters 4 and 5** describes unpublished data expanding on the optimisation of the CCS culturing parameters and culture protocols to refine and produce a more reliable CCS for patient use. Within **Chapter 5**, alternative methods for skin substitute fabrication were explored, collaborating with an internationally acknowledged expert, with long experience of producing engineered skins, to fabricate and trial a hybrid biopolymer scaffold for evaluation, *in vitro* and *in vivo,* in a porcine model. **Chapter 6** describes the

results of the *in vivo* biopolymer scaffold study in a manuscript submitted to the journal, *Wound Repair and Regeneration*. **Chapter 7** is an unpublished chapter that examines the refined polyurethane established in Chapter 5 and tests the layer-by-layer CCS approach in the bioreactor and an ISO 7 environment. This process is in preparation for clinical use, to identify the workflow and success of this scaled-up model. **Chapter 8** concludes the thesis narrative and presents results from the long-term follow-up of the burn survivor patient treated with CCS from Chapter 3, published in *Burns Open 2022*. **Chapter 9** is the overall discussion and provides a general summary elucidating new events not published in the presented paper discussions. It will suggest potential future directions of this project in the prospective development of engineered skin that may restore wounded tissue to the normal anatomy and physiology of uninjured human skin.

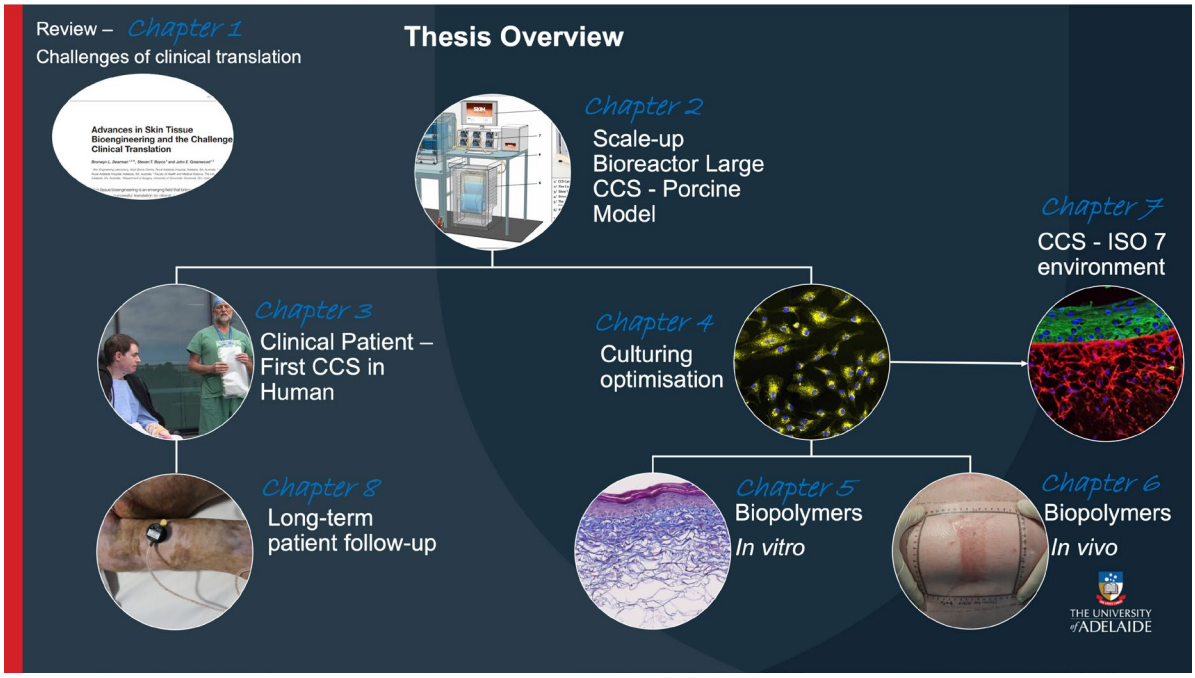

Figure 1.0. Schematic of thesis overview and related chapters.

1.2 The Structure and Function of Skin

Skin is a remarkably complex organ that provides a physical interface between body's internal and external environments. The skin has two defined layers, the epidermis and the dermis; both have distinctive (yet integrated) roles based on their structural constituents (Figure 1.1). The epidermis (an ectodermal derivative consisting predominantly of cells) comprises keratinocyte layers of varying maturity and morphology. From deep to superficial - stratum basale, stratum spinosum, stratum granulosum and stratum corneum represent the life cycle of the keratinocyte (Figure 1.2). These layers are renewed by proliferation, differentiation and final keratinisation of keratinocyte stem cells located within the stratum basale and the epidermal adnexal structures, renewing on average every 40 days [3]. The glabrous skin on the palms and soles of the feet has a thicker epidermis and an additional layer, the stratum lucidum, located between the stratum granulosum and the stratum corneum.

The stratum basale is the deepest layer, with a columnar shape and mitotically active cell population [4]. The keratinocytes of the stratum basale and overlying stratum spinosum produce several varieties of structural proteins, keratins. The basal keratinocytes express keratins 5 and 14, whereas the suprabasal spinous cells synthesise keratins K1 and K10 (Figure 1.2) [5]. The basal keratinocytes reside at the dermal-epidermal junction (DEJ) connecting the collagenous extracellular matrix (ECM) of the papillary dermis known as the basement membrane zone (Figure 1.3).

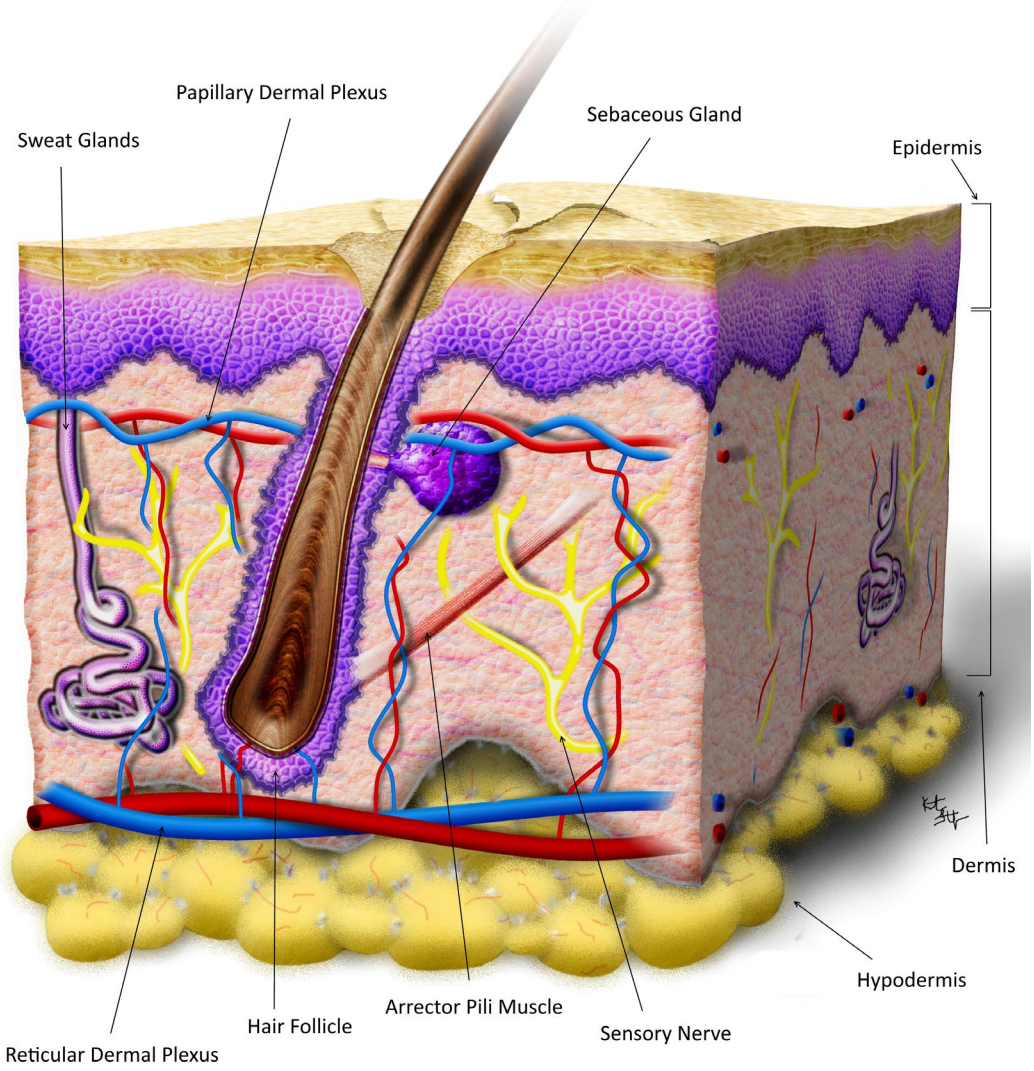

Figure 1.1. The structure of human skin. The skin comprises two main layers, the epidermis and dermis. The epidermis is divided into sublayers each with unique structures and functions. The dermis is a matrix consisting of loose connective tissue primarily of collagen and elastin fibres with blood and lymph vessels, nerves and contains the penetrating epidermal appendages: hair follicles, sebaceous and sweat glands. Illustration generated in paint.net by K.Stefani.

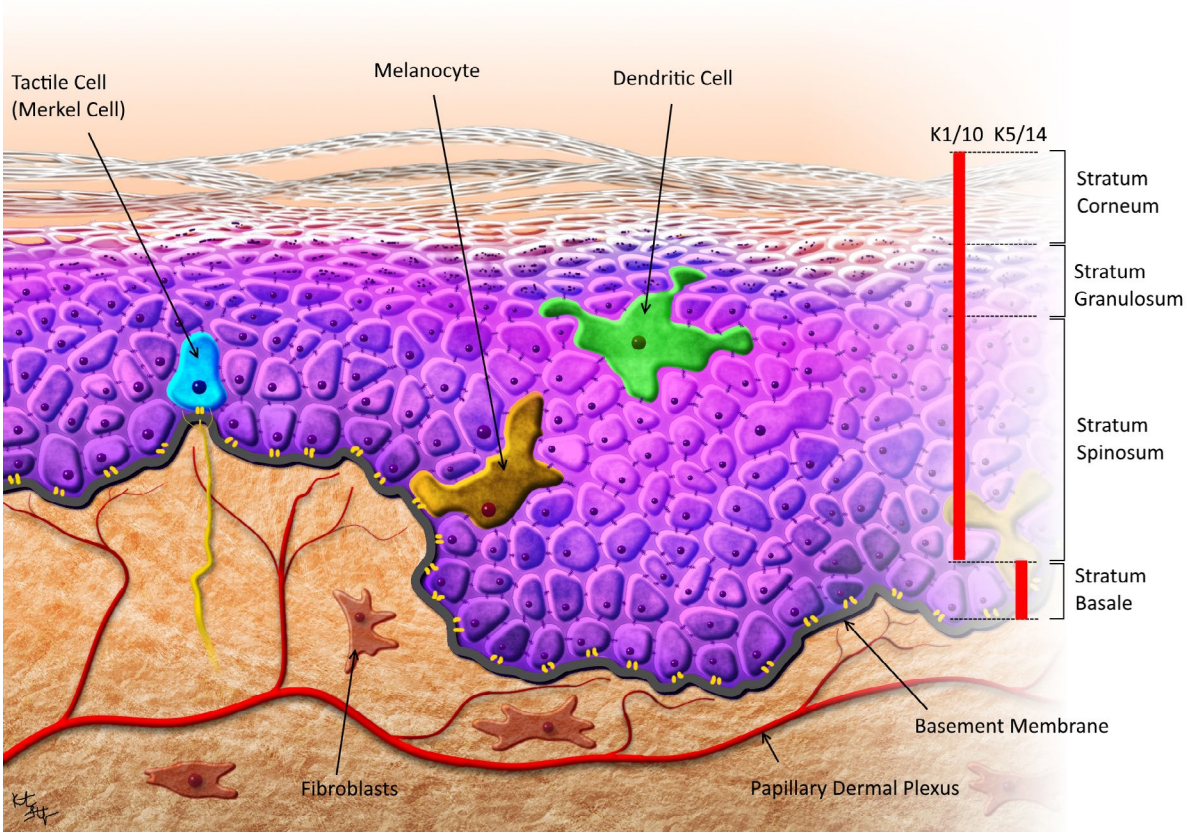

Figure 1.2. Epidermal skin layers and associated cell types. Basal keratinocytes express K14 and the suprabasal layers K10. Other cell types include the pigment-producing melanocytes, Dendritic langerhans cells, Merkel cells with associated nerve fibres and the extracellular matrix dermal collagen-producing fibroblasts. The basement membrane structure shows the link between the epidermal and dermal layer. Illustration generated in paint.net by K.Stefani.

The stratum granulosum is a thin 2-3 cell layer of irregularly shaped granular cells (containing keratohyalin granules) that have migrated from the underlying stratum spinosum, a 3-4 cell layer connected by multiple intercellular desmosomal junctions.

The outermost cornified layer, the stratum corneum consists of anucleated keratin-filled squamous cells (corneocytes). These keratin filaments and proteins are cross-linked tight bundles that form the cornified envelope of the corneocyte and gives it its flattened shape. Other structural proteins are subsequently cross-linked by transglutaminase reinforcing the cornified envelope. These compact flattened cells are cemented together in a ‘bricks and mortar’ model [6]. Corneocytes (bricks) are surrounded in a protective extracellular lipid-

matrix (mortar). This complex structure aids in the barrier function of skin providing a physical barrier to water loss and prevents external insults from exogenous chemicals or pathogens [7]. The corneocytes are linked to adjacent cells via corneodesmosomes, (modified desmosomes) and with final keratinisation these are degraded by proteases with cell exfoliation at the skin surface [8].

The junction between the ectodermally-derived epidermis and the mesodermally-derived dermis is structurally weak (representing an embryological cleavage plane). A specialised structure, the basement membrane, exists to assist in strengthening this junction. The basement membrane is comprised of two main layers – a superficial lamina lucida, and a deep lamina densa, firmly adhered via complex interconnecting adhesions. The lamina densa is the site of most of the structural protein, Collagen IV. Keratin filaments from the basal keratinocytes anchor the hemidesmosomes to the lamina lucida with anchoring filaments to the lamina densa. Anchoring fibrils of collagen VII then extend to adhere to the papillary dermis (Figure 1.3) [9]. The debilitating blistering diseases, Epidermolysis Bullosa, result from alterations in the genes specific for α6β4 integrin, laminin 332 and collagen VII, thus exploiting the weakness of the embryological cleavage plane and allowing 'shear' at the dermo-epidermal junction, with interlayer fluid accumulation, blistering and epidermal loss [10].

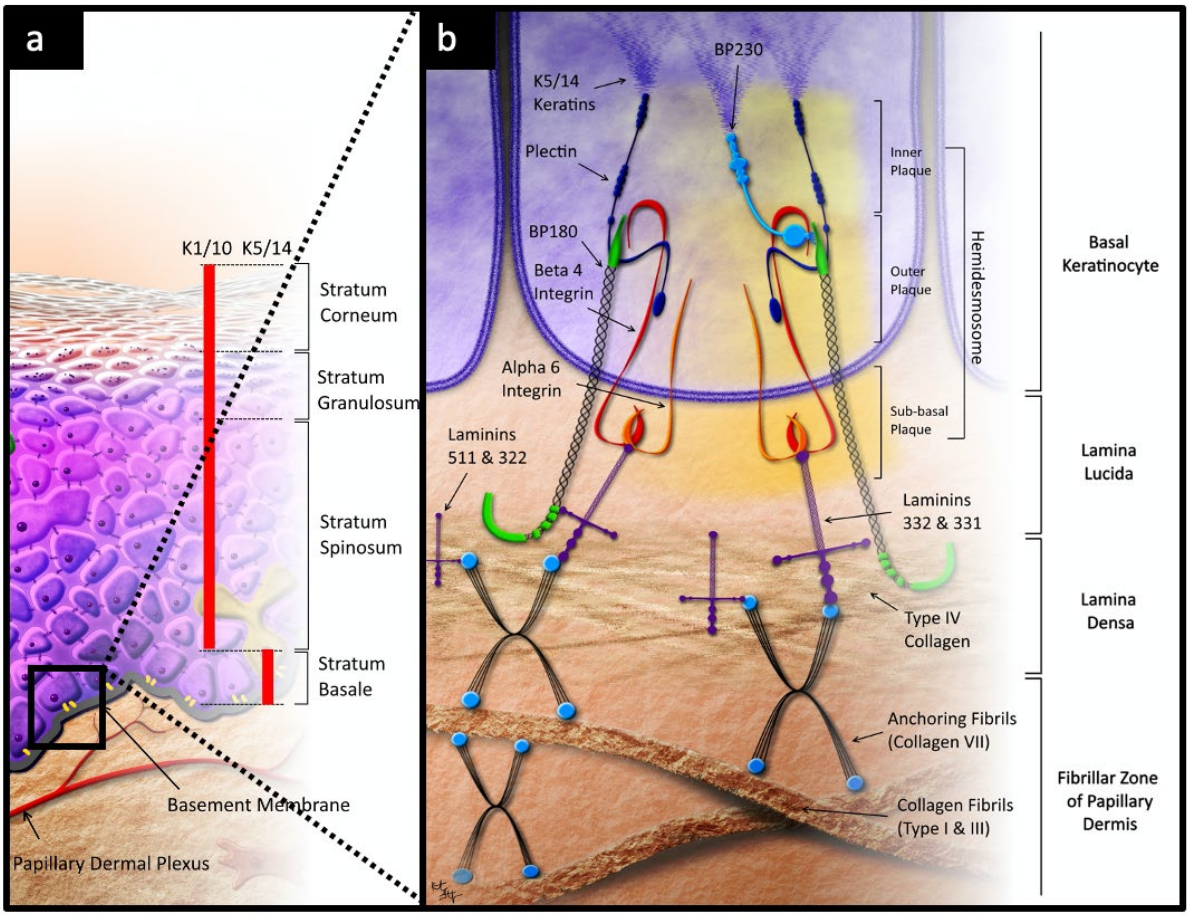

Figure 1.3. Skin microstructure (a) schematic overview of skin layers (b) showing the basement membrane structure with the lamina lucida and lamina densa at the molecular level. Illustration generated in paint.net by K.Stefani.

Other cell types exist within the epidermis. Melanocytes are pigment-producing cells derived from the neural crest. They produce melanin in two forms (in humans) – black/brown eumelanin, and red/yellow phaeomelanin [(11)]. Melanosome organelles within melanocytes transfer melanin into keratinocytes, forming an epidermal melanin unit, which forms a superficial cap over the nucleus of the stratum basale keratinocyte. The melanin protects the DNA in the nuclei of the potent stratum basale cells from DNA damage caused by ultraviolet ionising radiation by reflection and absorption. Langerhans cells (bone marrow-derived antigen-presenting immune cells), are tissue macrophages which reside predominantly in the stratum spinosum. They phagocytose foreign material and present derived antigens on their surface to initiate an immune response. Merkel cells are scattered among the epidermis, they are thought to be neuroendocrine derived and have a structure suggesting a mechanoreceptor function [(12)].

The dermis derived from mesoderm and is predominantly a molecular structure. The main cell type in the dermis is the fibroblast, a collagen-producing cell that deposits extracellular matrix components that proffer suppleness, flexibility, and tensile strength to the skin as a whole. The dermis can be up to twenty times the thickness of the epidermis (location dependent) and is divided into a superficial, loosely-arranged, papillary layer and a deep, denser, reticular layer. Although these layers are indistinct histologically, they differ in fibroblast density and have demonstrated different functions [13, 14]. The dermal extracellular matrix comprises macromolecular 'building blocks' of collagens, elastin, laminins, and proteoglycans. In normal human skin, collagen type I constitutes 75% of the collagen, with the remaining 25% being collagen III (Collagen ratio of normal skin; Collagen I: Collagen III = 3:1). The other main cell population present are endothelial cells, which form the intima of the blood vessels that provide oxygen and nutrients to the many cells involved for function and survival. The dermis also contains appendages of epidermal origin (adnexal structures), including hair follicles, sebaceous glands and sweat glands, as well as numerous nerve endings [15] (Figure 1.1). The subcutis (or hypodermis) is occasionally listed as a third layer of the dermis and resides deep to the reticular layer. It consists of a blood vessel network and fat-adipose cells that thermally insulate and act as a 'shock absorber' for underlying tissues.

1.3 Wound Healing

A wound is a pathological discontinuity of the epidermis. What loss of function results is determined by which other structures are coincidentally damaged/lost. Wound healing can be divided into phases with sequential molecular and cellular events. These phases overlap temporally and their durations are dependent on wound depth, size, type, and location (Figure 1.4) [16, 17]. Since the epidermis is a cellular structure, it is capable of regeneration. The molecular dermis, however, can only be repaired after injury with the aim to provide an environment over which epithelial differentiation, proliferation and migration can occur to 'close' the wound. In the ideal situation, the wound edges are either closely opposed as a result of the injury, or are brought into close opposition by surgical means (such as by debridement and direct suture). Such healing is said to progress by PRIMARY INTENTION. The processes involved, occurring in the dermis, begin with

a multi-step, multifactorial cascade, triggered immediately to initialise blood clotting and secure **haemostasis** at the site within minutes after injury [18]. The early response, **inflammation**, occurs from wounding and peaks around 48 hours later. This is characterised clinically by redness, heat, swelling and pain secondary to the immediate release of proinflammatory mediators (such as histamine from mast cells, serotonin from activated platelets) which result in precapillary arteriolar dilatation, increased capillary permeability and post-capillary venule constriction; resulting in increased blood flow (erythema and heat), movement of fluid and protein into the wound environment (oedema), and pain. Neutrophils are chemotactically summoned to the wound environment, peaking at 4-6 hours, where they function to enzymatically break down damaged tissue, phagocytose bacteria and foreign material and attract macrophages [17]. These cells co-ordinate the infiltrating immune response and continue the process of debridement, providing a framework for neovascularisation and a release of growth factors to initiate the next stage. The phase of **proliferation** can start from day 4-24 with fibroblasts depositing new tissue (collagens and ground substance) and angiogenetic ingrowth of vascular structures [19]. The collagen produced in the early proliferative phase is predominantly Collagen III, such that the collagen ratio in the wound is (Collagen I: Collagen III = 1:3), reversed from the normal skin ratio. Granulation tissue results (defined as the admixture of collagen and new vessels), enabling edge epithelial cells to migrate and initiate ultimate wound closure. The final phase, maturation, may last up to 2 years, involves tissue remodelling as skin matures (Figure 1.4) [20, 21]. The Collagen III deposited in the proliferative phase is replaced by Collagen I, enabling restoration of the normal collagen ratio. The repaired wound only has 70-80% the strength of the pre-injury skin [19, 22]. Under these circumstances, the scarring is as ‘good’ as it is destined to be, taking into account the general health of the individual, any systemic factors that might influence wound healing and the local environment of the original wound. Such wounds do not produce a high degree of scar contraction.

When the wound edges are not, and cannot surgically be, opposed (wounds > 4cm in diameter), the healing process is exaggerated. The phase of proliferation is lengthened, more granulation tissue is deposited. Fibroblasts in the granulation tissue differentiate into myofibroblasts, determined by the level of contractile protein alpha-smooth muscle actin,

and contraction occurs in an effort to make the wound smaller in area/width, which might allow epithelial migration across the wound [19]. Otherwise, migration will not extend more than 5mm from any edge. Excessive granulation tissue, contraction, rouching and delayed epithelialisation result in thickened (hypertrophic) scarring, functional disability, and aesthetic distortion. This healing process is known as healing by SECONDARY INTENTION.

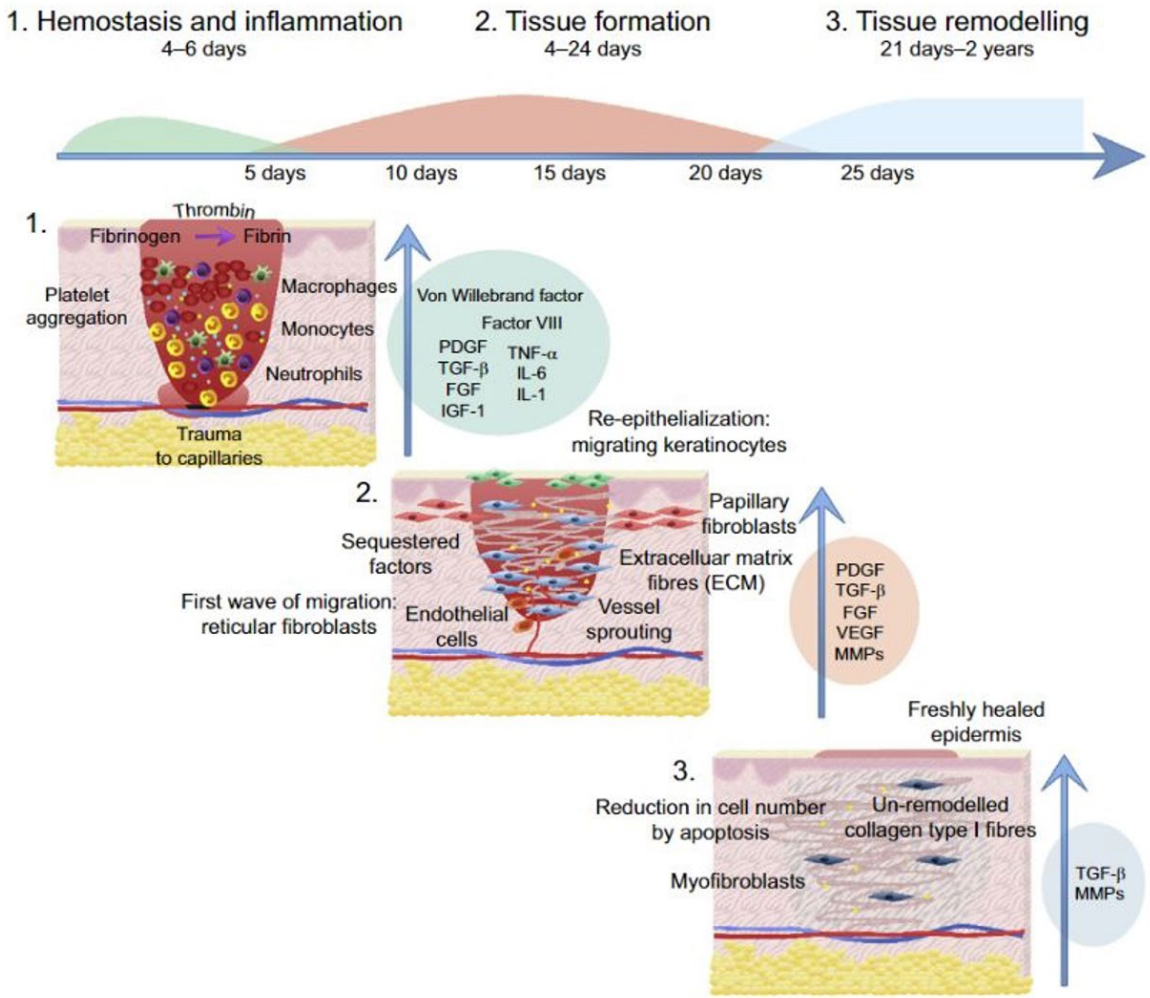

Figure 1.4. Phases of wound healing. The initial haemostasis and inflammatory phase lasts between 4-6 days triggering the immune system to prevent bacterial invasion. The proliferation phase from day 4-24 starts with deposition of granulation tissue to fill the wound to enable edge migration and re-epithelialisation and final tissue remodelling with maturation of the tissue from 21 days up to 2 years. (Image from Plotczyk et al. 2019 [21]).

As mentioned earlier, other factors can affect wound healing, resulting in impaired or non-healing wounds. In the local wound environment, they include decreased oxygen and hypoxic conditions, heavy bacterial colonisation or infection, and prolonged inflammatory response. Systemic factors also play a role, for example patient age, sex, presence of stress, diabetes and certain medications. A non-healing (chronic) wound is classified as a wound persisting longer than 4 weeks to three months [23]. They represent an immense burden on healthcare systems, costing in excess of AU$3.5 billion per year in Australia, and US$25-39 billion annually in the United States [24]. Putting aside cost, the diminution of quality of life mandates aggressive investigation into chronic wounds. Pathological scarring resulting from delayed wound healing (hypertrophic or keloid scarring) magnifies cost, dysfunction, disability and dysaesthesia. Extensive, deep burn injury is often associated with significant hypertrophic scar formation [25]. Failure to 'close' the wounds within 14 days of injury, results in 'overgranulation' with excess collagen deposition, raised and firm tissue, red-pink in colour, borders within the initial wound site and are painful and pruritic [25]. Such scars, when affecting function in particular, but also when causing unsightly socially-disfiguring scars, often require surgical correction. Latterly, this has been performed using laser therapy, but in severe cases, surgical release using a variety of techniques (some enormously complex, or requiring serial surgery) is required to release contracture. Tissue-engineered concepts have roles not only in the acute wound healing phase to close wounds expeditiously when techniques like skin grafting are impossible due to donor site paucity, but also in resource-sparing reconstructive surgery (where major free flap surgery can potentially be replaced by cultured alternatives). The aim is always to improve outcome, achieve independent living, regain pre-injury function and appearance as closely as possible, and reduce ongoing societal and medical strains. With an aging population faced with global increases in obesity and diseases such as diabetes, who are no longer robust enough to undergo the physical insult of major surgical procedures, we must focus our attention to expedite the transition of these research technologies into novel therapeutic treatments.

1.4 Burn Injury

As depicted in the wound healing section 1.3 above, a severe burn (or open) wound, heals differently from a normal cutaneous wound due to the degree of complexity (Figure 1.5). Thermal injury is the most common type of burn. Other causes include chemical, radiation, and electrical, requiring altered burn care practices and treatments. Burn injuries induce physiological and pathological systemic effects that lead to a compromised adaptive immune response, increasing infection risks and bacterial sepsis with the potential for organ dysfunction and death. Other related injuries include smoke inhalation, comorbidities, and any associated trauma injuries.

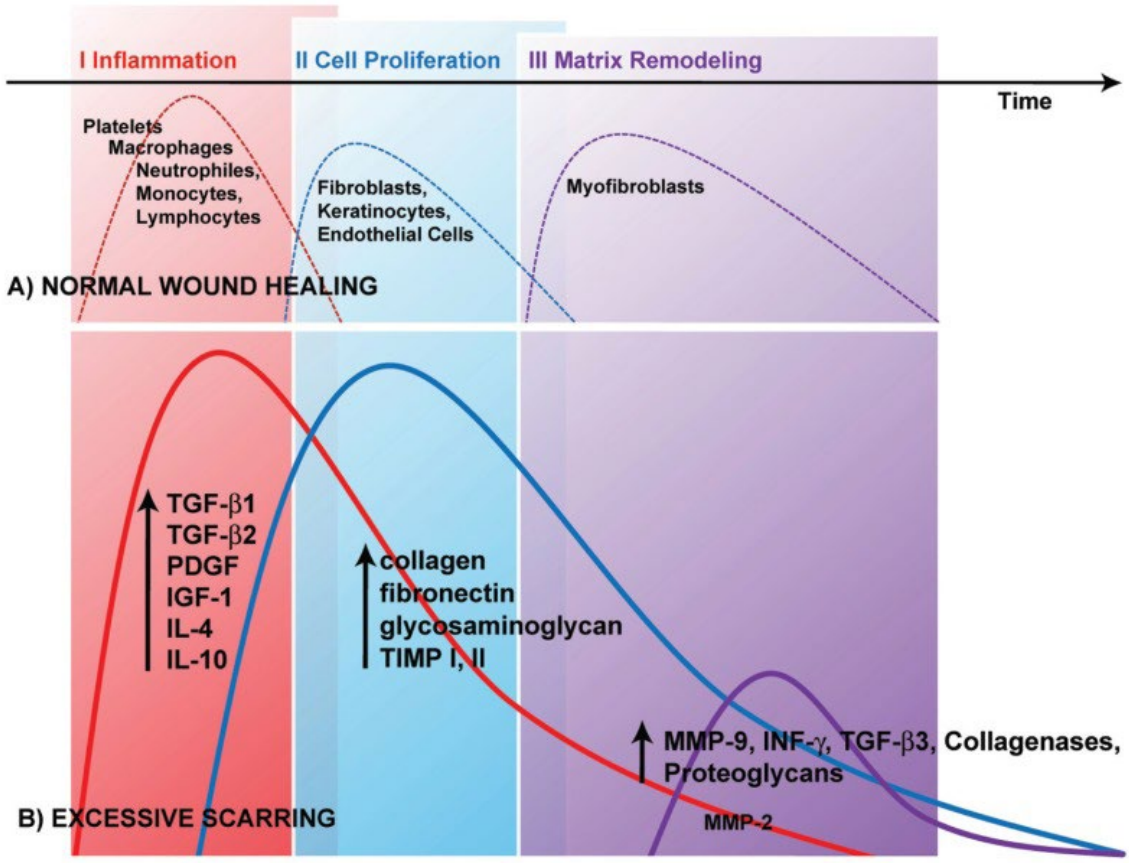

Figure 1.5. Differences between normal wound healing and excessive scarring. (Image from Gauglitz et al. 2011 [25]).

Together with the cause of injury, burns are classified according to the depth (the thickness of destroyed tissue), size, mode of healing, and are treatment dependent. Burn depths can essentially be classified into two groups, one where the wound will heal spontaneously (primary healing), and the other requires intervention (heals by secondary intention) (Figure 1.6). These can be further classified into superficial partial-thickness burns that involve loss of epidermal layers and present with blistering, minor pain and erythema. They heal with no scarring and require minimal intervention. Deep partial-thickness burns cause loss of the epidermis deep into the reticular dermal region and repairs by a process resulting in pathological scarring [17]. The deep to full-thickness burns result in total loss of epidermis, dermis, appendages and even subcutaneous fat to muscle and are often less painful due to the damage of sensory receptors (deep-partial) or no pain with total nerve obliteration (full-thickness). Contraction occurs due to fibroblasts transforming to a myofibroblast phenotype within the granulation tissue [26]. The result of contraction is 'contracture', which creates the disfiguring disability that, until recently, characterised major burn outcomes and may cause societal withdrawal and isolation. A full-thickness defect greater than 4cm requires a form of graft closure as the injury healed by re-epithelialisation is limiting and will have considerable contraction [27].

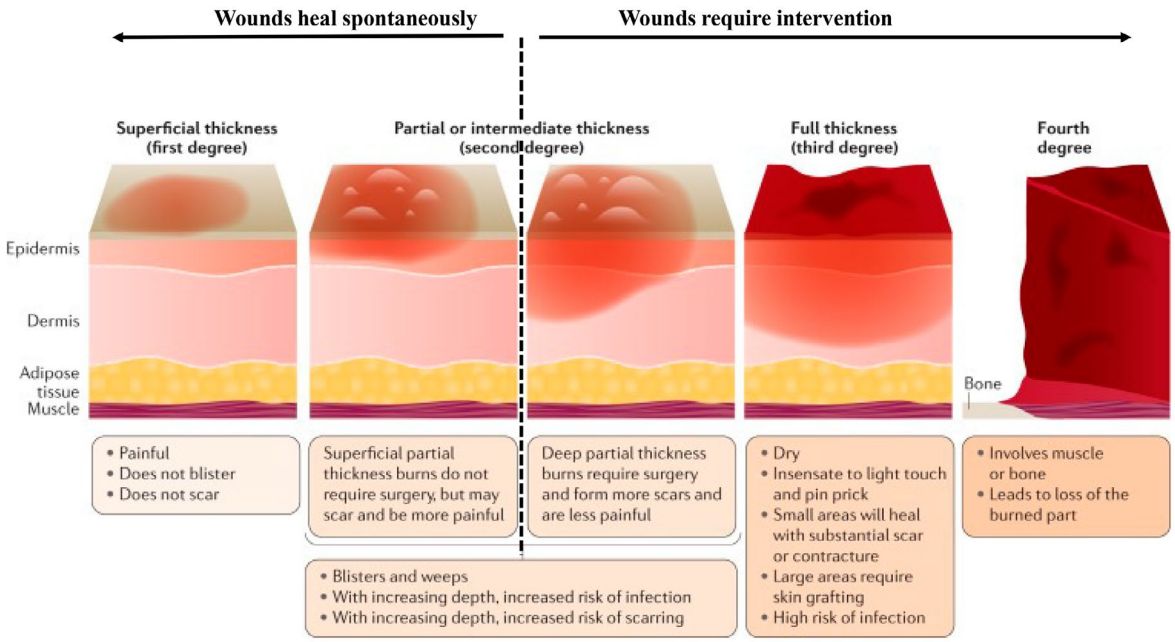

Figure 1.6. Burn classification of depths, dotted line delineates the two modes of burn depths and healing courses (Adapted from Jeschke et al. 2020 [28]).

Dysfunction requires reconstruction, often by multiple surgery episodes to release contracture and produce a functionally aesthetic result [29]. Extensive full-thickness burn injuries (greater than 50% of the Total Body Surface Area) are problematic and require considerable external interventions, with more medical complications than less severe burns, and may require intensive care during hospitalisation. The health-related quality of life parameters for patients that sustain a burn are lower when compared to the general population [30], alongside mental health issues that are substantially increased post-burn [31]. The effects are evident over years, long-term outcomes and quality of life are elements the burns community are only now starting to engage.

Since the 1980's early excision of eschar, and skin grafting for wound closure have been the principal therapeutic approaches for full-thickness burns [32], this has decreased infection rates, shortened hospital stays and improved patient outcomes and survival [33]. Over the last decade, technology and research have shown continual progress with the enhancement and increased use of dermal substitutes, multifaceted wound dressings, and life-saving tissue-engineered techniques (Bioengineered skin). Patients who suffer extensive burns will now benefit from this paradigm shift in burn care that will increase chances of survival with a more functional and aesthetic outcome, and better quality of life.

1.5 Milestones for Skin Tissue Engineering and Burns

The term “tissue engineering” (TE) has evolved over history, adopted in the mid-1980s and coined in 1987 at a US National Science Foundation meeting [34]. Tissue engineering assists with the regeneration and repair of tissues. The complex structures require a three-dimensional scaffold that incorporate a patients own cells that can produce growth factors to replicate new tissue growth for transplantation [35]. Research and animal studies have shown promise for skin tissue engineering; however, the transition to clinical practice is lengthy, marred by the complexity of financial and regulatory requirements. An overview of these challenges is in the following review (1.7 Advances in skin bioengineering and challenges of clinical translation). This section will elucidate the history behind skin tissue engineering with skin research and its parallel associations with burns (Figure 1.7). The first initial advancements occurred in the early 1950s with the successful separation of the epidermis from the dermis [36] and then in the 1960s the *in vitro* culture of keratinocytes, but it wasn’t until 1975, when the first serial cultivation of human epidermal keratinocytes was described by Rheinwald and Green [37]. This method involved the co-culture of lethally-irradiated 3T3 mouse fibroblasts and was the symbiotic foundation for burns. Formative investigations followed regarding colony formation, proliferation, differentiation and adhesion of keratinocytes [38]. The first clinical use of cultured epithelial autografts for burns occurred in 1981 [39] through to 1986 where it was used as an adjunct with donor skin [4].

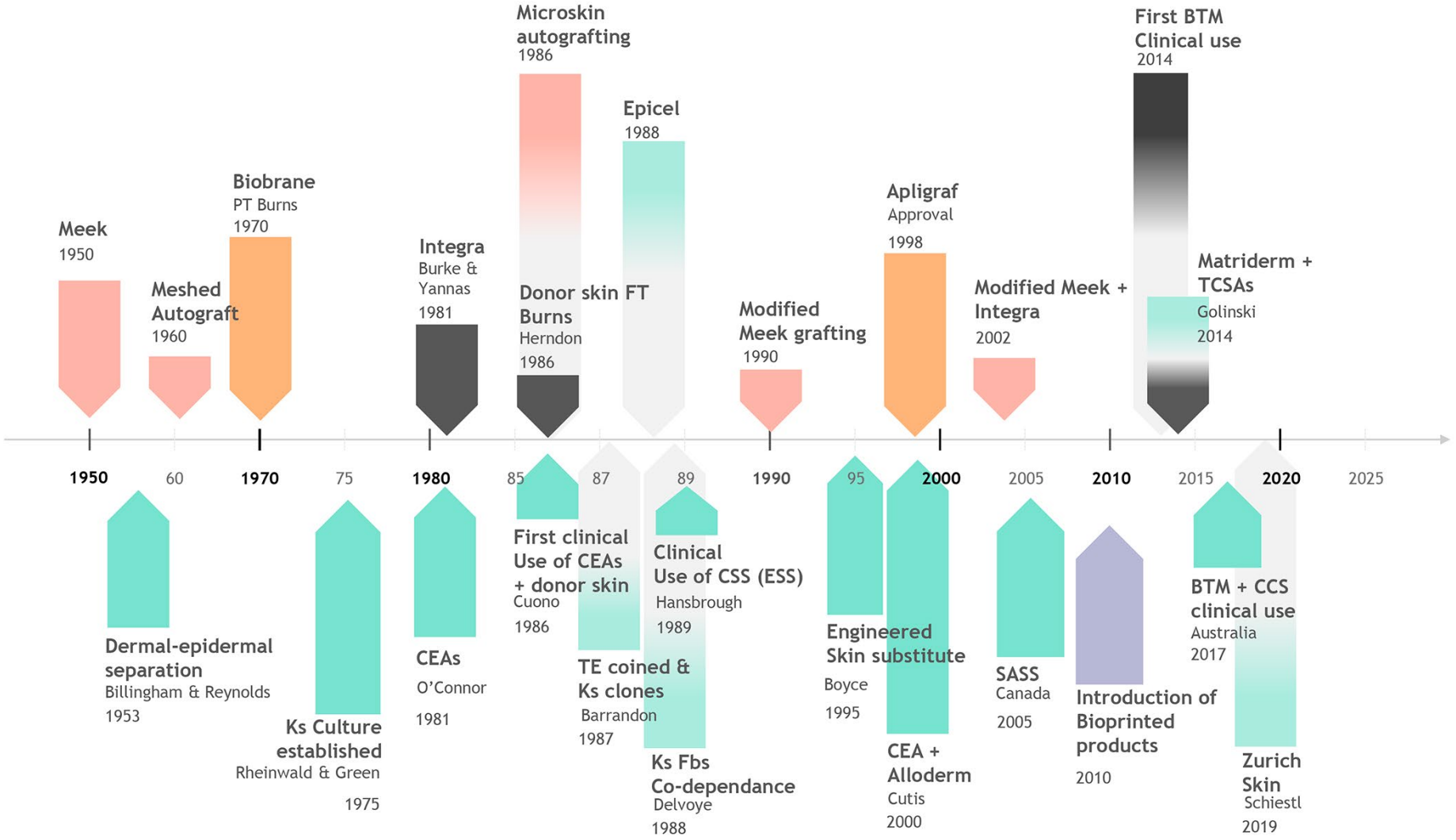

Figure 1.7. The fundamental developments and timeline of skin tissue engineering and burn techniques over the last 7 decades (Adapted from Chua et al. 2016 [40], Böttcher-Haberzeth et al. 2010 [41], Oberweis et al. 2020, [42] MacNeil S, 2007 [43]).

During the history of burns, a number of events including the development of a dermal substitute in 1981, known as Integra [44], gave promise for extensive wound defects. Following Integra, Bell and colleagues in 1983 [45] produced an animal model of a "living skin equivalent", consisting of a dermal component with collagen and epidermis known as Apligraf®. Comprising allogeneic fibroblasts and indicated for small ulcerated wounds, Apligraf® became the first product regulated by FDA, although this was in the late 1990s. A few years after Bell, in 1986, Herndon used donor allograft skin for full-thickness burns as temporary biologic dressings enabling these deep wounds to be covered, reducing mortality and morbidity [46]. Another product to receive market authorisation by the FDA was developed in 1988 on Green's technology. Epicel® is a cell-based tissue-engineered product now authorised for use in burns greater than 30% [4, 42]. Although the use of cultured epidermal autograft is limited. The following section, 1.6, provides a brief overview of cultured epithelial autografts (CEAs) and their shortcomings. However, two milestone events, (1) the co-dependence of keratinocytes on fibroblasts [47] and (2) the conclusion donor keratinocytes do not survive long-term [48], helps to explain the failure rates of CEAs or cell sprays.

The inherent nature of a large burn is the limited availability of donor site skin. Techniques to maximise and expand the ratio of autologous skin graft such as Meek-Wall technique, where small micrografts are expanded and mesh grafts are used to expediate wound coverage for these large burns [49]. Modifications occurred with the developed Meek (1950s) and meshed (1960s) autograft techniques in the 1990s to advance patient outcomes, but the known disadvantages of skin grafts were still confronting. To reduce the use of skin grafts, Boyce and colleagues were one of the first skin engineering groups to produce a clinically viable skin substitute (formally Cultured skin substitute with current reference to the model as Engineered skin substitute, ESS). These showed comparable outcomes to meshed skin autograft, and reduced donor skin requirements for extensive full-thickness wounds [50-54] (Figure 1.8).

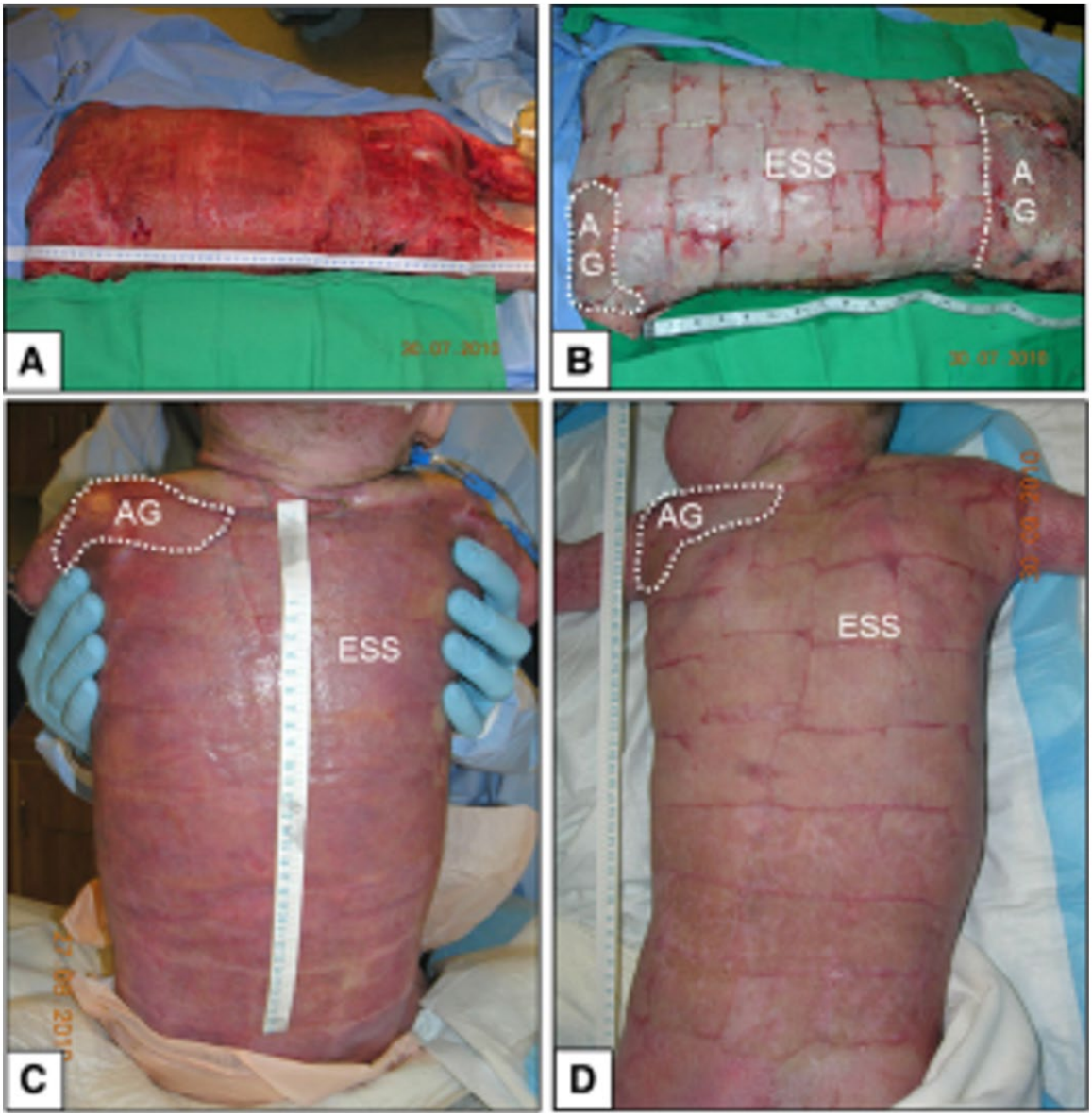

Figure 1.8. Use of Engineered skin substitute 1989-2017. A-D represents clinical observations of skin autograft (AG) and ESS application on the left shoulder and chest, respectively. D, POD 62 depicts multiple applications of small ESS. ESS, engineered skin substitute; POD, post-operative day. Adapted and reproduced from Boyce et al. 2017 [54].

Since this milestone, the increasing interest in tissue engineering has progressed exponentially including the beginning of tissue engineering societies [55]. Since the mid-twenty-tens to current, a minority of groups worldwide have attempted clinical use of modified designs of skin substitutes for wound loss conditions and, more recently major burns [56-58]. Most utilising a special access scheme (country-specific) as none have encountered clinical regulatory bodies or phase II trials at the commencement of this candidature. The review explores these challenges for skin tissue bioengineering with further introductive information for the types of skin substitutes, bioreactors, and scaffolds detailed in the related manuscript introduction section.

1.6 The Biology of Bioengineered Skin Substitutes

To regenerate *in vitro* skin, primary cell isolation and expansion of each main cell type is required from a small skin biopsy (Figure 1.9). With the correct techniques and methods a 'postage stamp', 2cm^2 biopsy can be exponentially expanded to cover 1m^2 of a human body in 3 weeks [59]. The dynamic biological processes of skin are barriers to re-engineering native skin and are challenges still to be met. Advances in the understanding of wound healing and skin biology will eventually enable the incorporation of multiple cell types and epidermal appendages.

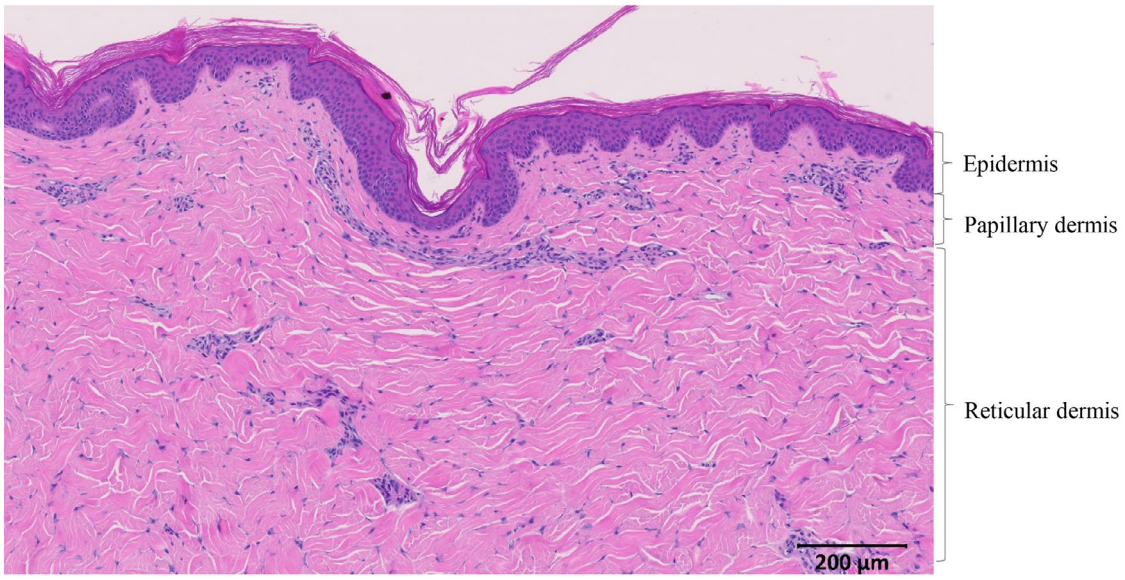

Figure 1.9. Haematoxylin and Eosin (H&E) stained section of human skin tissue. The epidermis contains stratified squamous epithelial cells, these keratinocytes are shed from the surface. The dermis divides into two layers, the papillary layer that interconnects with the epidermal ridges and consists of the main fibroblast population with thin collagen fibres. The deeper reticular layer has a thicker collagen network. Scale bar: 200µm.

The two essential cell types, keratinocytes and fibroblasts, are necessary to fabricate a rudimentary skin substitute. These can generate epidermal and dermal components including the crucial basement membrane. Skin cell culture is a multifaceted process, with each cell type requiring specific media and culture conditions. Firstly, a biopsy is separated using enzymes to cleave the two layers (Figure 1.10). Dispase separates at the basement membrane (BM) and trypsin isolates the epidermal keratinocytes. Collagenase then digests the dermis, isolating the fibroblasts for collagen production. These are mass expanded and cultured in monolayer with the premise of formulating a skin construct.

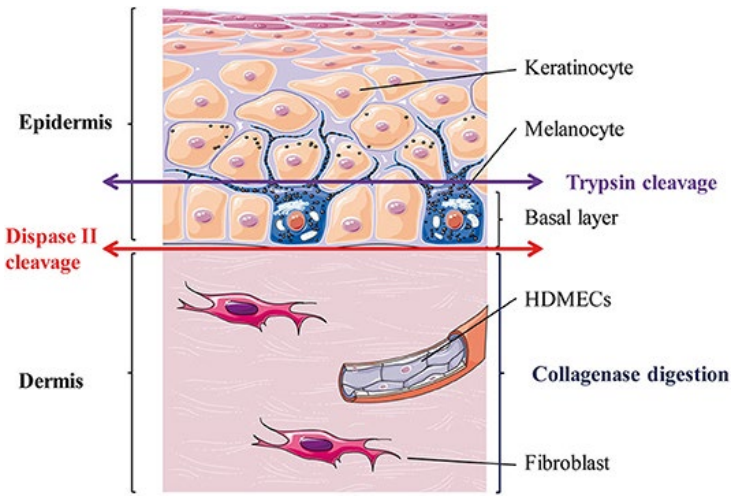

Figure 1.10. Separation of skin layers with Dispase II for basal cell keratinocyte isolation with trypsin and collagenase for dermal digest for fibroblast and endothelial isolation (Adapted from Henrot et al. 2020) [60].

A 3D culture environment assists in replicating a skin analogue, with the incorporation of a substrate/template or scaffold to provide the dermal matrix. Numerous fabrication steps are involved to produce a tissue-engineered product (Figure 1.11) and are the foundations of this thesis. The remaining introductive information is further explored within each related paper/chapter and expands on the current available skin substitutes, bioreactor developments for scale-up and further background into biopolymer dermal scaffolds.

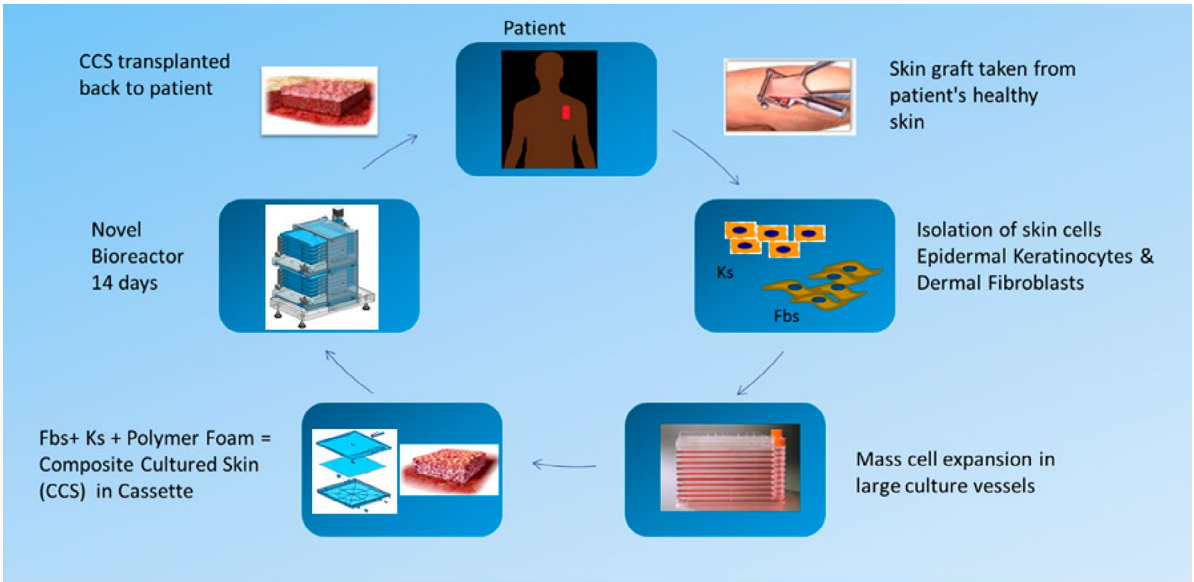

Figure 1.11. Skin Tissue Engineering fabrication approach – from biopsy to transplantation.

1.7 Advances in Skin Tissue Bioengineering and the Challenges of Clinical Translation

Dearman BL, Boyce ST, Greenwood JE

Published in

Frontiers in Surgery

2021

Statement of Authorship

Title of Paper	Advances in Skin Tissue Bioengineering and the Challenges of Clinical Translation
Publication Status	☑ Published ☐ Accepted for Publication ☐ Submitted for Publication ☐ Unpublished and Unsubmitted w ork w ritten in manuscript style
Publication Details	Dearman, BL, Boyce, ST & Greenwood, JE 2021, 'Advances in Skin Tissue Bioengineering and the Challenges of Clinical Translation', *Frontiers in Surgery*, vol. 8, pp. 640879–640879.

Principal Author

Name of Principal Author (Candidate)	Bronwyn Dearman		
Contribution to the Paper	Manuscript concept, design, writing and editing with submission.		
Overall percentage (%)	80%		
Certification:	This paper reports on original research I conducted during the period of my Higher Degree by Research candidature and is not subject to any obligations or contractual agreements with a third party that would constrain its inclusion in this thesis. I am the primary author of this paper.		
Signature		Date	05/01/2022

Co-Author Contributions

By signing the Statement of Authorship, each author certifies that:

i. the candidate's stated contribution to the publication is accurate (as detailed above);
ii. permission is granted for the candidate to include the publication in the thesis; and
iii. the sum of all co-author contributions is equal to 100% less the candidate's stated contribution.

Name of Co-Author	Professor John Greenwood		
Contribution to the Paper	Review and editing of manuscript.		
Signature		Date	05/01/2022

Name of Co-Author	Professor Steven Boyce		
Contribution to the Paper	Review and editing of manuscript.		
Signature		Date	05/01/2022

Please cut and paste additional co-author panels here as required.

frontiers in Surgery

MINI REVIEW
published: 24 August 2021
doi: 10.3389/fsurg.2021.640879

Advances in Skin Tissue Bioengineering and the Challenges of Clinical Translation

Bronwyn L. Dearman[1,2,3]*, *Steven T. Boyce*[4] *and John E. Greenwood*[1,2]

[1] Skin Engineering Laboratory, Adult Burns Centre, Royal Adelaide Hospital, Adelaide, SA, Australia, [2] Adult Burns Centre, Royal Adelaide Hospital, Adelaide, SA, Australia, [3] Faculty of Health and Medical Science, The University of Adelaide, Adelaide, SA, Australia, [4] Department of Surgery, University of Cincinnati, Cincinnati, OH, United States

Skin tissue bioengineering is an emerging field that brings together interdisciplinary teams to promote successful translation to clinical care. Extensive deep tissue injuries, such as large burns and other major skin loss conditions, are medical indications where bioengineered skin substitutes (that restore both dermal and epidermal tissues) are being studied as alternatives. These may not only reduce mortality but also lessen morbidity to improve quality of life and functional outcome compared with the current standards of care. A common objective of dermal-epidermal therapies is to reduce the time required to accomplish stable closure of wounds with minimal scar in patients with insufficient donor sites for autologous split-thickness skin grafts. However, no commercially-available product has yet fully satisfied this objective. Tissue engineered skin may include cells, biopolymer scaffolds and drugs, and requires regulatory review to demonstrate safety and efficacy. They must be scalable for manufacturing and distribution. The advancement of technology and the introduction of bioreactors and bio-printing for skin tissue engineering may facilitate clinical products' availability. This mini-review elucidates the reasons for the few available commercial skin substitutes. In addition, it provides insights into the challenges faced by surgeons and scientists to develop new therapies and deliver the results of translational research to improve patient care.

Keywords: skin, bioengineering, burns, wound closure, skin substitutes, clinical translation, tissue engineering, biopolymers

OPEN ACCESS

Edited by:
Claudia Di Bella,
The University of Melbourne, Australia

Reviewed by:
Marc G. Jeschke,
University of Toronto, Canada
Lars-Peter Kamolz,
Medical University of Graz, Austria

***Correspondence:**
Bronwyn L. Dearman
bronwyn.dearman@sa.gov.au

Specialty section:
This article was submitted to Visceral Surgery, a section of the journal Frontiers in Surgery

Received: *12 December 2020*
Accepted: *31 July 2021*
Published: *24 August 2021*

Citation:
Dearman BL, Boyce ST and Greenwood JE (2021) Advances in Skin Tissue Bioengineering and the Challenges of Clinical Translation. Front. Surg. 8:640879. doi: 10.3389/fsurg.2021.640879

INTRODUCTION

The challenges of translational medicine are becoming more prevalent with developing new technologies as novel therapies for personalised medicine. One therapy where translational research is at the forefront is reducing the use of skin autografts for extensive full-thickness burns with laboratory-generated skin (1–7). The split-thickness meshed and expanded skin autograft has been the prevailing standard of care for burns surgeons for decades and remains the preferred method of wound closure due to its relatively high efficacy of stable wound closure (3, 8, 9). However, if the burn area massively exceeds the area of available donor site for skin autografts, the advantages of autologous engineered skin substitutes is compelling. To regenerate a substitute of uninjured human skin that definitively provides wound closure both anatomically and physiologically (6) is a common challenge for tissue engineers, and may involve polymer chemists, cellular and molecular biologists, surgeons, nurses, and therapists. A systematic review of clinical studies investigating

autologous bilayered skin substitutes as epithelial stem cell niches after grafting, identified 16 potential studies and nine types of autologous skin substitutes over a 25-year period (10). Currently, only a small number of these are still available for therapeutic use, with no ideal substitute in the market. The current models have distinct attributes, for the majority, the scaffold type is a source or derivation of collagen (biologic) with autologous fibroblasts and keratinocytes. Another novel synthetic scaffold utilising a polyurethane (PUR) has also been used to generate a skin composite (composite cultured skin, CCS) and has reported its use for the treatment of a 95% total body surface area burn patient (11). However, these all remain deficient in pigmentation, hair, and other dermal appendages. The authors draw on combined experiences from taking the research bench to bedside. This review will describe the distinct models of bilayered tissue engineered products that have been used therapeutically, which there are few, but all address the same clinical challenges.

The Need for an Alternative to Skin Autografts for Extensive Full-Thickness Burns

Burns are a global health concern, especially for low to middle-income countries, accounting for over 95% of burn deaths (12). Burn injuries of all depths make up only a small proportion (1%) of trauma hospitalisations in Australia (13), but are one of the most costly, due to long hospital and rehabilitation stays (14, 15). In the United States, hospitalised burns cost over $1billion per year (16) and in high income countries the mean cost per 1% TBSA is US$4159.00 (17). These costs are significant, but the major indirect cost is the patient's lifelong scars and disfigurements. As the percentage of total body surface area (TBSA) burn and burn depth increases, the costs increase exponentially (14). Extensive, full-thickness burn injuries (>50% TBSA) usually require intensive care, multiple surgical procedures, physical and occupational therapy and psycho-social interventions to recover. Patients with these degrees of burn often die which obviates skin graft paucity (18). However, advances in burn care have led to increased survival rates due to early excision of eschar, temporary wound closure, advanced nutritional support, infection prevention, and improvements in critical care medicine (19–22). Although, burns in the elderly and those with coincident trauma such as inhalation injury, remain challenging.

In this patient population, temporary wound coverage provides time for utilisation of donor sites from superficially burned skin and re-harvesting to allow multiple procedures of skin autografting (23). Maximising wound coverage with available donor site involves thin, widely-meshed, or expanded (Meek-Wall technique) (24) skin autografts, resulting in poor functional and aesthetic outcomes. In addition, donor sites generated by split-thickness skin graft harvesting are extremely painful, may require opiate analgesia, limit mobilisation, and discourage compliance with physical therapy (25). Skin autografts, however, have properties that promote their continued widespread use for the closure of large, deep skin wounds (no rejection, vascular inosculation, high efficacy, long-term stability), but their correlation with increased morbidity, especially in the elderly, is a significant disadvantage, which motivates the search for alternatives (26, 27).

An ideal skin substitute should adhere, vascularise, and integrate quickly, contain both epidermal and dermal components, provide permanent and definitive wound closure, be autologous, resist infection, be easy to prepare, handle well, easy to apply, cost-effective, and resist mechanical shear forces (28). They should demonstrate high engraftment rates, restore natural pigmentation, and provide all skin appendages and sensory networks in uninjured skin. This list of qualities is comprehensive, and to simultaneously replicate these features *in vivo* requires complex engineering in the laboratory. Engineered skin fabrication is a specialised professional field with many aspects still to be elucidated and reduced to practise. A standardised universal classification system for "skin substitutes" was published by Davison-Kotler et al. in 2018 to encapsulate all adaptations (research and clinical) using a factorial design (29). Primary categories include acellular dermal substitutes, temporary skin substitutes, and permanent skin substitutes, further expanding into sub-categories (2). The many variations have been tabulated in former reviews and will not be detailed here (6, 7, 29–38). This review focuses on permanent, cellular, and mainly autologous products with dermal and epidermal components. It will explore a few commercially available products and some clinically used in extensive wounds (**Table 1**).

Large, Excised Wounds—Temporising the Wound Bed for Definitive Closure

The loss of the epidermis, and sufficient dermis to ensure loss of all the epidermal adnexa, requires rapid wound closure. The primary focus is on reducing inflammation and granulation, preventing infection and limiting contraction. The associated mortality and morbidity rates decrease with the successful implementation of the above and achieved by staged closure (69). Acellular dermal substitutes comprising a dermal and a pseudo-epidermal component have been widely used to achieve physiological closure. Their implementation has produced a paradigm shift in burn care (21, 70, 71). The dermal components may originate from decellularised human skin, biological polymers, or synthetic polymers. Their function is to temporarily close the excised wound to decrease fluid loss, allow integration and controlled granulation tissue invasion inducing a vascularised wound bed. Commercial examples include Integra® Dermal Regeneration Template, Pelnac, Terudermis, Hyalomatrix, and RenoSkin (69). These products and similar ones have limitations, including a risk of transmissible disease, loss from infection and high costs (5, 72). Despite regulatory approval for specific medical indications, most dermal substitutes have not achieved worldwide consensus as market leaders for large, deep dermal wounds. However, establishing a neo-dermis enhances structural stability and provides the time required for definitive epithelial wound closure, whether by serial grafting or by generating and applying autologous engineered skin.

TABLE 1 | Examples of clinically-available or investigative skin substitutes [adapted from Vig et al. (7), Boyce et al. (31)].

	Product-country of origin	Classification/components	Proposed clinical indication	Product limitations
Dermal-epidermal substitutes	TISSUEtech Autograft system (Hylomatrix + Laserskin)—Italy (39, 40)	Cellular, autologous Ks, Fbs with HA	Diabetic ulcers	Small wounds, difficult to use clinically
	Tissue-cultured skin autograft (TCSA's)—Germany (41)	Cellular, autologous Ks, Fbs with Matriderm™	Chronic ulcerations	Small wounds
	Engineered skin substitute (ESS)—USA (42–50)	Cellular, autologous Ks, Fbs, bovine collagen-GAG	Large burns and other skin loss conditions	Xenogeneic scaffold, small pieces, shrinkage of product, cost
	Composite cultured skin (CCS)—Australia (51–57)	Cellular, autologous Ks, Fbs, synthetic polymer	Full- thickness burns	Scaffold porosity, complex
	Self-assembled skin substitute (SASSs)—Canada (58)	Cellular, autologous Ks and Fbs	Burns	Labour intensive
	Autologous homologous skin construct (AHSC)—USA (59–61)	Cellular, autologous skin cells	Burns, acute trauma chronic wounds	Cell suspension/aggregate
	MyDerm—Malaysia (62–65)	Cellular, autologous Ks and Fbs, Fibrin	Burns, skin trauma and chronic wounds	Clinical efficiency
	StrataGraft™–USA (66, 67)	Cellular, allogeneic Ks and Fbs, non-bovine collagen	Burns and skin conditions	Allogeneic, temporary, size
	denovoSkin—Switzerland (68)	Cellular, autologous Ks and Fbs, bovine collagen	Burns	Xenogeneic scaffold

HA, Hyaluronic acid; Ks, Keratinocytes, Fbs, Fibroblasts.

The NovoSorb™ Biodegradable Temporising Matrix (BTM) is a synthetic scaffold that is currently in routine use for burns and complex wound repair (73–79). It is a scaffold that temporises the wound and biodegrades after integration and establishment of dermal elements (80). Furthermore, it resists infection, can be made in large sheets, is inexpensive to produce, easy to handle, and provides integration time (76–82). With the optimisation of a dermal replacement template and a major limitation addressed, i.e., acquisition of time for cellular growth, the prospective next step is the specification of a definitive wound closure alternative.

The Current State of Bioengineered Dermal-Epidermal Substitutes

Bioengineered skin substitutes involving dermal and epidermal components are the focus of this paper; however, epidermal replacements (cellular) require brief reference to appreciate the desirability of both components. A skin substitute is yet to be achieved that replaces the anatomy and physiology of uninjured skin or completely replaces all skin autograft properties- implying why an epidermal replacement alone will not replicate a meshed, or sheet, autograft. Cultured Epithelial Autografts (CEA's) have been used since 1986 (83), and other adaptations or iterations of keratinocyte suspensions [e.g., Epicel (84, 85), Cell Spray, RECELL® (86), BioSeed (87), Laserskin (39, 40)] have evolved. These are clinical adjuncts to therapies with traditional treatments of burn care to expedite reepithelialisation rate. Clinically applicable for small wounds (88), ulcers (87, 89–92), superficial burns (93) and skin graft donor sites; they have not been universally accepted by burns surgeons independently for deep large burns due to their limited expansion rate, mechanical fragility on handling, tendency to blister *in vivo* and vulnerability to shear after application (partly to deficiencies in basement membrane formation) (94). In addition, they are costly to produce, can take weeks to manufacture, and are epidermal derived replacements (95–100). Incorporating a substitute containing epidermal and dermal components is a logical progression toward regenerating a tissue more like uninjured skin (101).

A critical paracrine dialogue between fibroblasts and keratinocytes is essential for basement membrane synthesis, a beneficial feature for engineered skin substitutes (102–104). The basement membrane protects against shear by establishing a molecular bond that anchors the cellular epidermis to the extracellular matrix of the dermis. The most analogous to skin, and the most successful clinically to date, is an Engineered Skin Substitute (ESS) developed in Cincinnati, Ohio (105). Developed over the past 30 years, the ESS comprises autologous keratinocytes and fibroblasts in a bovine collagen-glycosaminoglycan (GAG) scaffold (42–50). The ESS model was the first to demonstrate stable closure of full-thickness burns by combination with Integra® Dermal Regeneration Template (106). In 2017, a report was published of ESS' clinical results in 16 subjects treated from 2007 to 2010. For patients with >50%, TBSA full-thickness burns, ESS's were able to reduce the need for harvesting donor skin grafts and reduce the mortality rate compared with data from similar patient populations reported in the National Burn Repository of the American Burn Association (107). The ESS results in a closed wound that has structural and functional similarities to native skin. However, this model also has limitations (lack of other cell types and adnexal structures, contraction of the collagen scaffold during ESS fabrication, relatively high cost and regulatory

complexity); and is not commercially available. Pre-clinical studies have recently demonstrated the successful incorporation of melanocytes (108, 109), microvascular endothelial cells (110), and hair follicles (111) into the ESS model.

Bovine collagen is also used in denovoSkin™ (Cutiss AG, Zurich), which consists of a collagen hydrogel and human dermal fibroblasts and keratinocytes. It has been classified as an Advanced Therapy Medical Product (ATMP) and has received FDA and EMA Orphan status to treat burns in the US and EU (112, 113). It is currently undergoing clinical trial recruitment for adult and children burns, with an estimated completion date of 2023. However, the production of a dermal-epidermal equivalent with xenogeneic (non-human)-derived biologicals, such as bovine, rat, or porcine collagens or glycosaminoglycans (42) raises the potential for immune recognition and rejection and risk of prion transmission. A synthetic scaffold and autologous cell approach may reduce these risks.

Several matrices using fibroblasts alone to provide the biological extracellular matrix environment (114–117) have shown the generated skin's long-term stability *in vitro* (118). Through the Special Access Program in Canada, a Self-Assembled Skin Substitute (SASS) has shown clinical effectiveness, reporting a case series of 14 severely burned subjects (58). This substitute contains autologous fibroblasts and keratinocytes, forming a human biopolymer fibroblast scaffold with subsequent keratinocyte seeding. The constraining factor for this type of substitute, like some others, is the production time, with an average of 9 weeks from the initial biopsy (58). In addition, the SASSs post-transplantation displayed visible junctions between applications, re-iterating the need for a sizeable sheet that can be generated and transplanted with fewer anaesthetics.

Improved scalability has now been reported using a biodegradable polyurethane (PUR) as the scaffold for a dermal-epidermal alternative, known as a composite cultured skin (CCS) (51–57). The attributes for an "ideal engineered skin," as mentioned previously (119), formulated the premise of combining an engineered-epidermis to a modified BTM dermal substitute. Compared to bovine collagen (a biologic), a synthetic biodegradable PUR showed lower toxicity and cytotoxicity, reduced immunogenic reaction, and minimal inflammatory response (51, 52, 120). The BTM-CCS provided a two-stage strategy, with the CCS as a definitive second stage wound closure material. The application of NovoSorb™ BTM, a temporising matrix, addresses one of the major limitations of available skin substitutes [i.e., time required for autologous cell expansion 3–5 weeks (38)]. The integration period enables the time required for cell isolation, expansion and bilayered construction (up to 7-weeks if needed) (11, 69). The CCS is a 1 mm thick PUR porous scaffold, populated with autologous fibroblasts in a fibrin network and layered with autologous keratinocytes (53, 54). Pre-clinical studies in a porcine model initially demonstrated the efficacy of small CCS, and later large pieces, generated in an automated bioreactor (54, 57). This custom-made novel bioreactor device has taken this from research to clinic (11, 57). The two-stage strategy of BTM-CCS has been used clinically in a 95% TBSA burn injury (covering 40% TBSA of original burn) (11). The patient not only survived but, at 1.5 years post-injury, required minimal contracture release in areas where autografts were applied and none to the CCS-applied areas. The result for CCS was a smooth, supple aesthetic appearance with varying pigmentation from primary epithelial engraftment. No delineation between junctions of CCSs can be observed. ROM and SOSS scores were comparable to sheet graft, but favourable over 1:3 meshed STSG and Meek.

The subcutaneous layer (the deepest layer of skin) is absent in many investigational and clinical substitutes. Polarity TE, a US company, produces an Autologous Homologous Skin Construct (AHSC). They claim that functional full-thickness skin can be regenerated by obtaining a full-thickness biopsy with immediate application (59). A retrospective, 15-patient post-AHSC application review case series was reported (60) for various wound types (burns, acute/traumatic injuries, and chronic wounds). It differs from the conventional dermal-epidermal substitute, in that it seems not to necessitate culture and is returned to the patient within days. These wounds were closed at 3 months post application; however, further studies are required to investigate and substantiate the claims of efficacy, especially in full-thickness, excised burns (61).

Several other dermal-epidermal constructs have been used clinically or gone to clinical trial pending commercialisation (**Table 1**). Some examples include, tissue cultured skin autograft (TCSAs using Matriderm™, Germany) (41), TISSUEtech Autograft system™ (using Hylomatrix, Anika Therapeutics Inc., Bedford) (121), and others using Allodermis (122, 123), Human plasma (124, 125), and Fibrin (MyDerm, Japan) (62–65). Another bi-layered product recently receiving (2021) FDA approval for adult deep partial-thickness burns is StrataGraft® (Mallinckrodt, USA) (66, 67). Although it is not autologous, this bilayered allogeneic product comprises murine collagen and allogeneic fibroblasts and keratinocytes, this acts indirectly on the autologous cells to assist with wound closure (66). This type of treatment is limited for deep full-thickness burns as it needs another source of autologous cells e.g., meshed graft or other skin appendages, to close the wound. However, it is readily available and "off-the-shelf" ready for immediate use, whereas typical bilayered autologous substitutes can take weeks to fabricate. As with any graft, there is potential for loss if there is no neovascularization. The majority of clinically available engineered skins are avascular; however, this is under investigation by researchers (126). The loss of graft can be due to an accumulation of blood (haematoma), fluid (seroma), contamination, or mechanical shear. The different skin models mentioned have varying pore sizes and can contribute to the success of the engraftment. The density of the dermal component (i.e., too small or large pores) can inhibit or promote vascularisation (57, 127). Shear of a substitute graft or blistering will also occur if there is loss or no basement membrane and reiterates the importance of cell-cell contact of the epidermal-dermal component *in vitro* culture. When this loss occurs, the wound heals by secondary reepithelialisation and healing is delayed. Although, a systematic review of bilayered skin substitutes showed wound healing rates for leg ulcers were comparable with the standard of care (RR 1.51, 95%

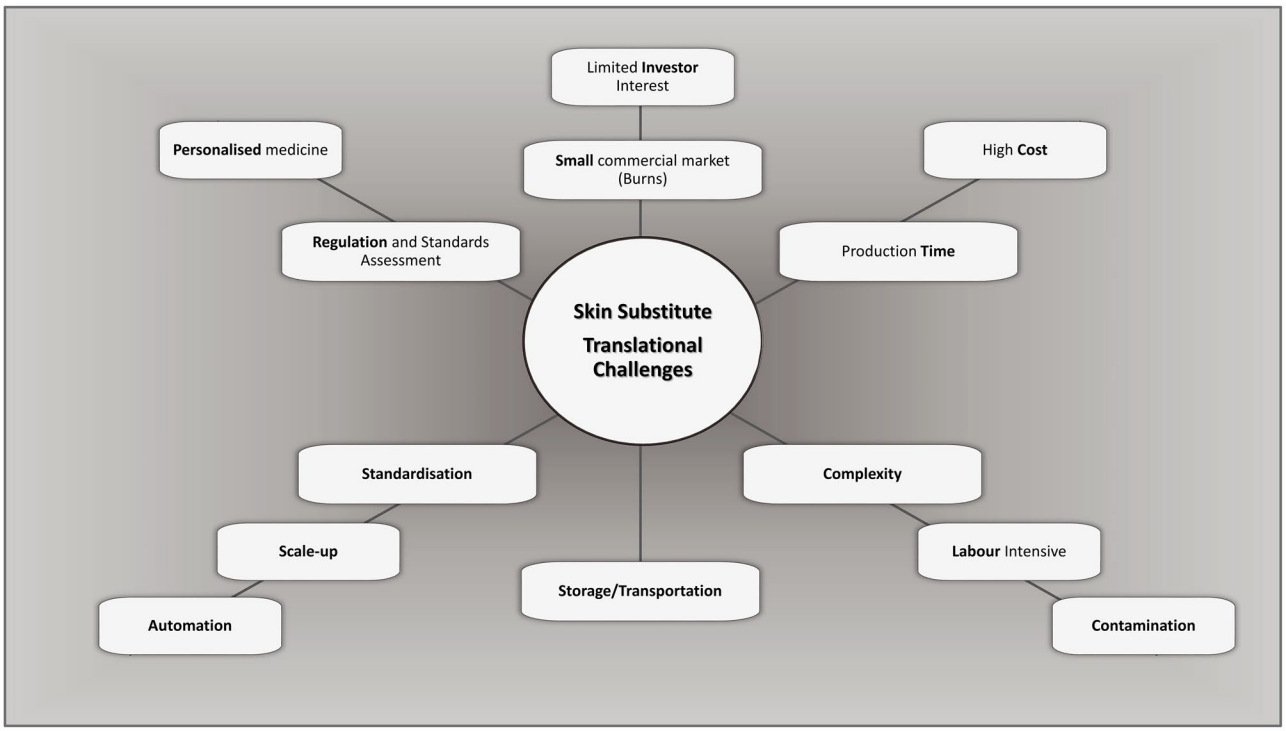

FIGURE 1 | Challenges and considerations in bioengineering of bilayered skin substitutes. Adapted from Al-Himdani et al. (133).

1.22–1.88) (128). A widely meshed STSG used for extensive wound coverage results in a weave-like pattern, producing a poor aesthetic result. In contrast, autologous engineered skin provides immediate coverage with a stratified epidermis that suppresses granulation tissue and arrests the scarring process. Producing a favourable smooth, pliable, even skin, with a reduction in pain and itch (55, 68, 107). Another major strength and benefit over skin autografts is the reduction of autologous donor skin and its associated morbidities. The diverse bilayered approaches mentioned all have their strengths and weaknesses, and in review, the ideal model may likely be combinations of biopolymer scaffolds and stem cells that can produce a functional, clinically safe and effective alternative (129, 130). Any of these tissue engineered products will face regulatory reviews and reimbursement requirements.

Clinical Challenges for Skin Substitutes

As cell-based therapeutic inventions, these products require approval by regulatory authorities to ensure high quality, safety and proven efficacy (131) (Therapeutic Goods Administration, TGA in Australia; Food and Drug Administration, FDA in the United States; European Medicines Agency (EMA), in the European Union, etc.). Several pre-clinical substitutes are being used through Special Access Programs (SAP) in designated countries. This scheme is a way of using non-licenced products to treat life-threatening injuries where other methods are not suitable, or non-existent. In the United States, the passage of the 21st Century Cures Act, in 2016 (31) and new agency programs will facilitate the clinical use of novel products and devices to treat patients at severe medical risk.

The generation of highly manipulated tissue-engineered products follows the standards for current Good Manufacturing Practices (cGMP) (132). They should ideally be free of any xenogeneic product (131) and include mandatory testing for microbiological assessment [sterility assurance level (SAL) of 10^{-6}] and transportation validation to ensure that product integrity is maintained. Generating a clinically viable, and ethical, product suitable for market is a lengthy and labour intensive process, with high initial capital costs. These infrastructure costs, process complexity, and stringent quality control result in expensive products, making commercialisation less practical (133, 134) and are translational challenges a therapeutic product may encounter (**Figure 1**). The cost of such substitutes, however, should not be assessed directly by the cost per unit of production only (31, 135), but also indirectly by assessing overall hospital cost reductions concerning length of stay, the number of reconstructive surgeries post-major burn, patient outcome and aesthetics. Although, an experienced highly trained medical team, including specialised nurses and therapy protocols are required during the intense early stages of treatment until they become the prevailing standard of care.

The Future Opportunities of Skin Substitutes

The generation of laboratory-generated "skin substitutes," irrespective of classification, have to date only partially

addressed the requirements for achieving stable wound closure. They currently produce inadequate pigmentation (hypo- or hyperpigmentation), they lack vasculature, hair, glands, and none have replicated the results of unmeshed autograft or duplicated the anatomy and physiology of uninjured skin. Due to cost, regulatory restraints, and the significant scientific challenge to incorporate all skin features simultaneously (136–139). Approaches to the refinement of fabrication systems for skin substitutes will facilitate advanced models of engineered skin to reach their markets with a consequent decrease in costs. The requirement for scalability is a compelling demand for large burn injuries and can be met by incorporating automated bioreactors (57, 140). These may assist production and provide complete automation and standardisation to improve product quality. The robotic systems are engineering advances that will move forward in parallel with medical advances. The 3D and 4D bioprinting fields coupled with the latest compatible bioinks are novel techniques that may rapidly advance the tissue engineering field (141–145).

In time, these technologies and advances in tissue engineering will at least reduce, and possibly replace, the need for skin autografts and enable easier clinical translation of an acceptable autologous engineered skin, suitable for patient use. The significance of this is that patients with life-threatening burns will no longer suffer the painful acute morbidity and later scarring that donor sites generate. Time in ICU and total hospitalisation will be reduced, the need for reconstructive surgery will decrease, with overall costs reduced. The success will also have implications for other dermatologic conditions, including but not limited to giant congenital naevi excision and engraftment, epidermolysis bullosa treatment, certain surgical reconstructions, and vitiligo. It can also contribute to the investigation and requirement for epidermal appendages, naturally matched skin pigmentation, vascular plexus, and sensory nerves (2, 139, 146, 147). As each of these advances is currently under investigation, there can be high degrees of confidence that many, if not most of these skin components (uniform skin colour, sweat glands, and hair follicles) will be incorporated into future models of skin substitutes and available clinically for the treatment of full-thickness skin wounds, including burns.

AUTHOR CONTRIBUTIONS

BD developed the outline with contributions from both JG and SB. BD wrote the manuscript with editing by JG and SB.

FUNDING

The CCS studies were supported by a grant from Lifetime Support Authority (LSA, GA-00061) and the Health Services Charitable Gifts Board (HSGB, 05-88). The NovoSorb® biodegradable polyurethane platform is produced by PolyNovo Biomaterials Pty. Ltd. based in Port Melbourne, Victoria, Australia.

REFERENCES

1. Supp DM, Boyce ST. Engineered skin substitutes: practices and potentials. *Clin Dermatol.* (2005) 23:403–12. doi: 10.1016/j.clindermatol.2004.07.023
2. Boyce S, Supp D. Chapter 11 - biologic skin substitutes. in *Skin Tissue Engineering and Regenerative Medicine*, eds M. Z. Albanna and J. H. Holmes Iv (New York, NY: Academic Press/Elsevier), (2016). p. 211–38. doi: 10.1016/B978-0-12-801654-1.00011-5
3. MacNeil S. Progress and opportunities for tissue-engineered skin. *Nature.* (2007) 445:874–80. doi: 10.1038/nature05664
4. Chua AW, Khoo YC, Tan BK, Tan KC, Foo CL, Chong SJ. Skin tissue engineering advances in severe burns: review and therapeutic applications. *Burns Trauma.* (2016) 4:3. doi: 10.1186/s41038-016-0027-y
5. Nicholas MN, Yeung J. Current status and future of skin substitutes for chronic wound healing. *J Cutan Med Surg.* (2017) 21:23–30. doi: 10.1177/1203475416664037
6. Shevchenko RV, James SL, James SE. A review of tissue-engineered skin bioconstructs available for skin reconstruction. *J R Soc Interface.* (2010) 7:229–58. doi: 10.1098/rsif.2009.0403
7. Vig K, Chaudhari A, Tripathi S, Dixit S, Sahu R, Pillai S, et al. Advances in skin regeneration using tissue engineering. *Int J Mol Sci.* (2017) 18:789-807. doi: 10.3390/ijms18040789
8. Ong YS, Samuel M, Song C. Meta-analysis of early excision of burns. *Burns.* (2006) 32:145–50. doi: 10.1016/j.burns.2005.09.005
9. Ben-Bassat H, Chaouat M, Segal N, Zumai E, Wexler MR, Eldad A. How long can cryopreserved skin be stored to maintain adequate graft performance? *Burns.* (2001) 27:425–31. doi: 10.1016/S0305-4179(00)00162-5
10. Cortez Ghio S, Larouche D, Doucet EJ, Germain L. The role of cultured autologous bilayered skin substitutes as epithelial stem cell niches after grafting: a systematic review of clinical studies. *Burns Open.* (2021) 5:56–66. doi: 10.1016/j.burnso.2021.02.002
11. Greenwood JE, Damkat-Thomas L, Schmitt B, Dearman B. Successful proof of the 'two-stage strategy' for major burn wound repair. *Burns Open.* (2020) 4:121–31. doi: 10.1016/j.burnso.2020.06.003
12. World Health Organization. *A WHO Plan for Burn Prevention and Care.* World Health Organization (?2008). Available online at: https://apps.WHO.Int/iris/handle/10665/97852
13. Pointer S, Tovell A. *Hospitalised Burn Injuries, Australia, 2013–14 Injury Research and Statistics Series no 102 Cat no INJCAT 178.* Canberra, ACT: AIHW (2016).
14. Ahn CS, Maitz PK. The true cost of burn. *Burns.* (2012) 38:967–74. doi: 10.1016/j.burns.2012.05.016
15. Cleland H, Greenwood JE, Wood FM, Read DJ, Wong She R, Maitz P, et al. The burns registry of Australia and New Zealand: progressing the evidence base for burn care. *Med J Austral.* (2016) 204:1951e. doi: 10.5694/mja15.00989
16. Finkelstein EA, Corso PS, Miller TR. *The Incidence and Economic Burden of Injuries in the United States.* New York, NY: Oxford University Press (2006).
17. Hop MJ, Polinder S, van der Vlies CH, Middelkoop E, van Baar ME. Costs of burn care: a systematic review: costs of burn care. *Wound Repair Regener.* (2014) 22:436–50. doi: 10.1111/wrr.12189
18. Chua A, Song C, Chai A, Kong S, Tan KC. Use of skin allograft and its donation rate in Singapore: an 11-year retrospective review for burns treatment. *Transplant Proc.* (2007) 39:1314–6. doi: 10.1016/j.transproceed.2006.11.028
19. Herndon DN, Barrow RE, Rutan RL, Rutan TC, Desai MH, Abston S. A comparison of conservative versus early excision. Therapies in severely burned patients. *Annal Surg.* (1989) 209:547. doi: 10.1097/00000658-198905000-00006
20. Rose J, Herndon D. Advances in the treatment of burn patients. *Burns.* (1997) 23:S19–26. doi: 10.1016/S0305-4179(97)90096-6

21. Price LA, Milner SM. The totality of burn care. *Trauma.* (2012) 15:16–28. doi: 10.1177/1460408612462311
22. Fratianne RB, Brandt CP. Improved survival of adults with extensive burns. *J Burn Care Rehab.* (1997) 18:347. doi: 10.1097/00004630-199707000-00013
23. Wurzer P, Keil H, Branski LK, Parvizi D, Clayton RP, Finnerty CC, et al. The use of skin substitutes and burn care-a survey. *J Surg Res.* (2016) 201:293–8. doi: 10.1016/j.jss.2015.10.048
24. Meek CP. Successful microdermagrafting using the meek-wall microdermatome. *Am J Surg.* (1958) 96:557–8. doi: 10.1016/0002-9610(58)90975-9
25. Huang G, Ji S, Luo P, Zhang Y, Wang G, Zhu S, et al. Evaluation of dermal substitute in a novel co-transplantation model with autologous epidermal sheet. *PLoS ONE.* (2012) 7:e49448. doi: 10.1371/journal.pone.0049448
26. Ashcroft GS, Mills SJ, Ashworth JJ. Ageing and wound healing. *Biogerontology.* (2002) 3:337. doi: 10.1023/A:1021399228395
27. Gore DC. Utility of acellular allograft dermis in the care of elderly burn patients. *J Surg Res.* (2005) 125:37–41. doi: 10.1016/j.jss.2004.11.032
28. Shores JT, Gabriel A, Gupta S. Skin substitutes and alternatives: a review. *Adv Skin Wound Care.* (2007) 20:493. doi: 10.1097/01.ASW.0000288217.83128.f3
29. Davison-Kotler E, Sharma V, Kang NV, García-Gareta E. A new and universal classification system of skin substitutes inspired by factorial design. *Tissue Eng Part B Rev.* (2018) 24:279–88. doi: 10.1089/ten.teb.2017.0477
30. Boyce ST, Lalley AL. Tissue engineering of skin and regenerative medicine for wound care. *Burns Trauma.* (2018) 6:4. doi: 10.1186/s41038-017-0103-y
31. Boyce S, Cheng P, Warner P. Chapter 2.5.8 - burn dressings and skin substitutes. In: Wagner W, Sakiyama-Elbert SE, Zhang G, Yaszemski MJ, editors. *Biomaterials Science, An Introduction to Materials in Medicine.* 4th ed. (San Diego: CA, Academic Press/Elsevier) (2020). p. 1169–80.
32. Sun BK, Siprashvili Z, Khavari PA. Advances in skin grafting and treatment of cutaneous wounds. *Science.* (2014) 346:941–5. doi: 10.1126/science.1253836
33. Metcalfe AD, Ferguson MW. Tissue engineering of replacement skin: the crossroads of biomaterials, wound healing, embryonic development, stem cells and regeneration. *J R Soc Interface.* (2007) 4:413–37. doi: 10.1098/rsif.2006.0179
34. Chocarro-Wrona C, Lopez-Ruiz E, Peran M, Galvez-Martin P, Marchal JA. Therapeutic strategies for skin regeneration based on biomedical substitutes. *J Eur Acad Dermatol Venereol.* (2019) 33:484–96. doi: 10.1111/jdv.15391
35. Zeng Q, Macri LK, Prasad A, Clark RAF, Zeugolis DI, Hanley C, et al. *5.534 - Skin Tissue Engineering*, (Amsterdam, NL: Elsevier Ltd) (2011). p. 467–99. doi: 10.1016/B978-0-08-055294-1.00186-0
36. Zeng R, Lin C, Lin Z, Chen H, Lu W, Li H. Approaches to cutaneous wound healing: basics and future directions. *Cell Tissue Res.* (2018) 374:217–32. doi: 10.1007/s00441-018-2830-1
37. Moiemen NS, Lee KC. The role of alternative wound substitutes in major burn wounds and burn scar resurfacing. In: Herndon D, editor. *Total Burn Care*, 5th edn. Edinburgh, UK: Elsevier Ltd (2018). p. 633–9.e1.
38. Stojic M, López V, Montero A, Quílez C, de Aranda Izuzquiza G, Vojtova L, et al. Skin tissue engineering. In: *Biomaterials for Skin Repair and Regeneration*, ed. E. García-Gareta (Duxford, UK: Woodhead Publishing) (2019). p. 59–99.
39. Price RD, Das-Gupta V, Leigh IM, Navsaria HA. A comparison of tissue-engineered hyaluronic acid dermal matrices in a human wound model. *Tissue Eng.* (2006) 12:2985. doi: 10.1089/ten.2006.12.2985
40. Chan ES, Lam PK, Liew CT, Lau HC, Yen RS, King WW. A new technique to resurface wounds with composite biocompatible epidermal graft and artificial skin. *J Trauma.* (2001) 50:358–62. doi: 10.1097/00005373-200102000-00028
41. Golinski P, Menke H, Hofmann M, Valesky E, Butting M, Kippenberger S, et al. Development and characterization of an engraftable tissue-cultured skin autograft: alternative treatment for severe electrical injuries? *Cells Tissues Organs.* (2015) 200:227–39. doi: 10.1159/000433519
42. Boyce ST, Christianson DJ, Hansbrough JF. Structure of a collagen-GAG dermal skin substitute optimized for cultured human epidermal keratinocytes. *J Biomed Mater Res.* (1988) 22:939–57. doi: 10.1002/jbm.820221008
43. Powell HM, Boyce ST. EDC cross-linking improves skin substitute strength and stability. *Biomaterials.* (2006) 27:5821–7. doi: 10.1016/j.biomaterials.2006.07.030
44. Smiley AK, Klingenberg JM, Boyce ST, Supp DM. Keratin expression in cultured skin substitutes suggests that the hyperproliferative phenotype observed *in vitro* is normalized after grafting. *Burns.* (2006) 32:135–8. doi: 10.1016/j.burns.2005.08.017
45. Barai ND, Boyce ST, Hoath SB, Visscher MO, Kasting GB. Improved barrier function observed in cultured skin substitutes developed under anchored conditions. *Skin Res Technol.* (2008) 14:418–24. doi: 10.1111/j.1600-0846.2008.00225.x
46. Kalyanaraman B, Supp DM, Boyce ST. Medium flow rate regulates viability and barrier function of engineered skin substitutes in perfusion culture. *Tissue Eng Part A.* (2008) 14:583–93. doi: 10.1089/tea.2007.0237
47. Kalyanaraman B, Boyce ST. Wound healing on athymic mice with engineered skin substitutes fabricated with keratinocytes harvested from an automated bioreactor. *J Surg Res.* (2009) 152:296–302. doi: 10.1016/j.jss.2008.04.001
48. Klingenberg JM, McFarland KL, Friedman AJ, Boyce ST, Aronow BJ, Supp DM. Engineered human skin substitutes undergo large-scale genomic reprogramming and normal skin-like maturation after transplantation to athymic mice. *J Invest Dermatol.* (2010) 130:587–601. doi: 10.1038/jid.2009.295
49. Lander JM, Supp DM, He H, Martin LJ, Chen X, Weirauch MT, et al. Analysis of chromatin accessibility in human epidermis identifies putative barrier dysfunction-sensing enhancers. *PLoS ONE.* (2017) 12:e0184500. doi: 10.1371/journal.pone.0184500
50. Lloyd C, Besse J, Boyce S. Controlled-rate freezing to regulate the structure of collagen-glycosaminoglycan scaffolds in engineered skin substitutes. *J Biomed Mater Res B Appl Biomater.* (2015) 103:832–40. doi: 10.1002/jbm.b.33253
51. Greenwood JE, Li A, Dearman BL, Moore TG. Evaluation of novosorb novel biodegradable polymer for the generation of a dermal matrix part 2: *in-vivo* studies. *Wound Prac Res.* (2010) 18:24–34.
52. Greenwood JE, Li A, Dearman BL, Moore TG. Evaluation of novosorb novel biodegradable polymer for the generation of a dermal matrix part 1: *in-vitro* studies. *Wound Prac Res.* (2010) 18:14–22.
53. Dearman BL, Stefani K, Li A, Greenwood JE. "Take" of a polymer-based autologous cultured composite "skin" on an integrated temporizing dermal matrix: proof of concept. *J Burn Care Res.* (2013) 34:151–60. doi: 10.1097/BCR.0b013e31828089f9
54. Dearman BL, Li A, Greenwood JE. Optimization of a polyurethane dermal matrix and experience with a polymer-based cultured composite skin. *J Burn Care Res.* (2014) 35:437–48. doi: 10.1097/BCR.0000000000000061
55. Dearman B, Greenwood J. Treatment of a 95% total body surface burns patient with a novel polyurethane-based composite cultured skin. *eCM Periodical.* (2020) Collection 1(TERMIS EU Abstracts):187.
56. Dearman B, Greenwood J. A novel polyurethane-based composite cultured skin and a bespoke bioreactor in a porcine wound. *eCM Periodical.* (2020) Collection 1(TERMIS EU Abstracts):315.
57. Dearman BL, Greenwood JE. Scale-up of a composite cultured skin using a novel bioreactor device in a porcine wound model. *J Burn Care Res.* (2021). doi: 10.1093/jbcr/irab034
58. Germain L, Larouche D, Nedelec B, Perreault I, Duranceau L, Bortoluzzi P, et al. Autologous bilayered self-assembled skin substitutes (SASSs) as permanent grafts: a case series of 14 severely burned patients indicating clinical effectiveness. *Eur Cell Mater.* (2018) 36:128–41. doi: 10.22203/eCM.v036a10
59. Isbester K, Wee C, Boas S, Sopko N, Kumar A. Regeneration of functional, full-thickness skin with minimal donor site contribution using autologous homologous skin construct. *Plastic Surg Case Stud.* (2020) 6:2513826X1989881. doi: 10.1177/2513826X19898810
60. Mundinger GS, Armstrong DG, Smith DJ, Sailon AM, Chatterjee A, Tamagnini G, et al. Autologous homologous skin constructs allow safe closure of wounds: a retrospective, noncontrolled, multicentered case series. *Plast Reconstr Surg Glob Open.* (2020) 8:e2840. doi: 10.1097/GOX.0000000000002840
61. Granick MS, Baetz NW, Labroo P, Milner S, Li WW, Sopko NA. *In vivo* expansion and regeneration of full-thickness functional skin with an autologous homologous skin construct: clinical proof of concept for chronic wound healing. *Int Wound J.* (2019) 16:841–46. doi: 10.1111/iwj.13109

62. Mazlyzam AL, Aminuddin BS, Fuzina NH, Norhayati MM, Fauziah O, Isa MR, et al. Reconstruction of living bilayer human skin equivalent utilizing human fibrin as a scaffold. *Burns.* (2007) 33:355–63. doi: 10.1016/j.burns.2006.08.022
63. Seet WT, Manira M, Khairul Anuar K, Chua KH, Ahmad Irfan AW, Ng MH, et al. Shelf-life evaluation of bilayered human skin equivalent, Myderm. *PLoS ONE.* (2012) 7:e40978. doi: 10.1371/journal.pone.0040978
64. Bt Hj Idrus R, Abas A, Ab Rahim F, Saim AB. Clinical translation of cell therapy, tissue engineering, and regenerative medicine product in Malaysia and its regulatory policy. *Tissue Eng Part A.* (2015) 21:2812–6. doi: 10.1089/ten.tea.2014.0521
65. Mohamed Haflah NH, Ng MH, Mohd Yunus MH, Naicker AS, Htwe O, Abdul Razak KA, et al. Massive traumatic skin defect successfully treated with autologous, bilayered, tissue-engineered myderm skin substitute: a case report. *JBJS Case Connect.* (2018) 8:e38. doi: 10.2106/JBJS.CC.17.00250
66. Centanni JM, Straseski JA, Wicks A, Hank JA, Rasmussen CA, Lokuta MA, et al. Stratagraft skin substitute is well-tolerated and is not acutely immunogenic in patients with traumatic wounds: results from a prospective, randomized, controlled dose escalation trial. *Ann Surg.* (2011) 253:672–83. doi: 10.1097/SLA.0b013e318210f3bd
67. Sheryl R. *Stratatech Corporation Biologics License Application (Approval Letter).* (2021). Available online at: https://www.FDA.Gov/media/150131/download
68. Schiestl C, Meuli M, Vojvodic M, Pontiggia L, Neuhaus D, Brotschi B, et al. Expanding into the future: combining a novel dermal template with distinct variants of autologous cultured skin substitutes in massive burns. *Burns Open.* (2021) 5:145–53. doi: 10.1016/j.burnso.2021.06.002
69. Greenwood JE. Chapter 10 - hybrid biomaterials for skin tissue engineering. in *Skin Tissue Engineering and Regenerative Medicine*, eds M. Z. Albanna and J. H. Holmes Iv (Amsterdam, NL: Academic Press) (2016). p. 185–210.
70. Yannas IV, Burke JF, Huang C, Gordon PL. Correlation of *in vivo* collagen degradation rate with *in vitro* measurements. *J Biomed Mater Res.* (1975) 9:623–28. doi: 10.1002/jbm.820090608
71. Yannas IV, Burke JF. Design of an artificial skin. I. Basic design principles. *J Biomed Mater Res.* (1980) 14:65–81. doi: 10.1002/jbm.820140108
72. MacNeil S. Biomaterials for tissue engineering of skin. *Mater Today.* (2008) 11:26–35. doi: 10.1016/S1369-7021(08)70087-7
73. Wagstaff MJD, Schmitt BJ, Coghlan P, Finkemeyer JP, Caplash Y, Greenwood JE. A biodegradable polyurethane dermal matrix in reconstruction of free flap donor sites: a pilot study. *Eplasty.* (Springfield, IL: Open Science Co.) (2015) 15:e13.
74. Cheshire PA, Herson MR, Cleland H, Akbarzadeh S. Artificial dermal templates: a comparative study of novosorb biodegradable temporising matrix (btm) and integra((r)) dermal regeneration template (drt). *Burns.* (2016) 42:1088–96. doi: 10.1016/j.burns.2016.01.028
75. Lodescar RJ, Gibson CJ, Gallagher J. 722 an experience with a biodegradable temporizing matrix in a metropolitan burn center. *J Burn Care Res.* (2020) 41:S192. doi: 10.1093/jbcr/iraa024.306
76. Wagstaff MJ, Caplash Y, Greenwood JE. Reconstruction of an anterior cervical necrotizing fasciitis defect using a biodegradable polyurethane dermal substitute. *Eplasty.* (2017) 17:e3.
77. Greenwood JE, Schmitt BJ, Wagstaff MJ. Experience with a synthetic bilayer biodegradable temporising matrix in significant burn injury. *Burns Open.* (2018) 2:17–34. doi: 10.1016/j.burnso.2017.08.001
78. Damkat-Thomas L, Greenwood JE, Wagstaff MJD. A synthetic biodegradable temporising matrix in degloving lower extremity trauma reconstruction: a case report. *Plast Reconstr Surg Glob Open.* (2019) 7:e2110. doi: 10.1097/GOX.0000000000002110
79. Sreedharan S, Morrison E, Cleland H, Ricketts S, Bruscino-Raiola F. Biodegradable temporising matrix for necrotising soft tissue infections: a case report. *Austral J Plastic Surg.* (2019) 2:106–9. doi: 10.34239/ajops.v2i1.72
80. Greenwood JE, Dearman BL. Comparison of a sealed, polymer foam biodegradable temporizing matrix against integra(r) dermal regeneration template in a porcine wound model. *J Burn Care Res.* (2012) 33:163–73. doi: 10.1097/BCR.0b013e318233fac1
81. Greenwood JE, Wagstaff MJD, Rooke M, Caplash Y. Reconstruction of extensive calvarial exposure after major burn injury in 2 stages using a biodegradable polyurethane matrix. *Eplasty.* (2016) 16:e17.
82. Solanki NS, York B, Gao Y, Baker P, Wong She RB. A consecutive case series of defects reconstructed using novosorb® biodegradable temporising matrix: initial experience and early results. *J Plastic Reconstruc Aesthetic Surg.* (2020) 73:1845. doi: 10.1016/j.bjps.2020.05.067
83. Cuono C, Langdon R, McGuire J. Use of cultured epidermal autografts and dermal allografts as skin replacement after burn injury. *Lancet.* (1986) 1:1123. doi: 10.1016/S0140-6736(86)91838-6
84. Compton CC, Hickerson W, Nadire K, Press W. Acceleration of skin regeneration from cultured epithelial autografts by transplantation to homograft dermis. *J Burn Care Rehabil.* (1993) 14:653. doi: 10.1097/00004630-199311000-00010
85. Carsin H, Ainaud P, Le Bever H, Rives J-M, Lakhel A, Stephanazzi J, et al. Cultured epithelial autografts in extensive burn coverage of severely traumatized patients: a five year single-center experience with 30 patients. *Burns.* (2000) 26:379–87. doi: 10.1016/S0305-4179(99)00143-6
86. Holmes JH, Molnar JA, Shupp JW, Hickerson WL, King BT, Foster KN, et al. Demonstration of the safety and effectiveness of the recell® system combined with split-thickness meshed autografts for the reduction of donor skin to treat mixed-depth burn injuries. *Burns.* (2019) 45:772–82. doi: 10.1016/j.burns.2018.11.002
87. Vanscheidt W, Ukat A, Horak V, Bruning H, Hunyadi J, Pavlicek R, et al. Treatment of recalcitrant venous leg ulcers with autologous keratinocytes in fibrin sealant: a multinational randomized controlled clinical trial. *Wound Repair Regen.* (2007) 15:308–15. doi: 10.1111/j.1524-475X.2007.00231.x
88. Ortega-Zilic N, Hunziker T, Lauchli S, Mayer DO, Huber C, Baumann Conzett K, et al. Epidex® Swiss field trial 2004-2008. *Dermatology.* (2010) 221:365–72. doi: 10.1159/000321333
89. Tausche AK, Skaria M, Böhlen L, Liebold K, Hafner J, Friedlein H, et al. An autologous epidermal equivalent tissue-engineered from follicular outer root sheath keratinocytes is as effective as split-thickness skin autograft in recalcitrant vascular leg ulcers. *Wound Repair Regener.* (2003) 11:248–52. doi: 10.1046/j.1524-475X.2003.11403.x
90. Limat A, Mauri D, Hunziker T. Successful treatment of chronic leg ulcers with epidermal equivalents generated from cultured autologous outer root sheath cells. *J Investigative Dermatol.* (1996) 107:128–35. doi: 10.1111/1523-1747.ep12298415
91. Moustafa M. Randomized, controlled, single-blind study on use of autologous keratinocytes on a transfer dressing to treat nonhealing diabetic ulcers. *Regen Med.* (2007) 2:887–902. doi: 10.2217/17460751.2.6.887
92. Moustafa M, Simpson C, Glover M, Dawson RA, Tesfaye S, Creagh FM, et al. A new autologous keratinocyte dressing treatment for non-healing diabetic neuropathic foot ulcers. *Diabet Med.* (2004) 21:786–9. doi: 10.1111/j.1464-5491.2004.01166.x
93. Zhu N, Warner RM, Simpson C, Glover M, Hernon CA, Kelly J, et al. Treatment of burns and chronic wounds using a new cell transfer dressing for delivery of autologous keratinocytes. *Euro J Plastic Surg.* (2005) 28:319–30. doi: 10.1007/s00238-005-0777-4
94. Middelkoop E, Sheridan RL. 15 - skin substitutes and the next level'. in: *Total Burn Care*, ed. D. Herndon, 5th edn. Edinburgh: Elsevier Ltd (2018). p. 167–73.e2.
95. Blight A, Mountford EM, Cheshire IM, Clancy JMP, Levick PL. Treatment of full skin thickness burn injury using cultured epithelial grafts. *Burns.* (1991) 17:495–98. doi: 10.1016/0305-4179(91)90079-V
96. Donati L, Magliacani G, Bormioli M, Signorini M, Baruffaldi Preis FW. Clinical experiences with keratinocyte grafts. *Burns.* (1992) 18:S19–26. doi: 10.1016/0305-4179(92)90106-5
97. Munster AM. Cultured skin for massive burns: a prospective, controlled trial. *Ann Surg.* (1996) 224:372–7. doi: 10.1097/00000658-199609000-00013
98. Raghunath M, Meuli M. Cultured epithelial autografts: diving from surgery into matrix biology. *Pediatric Surg Int.* (1997) 12:478–83. doi: 10.1007/s003830050188
99. Paddle-Ledinek JE, Cruickshank DG, Masterton JP. Skin replacement by cultured keratinocyte grafts: an Australian experience. *Burns.* (1997) 23:204–11. doi: 10.1016/S0305-4179(96)00123-4

100. Atiyeh BS, Costagliola M. Cultured epithelial autograft (CEA) in burn treatment: three decades later. *Burns.* (2007) 33:405–13. doi: 10.1016/j.burns.2006.11.002
101. Greaves NS, Iqbal SA, Baguneid M, Bayat A. The role of skin substitutes in the management of chronic cutaneous wounds. *Wound Repair Regen.* (2013) 21:194–210. doi: 10.1111/wrr.12029
102. Boyce ST, Supp AP, Swope VB, Warden GD. Vitamin C regulates keratinocyte viability, epidermal barrier, and basement membrane *in vitro*, and reduces wound contraction after grafting of cultured skin substitutes. *J Invest Dermatol.* (2002) 118:565–72. doi: 10.1046/j.1523-1747.2002.01717.x
103. Boyce ST, Warden GD. Principles and practices for treatment of cutaneous wounds with cultured skin substitutes. *Am J Surg.* (2002) 183:445–56. doi: 10.1016/S0002-9610(02)00813-9
104. Harriger MD, Warden GD, Greenhalgh DG, Kagan RJ, Boyce ST. Pigmentation and microanatomy of skin regenerated from composite grafts of cultured cells and biopolymers applied to full-thickness burn wounds. *Transplantation.* (1995) 59:702–7. doi: 10.1097/00007890-199503150-00011
105. Boyce ST, Kagan RJ, Yakuboff KP, Meyer NA, Rieman MT, Greenhalgh DG, et al. Cultured skin substitutes reduce donor skin harvesting for closure of excised, full-thickness burns. *Ann Surg.* (2002) 235:269. doi: 10.1097/00000658-200202000-00016
106. Boyce ST, Kagan RJ, Meyer NA, Yakuboff KP, Warden GD. The 1999 clinical research award. Cultured skin substitutes combined with Integra artificial skin to replace native skin autograft and allograft for the closure of excised full–thickness burns. *J Burn Care Rehabil.* (1999) 20:453–61. doi: 10.1097/00004630-199920060-00006
107. Boyce ST, Simpson PS, Rieman MT, Warner PM, Yakuboff KP, Bailey JK, et al. Randomized, paired-site comparison of autologous engineered skin substitutes and split-thickness skin graft for closure of extensive, full-thickness burns. *J Burn Care Res.* (2017) 38:61–70. doi: 10.1097/BCR.0000000000000401
108. Boyce ST, Zimmerman RL, Supp DM. Tumorigenicity testing in athymic mice of cultured human melanocytes for transplantation in engineered skin substitutes. *Cell Transplant.* (2015) 24:1423–9. doi: 10.3727/096368914X683052
109. Boyce ST, Lloyd CM, Kleiner MC, Swope VB, Abdel-Malek Z, Supp DM. Restoration of cutaneous pigmentation by transplantation to mice of isogeneic human melanocytes in dermal-epidermal engineered skin substitutes. *Pigment Cell Melanoma Res.* (2017) 30:531–40. doi: 10.1111/pcmr.12609
110. Supp DM, Wilson-Landy K, Boyce ST. Human dermal microvascular endothelial cells form vascular analogs in cultured skin substitutes after grafting to athymic mice. *FASEB J.* (2002) 16:797–804. doi: 10.1096/fj.01-0868com
111. Sriwiriyanont P, Lynch KA, McFarland KL, Supp DM, Boyce ST. Characterization of hair follicle development in engineered skin substitutes. *PLoS ONE.* (2013) 8:e65664. doi: 10.1371/journal.pone.0065664
112. Oostendorp C, Meyer S, Sobrio M, van Arendonk J, Reichmann E, Daamen WF, et al. Evaluation of cultured human dermal- and dermo-epidermal substitutes focusing on extracellular matrix components: comparison of protein and rna analysis. *Burns.* (2017) 43:520–30. doi: 10.1016/j.burns.2016.10.002
113. Pontiggia L, Klar A, Bottcher-Haberzeth S, Biedermann T, Meuli M, Reichmann E. Optimizing *in vitro* culture conditions leads to a significantly shorter production time of human dermo-epidermal skin substitutes. *Pediatr Surg Int.* (2013) 29:249–56. doi: 10.1007/s00383-013-3268-x
114. Grinnell F, Fukamizu H, Pawelek P, Nakagawa S. Collagen processing, crosslinking, and fibril bundle assembly in matrix produced by fibroblasts in long-term cultures supplemented with ascorbic acid. *Exp Cell Res.* (1989) 181:483–91. doi: 10.1016/0014-4827(89)90105-5
115. Ishikawa O, Kondo A, Okada K, Miyachi Y, Furumura M. Morphological and biochemical analyses on fibroblasts and self-produced collagens in a novel three-dimensional culture. *Br J Dermatol.* (1997) 136:6–11. doi: 10.1046/j.1365-2133.1997.d01-1134.x
116. El Ghalbzouri A, Lamme E, Ponec M. Crucial role of fibroblasts in regulating epidermal morphogenesis. *Cell Tissue Res.* (2002) 310:189–99. doi: 10.1007/s00441-002-0621-0
117. Ahlfors JE, Billiar KL. Biomechanical and biochemical characteristics of a human fibroblast-produced and remodeled matrix. *Biomaterials.* (2007) 28:2183–91. doi: 10.1016/j.biomaterials.2006.12.030
118. El Ghalbzouri A, Commandeur S, Rietveld MH, Mulder AA, Willemze R. Replacement of animal-derived collagen matrix by human fibroblast-derived dermal matrix for human skin equivalent products. *Biomaterials.* (2009) 30:71–8. doi: 10.1016/j.biomaterials.2008.09.002
119. Kailani MH, Jafar H, Awidi A. Chapter 9 - synthetic biomaterials for skin tissue engineering. in *Skin Tissue Engineering and Regenerative Medicine*, eds M. Z. Albanna and J. H. Holmes Iv (Amsterdam, NL: Academic Press/Elsevier Inc) (2016). p. 163–83.
120. Li A, Dearman BL, Crompton KE, Moore TG, Greenwood JE. Evaluation of a novel biodegradable polymer for the generation of a dermal matrix. *J Burn Care Res.* (2009) 30:717. doi: 10.1097/BCR.0b013e3181abffca
121. Uccioli L, TissueTech Autograph System Italian Study G. A clinical investigation on the characteristics and outcomes of treating chronic lower extremity wounds using the tissuetech autograft system. *Int J Low Extrem Wounds.* (2003) 2:140–51. doi: 10.1177/1534734603258480
122. Sheridan RL, Morgan JR, Cusick JL, Petras LM, Lydon MM, Tompkins RG. Initial experience with a composite autologous skin substitute. *Burns.* (2001) 27:421–24. doi: 10.1016/S0305-4179(00)00156-X
123. Takami Y, Yamaguchi R, Ono S, Hyakusoku H. Clinical application and histological properties of autologous tissue-engineered skin equivalents using an acellular dermal matrix. *J Nippon Med School.* (2014) 81:356–63. doi: 10.1272/jnms.81.356
124. Gomez C, Galan JM, Torrero V, Ferreiro I, Perez D, Palao R, et al. Use of an autologous bioengineered composite skin in extensive burns: clinical and functional outcomes. A multicentric study. *Burns.* (2011) 37:580–9. doi: 10.1016/j.burns.2010.10.005
125. Llames S, Garcia E, Garcia V, del Rio M, Larcher F, Jorcano JL, et al. Clinical results of an autologous engineered skin. *Cell Tissue Bank.* (2006) 7:47–53. doi: 10.1007/s10561-004-7253-4
126. Baltazar T, Merola J, Catarino C, Xie CB, Kirkiles-Smith NC, Lee V, et al. Three dimensional bioprinting of a vascularized and perfusable skin graft using human keratinocytes, fibroblasts, pericytes, and endothelial cells. *Tissue Eng Part A.* (2020) 26:227–38. doi: 10.1089/ten.tea.2019.0201
127. Dehghani F, Annabi N. Engineering porous scaffolds using gas-based techniques. *Curr Opin Biotechnol.* (2011) 22:661–6. doi: 10.1016/j.copbio.2011.04.005
128. Jones JE, Nelson EA, Al-Hity A, Jones JE. Skin grafting for venous leg ulcers. *Cochrane Libr.* (2013) 2013:CD001737-CD37. doi: 10.1002/14651858.CD001737.pub4
129. Sheikholeslam M, Wright MEE, Jeschke MG, Amini-Nik S. Biomaterials for skin substitutes. *Adv Healthc Mater.* (2018) 7:1700897. doi: 10.1002/adhm.201700897
130. Augustine R, Kalarikkal N, Thomas S. Advancement of wound care from grafts to bioengineered smart skin substitutes. *Progress Biomater.* (2014) 3:103–13. doi: 10.1007/s40204-014-0030-y
131. Zheng MH, Pembrey R, Niutta S, Stewart-Richardson P, Farrugia A. Challenges in the evaluation of safety and efficacy of human tissue and cell based products. *ANZ J Surg.* (2006) 76:843–9. doi: 10.1111/j.1445-2197.2006.03880.x
132. Rajab T, Rivard AL, Wasiluk KR, Gallegos RP, Bianco RW. Chapter III.2.7 - Ethical issues in biomaterials and medical devices. in *Biomaterials Science*, eds B. D. Ratner, A. S. Hoffman, F. J. Schoen and J. E. Lemons 3rd ed. (Amsterdam: NL, Academic Press/Elsevier) (2013). p. 1425–31.
133. Al-Himdani S, Jessop ZM, Al-Sabah A, Combellack E, Ibrahim A, Doak SH, et al. Tissue-engineered solutions in plastic and reconstructive surgery: principles and practice. *Front Surg.* (2017) 4:4. doi: 10.3389/fsurg.2017.00004
134. Tolkoff J, Anders R. Chapter III.2.2 - commercialization: what it takes to get a product to market. In: *Biomaterials Science.* eds B. D. Ratner, A. S. Hoffman, F. J. Schoen and J. E. Lemons. 3rd edn. (Amsterdam NL: Academic Press/Elsevier) (2013). p. 1389–99.
135. Dhasmana A SS, Kadian S, Singh L. Skin tissue engineering: principles and advances. *J Dermatol Skin.* (2018) 1:101.
136. Hendrickx B, Vranckx JJ, Luttun A. Cell-based vascularization strategies for skin tissue engineering. *Tissue Eng Part*

B Rev. (2011) 17:13–24. doi: 10.1089/ten.teb.2010.0315
137. Huang S, Xu Y, Wu C, Sha D, Fu X. *in vitro* constitution and *in vivo* implantation of engineered skin constructs with sweat glands. *Biomaterials.* (2010) 31:5520–25. doi: 10.1016/j.biomaterials.2010.03.060
138. Brandenburger M, Kruse C. Fabrication of a co-culture system with human sweat gland-derived cells and peripheral nerve cells. *Methods Mol Biol.* (2019) 1993:139–48. doi: 10.1007/978-1-4939-9473-1_11
139. Lalley AL, Boyce ST. Fabrication of chimeric hair follicles for skin tissue engineering. *Methods Mol Biol.* (2019) 1993:159–79. doi: 10.1007/978-1-4939-9473-1_13
140. Kalyanaraman B, Boyce S. Assessment of an automated bioreactor to propagate and harvest keratinocytes for fabrication of engineered skin substitutes. *Tissue Eng.* (2007) 13:983–93. doi: 10.1089/ten.2006.0338
141. Cubo N, Garcia M, Del Canizo JF, Velasco D, Jorcano JL. 3D bioprinting of functional human skin: production and *in vivo* analysis. *Biofabrication.* (2016) 9:015006. doi: 10.1088/1758-5090/9/1/015006
142. Pourchet LJ, Thepot A, Albouy M, Courtial EJ, Boher A, Blum LJ, et al. Human skin 3D bioprinting using scaffold-free approach. *Adv Healthc Mater.* (2017) 6:1601101–8. doi: 10.1002/adhm.201601101
143. Koch L, Michael S, Reimers K, Vogt PM, Chichkov B. Chapter 13 - bioprinting for skin. In: Zhang LG, Fisher JP and Leong KW, editors. *3D Bioprinting and Nanotechnology in Tissue Engineering and Regenerative Medicine.* London, UK: Elsevier Inc., Academic Press (2015). p. 281–306.
144. Albanna M, Binder KW, Murphy SV, Kim J, Qasem SA, Zhao W, et al. *In situ* bioprinting of autologous skin cells accelerates wound healing of extensive excisional full-thickness wounds. *Sci Rep.* (2019) 9:1856. doi: 10.1038/s41598-018-38366-w
145. Smandri A, Nordin A, Hwei NM, Chin KY, Abd Aziz I, Fauzi MB. Natural 3D-printed bioinks for skin regeneration and wound healing: a systematic review. *Polymers.* (2020) 12:1782–1800. doi: 10.3390/polym12081782
146. Supp DM, Hahn JM, McFarland KL, Combs KA, Lee KS, Inceoglu B, et al. Soluble epoxide hydrolase inhibition and epoxyeicosatrienoic acid treatment improve vascularization of engineered skin substitutes. *Plast Reconstr Surg Glob Open.* (2016) 4:e1151. doi: 10.1097/GOX.0000000000001151
147. Supp DM, Hahn JM, Lloyd CM, Combs KA, Swope VK, Abdel-Malek Z, et al. Light or dark pigmentation of engineered skin substitutes containing melanocytes protects against ultraviolet light-induced DNA damage *in vivo*. *J Burn Care Res.* (2020) 41:751–60. doi: 10.1093/jbcr/iraa029

Conflict of Interest: At the time of the CCS studies JG was a major shareholder in PolyNovo Biomaterials Pty Ltd., the company that produced the NovoSorb® Polyurethane material. JG and BD were stakeholders in Skin Tissue Engineering Pty Ltd. a company that had no protectable IP and was used as a vehicle for attracting and dispersing funding from non-grant awarding bodies.

The remaining author declares that the research was conducted in the absence of any commercial or financial relationships that could be construed as a potential conflict of interest.

Publisher's Note: All claims expressed in this article are solely those of the authors and do not necessarily represent those of their affiliated organizations, or those of the publisher, the editors and the reviewers. Any product that may be evaluated in this article, or claim that may be made by its manufacturer, is not guaranteed or endorsed by the publisher.

1.8 Hypothesis and Aims

Optimisation of the composite cultured skin (CCS) will enable definitive wound closure, consistently and reliably, after its engraftment *in vivo* in a large animal (porcine) wound model allowing its subsequent evaluation in extensive, full-thickness burn management in humans.

The overall aim of the project is to develop a sizable CCS that can be consistently produced and reliably transplanted to patients with extensive burns. The aim of the project can be further divided into:

- Develop and optimise 25cm x 25cm composite skins containing fibroblasts and keratinocytes, using the biodegradable polyurethane foam as a scaffold within the bioreactor system *in vitro*.
  - Optimise cell expansion conditions for both cell types (fibroblasts and keratinocytes) with cell characterisation.
  - Conduct further tests of the foam scaffold with the optimised, smaller pore configurations, using the plasma gel.
  - Compare the polymer scaffold/plasma gel composition with a collagen-based glycosamino-glycan (GAG) scaffold.
  - Evaluate a hybrid composite, i.e., determine whether any advantages/disadvantages are proffered by creating a combination polyurethane with collagen-GAG.
  - Within the bioreactor cassette, design and develop an air-liquid interface system which will support epidermal organisation into a stratified, squamous structure anchored by a basement membrane to the dermal component within the foam.
  - Refine the bioreactor system to initially support and maintain the CCS manually. Subsequently to move to an automated system driven by a computer-based software initialising program.
- Implant a 25cm x 25cm CCS into the porcine wound model, demonstrating successful and uniform engraftment utilising the bioreactor device.
- Progress the bioreactor device to meet ISO/NATA/TGA standards in preparation for manufacturing the CCS in an ISO 7 environment.
- To utilise the two-stage strategy to manufacture and transplant a CCS into a human burn-injured patient who has received BTM as the first stage.

CHAPTER 2:
Scale-up of a Composite Cultured Skin Using a Novel Bioreactor Device in a Porcine Wound Model

Dearman BL and Greenwood JE

Published in

Journal of Burn Care & Research

2021

2.1 Overview

The CCS has shown promise in a small 10cm x 10cm animal wound model; however, to enable coverage of a large burn, a scaling process of the CCS wound be advantageous. For this purpose, a bespoke bioreactor device that can support a 25cm x 25cm piece of CCS was designed and investigated. Six 24.5cm x 24.5cm CCS's were produced in a two-array system, utilising two shoes and six cassettes that were controlled automatically via the bioreactor software for media replenishment and waste removal. Six large 24cm x 12cm wounds were successfully created on the back of three pigs, with BTM integrating and producing a viable wound bed for CCS transplantation. CCS culture conditions and seeding densities have now been optimised. Four out of six wounds demonstrated engraftment and 'take' by day 53, producing a robust, stratified epithelium analogous to the control split-thickness skin. The bioreactor sustained 24 days of daily operation for the two-array system.

Statement of Authorship

Title of Paper	Scale-up of a Composite Cultured Skin Using a Novel Bioreactor Device in a Porcine Wound Model
Publication Status	☑ Published ☐ Accepted for Publication ☐ Submitted for Publication ☐ Unpublished and Unsubmitted w ork w ritten in manuscript style
Publication Details	Dearman, BL & Greenwood, JE 2021, 'Scale-up of a Composite Cultured Skin using a novel Bioreactor Device in a Porcine Wound Model', *Journal of Burn Care & Research*, vol. 42, no. 6, pp. 1199–1209.

Principal Author

Name of Principal Author (Candidate)	Bronwyn Dearman		
Contribution to the Paper	Conceptualisation of project. Study design, methodology execution and analysis of all samples. Manuscript writing, editing and review for submission. Corresponding author.		
Overall percentage (%)	85%		
Certification:	This paper reports on original research I conducted during the period of my Higher Degree by Research candidature and is not subject to any obligations or contractual agreements with a third party that would constrain its inclusion in this thesis. I am the primary author of this paper.		
Signature		Date	05/01/2022

Co-Author Contributions

By signing the Statement of Authorship, each author certifies that:

i. the candidate's stated contribution to the publication is accurate (as detailed above);

ii. permission is granted for the candidate to include the publication in the thesis; and

iii. the sum of all co-author contributions is equal to 100% less the candidate's stated contribution.

Name of Co-Author	Professor John Greenwood		
Contribution to the Paper	Project participation. Manuscript review and editing.		
Signature		Date	05/01/2022

Scale-up of a Composite Cultured Skin Using a Novel Bioreactor Device in a Porcine Wound Model

Bronwyn L. Dearman, BSc (Hons)*,† and John E. Greenwood AM, BSc(Hons), MBChB, MD, DHlthSc, FRCS(Eng), FRCS(Plast), FRACS‡

Extensive deep-burn management with a two-stage strategy can reduce reliance on skin autografts; a biodegradable polyurethane scaffold to actively temporize the wound and later an autologous composite cultured skin (CCS) for definitive closure. The materials fulfilling each stage have undergone in vitro and in vivo pretesting in "small" large animal wounds. For humans, producing multiple, large CCSs requires a specialized bioreactor. This article reports a system used to close large porcine wounds. Three Large White pigs were used, each with two wounds (24.5 cm × 12 cm) into which biodegradable dermal scaffolds were implanted. A sample from discarded tissue allowed isolation/culture of autologous fibroblasts and keratinocytes. CCS production began by presoaking a 1-mm-thick biodegradable polyurethane foam in autologous plasma. In the bioreactor cassette, fibroblasts were seeded into the matrix with thrombin until established, followed by keratinocytes. The CCSs were applied onto integrated dermal scaffolds on day 35, alongside a sheet skin graft (30% of one wound). Serial punch biopsies, trans-epidermal water loss readings (TEWL), and wound measurements indicated epithelialization. During dermal scaffold integration, negligible wound contraction was observed (average 4.5%). After CCS transplantation, the control skin grafts were "taken" by day 11 when visible islands of epithelium were clinically observed on 2/3 CCSs. Closure was confirmed histologically, with complete epithelialization by day 63 post-CCS transplantation (CCS TEWL ~ normal skin average 11.9 g/m²h). Four of six wounds demonstrated closure with robust, stratified epithelium. Generating large pieces of CCS capable of healing large wounds is thus possible using a specialized designed bioreactor.

Extensive deep burns result in large wounds that require definitive closure. As burn size increases, the nonburned areas of skin from which skin grafts might be harvested (donor sites) decrease. Definitive wound closure, even with maneuvers to maximize the utility of harvested skin (e.g., meshing, Meek–Wall technique), is serial, thus delayed and leads to suboptimal outcomes. A tissue engineered skin replacement, containing both dermal and epidermal components created by autologous cells, is one therapeutic approach. A two-stage strategy using a novel polyurethane (PUR) polymer platform was therefore designed, and subsequently developed, to assist with the issues of closure and functional coverage. A body of work began in 2004 that describes the translational pathway from laboratory to patient and our efforts to "retire the skin graft."[1–7] Briefly, a PUR material was sourced as the scaffolding for the two materials used in each stage. The first stage was designed as a biodegradable temporizing matrix (BTM), now marketed as NovoSorb® BTM.[1–8] This enables the wound to be temporarily but physiologically "closed" during its integration and then forms a uniform, well-vascularized wound bed. Since the material does not spontaneously delaminate, this provides the 4- to 5-week time period required for the second stage (composite cultured skin or CCS) to be produced. The first CCS was created using spun fibers of the biodegradable PUR in 2007, to determine biocompatibility both in vitro and in vivo.[1,5–7] The fiber structure was inherently unsuitable and following requests, the PUR was produced as an open-cell foam. The CCS subsequently underwent several iterations to overcome inherent issues with the PUR scaffold. A plasma gel was employed to rectify both buoyancy and the degree of cell loss from highly variable pore sizes. Two phenomena were noted during in vivo testing: CCS "take" where the polymer became integrated under the neo-epidermis, and "non-take" where the PUR acted as a delivery vehicle before being shed from the wound. Both routes enabled wound closure.[2,3] Generating a PUR foam with smaller pores was required to enable complete CCS engraftment, but attempted refinement by the manufacturer was only partially successful. The next issue to be addressed was how to generate large pieces of CCS as a meaningful resource for extensive wound conditions, such as burns.

The largest clinically available skin substitute was no bigger than 10 cm × 10 cm. Clinically, the application of many small pieces of engineered skin to cover large areas produces an

*From the *Skin Engineering Laboratory, Adult Burn Centre, Royal Adelaide Hospital, SA, Australia; †Faculty of Health Sciences, The University of Adelaide, SA, Australia; and ‡Adult Burn Centre, Royal Adelaide Hospital, SA, Australia*

Funding: This study was supported by a grant from Lifetime Support Authority (LSA) and the Health Services Charitable Gifts Board (HSCGB).

Conflict of interest statement: At the time of this study Professor John Greenwood was a major shareholder in PolyNovo Biomaterials Pty Ltd, the company that produced the NovoSorb® Polyurethane material. Skin Tissue Engineering Pty Ltd has no current protectable IP and is used as a vehicle for attracting and dispersing funding from non-grant awarding bodies in which Professor John Greenwood and Bronwyn Dearman are stakeholders.

Supplemental digital content is available for this article. Direct URL citations appear in the printed text and are provided in the HTML and PDF versions of this article on the journal's Web site.

Address correspondence to Bronwyn Dearman, BSc (Hons), Skin Engineering Laboratory, Adult Burn Centre, Royal Adelaide Hospital, Port Road, Adelaide, SA 5000, Australia. Email: Bronwyn.dearman@sa.gov.au

doi:10.1093/jbcr/irab034

outcome both dysaesthetic (a "quilt" appearance) and dysfunctional (due to multiple, scarred interpiece seams). Useful skin substitute production requires each piece to be large enough to be time efficient during application and scalable (so that many large pieces can be produced simultaneously). This requires a bespoke culture environment, a bioreactor capable not only of reducing the need for manipulation by scientists (thus reducing the chance of contamination and introducing infection into the substitutes), but also of being computer controlled to reduce the need for constant monitoring and time-expensive human processes.[9,10]

A bioreactor is broadly defined as a vessel in which a biological reaction or process occurs, particularly on a manufacturing scale.[11] Bioreactors exist for generation of other 3D engineered tissues, such as cartilage, bone, vascular tissue, and nerve.[12–14] The requirements of a skin tissue bioreactor generally include a support scaffold that relies on a nutrient supply via a perfusion and waste removal system, in a controlled environment, automated by computer-based software program. Designs for a skin tissue-expanding device have yielded only small machines with limited capabilities.[15–17] Custom bioreactors have been developed for organotypic skin grafts or skin equivalents,[18–20] cultured epithelial autografts,[21,22] and the mass expansion of keratinocytes, the Kerator.[9,22,23] However, commercially available bioreactors capable of meeting 3D composite skin scale-up requirements have not yet emerged.

A custom-designed prototype bioreactor was designed and built to assist the upscaling of CCS production to produce large 25 cm × 25 cm sheets. Several serial CAD designs were produced, and their parameters were analyzed to arrive at the final prototype that can produce (currently) up to 20 CCSs, each 25 cm × 25 cm, with automated feeding and waste removal, requiring manual handling only with the initial cell seeding of each cell type. This manuscript reports the use of scaled-up CCS in a porcine large wound model.

METHODS

The biodegradable PUR matrices for this study were manufactured by PolyNovo Biomaterials Pty. Ltd (Port Melbourne, Victoria, Australia).[2] Sterile sheets of 40 cm × 20 cm NovoSorb® BTM (sealed, 2 mm) and 25 cm × 25 cm CCS matrices (unsealed, 1 mm PUR) were used.

The previously published porcine animal model was used for this study.[2,3] Modifications to the protocol included wound size creation (8 cm × 8 cm to 24.5 cm × 12 cm). Surgical wounds were created (Figure 1A) to the level of the panniculus adiposus so that no skin remnant remained (Figure 1D). Skin biopsies were harvested using a Watson Humby skin graft knife (Figure 1B and C). NovoSorb® BTM was cut to size and implanted into these wounds, held by surgical staples (Figure 1E and F). The wounds were dressed with Acticoat® (a nanocrystalline silver dressing; Smith & Nephew, Hull, UK) held in place with Hypafix® adhesive tape (BSN Medical, Hamburg, Germany), with adherence to the surrounding skin facilitated by Tincture of Benzoin (Figure 1G). This reinforced dressing was then padded by cotton wool combines also held by Hypafix® and protected by a custom-made coat secured by Velcro strips (Figure 1H). The dressings were changed twice weekly until the CCSs were ready for transplantation. Due to the scale-up of CCS size, this required the design of a specialized culture vessel device, the bioreactor.

Novel Bioreactor Device

The Bioreactor prototype is housed within a large ULPA-filtered CO_2 incubator (Esco, Singapore); there are two towers, each consisting of a two-array system ("shoes") which can hold 5 cassettes each. The cassettes are 25 cm × 25 cm and comprise a media inlet and waste outlet. A drive and spigot assembly delivers the media to the cassettes and tips the array for waste extraction into a designated waste container. The cold media is stored in an in-built refrigerator prior to being pumped into a media reservoir assembly within the incubator to allow warming to occur before delivery to the cassettes. The pump housing includes an electronic interface and power supply to pump media both into and out of the reservoir bags. All these processes are finely controlled by specialized custom software. The Bioreactor and supporting equipment are designed to fit within a 2m × 1m floor area (Figure 2).

EXPERIMENT

Experimental Design

Animals. All animal work was performed in an accredited large animal facility following approval by the South Australian Health and Medical Research Institute (SAHMRI) Animal Ethics Committee (Approval Number: SAM282). Three Large White XLandrace pigs weighing on average 30 kg were obtained from Roseworthy piggery 1 week prior to the start date to allow for acclimatization to their new environment. One unit of blood (~400 ml) was collected from the jugular vein of each pig prior to initial surgery to isolate plasma for the generation of the CCSs.

Day 0—Skin Harvest and BTM Implantation. On the day of surgery, two sites were planned out, one on either side of the spine of the animal (Figure 1). Two skin biopsies per pig, ~20 cm × 10 cm at 12/1000s of an inch thick, were harvested as a source for the isolation of autologous fibroblasts and keratinocytes. NovoSorb® BTM were implanted and the wounds dressed according to the method. At dressing change, the wounds and surrounding areas were shaved, cleaned, and photographed. Wound measurements were recorded each week.

Days 0 to 35—Cell Culture and CCS Generation. For the creation of the CCS, the biopsies were processed on day 0[2,3] and the epidermal keratinocytes and dermal fibroblast cells isolated for mass cell expansion in culture. Fibroblasts were initially established in Dulbecco's modified Eagle's Medium with 10% fetal bovine serum (FBS) before being changed to 5% FBS for subsequent passages. Keratinocytes were co-cultured using irradiated Swiss albino mouse fibroblasts in a supplemented SEL-KGM-1% FBS.[2,3] All cells were cultured in an incubator (Sanyo MC0-20AIC, Quantum Scientific) with 5% CO_2 at 37°C. When sufficient cell numbers were achieved after expansion, they were frozen using a control rate freezer (Planer Kryo 10 Freezer, Quantum Scientific), pending the sequential seeding of the CCS PUR foams.

Two 25 cm × 25 cm CCSs were produced per pig, CCSa and CCSb.[2,3] PUR Foams were presoaked with autologous plasma in

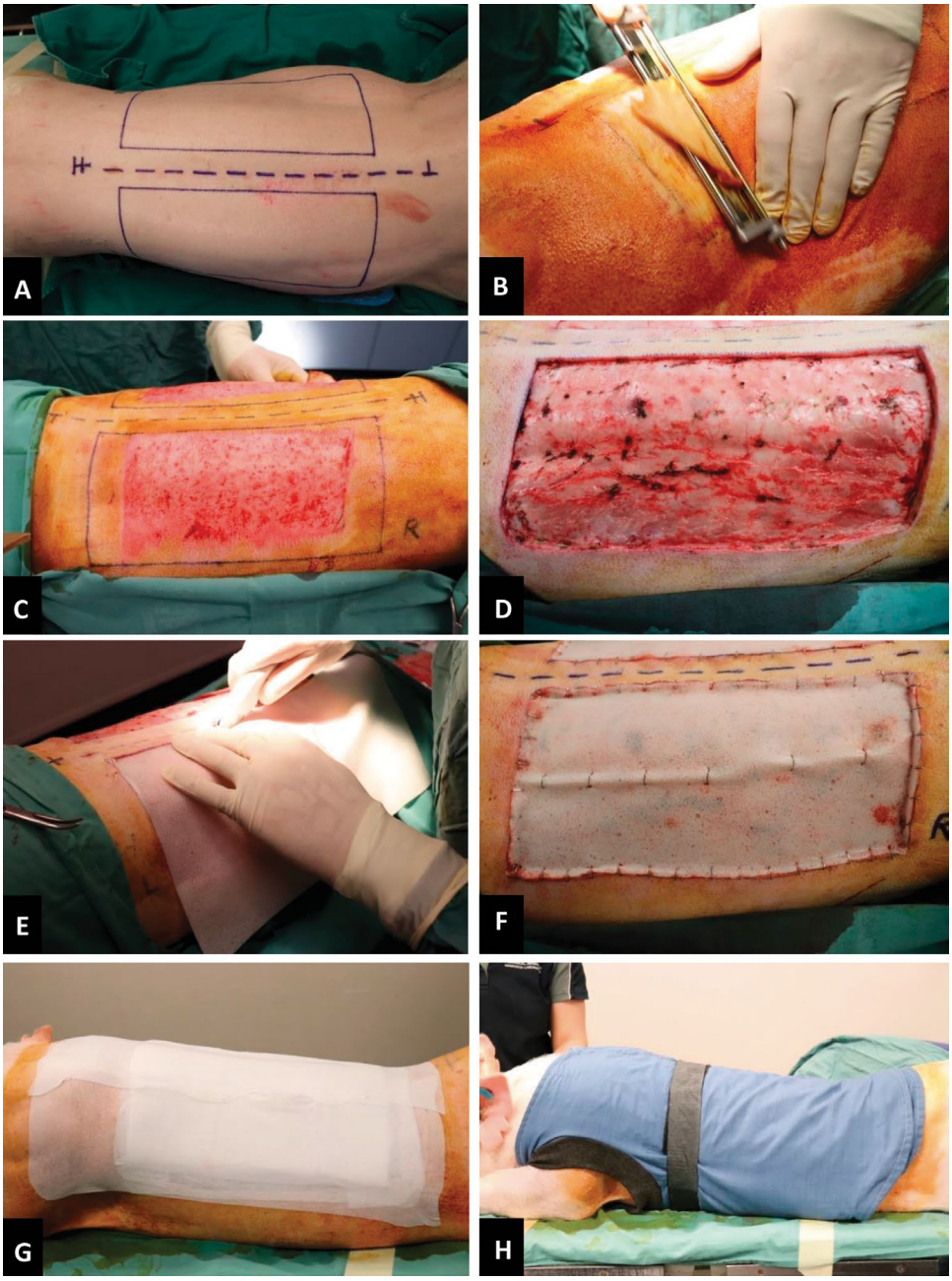

Figure 1. Wound creation and BTM implantation. (A) 24.5 cm × 12 cm wound areas marked out with a surgical marker pen and template, (B, C) harvesting tissue for an autologous source of skin cells, (D) removal of the full-thickness skin to the panniculus adiposus layer, (E, F) implantation of the BTM into the wound by cutting and affixing with surgical staples, (G) outer layers of wound dressings of combine and hypafix, (H) custom-made pig jackets complete the dressing.

preparation for fibroblast inoculation with autologous thrombin at $6 \times 10^4/cm^2$ for CCSa for 17 days and $2.5 \times 10^5/cm^2$ for CCSb for 7 days. Keratinocytes were then inoculated at $5 \times 10^5/cm^2$ and $1 \times 10^6/cm^2$, respectively, for another 7 days. The keratinocyte co-culture period was identical for both CCSa and CCSb (7 days). After initial cell inoculations, media in the CCSs were changed daily with the automated bioreactor. The media used for co-culture was a modified SEL-KGM with 2% FBS.

Day 35—BTM Delamination and CCS Transplantation. The BTM was delaminated on day 35 postimplantation (Figure 3A–C), exposing the vascularized wound bed. Precultured CCSs were cut to size and affixed with surgical steel staples (Figure 3D–G). An autologous split-thickness skin graft (STSG) was taken from the shoulder area as a control site, covering approximately one third of one wound on each animal (Figure 3H).

Wound Assessment and CCS Analysis. Dressings were changed every Monday afternoon and Friday morning with punch biopsies taken at clinically relevant time points; photos, wound measurements, and evaporative water loss readings (Vapometer, Delfin Technologies Ltd., Helsinki, Finland) were recorded to indicate wound closure.

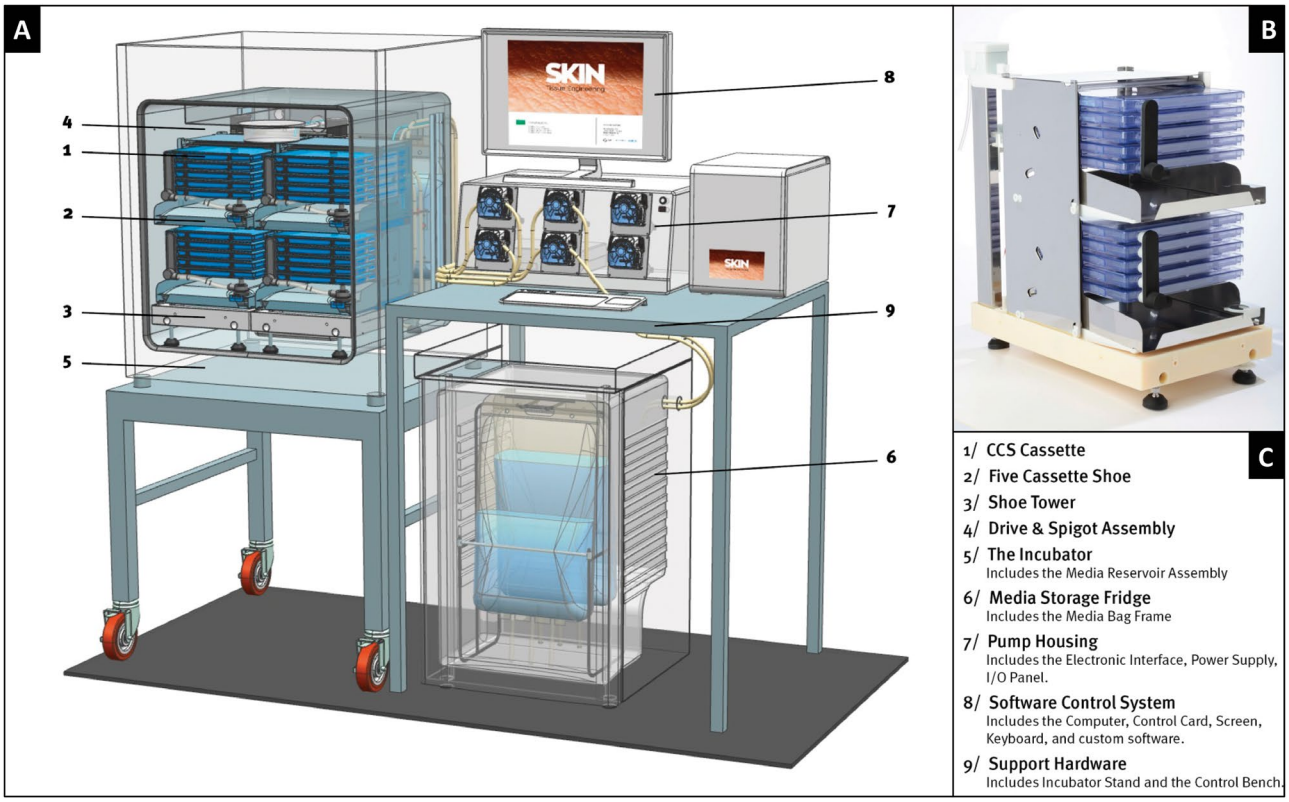

Figure 2. In-house novel bioreactor design and setup. (A) CAD schematic of the prototype design resolved to fit 20 cassettes into an ESCO 240-l incubator (shown here with its supporting equipment on a 2 m × 1 m floor area for scale), (B) actual tower holding 10 cassettes in two shoes, (C) itemized descriptions for each part of the bioreactor.

Biopsies of the CCS were taken pre-application and stained to view with fluorescence microscopy. A LIVE/DEAD® viability stain (L3224, Life Technologies) was used; green fluorescent calcein-AM activity indicating live and red fluorescent ethidium homodimer-1 indicating dead, or loss of plasma membrane integrity. Collagen formation was assessed with the use of dichlorotriazinyl aminofluorescein stain (D0531; Sigma–Aldrich). Immunostaining was performed to affirm the presence of Cytokeratin (AE1/AE3 + 5D3, ab86734, Abcam), and Collagen I (ab34710 and ab90395; Abcam), although success was limited due to the unavailability of a wide range of reactive pig antibodies. In brief, samples were fixed for 10 min in 4% paraformaldehyde, washed, primary antibody applied for 1 hr at room temperature, washed again, and corresponding secondary antibody applied. Samples were then counterstained with either propidium iodide (P4864; Sigma–Aldrich) or DAPI (P36935; Life Technologies). A FluoroDish™ was used to aid viewing on the Nikon confocal microscope.

Wound punch biopsies and large full-thickness excisional samples were fixed in 10% neutral-buffered formalin, dehydrated, and embedded in paraffin. Specimens were cut at 5-µm sections and stained with hematoxylin and eosin (H&E) and Periodic acid–Schiff (PAS) for structural integrity and basement membrane identification.

Statistical Analysis

The statistical software used was SAS 9.4 (SAS Institute Inc., Cary, NC). A linear mixed-effects model was used to test for the effect of flank treatment and then for the effect of flank treatment across time. In the latter model, flank treatment and the continuous term for time period were included in addition to the interaction of time period and flank treatment group. Adjusted models (controlling for pig weight, length, and girth) were also employed. A compound symmetry covariance matrix was used to account for repeated measurements over time and a Variance Components covariance structure was used to adjust for clustering on time (there are measurements on two flanks for each time period). Assumptions of a linear mixed-effects model were found to be upheld by inspection of histograms and scatter plots of residuals, variance, and predicted values. Treatment effects are described as mean differences with 95% confidence intervals.

EXPERIMENTAL RESULTS

All pigs gained weight and were healthy for the entirety of the experimental period. Pig 1 was euthanized on day 49 post-CCS application due to <50% CCS engraftment.

BTM Observations

All BTMs showed complete integration and consolidation by day 18. The wounds with BTM displayed negligible contraction (4.5%), prior to their delamination for CCS transplantation (Figure 3). There was not a statistically significant association between wound contraction for the flank treatments in either an unadjusted model ($P = .5602$) or an adjusted model controlling

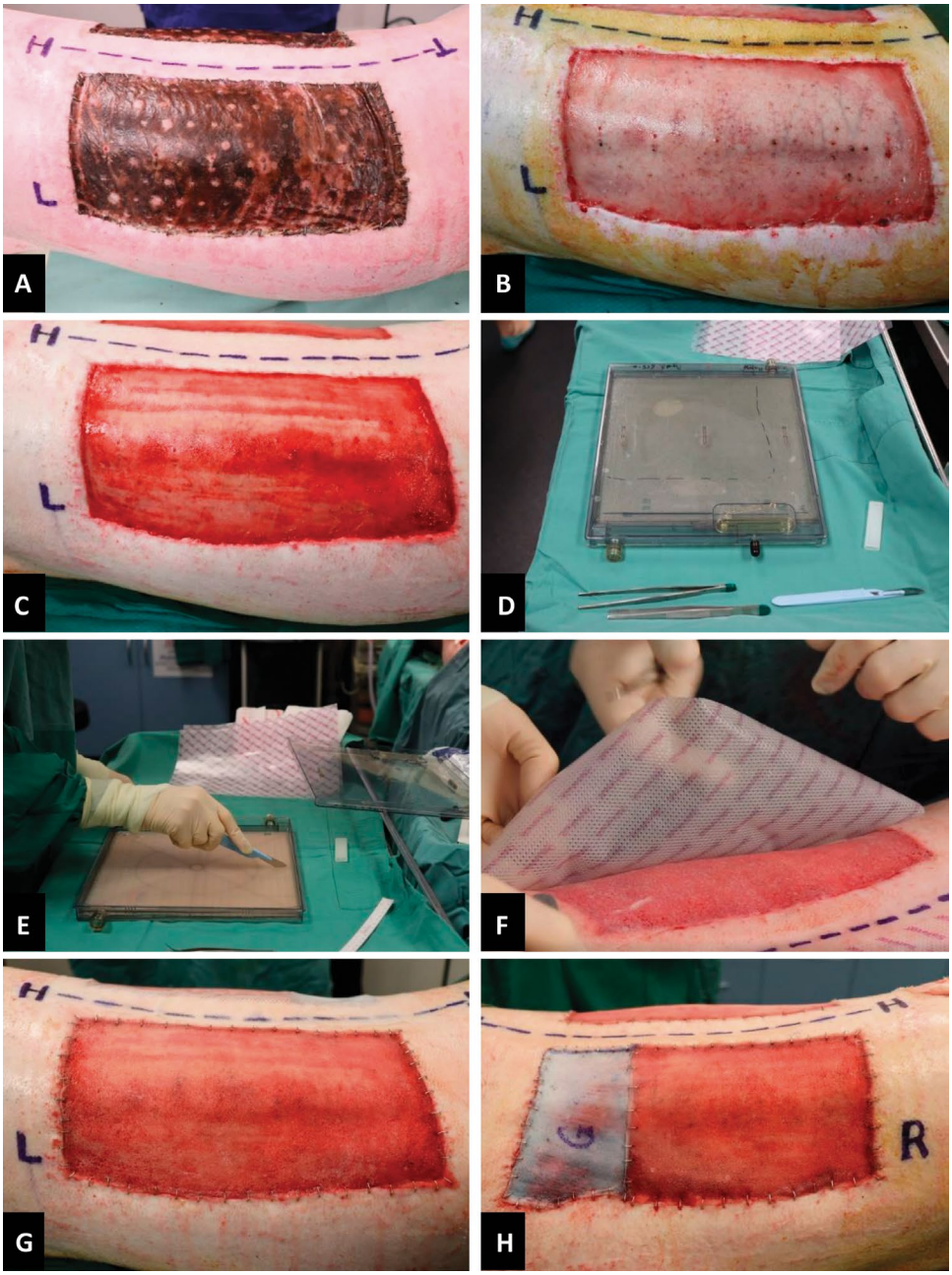

Figure 3. BTM delamination and CCS transplantation. (A) On day 35, after BTM implantation when CCSs were ready to be transplanted, (B, C) BTM delaminated to expose the well-vascularized wound bed which was prepared by light dermabrasion, (D–H) the CCS was cut to size and affixed to the freshly prepared wound bed followed by an additional dressing layer, Mepitel™, which preceded the dressing regime. (H) A split-thickness skin graft was taken from the shoulder area of each pig as a control site, covering approximately one third of one of the wounds.

for pig weight, length, and width (P = .5792), adjusting for repeated measurements over time and clustering on time (two flanks for each time period). Pig 1 clinically presented a superior BTM with negligible seal delamination, whereas Pig 3's BTMs were traumatized, and presented with areas of superficial scar secondary to traumatic early delamination, producing a suboptimal wound bed for grafting.

CCS and Bioreactor

CCS Before Application (In Vitro) The CCS matrices were presoaked with autologous pig plasma prior to fibroblast inoculation. The 1-mm batches of PUR foam presented with an "L-shaped" area that had significantly larger pores on two edges of the 25 cm × 25 cm sheet. As only half of each CCS was to be transplanted per pig, we could manipulate it so that only a small proportion of the larger pore foam was applied onto a wound, and its subsequent location was noted upon application. Due to the extra-large pores (>1 mm) cell fall through and growth on the bottom plate in the cassette was apparent; however, fibroblasts were able to span the smaller pores to produce confluent layers (Figure 4A and B). Immunostaining confirmed the presence of collagen type 1 (Figure 4C).

Keratinocytes seeded on the surface were apparent prior to transplantation (Figure 4D and E, see Supplemental Video File) and positively stained with pancytokeratin (AE1–AE3) (Figure 4D, inset).

CCS After Application Between days 4 and 7 post-CCS transplantation, the pigs inflicted varying degrees of trauma on the CCSs, both during normal behavior and physical trauma during induction of anesthesia for dressing changes. Two of three pig skin grafts showed 100% take by day 11, with substantial skin graft loss (65.5%) in the third pig. Small islands of epithelium were also observed clinically on day 11 in the CCS conditions (Figure 5A and B). Split-thickness skin and CCS engraftment were confirmed by punch biopsies and histological analysis with H&E and PAS staining (Figure 5C–E). CCS biopsies displayed superficial 1-mm PUR fragments with developing interwoven epidermis with a small band of granulation tissue and residual 2-mm BTM in the lower portions

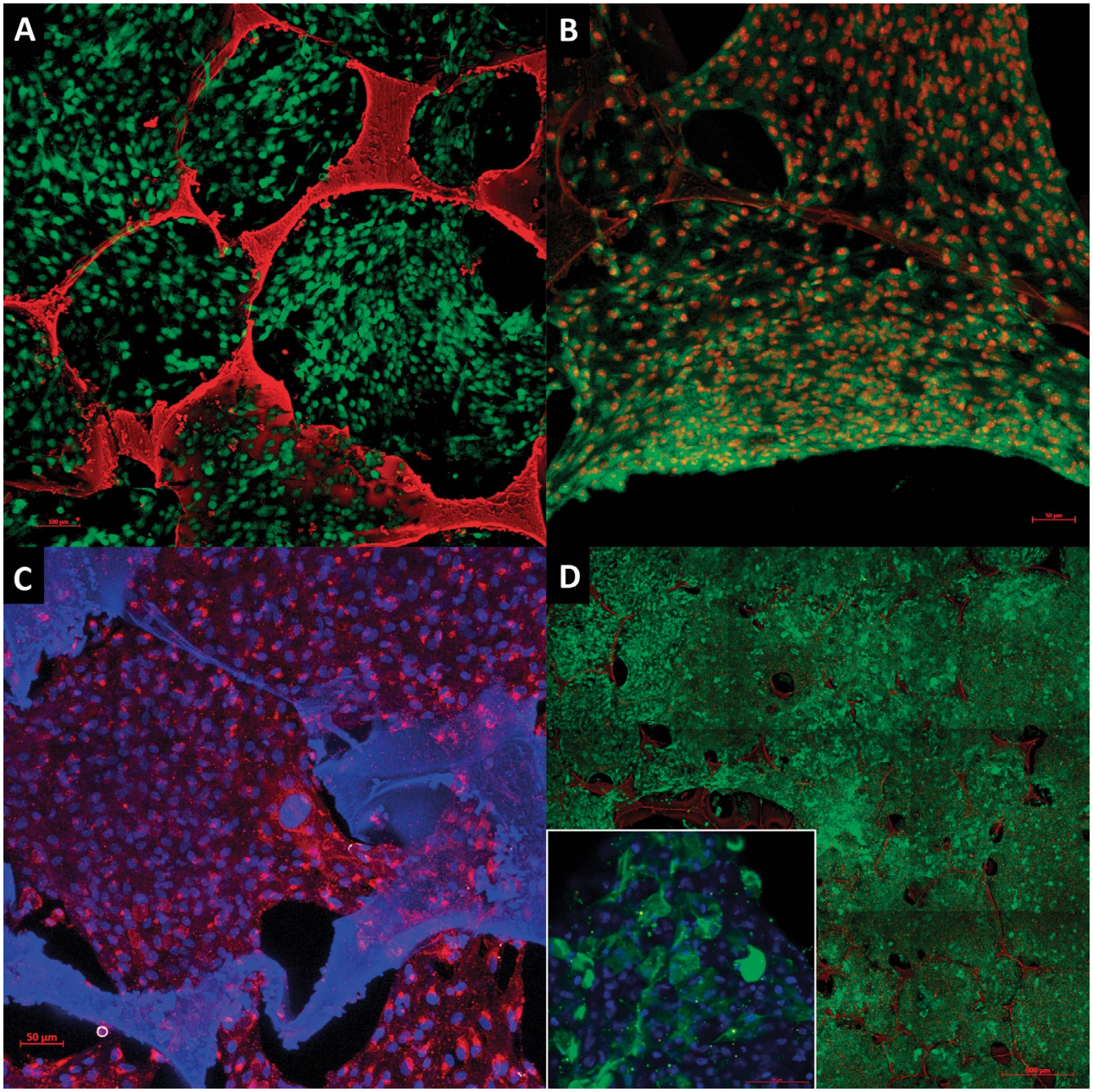

Figure 4. Representative staining of CCSs prior to application. (A) Live/dead stain (calcein—green, ethidium—red) showing fibroblasts (Fbs) stained green, filling the polymer pores (PUR stained red), (B) fibroblasts stained with dichlorotriazinyl aminofluorescein depicting collagen production, (C) Collagen type I staining red, and blue fibroblast nuclei stained with auto-fluorescent blue PUR foam structure, (D) confocal micrograph, 3 × 3 tile showing a lawn of green cells prior to transplantation note the >1-mm open pore section where cells were unable to bridge, (D-inset) AE1–AE3 green staining for keratin with blue DAPI-stained nuclei, (E) confocal micrograph video of CCS before application showing z-stack of cellular morphology from keratinocytes to fibroblast layer. Scale bars = 100 µm (A), 50 µm (B, C, D-inset, E), and 500 µm (D).

(Figure 5C). PAS staining, indicative of basement membrane, was observed in Figure 5D from a section of CCS engraftment. The skin graft showed normal epidermis (with continuous and well-developed basement membrane) and dermis (Figure 5E), showing perivascular lymphoplasmacytic and eosinophil cuffing, with an edematous layer with active fibroplasia, merging into more mature collagenous connective tissue with compact collagen. The PUR foam material from the BTM was present in the subcutis, surrounded by multinucleate giant cells and epithelioid macrophages.

The majority of CCS healing and engraftment on pigs 2 and 3 occurred by day 53 post-CCS transplantation, when they were sufficiently healed to no longer require dressings, although these wounds were being moisturized and massaged to aid with the tissue repair process and produce a soft and supple scar from a week earlier. On day 63 post-CCS transplantation, the evaporative water loss readings were comparable to normal skin (average 11.9 g/m^{2}h) and the healed skin graft (average 11 g/m^{2}h) with readings for sites a and b averaging between 9.4 and 13.3 g/m^{2}h, indicating definitive wound closure.

Pig 1 achieved limited success due to major trauma on day 4 post-CCS application, causing an initial total CCS loss of 48%. By day 32, only 7.5% of the original wound displayed central re-epithelialization from CCS and, on day 49 (7 weeks post-CCS application), this animal was euthanized. However, areas of viable epithelium appeared both clinically and histologically within the CCS PUR over residual NovoSorb® BTM in the subcutis. This ranged from superficial thick viable epithelium (early CCS take), adjacent thin epithelium (secondary edge migration) to ulceration (no take) with deep inflammatory infiltration.

At 32 days post-CCS application, pig 2 displayed 73% wound closure for CCSa, and 85% for CCSb. The CCSb wound area was completely healed by day 53 postapplication. It was soft and supple to manipulate but had a central scar band present due to some delayed healing (Figure 6A). The sheet skin graft applied at the same time was clinically similar to normal skin, bearing in mind the effect of the integrated BTM deep to the graft. Figure 6B shows the area at 4.5 months postapplication with minimal delineation between the STSG site and CCS applied area. CCSa also

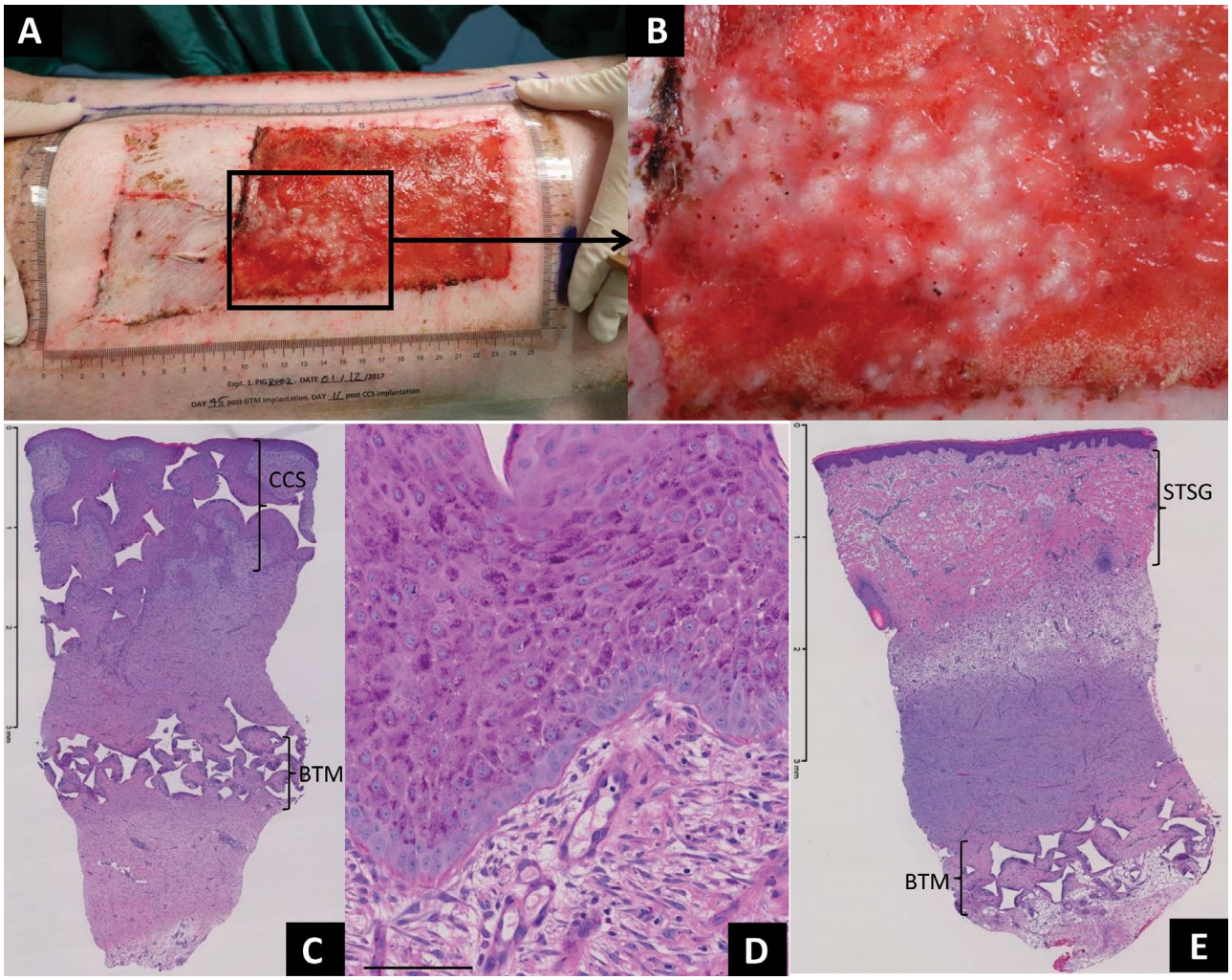

Figure 5. Areas of successful CCS and STSG engraftment at day 11. (A, B) Pig 2, CCSb displaying small islands of clinical re-epithelialization, (C, D) H&E and Periodic acid–Schiff staining of punch biopsies from CCS engraftment day 11, and (E) H&E staining of split-thickness skin graft punch biopsy, day 11.

displayed a central scar band with visible edge scarring and contraction. In pig 3 at day 32, CCSa and CCSb were 56% and 55% healed, respectively. The remaining wounds healed by secondary re-epithelialization by day 63.

The wound areas stabilized at day 66, (32 post-CCS transplant), with an average of 18% contraction from the time of delamination/CCS transplant (Figure 7). Pig 2 displayed an increase in wound size from this time point to endpoint, indicating the ability of a healed wound to expand with pig growth.

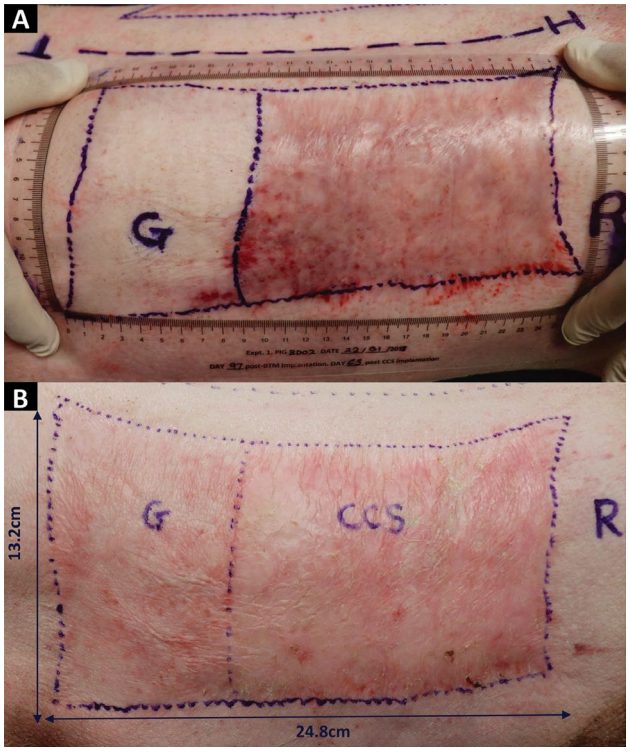

Figure 6. Healed wound at day 63 and 137 post-CCS transplantation. (A) Pig 2 CCSb wound size day 0, 281 cm^2 to day 63, 261 cm2 and (B) Pig 2 CCS at 137 days (4.5 months) post-transplant maintaining wound size, shape, and no obvious hypertrophic scarring. Note: pigs at this time point had been exposed to environmental factors and elements.

There was no statistically significant difference between the different areas, CCSa or CCSb ($P > .01$); however, aesthetically the epithelium produced from CCSb was initially thicker, more uniform, and at early time points covered a greater percentage of the wound. For CCSa wound, for every 1-day increase in time, the mean percent wound change increases by 0.18% (estimate = 0.18, 95% confidence interval: 0.09, 0.27, comparison $P = .0002$). For CCSb wounds, for every 1-day increase in time, the mean percent wound change increases by 0.29% (estimate = 0.29, 95% confidence interval: 0.20, 0.39, comparison $P < .0001$). However, there is not a statistically significant difference between these slopes/associations (interaction $P = .0900$). When controlled for pig weight, pig length, and pig girth, these post hoc comparisons are no longer significant (CCSa—$P = .4298$ and CCSb—$P = .7509$, interaction $P = .0915$).

Pigs 2 and 3 were penned outdoors from day 63 post-CCS application until euthanasia (25 weeks post-CCS application). At 137 days (4.5 months) postapplication, histological sections revealed the presence of BTM along the subcutaneous fat layer, with intermittent residual CCS PUR foam. The epidermis showed acanthosis with prominent rete ridges and prominent, laminated orthokeratotic hyperkeratosis. There was a thick dermal layer of mature collagenous connective tissue with PUR material evident in the subcutis.

At day 177, the full-thickness excisional histology (Figure 8) was similar to day 137, with abundant collagen deposition and epidermal integrity. The PUR implanted material was evident in the deeper dermis and was surrounded by multinucleate giant cells and epithelioid macrophages indicative of a granulomatous reaction (Figure 8C). This reaction was also observed deep to the STSG (Figure 8F). The two sites (CCS treated and control) presented similar histology, although CCS resulted in a greater dermal thickness, this outcome might be due to delayed re-epithelialization and increased fibrosis, but the fact that the CCS is 1 mm thick

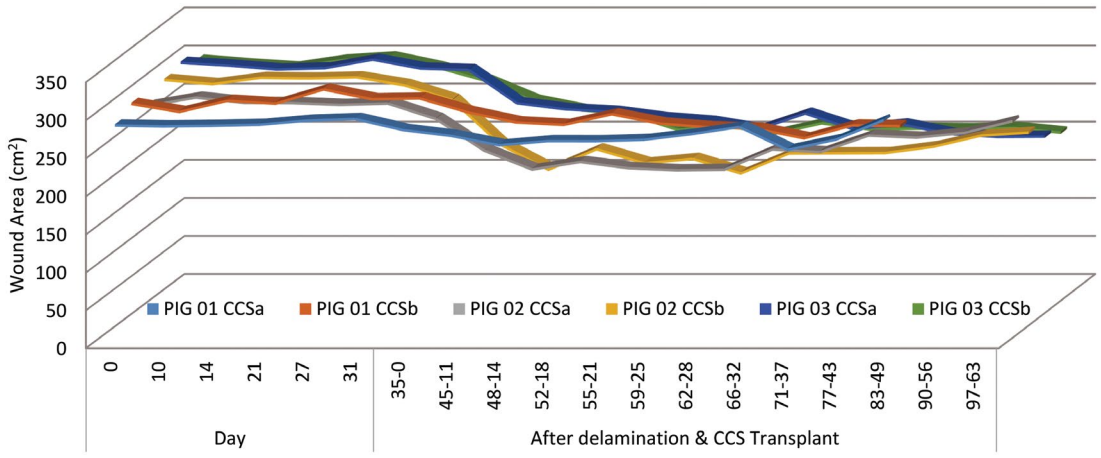

Figure 7. Wound area over time (cm^2), day 0 to 35 post-BTM implantation prior to CCS application and then day 35 until 2 months post-CCS application.

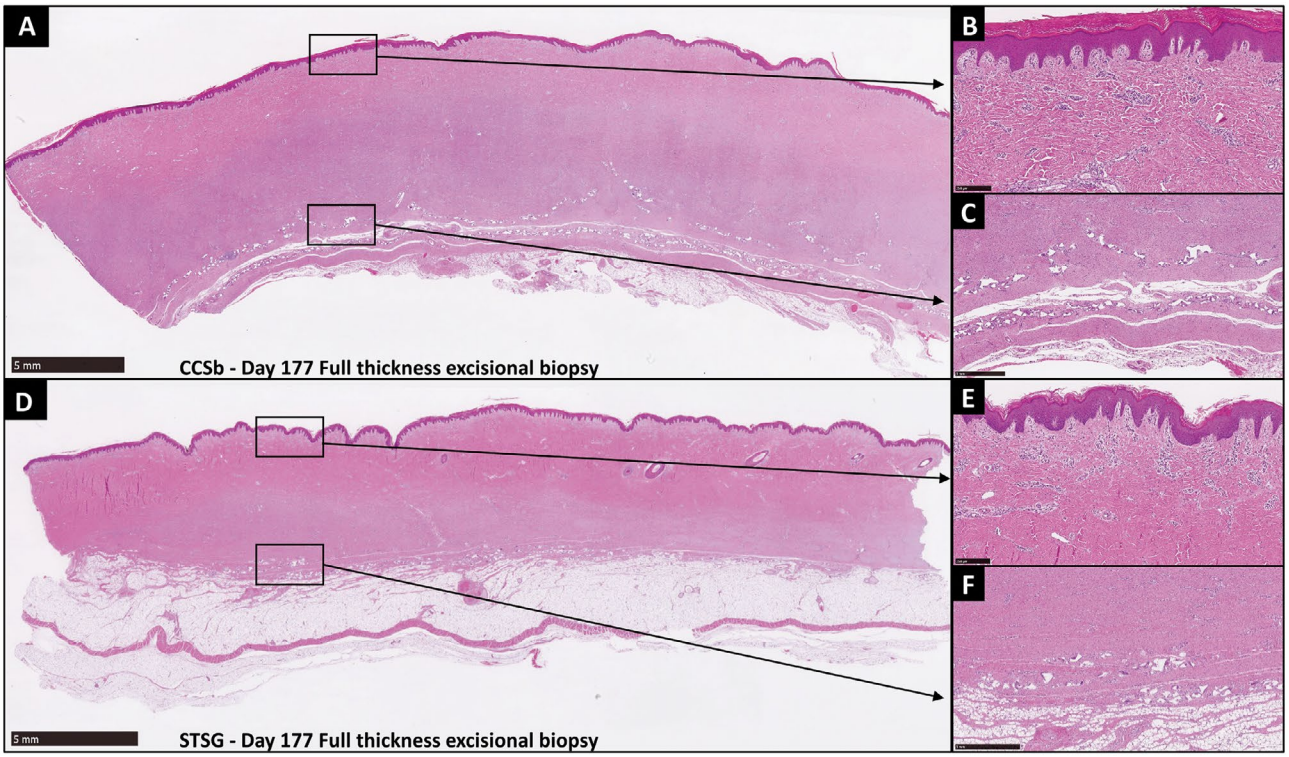

Figure 8. Representative histology of full-thickness sections from day 177 post-CCS application and STSG. (A–C) A 4.2-cm section from CCS healed wound with continual well-developed epidermis and residual PUR foam in the lower subcutis, 10.8-mm-overall-thick section, average 8.7-mm epidermis to dermis, average epidermal thickness 221 µm and (D–F) similar histology observed in a 3.5-cm section from STSG healed wound, with prominent rete ridges, 9.03 mm overall thickness, average 5.5-mm epidermis to dermis, and an average epidermal thickness 209 µm. Scale bar = 5 mm (A and D), 250 µm (B and E), 1 mm (C and F).

and the STSG is 12/1000 inch (0.305 mm) should also be considered as a possible mechanism.

Bioreactor

The bioreactor was able to maintain 24 days of operation, automatically supplying new nutrients and removing waste from the cassettes daily. Upon decommissioning the equipment, a few minor deficiencies were noted but easily rectifiable by machining the prototype parts to ensure rigidity and demonstrating that long-term use is sustainable. Minor software updates and changes are required that will refine the success of the bioreactor and the consistent reliability of the produced CCSs. Changes to the growth plate and an introduction of a lifting mechanism for the CCS transplant are underway and will further advance the bioreactor.

DISCUSSION AND CONCLUSIONS

Using a porcine large wound model, we demonstrated that upscaling the CCS from 8 cm × 8 cm, to 25 cm × 25 cm, is feasible by utilizing an in-house novel bioreactor device. This facilitated automated daily media changes and waste control. A total of six cassettes were setup over two shoes for the three pigs. Although CCS engraftment was variable over the three pigs, initial island epithelialization from the CCS was observed by day 11 with complete healing from secondary re-epithelialization. Numerous factors contributed to the final outcomes.

Early trauma to the wounds caused not only CCS loss but also graft loss. This was potentially due to the generation of the donor site for the STSG control area, as it is well reported that a donor site can be more painful for the patient than the actual wound site.[24] To enable the use of a sheet graft for the control site, a larger donor site was required. However, future studies will investigate the possibility of a designated research electric dermatome and porcine skin graft mesher to first enable smaller donor sites and second, it will align with that of a clinical setting for extensive full-thickness wounds, where 1:3 meshed grafts are more widely used. A direct comparison of a meshed 1:3 STSG to CCS may proffer similar healing times. Other skin substitutes that have been used clinically have also been meshed prior to application to expand the area of coverage.[25]

The range of PUR foam pore sizes/porosity is another contributing factor to island epithelialization and inconsistency. Although fibroblasts prefer a pore range (between 38 and 150 µm),[26,27] they can bridge much larger pores since adjacent cells act as support structures.[2] However, the CCS PUR matrices supplied contained pores > 1 mm, which made it impossible for fibroblasts to traverse. Other contributing factors that may produce a range of variability include a manual cell seeding technique, permitting operator-dependent deficiencies.[10] Bio-printing and automated cell seeding devices may assist with homogenous cell distribution, both improving the reproducibility and accuracy concerns.[28,29] Smaller scale bioreactor devices have been designed for other 3D tissues that can inoculate cells by

dynamic methods,[19,30–32] possible for single cell inoculations but more complicated for the creation of layered multi-cell structures.

A well-prepared wound bed is critical for full engraftment whether it be a split-thickness skin graft or a substitute graft. For a wound to heal it needs to be well vascularized, have reduced bacterial load and organized granulation tissue.[33] The NovoSorb® BTM is anecdotally one of the most robust and forgiving dermal templates currently available[34–37]; however, the unpredictable behaviors of a 35-kg pig might be overstretching its tolerance and is one drawback of using a large animal model. The porcine study model may have several disadvantages (size) but, as a close analog of human skin, it is a model that has enabled our translational research to move forward into clinic.

Tissue engineering is rapidly evolving, with the next generation of "skin substitute" requiring an interdisciplinary approach to ensure a clinically suitable product. Large-scale production of such materials not only needs to meet regulatory requirements but also proffers critical biological and engineering challenges that need a thoughtful approach to ensure an end product that is safe, of high quality, and efficacious. The principal limiting factor in the widespread production and use of any engineered tissue, not just skin, is production cost, which includes not merely the initial raw materials, but also cleanroom accessibility/fees, running expenditures, and labor.[38] If one or two of these can be reduced, then it might enable the expedition of engineered tissues to market. In the long term, a bioreactor will enable a reduction of costs by reducing the manual handling required through automation; however, scale-up and automation for standard cell culture techniques is also required. This will ease the labor required for the intensive expansion of cells and is another avenue where specialized bioreactors may assist.[9,39]

There are a number of research tissue engineered skins and in-house research bioreactors in the field that have shown potential[20,25,40] and is essential for extensive burns cases to consider the capability of scale-up to manufacture a product for clinical application.

In summary, the study suggests that the novel in-house prototype bioreactor can support the generation and scale-up of large CCSs, which can then provide a closure strategy for large wounds. The study employed the two-stage strategy of NovoSorb® BTM followed by CCS application. This has been designed to offer patients with large burn injuries at least a chance of survival with an acceptable outcome. The current CCS represents the first steps to a more complete cultured skin analog. Plans to include a micro-vasculature, pigmentary capability and other desirable appendages (such as hair) have been formulated, but having the capability to scale-up the basic model will be a major advantage for further long-term development, while saving lives in the short term.

ACKNOWLEDGMENTS

We thank Dr. John Finnie, Veterinary Pathologist, SA Pathology, for his help with interpreting the histological findings. Thanks to Ms. Amy Li for her assistance with the large demands of the required cell culture component. General veterinary and animal support from the Large Animal Research Imaging Facility at Gilles Plains (SAHMRI). Great thanks are extended to David Robertson, a meticulous Engineer, for all his patience and assistance with the bioreactor designs. Suzanne Edwards, Statistician within the Adelaide Health Technology Assessment (AHTA), School of Public Health, The University of Adelaide, for her assistance with the statistical analysis.

REFERENCES

1. Li A, Dearman BL, Crompton KE, Moore TG, Greenwood JE. Evaluation of a novel biodegradable polymer for the generation of a dermal matrix. J Burn Care Res 2009;30:717–28.
2. Dearman BL, Li A, Greenwood JE. Optimization of a polyurethane dermal matrix and experience with a polymer-based cultured composite skin. J Burn Care Res 2014;35:437–48.
3. Dearman BL, Stefani K, Li A, Greenwood JE. "Take" of a polymer-based autologous cultured composite "skin" on an integrated temporizing dermal matrix: proof of concept. J Burn Care Res 2013;34:151–60.
4. Greenwood JE, Dearman BL. Split skin graft application over an integrating, biodegradable temporizing polymer matrix: immediate and delayed. J Burn Care Res 2012;33:7–19.
5. Greenwood JE, Dearman BL. Comparison of a sealed, polymer foam biodegradable temporizing matrix against Integra® dermal regeneration template in a porcine wound model. J Burn Care Res 2012;33:163–73.
6. Greenwood JE, Li A, Dearman BL, Moore TG. Evaluation of NovoSorb™ novel biodegradable polymer for the generation of a dermal matrix. Part 2: in-vivo studies. Wound Pract Res 2010;18:24.
7. Greenwood JE, Li A, Dearman BL, Moore TG. Evaluation of NovoSorb™ novel biodegradable polymer for the generation of a dermal matrix. Part 1: in-vitro studies. Wound Practice Res 2010;18:14.
8. Greenwood JE, Wagstaff MJD. The use of biodegradable polyurethane in the development of dermal scaffolds. In: Cooper SL, Guan J, editors. Advances in polyurethane biomaterials. Duxford, UK: Woodhead Publishing Series in Biomaterials, Elsevier; 2016. p. 1.
9. Kino-Oka M, Ogawa N, Umegaki R, Taya M. Bioreactor design for successive culture of anchorage-dependent cells operated in an automated manner. Tissue Eng 2005;11:535–45.
10. Martin I, Wendt D, Heberer M. The role of bioreactors in tissue engineering. Trends Biotechnol 2004;22:80–6.
11. Wang S, Zhong J. Bioreactor Engineering. In: Yang S, editor. Bioprocessing for Value-Added Products from Renewable Resources. Elsevier; 2007. p. 131–61.
12. Pörtner R, Goepfert C, Wiegandt K, et al. Technical strategies to improve tissue engineering of cartilage-carrier-constructs. In: Kasper C, van Griensven M, Pörtner R, editors. Bioreactor Systems for Tissue Engineering. Advances in Biochemical Engineering/Biotechnology. Springer, Berlin, Heidelberg; 2009. p. 145–81.
13. Pörtner R, Nagel-Heyer S, Goepfert C, Adamietz P, Meenen NM. Bioreactor design for tissue engineering. J Biosci Bioeng 2005;100:235–45.
14. Zhao J, Griffin M, Cai J, Li S, Bulter PEM, Kalaskar DM. Bioreactors for tissue engineering: an update. Biochem Eng J 2016;109:268–81.
15. Ladd MR, Lee SJ, Atala A, Yoo JJ. Bioreactor maintained living skin matrix. Tissue Eng Part A 2009;15:861–68.
16. Jeong C, Chung HY, Lim HJ, et al. Applicability and safety of *in vitro* skin expansion using a skin bioreactor: a clinical trial. Arch Plast Surg 2014;41:661–7.
17. Huh MI, An SH, Kim HG, et al. Rapid expansion and auto-grafting efficiency of porcine full skin expanded by a skin bioreactor ex vivo. Tissue Eng Regen Med 2016;13:31–8.
18. Helmedag MJ, Weinandy S, Marquardt Y, et al. The effects of constant flow bioreactor cultivation and keratinocyte seeding densities on prevascularized organotypic skin grafts based on a fibrin scaffold. Tissue Eng Part A 2015;21:343–52.
19. Sun T, Norton D, Haycock JW, Ryan AJ, MacNeil S. Development of a closed bioreactor system for culture of tissue-engineered skin at an air–liquid interface. Tissue Eng 2005;11:1824–31.
20. Sriram G, Alberti M, Dancik Y, et al. Full-thickness human skin-on-chip with enhanced epidermal morphogenesis and barrier function. Mater Today 2018;21:326–40.
21. Prenosil JE, Kino-oka M. Computer controlled bioreactor for large-scale production of cultured skin grafts. Ann N Y Acad Sci 1999;875:386–97.
22. Prenosil JE, Villeneuve PE. Automated production of cultured epidermal autografts and sub-confluent epidermal autografts in a computer controlled bioreactor. Biotechnol Bioeng 1998;59:679–83.

23. Kalyanaraman B, Boyce S. Assessment of an automated bioreactor to propagate and harvest keratinocytes for fabrication of engineered skin substitutes. Tissue Eng 2007;13:983–93.
24. Sinha S, Schreiner AJ, Biernaskie J, Nickerson D, Gabriel VA. Treating pain on skin graft donor sites: review and clinical recommendations. J Trauma Acute Care Surg 2017;83:954–64.
25. Boyce ST, Simpson PS, Rieman MT, et al. Randomized, paired-site comparison of autologous engineered skin substitutes and split-thickness skin graft for closure of extensive, full-thickness burns. J Burn Care Res 2017;38:61–70.
26. Zeltinger J, Sherwood JK, Graham DA, Müeller R, Griffith LG. Effect of pore size and void fraction on cellular adhesion, proliferation, and matrix deposition. Tissue Eng 2001;7:557–72.
27. Salem AK, Stevens R, Pearson RG, et al. Interactions of 3T3 fibroblasts and endothelial cells with defined pore features. J Biomed Mater Res 2002;61:212–7.
28. Varkey M, Visscher DO, van Zuijlen PPM, Atala A, Yoo JJ. Skin bioprinting: the future of burn wound reconstruction? Burns Trauma 2019;7:4.
29. Baltazar T, Merola J, Catarino C, et al. Three dimensional bioprinting of a vascularized and perfusable skin graft using human keratinocytes, fibroblasts, pericytes, and endothelial cells. Tissue Eng Part A 2020;26:227–38.
30. Wendt D, Marsano A, Jakob M, Heberer M, Martin I. Oscillating perfusion of cell suspensions through three-dimensional scaffolds enhances cell seeding efficiency and uniformity. Biotechnol Bioeng 2003;84:205–14.
31. Zhao F, Ma T. Perfusion bioreactor system for human mesenchymal stem cell tissue engineering: dynamic cell seeding and construct development. Biotechnol Bioeng 2005;91:482–93.
32. Campos Marín A, Brunelli M, Lacroix D. Flow perfusion rate modulates cell deposition onto scaffold substrate during cell seeding. Biomech Model Mechanobiol 2018;17:675–87.
33. Borgquist O, Gustafsson L, Ingemansson R, Malmsjö M. Micro- and macromechanical effects on the wound bed of negative pressure wound therapy using gauze and foam. Ann Plast Surg 2010;64:789–93.
34. Damkat-Thomas L, Greenwood JE, Wagstaff MJD. A synthetic biodegradable temporising matrix in degloving lower extremity trauma reconstruction: a case report. Plast Reconstr Surg Glob Open 2019;7:e2110.
35. Wagstaff MJD, Salna IM, Caplash Y, Greenwood JE. Biodegradable temporising matrix (BTM) for the reconstruction of defects following serial debridement for necrotising fasciitis: a case series. Burns Open 2019;3:12–30.
36. Sreedharan S, Morrison E, Cleland H, Ricketts S, Bruscino-Raiola F. Biodegradable temporising matrix for necrotising soft tissue infections: a case report. Aust J Plas Surg 2019;2:106–9.
37. Liu X, Hickerson W, Velamuri S. 330 A case of successful reconstruction of facial chemical burn by using biodegradable temporising matrix. J Burn Care Res 2018;39 Suppl 1:S135.
38. Abraham E, Gupta S, Jung S, McAfee E. Bioreactor for scale-up: process control. In: Viswanathan S, Hematti P, editors. Mesenchymal stromal cells. Elsevier Inc; 2017. p. 139–78.
39. Wendt D, Riboldi SA. Bioreactors in tissue engineering: from basic research to automated product manufacturing. In: Meyer U, Handschel J, Wiesmann HP, Meyer T, editors. Fundamentals of tissue engineering and regenerative medicine. Berlin, Germany: Springer; 2009. p. 595.
40. Navarro J, Clohessy RM, Holder RC, et al. In vivo evaluation of three-dimensional printed, keratin-based hydrogels in a porcine thermal burn model. Tissue Eng Part A 2020;26:265–78.

CHAPTER 3:
Successful Proof of the 'Two-stage Strategy' for Major Burn Wound Repair

Greenwood JE, Damkat-Thomas LL, Schmitt B, **Dearman BL**

Published in

Burns Open

2020

3.1 Overview

Pre-optimisation studies to refine the CCS process, culturing methods and bioreactor improvements were in progress prior to the preparation of the second porcine study scheduled to start in December 2018. However, due to unforeseen and extenuating circumstances (95% Burn patient), these and the porcine trial were deferred to undertake the first CCS trial in man. Although the approval of the human research ethics committee had been granted (Appendix I), governance had not been successfully cleared prior to December 2018 and this patient was treated via the Special Access Scheme (SAS) through the Therapeutic Goods Administration (TGA). Overall, 26 pieces of CCS (16,250 cm^2) were generated to assist with closing a 95% wound. Along with the results from Chapter 2, the culturing methods and CCS fabrication methods employed for this patient have been previously published [1, 2]. The results and information obtained from this first human trial is a major step in developing a second paradigm shift in burn care, the first being BTM. Although further optimisation to enable consistent 'take' is a necessity and is further explored in Chapters 4-6.

Statement of Authorship

Title of Paper	Successful proof of the "two-stage strategy" for major burn wound repair
Publication Status	☑ Published ☐ Accepted for Publication ☐ Submitted for Publication ☐ Unpublished and Unsubmitted w ork w ritten in manuscript style
Publication Details	Greenwood, JE, Damkat-Thomas, L, Schmitt, B & Dearman, B 2020, 'Successful proof of the "two-stage strategy" for major burn wound repair', *Burns Open : an International Open Access Journal for Burn Injuries*, vol. 4, no. 3, pp. 121–131.

Principal Author

Name of Principal Author (Candidate)	Bronwyn Dearman
Contribution to the Paper	Study design, methodology execution, data collation/analysis, manuscript figure preparation, writing, review and editing.
Overall percentage (%)	45%
Certification:	This paper reports on original research I conducted during the period of my Higher Degree by Research candidature and is not subject to any obligations or contractual agreements with a third party that would constrain its inclusion in this thesis. I am the senior author of this paper.
Signature	Date 23/3/22

Co-Author Contributions

By signing the Statement of Authorship, each author certifies that:

i. the candidate's stated contribution to the publication is accurate (as detailed above);
ii. permission is granted for the candidate to include the publication in the thesis; and
iii. the sum of all co-author contributions is equal to 100% less the candidate's stated contribution.

Name of Co-Author	Professor John Greenwood
Contribution to the Paper	Study participation, data collation, concept of paper, writing, editing and submission.
Signature	Date 5th April 2022

Name of Co-Author	Dr Lindsay Damkat-Thomas		
Contribution to the Paper	Study participation with manuscript review.		
Signature		Date	09/04/2022

Name of Co-Author	Brad Schmitt		
Contribution to the Paper	Data collation, manuscript review.		
Signature		Date	23/3/22

Please cut and paste additional co-author panels here as required.

Burns Open 4 (2020) 121–131

Contents lists available at ScienceDirect

Burns Open

journal homepage: www.burnsopen.com

Case Report

Successful proof of the 'two-stage strategy' for major burn wound repair

John E. Greenwood *, Lindsay Damkat-Thomas, Brad Schmitt, Bronwyn Dearman

Adult Burn Service, Royal Adelaide Hospital, 1 Port Road, Adelaide 5000, South Australia, Australia

ARTICLE INFO

Article history:
Received 30 April 2020
Received in revised form 2 June 2020
Accepted 15 June 2020
Available online 21 June 2020

ABSTRACT

In 2004, in response to inadequacies in wound management techniques employed in the management of massive burns and the consequent high mortality and morbidity, a two stage strategy was conceived to reduce the traditional reliance on autograft, where donor sites were scarce, or absent. Over the next 14 years, two products were developed based in a novel, biodegradable polyurethane foam – a Biodegradable Temporising Matrix (BTM) and an autologous, bilayer (dermis and epidermis) Composite Cultured Skin (CCS). Following immediate burn escharectomy, the 1st stage of the strategy (either at the same operation or a few days later) would involve BTM implantation into the resultant wounds and harvesting of a small autograft for keratinocyte and fibroblast isolation for culture and CCS production. The 2nd stage, five weeks later, would involve delamination of the BTM and the application of the prepared CCS to the BTM 'neo-dermis'. The two stages together designed to reduce the requirement for autograft to the small piece harvested to provide the cells for CCS production. At the end of 2018, an adult male with 95% TBSA burns (85% full-thickness) and significant smoke inhalation was received and was the first to undergo the 'two-stage strategy'. His treatment course and outcome are described herein.

1. Introduction

In 2004, the senior author (JG) postulated that in order to abolish the requirement for the split skin graft in the repair of the post-debridement wounds of patients after major burn injury, two serially-applied materials would be necessary. This 'two-stage strategy' suggested that definitive closure would be best achieved by an autologous composite cultured skin (CCS), derived from a small split skin graft biopsy where dermal and epidermal elements could be individually cultured for expansion and then serially seeded into a suitable 'scaffold'. However, whilst keratinocytes are happy to form confluent cellular layers under suitable culture conditions (the epidermis, derived from ectoderm in the embryo, is a completely cellular organ); a confluent layer of cultured fibroblasts does not constitute a dermis. The dermis, derived from mesoderm, is not a cellular, but a molecular structure. The function of the dermal cell, the fibroblast, is to maintain this structure and occasionally to repair it after injury. Rather than merely culturing fibroblasts, these cells must be allowed to establish themselves within a three-dimensional scaffold in which, with time and nurturing, they will lay down collagen and the other macromolecules that characterise the dermal structure. Thus, the senior author determined that the three-dimensional scaffold did not need to be composed of biological materials, since its role was the temporary support of fibroblast proliferation and collagen deposition, and sourced a biodegradable polyurethane from a CSIRO-spin out company, PolyNovo Biomaterials in 2004.

The initial work on producing CCS demonstrated that the polyurethane was biocompatible, bio-tolerated and suitably biodegradable (a property which could be tailored by altering aspects of the chemistry) [1]. However, it became apparent that the time taken to produce these early bi-layer 'skin analogues' (at least four weeks), would require the development of a second material, a biodegradable temporising matrix (BTM, now marketed as NovoSorb BTM™ by PolyNovo Biomaterials Pty Ltd, Port Melbourne, Victoria, Australia). The function of NovoSorb BTM™ (idiosyncratically to be applied first) would be to 'physiologically' close the wound by virtue of a superficial pseudo-epidermal layer, and then have a deeper, biodegradable dermal layer integrate into the wound bed, preventing wound contraction and improving the wound bed for the subsequent receipt of CCS.

The development of the NovoSorb BTM™ has been the subject of a series of articles and book chapters [1–20].

The background of the CCS has similarly received some mention in the literature [1–3,6,8,13–15], but its progress was postponed by several years because of some fundamental issues. One of these has already been highlighted - the culture/preparation time of CCS, which mandated the development of the NovoSorb BTM™. With

* Correspondence author: Adult Burn Service, Royal Adelaide Hospital, 1 Port Road, Adelaide 5000, South Australia, Australia.
E-mail address: john.greenwood@sa.gov.au (J.E. Greenwood).

https://doi.org/10.1016/j.burnso.2020.06.003
2468-9122/

the processes of CCS production fully developed and optimised, this preparation time is now five weeks. Some issues were remedied more simply - for instance, the polymer scaffold was buoyant in culture and necessitated the identification of a means of holding it submerged in fibroblast media, and simultaneously negating the tendency for seeded fibroblasts to be lost by 'falling-through' the open-cell nature of the polyurethane foam. More difficult was the problem of scale. This was solved with the bespoke design and construction of a 'bioreactor' [14,15], which necessitated both advanced engineering and computer software designer input.

Experimentation with autologous, bioreactor-yielded CCS in a porcine large wound models demonstrated 'proof of concept' of the two-stage strategy [21]. The results of these studies, together with the published background work, led to the Human Research Ethics Committee granting approval for a three patient pilot study of CCS in the repair of post-debridement wounds in patients with extensive, full thickness burn injuries. This was due to start recruitment on 1st January 2019. However, these intentions were pre-empted when, a month earlier, a desperate case was admitted to the Royal Adelaide Hospital.

2. Case report

2.1. Admission and debridement surgeries

A 34-year old male sustained very significant burns during a house fire at midnight in a small town 147Km north of Adelaide. He was taken by ambulance to the local hospital and from there was retrieved by air ambulance to the Royal Adelaide Hospital, which houses the Adult Burn Service (the tertiary burn service for South Australia, the Northern Territory, western New South Wales and western Victoria). Passing rapidly through trauma clearance, he arrived five hours post-injury in the burns operating theatre (which had been pre-heated to 34 °C). His burns were formally mapped at this stage (Fig. 1a). Bronchoscopy demonstrated significant lower airway inhalation injury (Fig. 1b). Significant haemochromogenuria was noted on arrival (Fig. 1c) although within 3 h, the urine was clear (Fig. 2a–d) and was being produced in good volume (>0.5 ml/Kg/hr). Due to the time delay between burn and surgery, the burns were aggressively scrubbed clean with betadine-impregnated brushes and full torso and four limb escharotomies were performed (Fig. 3a–d), to facilitate anaesthesia and reduce compartment pressures during the ongoing aggressive fluid resuscitation. To further decontaminate his facial wounds, his hair was shaved and his face and scalp washed. As soon as the escharotomies were complete, the patient, lying on an Inditherm™ patient warming system (Inditherm PLC, Crawley, West Sussex, UK) was covered with a 3 M Bair Hugger™ (3 M, St. Paul, Minnesota, USA) and sterile warmed blankets. Since we anticipated performing tangential excision and expected blood loss, serial exposure of limbs allowed sub-eschar tumescence of all limb and anterior trunk tissues with 1:500,000 adrenaline and 0.05% bupivacaine by our standard technique [22]. Once we realised that the patient had very little body fat and that the fat layer looked to be compromised by the mechanism of injury, we performed fascial excision of 63% total body surface area (TBSA) full thickness burns using a Colorado Microdissection Needle™ (Stryker Corporation, Kalamazoo, Michigan, USA) and cutting monopolar diathermy. Once a limb eschar excision was complete, it was wrapped in Biobrane™ (Smith & Nephew Ltd., London, UK), held with staples, overdressed with Acticoat™ (Smith & Nephew Ltd., London, UK) and wrapped with a single crêpe bandage. Biobrane is used in this situation as a 'passive' temporiser, in the knowledge that once the escharectomy is complete, the patient has already suffered extreme physiological insults from injury and surgery and

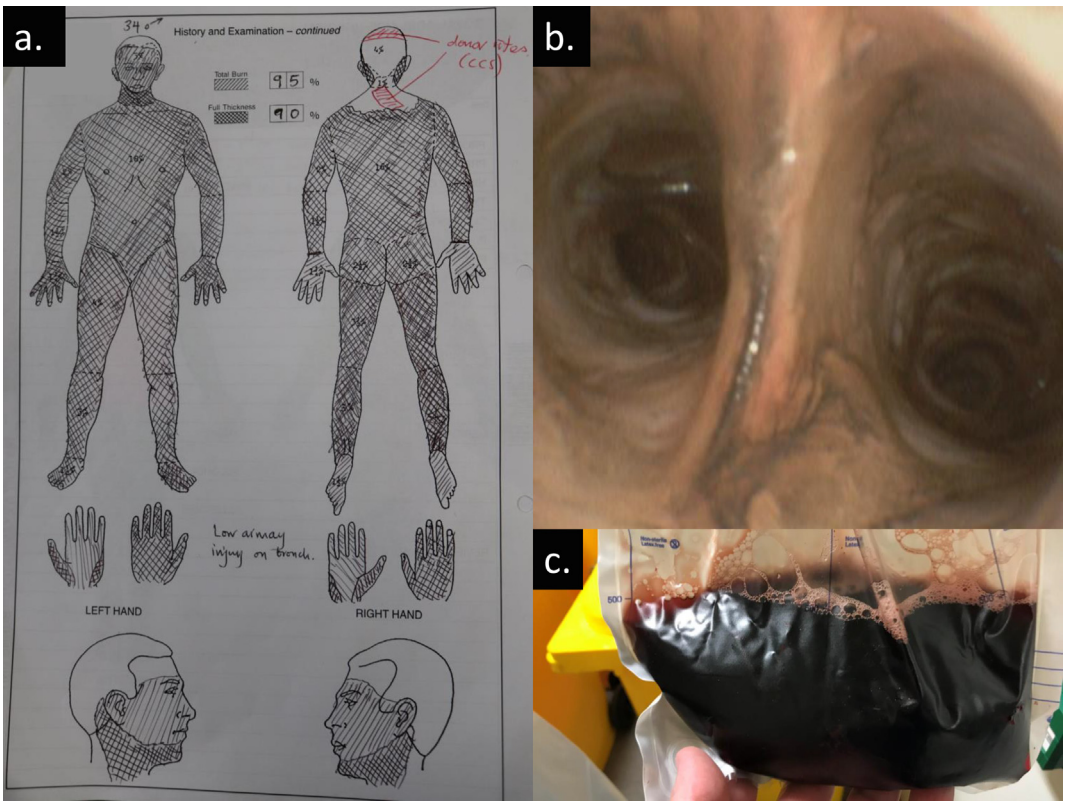

Fig. 1. Burn assessment upon arrival. a. Burn depth and estimation recorded using the Lund and Browder diagram (full thickness areas cross-hatched, mid-dermal areas hatched). b. Visualisation of the airway on bronchoscopy. c. Urine on arrival in theatre (5.05am).

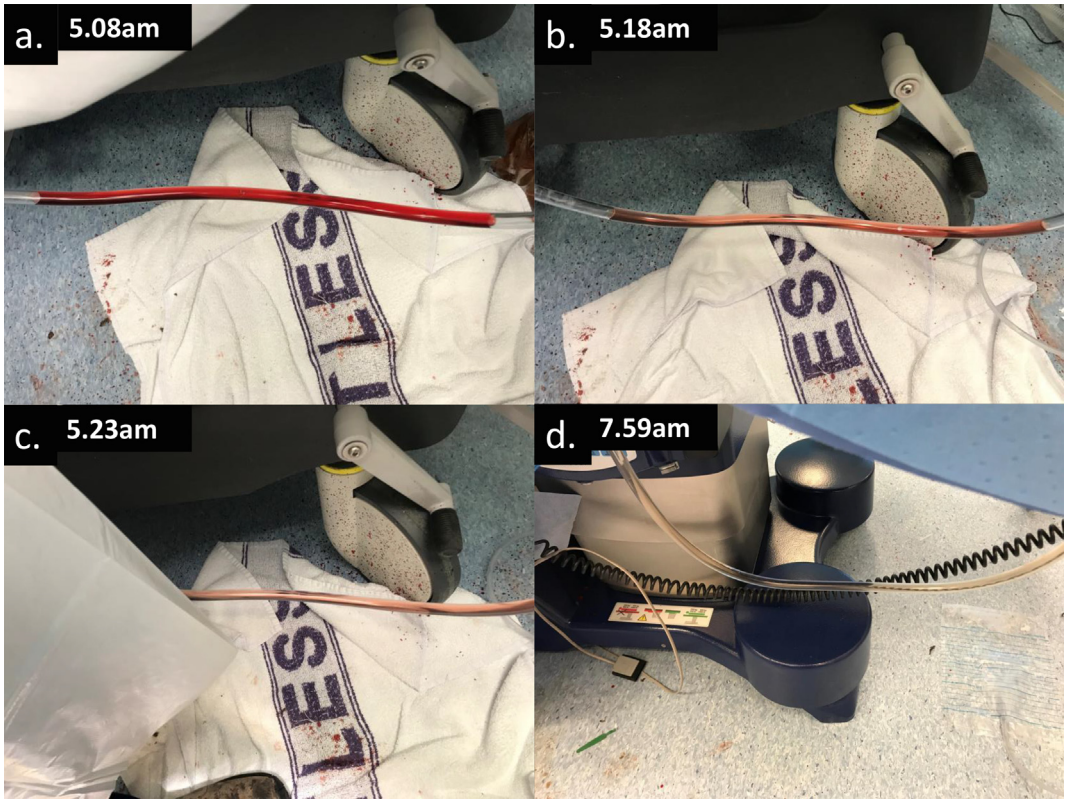

Fig. 2. Serial photographs showing the effect of rapid and aggressive fluid resuscitation on urine haemochromogenuria. Clear urine was achieved within the first three hours of the first operation. 2a. - d. indicate progression with time.

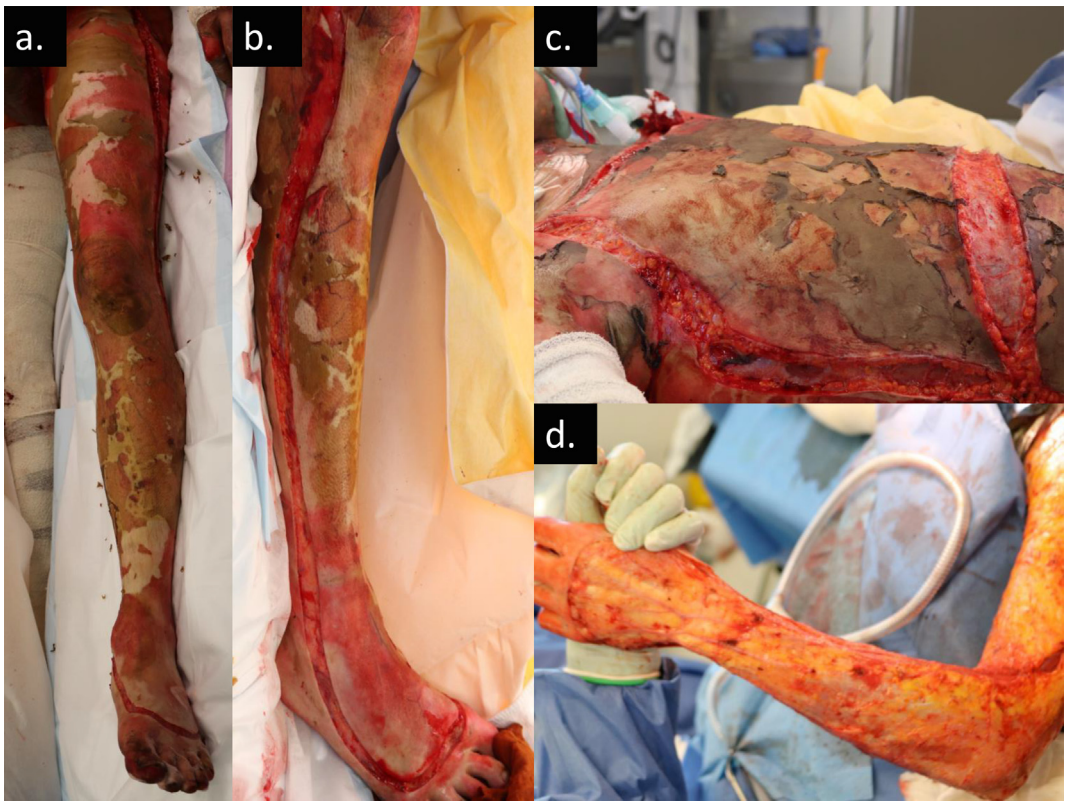

Fig. 3. a. & b. Escharotomies of lower limbs performed on admission in theatre while ongoing fluid resuscitation was performed. c. Chest escharotomy and d. arm escharotomy.

everyone involved in the surgery is exhausted after working for a long period in a hot theatre. Prologing surgery and anaesthesia to perform definitive closure (or in this case even 'active' temporisation with BTM) is not sensible. Biobrane is relatively inexpensive, quick (dry packed, easy to apply with staples), hypothetically has an evaporative water loss barrier function (thus abolishing a prime physiological stimulus to wound recognition and continued inflammation, facilitating physiological improvement) and doesn't affect the appearance of, or allow dessication of, the wound bed. Acticoat is applied because it is also easy and quick to apply to the whole body if necessary, profoundly antibacterial (Ag^{o}) and anti-inflammatory (Ag^{3+}). The Biobrane also prevents the Acticoat from staining the debrided wound bed with silver deposition or pseudoeschar formation. These materials make the wound bed easier to assess at the next operation, needing minimal refreshment before BTM application. The next limb was then exposed (Fig. 4a–d). The anterior trunk was then debrided to fascia from the limit of lower limb debridement inferiorly, to the angle of the mandible superiorly and to the mid-axial lines of the trunk and proximal limit of the upper limb eschar excisions laterally. A full platysmectomy was performed. These wounds were similarly passively temporised with Biobrane™, and overdressed with Acticoat™. A split skin graft, 7.7 cm × 15 cm, was harvested from the shaved scalp to provide the cellular components for CCS production and completed the first operation. This size of split skin graft was taken because we have calculated previously that 10 cm × 20 cm provides a sufficient number of dermal fibroblasts and epidermal keratinocytes, after isolation and individual culture, to seed up to 40 pieces of CCS, 25 cm × 25 cm (2.5 m^2) [15]. He was transferred to the Intensive Care Unit (ICU). His initial surgery had lasted 10 h.

On the ICU, over the next 48 h, he received nebulised HEPNAC (a solution of 10,000 IU of heparin with 3mls of 20% N-acetylcysteine every four hours) via his endotracheal tube. By 48 h, he was surprisingly well by all physiological parameters. However, due to the normal hair flora, the fibroblast culture created from the scalp biopsy became contaminated with Cutibacterium acne (confirmed by sterility results) and a second biopsy was required.

Two days following his admission, the patient returned to the operating theatre. Placed in the prone position, the final 22% TBSA deep burn eschar was excised from his posterior trunk and both buttocks after sub-eschar tumescence. The eschar excision again extended to fascia (Fig. 5a & b). Whilst in this position, and following limited haemostasis (with only adrenaline-soaked gauze packs and minimal bipolar diathermy), NovoSorb BTM™ was applied to his entire posterior trunk and buttock wounds and affixed with surgical staples (Fig. 5c). He was then transferred to a second operating table to place him in the supine position. The excised burn wounds to all limbs and the anterior trunk and neck were refreshed by scraping with a metal ruler and NovoSorb BTM™ was similarly applied. In areas like the neck, and axillae, the BTM is applied in 'tailored' sections to exactly fit the contours of the wounds with these areas in extension (and abduction in the case of the axillae). These sections are then 'quilted' using staples to maintain good apposition to the wound bed. By the end of the second procedure, 85% TBSA full thickness burns had been excised and NovoSorb BTM™ had been implanted into all of the resultant deep wounds (Fig. 6).

On Day 6, during a general anaesthetic dressing change, an 8 cm × 11 cm split-skin graft was harvested for the isolation and culture of fibroblasts for CCS generation from a small, unburned area of his posterior right shoulder.

2.2. Airway recovery, extubation and the initiation of therapy

The patient continued to receive HEPNAC via the endotracheal tube but, as his physiological status improved, his sedation was

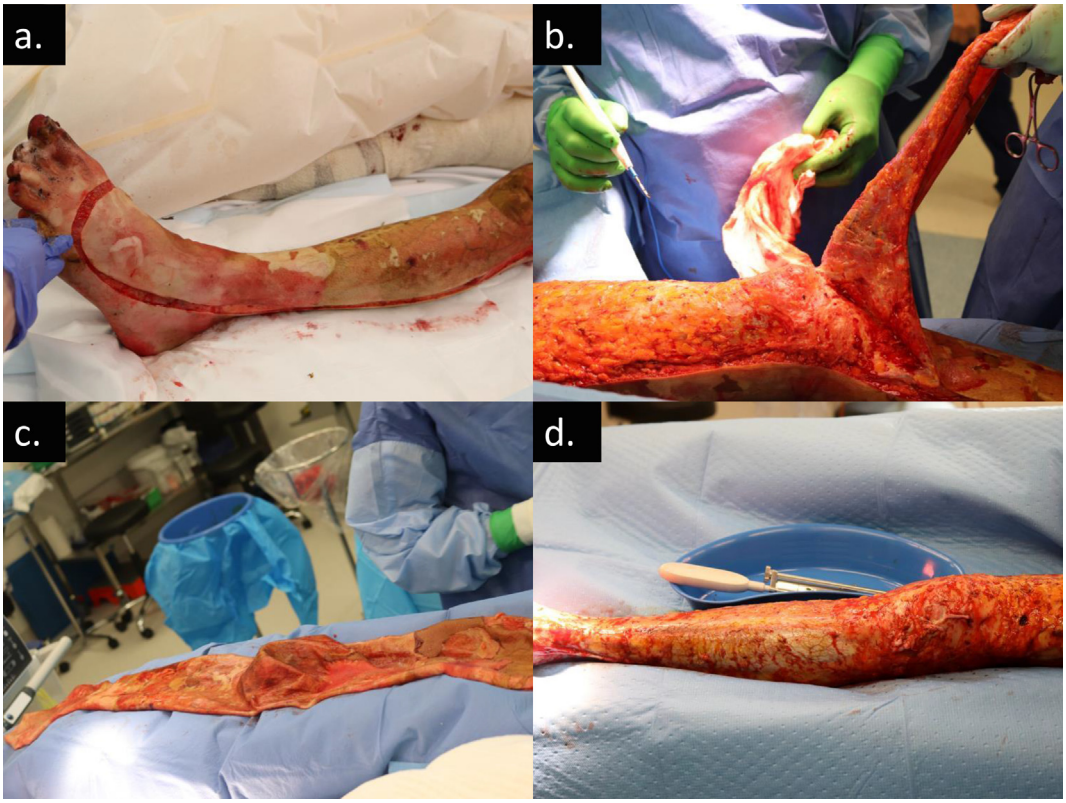

Fig. 4. a. - d. Full fascial excision of the lower limb performed at first debridement using cutting diathermy.

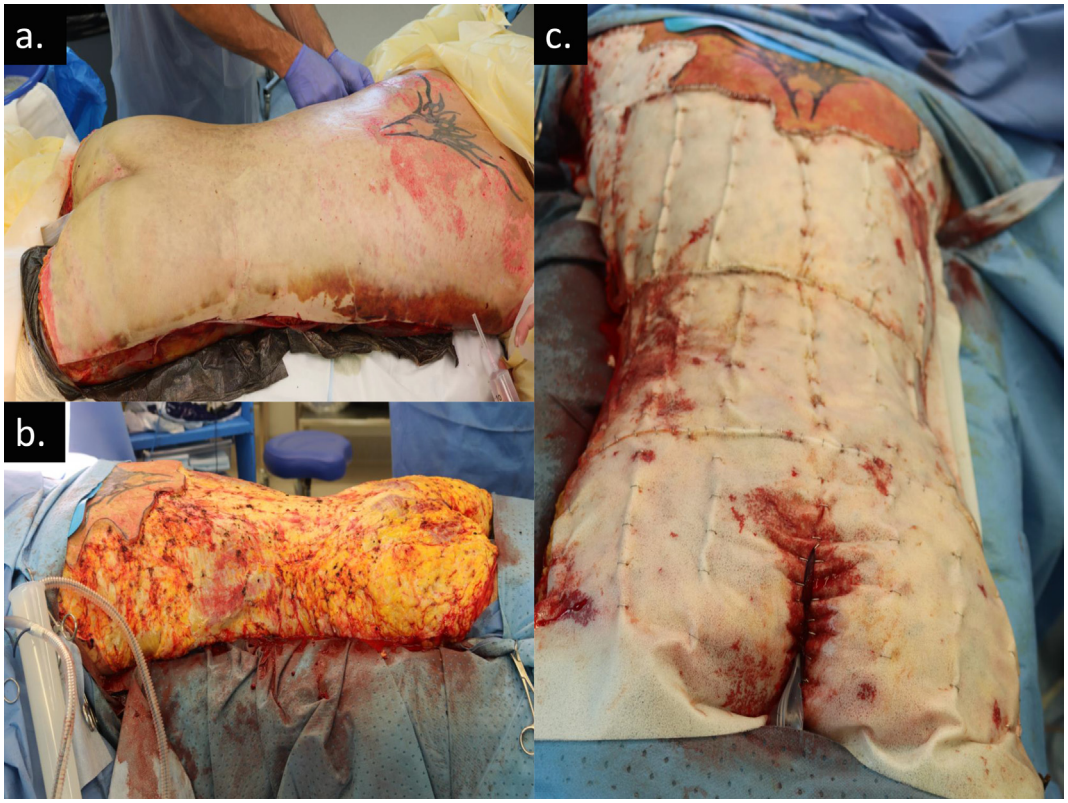

Fig. 5. a. Full-thickness burn on posterior trunk at the time of second procedure on Day 2, b. wound following burn excision, and c. freshly applied NovoSorb BTM™.

reduced. In addition, he required no vasopressor/inotrope administration. By 8 days post-burn, he was conscious and thus extubated (Fig. 7). The following day, he was transferred to the Burns Unit. Passive physiotherapy had been commenced on Day 5 post-burn (Day 3 post-NovoSorb BTM™ application) and continued on the Burns Unit, although this was progressively supplemented with

Fig. 6. At the end of the second procedure on Day 2, 85% TBSA full-thickness burns excised and NovoSorb BTM™ implanted into the resultant wounds.

Fig. 7. The first 'awake' dressing change on Day 9 following extubation the day before.

active exercises as the patient's analgesic requirements reduced. From Day 20 post-burn, the physiotherapists had him sitting on the edge of his bed, on Day 25 he stood with assistance and on Day 28, he walked with the aid of a frame in his room and then a short distance down the corridor and back. This was video-recorded when he repeated the feat 4 days later (Video 1).

2.3. BTM integration

The patient's outer dressings, Acticoat™ held by Hypafix™ (3 M, St. Paul, Minnesota, USA) on the trunk and by Hypafix™ and crêpe bandages on the limbs, were changed every three days. Whilst intubated and on the ICU, these dressing changes were performed under sedation. Once extubated, the first two dressing changes were performed in the operating theatre to ensure a rapid and painless procedure, but thereafter his dressing changes were usually performed on the ward, unless another procedure accompanied the dressing change (such as central line changes, or aggressive passive major joint mobilisation by the therapists). During each dressing change, the BTM was left open (aired) for up to 1 h and washed with a chlorhexidine-impregnated sponge before fresh Acticoat™ was re-applied. Almost all of the 85% TBSA NovoSorb BTM™ integrated evenly and completely by Day 40 post-application (Day 42 post-burn) (Fig. 8). There were no infections in the BTM. The only disappointing areas were over the subcutaneous borders of both tibiae (Fig. 9a). On Day 44 post application, the non-integrated NovoSorb BTM™ seal and foam overlying these bones was removed. The underlying periosteum was found to be non-viable and was detached with a periosteal

Fig. 8. Integrated NovoSorb BTM™ on Day 40 with the characteristic 'peach-coloured' appearance.

Video 1.

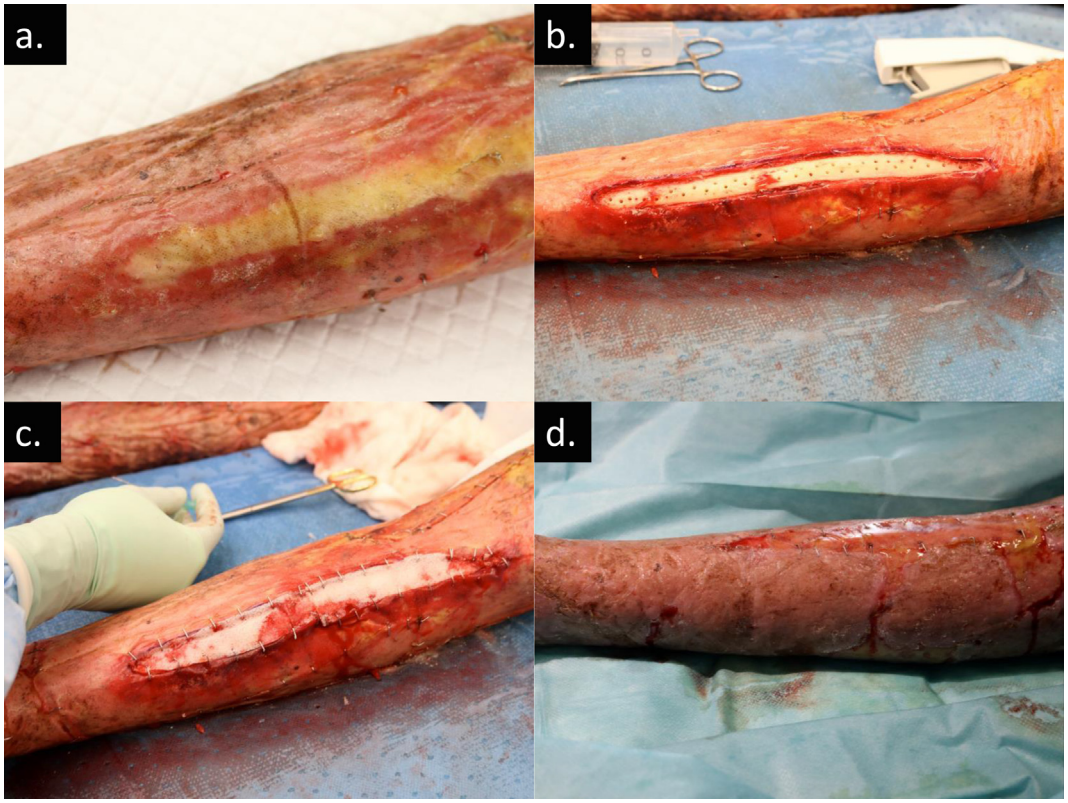

Fig. 9. a. The majority of BTM lower leg integrated, except for the anterior border of the tibia (Day 46). b. Periosteum removed and cortical drill holes in tibia. c. Fresh BTM applied and secured to surrounding tissue with staples. d. Following successful BTM integration ready for CCS application over the tibia on Day 123). This is surrounded by previously applied and healed CCS.

elevator. Multiple holes were drilled into the tibial cortices with a dental burr and fresh NovoSorb BTM™ was applied (Fig. 9b & c). Tissue from the tibial medulla filled and integrated the new NovoSorb BTM™ strips over the next 77 days, by which time the previously integrated NovoSorb BTM™ around them had undergone delamination, CCS application and healing (Fig. 9d).

2.4. CCS production

In an ISO 7 Cleanroom environment, the split skin graft biopsies had been enzymatically divided into dermis and epidermis, for individual cell isolation and culture. The CCS polyurethane scaffold (25 cm × 25 cm × 1 mm) was prepared with Fresh Frozen Plasma (FFP) and seeded with the cultured fibroblasts. These were kept in submerged culture until they were seen to fill the foam pores and lay down collagen inside the 'dermal' foam component of the CCS (1 mm thick, unsealed, biodegradable NovoSorb™ polyurethane foam, Fig. 10a). At this time point, cultured keratinocytes were seeded and the media changed to supplement both cells types. The CCS was cultured for a total of 14 days (Fig. 10b). Unfortunately, some components of the bioreactor were not available at the time of patient admission requiring an enormous amount of time, both day and night, to create the CCSs semi-manually. They thus had to be created in 'batches', and the first batch (of 5 pieces of CCS) was ready by Day 50 post-burn.

2.5. Non-CCS wound closure

Conservatively managed - Certain areas of this patient's burn injuries were deemed superficial enough, or critically important enough, to heal spontaneously. These amounted to 7% TBSA and included face, genitalia, both palms, right sole and the lower portion of the 'donor site' on his posterior upper back. In retrospect, the left palm and the right sole would have benefitted from sharp surgical debridement, but the desire/need to re-establish glabrous skin with deep attachment to the palmar/plantar fascia required a conservative approach.

Use of available skin graft - The extended anterior neck (2% TBSA) and the posterior trunk and buttocks (15% TBSA) received meshed split skin graft (1:1.5 on the neck on Day 41, and 1:3 on the back/buttocks on Day 71) from serial harvest of the posterior shoulder donor sites. The dorsum of both hands received sheet autograft from the scalp, the right on Day 41 and the left on Day 57.

Additionally, on Day 113, small pieces of scalp graft were subjected to Meek™ treatment (Humeca, Borne, Netherlands) at two different ratios. The anterior trunk and the left circumferential forearm received 1:4, whereas 1:9 was used on the left circumferential arm. The total area receiving Meek™ grafting was 13.5% TBSA. Some residual wounds (dorsum right foot, posterior right lower limb) totalling 2% TBSA, received meshed SSG to complete his wound healing on Day 215.

2.6. CCS application and result

In total, 6 batches of CCS were produced and applied (although batches 5 and 6 were merely used to 'touch-up' areas predominantly already healed by previous CCS application). The first batch was applied on Day 50 following delamination of the NovoSorb BTM™ over his anterior trunk, groins and bilateral anterior thighs. These neo-dermal surfaces were refreshed by gentle dermabrasion. The lateness of this application followed a delay in CCS production resulting from Christmas Holiday closures of media suppliers and the almost complete Australia-wide exhaustion of the supply of cell factories for cell culture. Five pieces were applied, covering

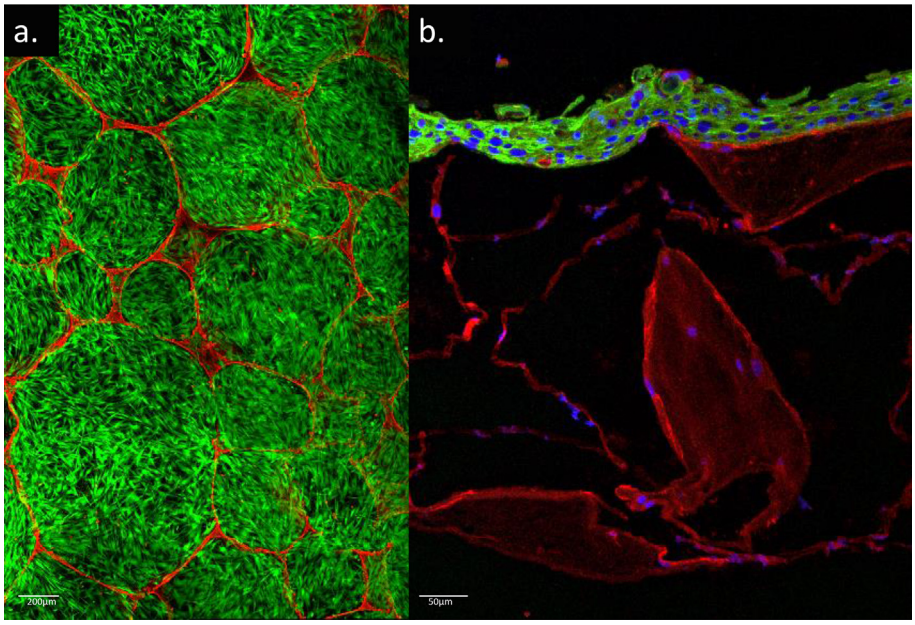

Fig. 10. Composite cultured skin (CCS) confocal micrographs before application showing a. Live/dead staining of the foam (red) filled pores with live fibroblasts (green) before keratinocyte inoculation b. showing positive superficial cytokeratin staining and fibroblasts (nuclei blue) . (For interpretation of the references to colour in this figure legend, the reader is referred to the web version of this article.)

15% TBSA. The CCS foam with the cultured keratinocytes and fibroblasts was carefully removed from the cassette onto square sheets of Mepitel™ One (Mölnlycke Health Care, Gothenburg, Sweden), which were then placed onto the prepared wound bed. The Mepitel™ was fixed with staples to the wound (Fig. 11a & b) and overdressed with Acticoat™. The first batch of CCS successfully closed only 4% TBSA correlating closely with margins between the pieces and indicating that, centrally, they were deficient. A second 5-piece batch, covering 14% TBSA (circumferential left upper limb, anterior shoulders and circumferential left thigh), was applied on Day 57, successfully closing 7% TBSA. Disappointed with a successful closure rate of only 18% (7 of 39% TBSA) for these two initial batches, fundamental changes were introduced into the culture regimen.

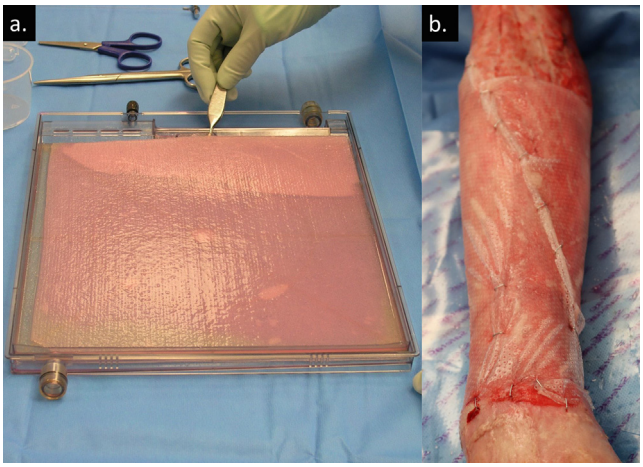

Fig. 11. a. The bioreactor cassette with the CCS foam containing co-cultured cells being gently prepared for application. b. The CCS applied with Mepitel One onto the lower arm and stapled.

Batches 3 and 4 were applied on Day 78, covering 32% TBSA (upper chest, circumferential right upper limb, circumferential right lower limb, circumferential left leg, the dorsum of both feet and an area on the left sole of foot). The introduced changes were highly effective and the CCS healed 30% TBSA, with a 94% success rate for this optimised CCS variant. In total, CCS effected complete and robust healing of 42% TBSA. Progression of *in vivo* CCS integration was demonstrated by histological preparation on/staining of punch biopsies on Day 21, and at 3 and 6 months (Fig. 12a–c).

3. Outcome

The patient was discharged 249 days post-injury (just over 35 weeks), delayed by the unavailability of a bed at the rehabilitation hospital. Fig. 13a–c demonstrate wound closure of the chest, right upper limb and both lower limbs with BTM and CCS alone. The contrast between CCS and meek grafting at this stage was obvious (Fig. 14). Non-compliance with hand splinting contributed to the development of a significant intrinsic-minus deformity of his left hand. He self-discharged from rehabilitation after 107 days (9 days before the anniversary of his injury) to live with his 97-year old Grandmother. He has since undergone some left hand and left elbow release, but has not required any reconstructive surgery to other major joints, including all areas treated with CCS. He is walking independently and occasionally uses a walking stick. In a recent 6-minute walk test, he recorded a distance of 245 m. For long distances, he has an electric wheelchair.

Scar Outcomes (Fig. 15) were recorded at approximately 1-year post CCS application (Table 1) by a Senior Physiotherapist. The Patient and Observer Scar Assessment Scale v2.0 (POSAS) [23] was used and has been recommended for use where only one measure of the scar is required and to gain the patient's perspective of their scar [24]. Patient scores for all types of wound closure indicated a very good cosmetic outcome. This is despite the patient being non-compliant with pressure garment therapy and only minimally compliant with scar massage. No pain or itch was reported at any of the assessed sites. Observer scores also indicated

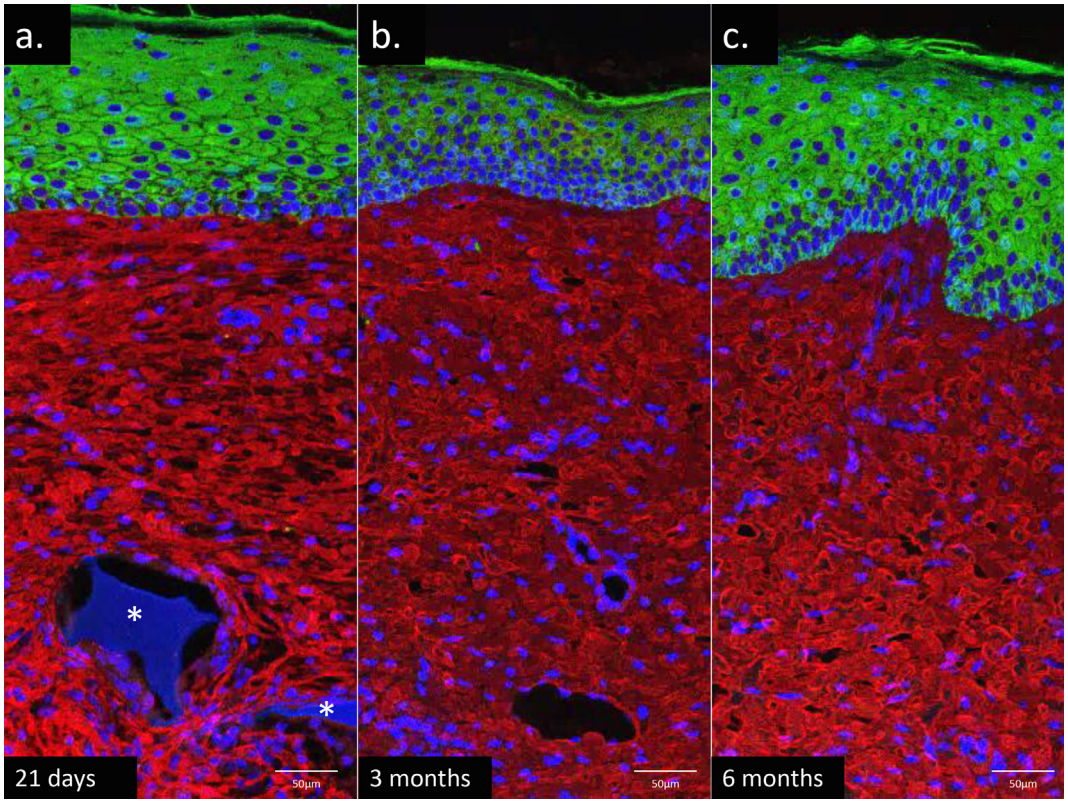

Fig. 12. a. At 21 days Collagen I (red) and Cytokeratin (green) staining *in vivo* of CCS punch biopsies. This demonstrates the gradual disappearance of the polyurethane foam (*), predominantly by simple hydrolysis (99%). b. At 3 months, and c. At 6 months. Final microscopic remnants of hard segment are phagocytosed by giant cells. (For interpretation of the references to colour in this figure legend, the reader is referred to the web version of this article.)

Fig. 13. a. Left lower leg at discharge (Day 249 post-admission), with wound closure obtained by BTM and CCS only. b. Anterior trunk and arms on the same day (dotted lines enclose CCS areas) and c. Bilateral lower legs (172 days post-CCS application).

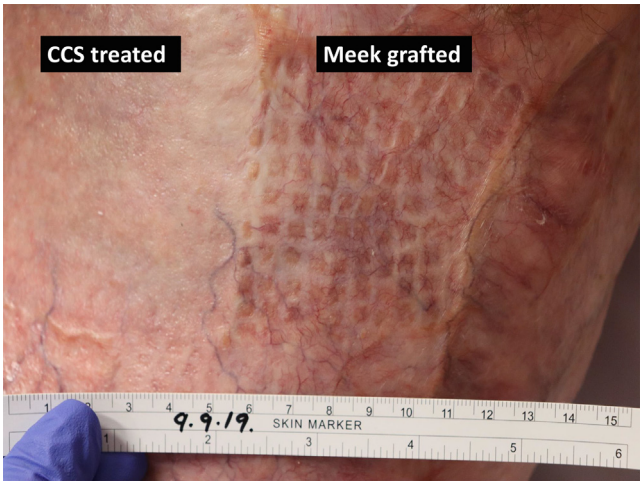

Fig. 14. Meek mesh-grafting pattern (165 days post-application) grafting versus CCS on the left anterior trunk (200 days post-application).

very good scar outcomes for all types of wound closure with a tendency for CCS and sheet skin graft wounds having better outcomes. These very good scar outcomes mirror those previously reported in other NovoSorb BTM™ studies [9,10,16].

4. Patient consent statement

The patient described in this article has consented to the publication of his images and discussion of his case.

Declaration of Competing Interest

The authors declare the following financial interests/personal relationships which may be considered as potential competing interests: Professor Greenwood developed Biodegradable Temporising Matrix (BTM) between 2004 and 2016 in collaboration with PolyNovo Biomaterials Pty Ltd. He has no current affiliation with PolyNovo Biomaterials Pty Ltd, and does not receive any fee for

Fig. 15. a & b One year post CCS (Day 405 post injury), showing good bilateral shoulder movement.

Table 1
POSAS Scores for CCS, sheet and meshed skin graft and Meek graft at 12 months post-healing.

Wound closure technique	Site	Timeframe (months, days)	POSAS observer	POSAS observer overall	POSAS patient	POSAS patient overall
CCS	L) abdo	12 m 14 d	12	2	8	1
	L) knee	12 m 7 d	19	3	12	1
	R) calf	11 m 17 d	17	2	10	2
	L) chest	11 m 17 d	15	2	18	1
	R) forearm	11 m 17 d	16	2	8	1
	R) arm	11 m 17 d	11	2	8	1
SSG sheet	R) hand dorsum	12 m 23 d	17	2	8	2
MEEK 1:4	L) forearm	10 m 12 d	24	3	10	2
	secondary intention	11 m 17 d+	25	3	14	2
SSG meshed 1:3	back	12 m	18	3	10	1

consultation, presentation, travel or promotion. He retains a small shareholding.

References

[1] Li A, Dearman BL, Crompton KE, Moore TG. JE Greenwood 'Evaluation of a novel biodegradable polymer for the generation of a dermal matrix'. J Burns Care Res 2009;30(4):717–28.

[2] JE Greenwood, A Li, B Dearman, TG Moore 'Evaluation of NovoSorb™ novel biodegradable polymer for the generation of a dermal matrix. Part 1: In-vitro studies' Wound Practice and Research February 2010;18(1):14-22.

[3] JE Greenwood, A Li, B Dearman, TG Moore 'Evaluation of NovoSorb™ novel biodegradable polymer for the generation of a dermal matrix. Part 2: In-vivo studies' Wound Practice and Research February 2010;18(1):24-34.

[4] JE Greenwood, BL Dearman 'Split-skin graft application over an integrating, biodegradable temporising polymer matrix: Immediate and delayed' Journal of Burn Care and Research Jan/Feb2012;33(1):7-19.

[5] JE Greenwood, BL Dearman 'Comparison of a sealed, polymer foam biodegradable temporising matrix against Integra™ dermal regeneration template in a porcine wound model' Journal of Burn Care and Research Jan/Feb2012;33(1):163-173.

[6] Dearman BL, Stefani K, Li A, Greenwood JE. 'Take of a polymer-based autologous cultured composite 'Skin' on an integrated temporising dermal matrix: proof of concept'. J Burn Care Res 2013;34(1):151–60.

[7] Wagstaff MJD, Driver S, Coghlan P, Greenwood JE. 'A randomised, controlled trial of Negative Pressure Wound Therapy of pressure ulcers via a novel polyurethane foam'. Wound Repair Regen 2014;22:205–11.

[8] Dearman BL, Li A, Greenwood JE. Optimisation of a polyurethane dermal matrix and experience with a polymer-based cultured composite skin. J Burn Care Res 2014;35(5):437–48.

[9] Wagstaff MJD, Schmitt BJ, Coghlan P, Finkemeyer JP, Caplash Y, Greenwood JE. A biodegradable polyurethane dermal matrix in reconstruction of free flap donor sites: a pilot study. ePlasty 2015;15:102–18.

[10] Wagstaff MJD, Schmitt BJ, Caplash Y, Greenwood JE. Free flap donor site reconstruction: a prospective case series using an optimized polyurethane temporizing matrix. ePlasty 2015;15:231–48.

[11] Greenwood JE, Wagstaff MJD, Rooke M, Caplash Y. Reconstruction of extensive calvarial exposure after major burn injury in two stages using a biodegradable polyurethane matrix. ePlasty 2016;16:151–60.

[12] Wagstaff MJD, Caplash Y, Greenwood JE. Reconstruction of an anterior cervical necrotizing fasciitis defect using a biodegradable dermal substitute. ePlasty 2017;17:29–36.

[13] JE Greenwood, MJD Wagstaff. 'The use of biodegradable polyurethane in the development of dermal scaffolds' Chapter 22 In Cooper SL & Guan J (Eds) 'Advances in Polyurethane Biomaterials' 2016. Woodhead Publishing Series in Biomaterials, (Elsevier Inc.), Duxford, UK. ISBN:978-0-08-100614-6.

[14] JE Greenwood 'Hybrid biomaterials for skin tissue engineering' Chapter 9 In Albanna MZ & Holmes JH IV (Eds) 'Skin Tissue Engineering and Regenerative Medicine' 2016. Academic Press (Elsevier Inc.), London, UK. ISBN:978-0-12-801654-1.

[15] Greenwood JE. The evolution of acute burn care - retiring the split skin graft (Hunterian Lecture). Ann R Coll Surg Engl 2017;99:432–8. https://doi.org/10.1308/rcsann.2017.0110.

[16] Greenwood JE, Schmitt BJ, Wagstaff MJD. Experience with a synthetic bilayer biodegradable temporising matrix in significant burn injury. Burns Open 2018;2(1):17–34.

[17] MJD Wagstaff, I Salna, Y Caplash, JE Greenwood 'Use of a biodegradable synthetic dermal matrix in the reconstruction of defects after serial debridement for necrotising fasciitis: a case series' Burns Open January 2018;3(1):12-30. DOI: https://doi.org/10.1016/j.burnso.2018.10.002.

[18] L Damkat-Thomas, JE Greenwood, MJD Wagstaff 'A synthetic Biodegradable Temporising Matrix in degloving lower extremity trauma reconstruction: A case report' Plastic and Reconstructive Surgery Global Open April 2019;7(4): e2110. DOI: https://doi.org/10.1097/GOX.0000000000002110

[19] L Damkat-Thomas, JE Greenwood 'Scarring after burn injury'. Published in 'Scars' (online book) by InTech Open, 2019. DOI: 10.5772/intechopen.85411.

[20] Greenwood JE. A paradigm shift in practice - the benefits of early active wound temporisation rather than early skin grafting after burn eschar excision. Anaesth Intensive Care 2019. in press.

[21] Greenwood JE. Bioreactor Development for Composite Cultured Skin production. J Burn Care Res 2016;37(3). Suppl:S266.

[22] JE Greenwood 'Development of patient pathways for the surgical management of burn injury' ANZ Journal of Surgery Sep 2006:76(9);805-811.

[23] Draaijers LJ, Tempelman FR, Botman YA, Tuinebreijer WE, Middelkoop E, Kreis RW, van Zuijlen PP (2004). The patient and observer scar assessment scale: a reliable and feasible tool for scar evaluation. Plastic and Reconstructive Surgery 2004;113(7):1960-1965.

[24] Tyack Z, Simons M, Spinks A, Wasiak J. A systematic review of the quality of burn scar rating scales for clinical and research use. Burns 2012;38(1):6–18.

CHAPTER 4:
Assessment of Skin Culturing Parameters for Clinical Use

4.1 Overview

As mentioned in the Chapter 3 overview, optimisation studies were in progress when a 95% burn patient presented. The following changes tested and described within were not yet validated to the level of Good Manufacturing Practice and therefore could not be implemented for the clinical use of that patient. The main aim of refining the culturing techniques is to direct them towards animal origin free methods for clinical use. The current procedures for fabrication of CCS and many skin substitute models use animal-derived products for optimal proliferation and differentiation of skin cells. A clinical product that will be translatable is one that can eliminate or reduce these components. Optimising the primary culturing elements to remove animal-origin products endorsed an inquiry into keratinocyte and fibroblast media and the use of lethally irradiated fibroblasts for co-culture of keratinocytes. These parameters require assessment of cost, effectiveness, and product availability before any modifications. The porcine skin culture model was also challenged with these changes. The following chapter is divided into subsections for each parameter tested with separate materials and methods followed by results and an inclusive discussion.

4.2 Comparison of Keratinocyte Media and Feeder Layer Removal

The use of serum-free media to eliminate the traditional use of foetal bovine serum (FBS) and feeder layer cells for keratinocyte proliferation has been well established [61, 62]. Based on the original MCDB-153 serum-free medium, multiple defined formulations now exist from commercial sources. Although, additional growth factors, hormone supplements (e.g., bovine pituitary extract (BPE)) or matrices that promote cell attachment are still required for *in vitro* culture. One suggested prerequisite with serum-free media is the addition of a collagen coating matrix before cell inoculation. For clinical purposes and testing, an animal origin-free recombinant matrix was purchased from Cascade Biologics (Invitrogen, Carlsbad, CA, USA) (R-011-K). The coating matrix comprises two components, a Dilution Medium (DM) and a Coating Matrix (CM), added directly to each culture vessel. This matrix is intended to be used in conjunction with serum-free keratinocyte media. EpiLife™ is a basal medium (M-EPI-500-CA) requiring supplemental additives, supplement S7 (S-017-5) (GIBCO, Thermo Fisher Scientific, Grand Island, NY, USA). This medium was

chosen for comparison testing for its potential in clinical applications. However, at this time point, the matrix and the medium are not intended for human therapeutic use. Another serum-free keratinocyte media from GIBCO™ (Thermo Fisher Scientific, Grand Island, NY, USA) is the Defined keratinocyte-serum free medium (dKGM) (1x) (10744-019) kit, also requiring the use of a coating matrix kit for optimal cell growth. This formulation is advantageous as it already has an FDA master file. The three media tested to support keratinocyte cell growth include EpiLife™, dKGM and SEL-KGM (in-house prepared media). The current SEL-KGM media and culture system is based on Rheinwald and Green's original advancements which necessitates co-culture with irradiated fibroblasts as the feeder layer. The feeder layer is growth-arrested and secretes grow factors and extracellular matrix proteins to support keratinocyte proliferation. Irradiated mouse 3T3 feeder cells were originally used to support keratinocyte culture [37, 63], but with the aim of animal origin-free, it has been shown they can be replaced with screened human fibroblasts donated from discarded surgical skin operations [64, 65]. This method is well established within the Skin Engineering Laboratory and has been used by other laboratories aiming for animal component-free processes [66]. The human feeder layer and SEL-KGM media will be used in all experiments to compare alternative media types and conditions.

Another substitute to replace the feeder cell layer is a product from Corning®, PureCoat ECM Mimetic cultureware (Corning, NY, USA). The Mimetic cultureware is coated with synthetic animal-free peptides (collagen I) linked to a proprietary surface and has been previously tested with keratinocyte culture [67]. It is a ready to use coated surface with no special pre-handling requirements. However, at the time of investigation, large vessel sizes were not available, and although they are now under development for scale-up, the cost may be a limiting factor.

4.2.1 Materials and Methods

4.2.1.1 Buffers

All chemicals used were of analytical grade. For cell culture, all solutions and media were sterile and stored according to manufacturers' instructions. Buffers included phosphate buffered saline (without calcium chloride and magnesium chloride) (DPBS) 1x sterile

(Sigma-Aldrich, St. Louis, MO, USA - D8537-500mL), and Hanks' balanced salt solution (HBSS) (Sigma-Aldrich, H6648-500mL). These buffers were used as a base for wash buffers with the addition of serum. For non-sterile analyses (e.g., immunofluorescence staining), a 20x DPBS stock solution was diluted with MilliQ water to 1x. Other wash buffers included PBS + 0.1% Tween 20 and PBS + 0.1% Triton X-100. Blocking buffer, 0.5% human serum albumin (HSA) and 2% FBS in 1x PBS. Washing buffer, HBSS + 5% FBS.

4.2.1.2 Antibodies and staining reagents

Staining keratinocytes for intracellular proteins for flow cytometric analysis and immunofluorescence, cytokeratins K14, K10, and negative controls were used (Appendix II -method and Appendix III- antibodies). Keratinocyte colonies were stained using Rhodamine B and read on a microplate reader for fluorescence analysis. FACS fix (1x PBS, 1% formalin, 0.1m D-glucose, 0.02% sodium azide) and 4% formaldehyde (Invitrogen, Thermo Fisher Scientific, FB002) were the fixatives used.

4.2.1.3 Media and associated subculture reagents

EpiLife™ Medium contains 60µM calcium (M-EPI-500-CA) and is combined with Supplement S7 (S-017-5) from ThermoFisher Scientific. dKGM from GIBCO-Life technologies consists of a basal medium (10785-012) and supplement (10784-015). SEL-KGM is abbreviated for Skin Engineering Laboratory (SEL) keratinocyte growth medium (KGM). This formulation is based on Green's original medium [37], see Table 4.1 for listed SEL-KGM components. This contains Dulbecco's Modified Eagle Medium: Nutrient Mixture F-12 (DMEM/F12) with GlutaMAX (ThermoFisher, 10565041 or 195253), 1% (v/v) serum, 0.5µg/mL hydrocortisone, 10ng/mL human recombinant epidermal growth factor (hEGF), 5µg/mL Insulin Actrapid (Novo Nordisk, AUST-R 16923), 10ng/mL cholera toxin and 25µg/mL Adenine. All SEL-KGM supplements were purchased from Sigma-Aldrich and prepared in house for sterility and batch testing. The serum used can be either pooled AB+ve normal human serum or foetal bovine serum (FBS) (CellSera, NSW, AUS, AU-FBS/PG). Antibiotic antimycotic (AA) solution (Sigma-Aldrich, A5955-100ML) was standardised at 1% (v/v) for all keratinocyte media.

Table 4.1 SEL-KGM list of supplements.

SEL-KGM				
Component	**Concentration**	**Catalogue #**	**Company**	**Location**
DMEM/F12 + GlutaMAX™	1:1	1065-018	GIBCO™, Thermo Fisher Sci-entific	Grand Island, NY, USA
FBS	1% (v/v)	1608A	CellSera	NSW, AUS
Hydrocortisone	0.5µg/mL	H0396	Sigma-Aldrich	St. Louis, MO, USA
Human recombinant epidermal growth factor (hEGF)	10ng/ mL	E9644	Sigma-Aldrich	St. Louis, MO, USA
Insulin Actrapid	5µg/mL	AUST-R 16923	Novo Nordisk	Clayton, North Carolina, USA
Cholera toxin	10ng/mL	C8052	Sigma-Aldrich	St. Louis, MO, USA
Adenine	25µg/mL	A-2786	Sigma-Aldrich	St. Louis, MO, USA
Antibiotic antimycotic	1% (v/v)	A5955-100ML	Sigma-Aldrich	St. Louis, MO, USA

For subculture of keratinocytes, Trypsin-EDTA 0.05% (1X) (GIBCO-ThermoFisher Scientific, 25300) and Trypsin inhibitor from Glycine max (soybean) (SBTI) (Sigma-Aldrich, T6522) prepared at 1x working solution of 1mg/mL were used along with two rinsing media containing Dulbecco's Modified Eagle's Medium (DMEM) (Sigma-Aldrich, D1145) 5% FBS and 2% FBS. Cell counting was performed using Trypan Blue solution (Sigma-Aldrich, T8154).

4.2.1.4 Cell culture and experimental design

The use of discarded skin samples and human cells was approved by the Royal Adelaide Hospital ethics committee, HREC/18/CALHN/539 and R20180811 (Appendix I). Normal human epidermal keratinocytes were isolated from donated skin samples and were pre-cultured using the laboratories standard operating procedure for keratinocyte isolation and culture (Appendix IV). The culture conditions for the human feeder layer are also described within appendix IV. In brief, cells were grown in SEL-KGM with a layer of irradiated human dermal fibroblasts (iHFbs) until 80-90% confluence and cryopreserved until required. These experiments used three different biological cell lines for each experiment. Before testing, each cell line was passaged once in the corresponding medium to prevent a lag phase from transitioning media. Primary to passage two cells were used for testing. Subculture was performed by removing the feeder layer with a co-trypsinisation method of pre-warmed trypsin-EDTA 0.05% for two minutes followed by a PBS wash and a second trypsin-EDTA incubation at 37°C for up to 20 minutes. Cells were then quenched with soybean trypsin inhibitor and washed with DMEM 2% Serum and DMEM. Centrifuged at 220g for five minutes and cell suspensions were resuspended in the appropriate medium for cell counting using trypan blue. Cells were plated according to experimental design (see outline below). T75, T175 culture flasks or cell stackers were used for expansion and cell counting analysis. T25 culture flasks (for flow cytometry), six and 24 well-plates (for Rhodamine B), and 8-well plates (Ibidi GmbH) (for immunofluorescence). For EpiLife™ and dKGM culture, the vessels were pre-coated with the coating matrix (as per manufacturers instructions- Appendix V) prior to cell inoculation, and SEL-KGM vessels were pre-inoculated with iHFbs. Media were exchanged every 2-3 days until experimental end. Vessels were washed once with PBS and stained or used accordingly. The media testing was co-aligned with the feeder removal testing, and therefore, the Mimetic cultureware was tested in parallel.

Experiment 1. Primary keratinocytes and coating substrates – 6-well plates and Mimetic 6-well cultureware plates, three biological replicates of primary keratinocytes. Media compared included (1) SEL-KGM + feeders, (2) EpiLife™ + CM, and (3) dKGM + CM. Plated at 20,000 hKs/cm^2. Duplicate experiments were performed. Conditions were assessed by Rhodamine B staining and cell morphology by phase-contrast microscopy. The three media conditions and coating substrates were further tested in larger culture vessels (T75/T175 flasks or cell factories) (excluding Mimetic cultureplates from subsequent experiments). The fold-increase in cell number, population doubling time (hrs) and day of harvest were assessed for each media type. Five biological replicates were tested for establishing primary cells. Figures 4.1-4.3.

Experiment 2. Keratinocyte characterisation, (a) – T25 flasks, at 5,000 hKs/cm^2 harvested on Day 6 for cell count comparison and flow cytometry staining for cytokeratin 10 and 14. Media conditions were (1) SEL-KGM + feeders, (2) EpiLife™ + CM, and (3) dKGM + CM. 50,000 cells were removed for flow cytometry analysis using Becton Dickinson FACSAria II. **(b)** – 8-well plates (Ibidi GmbH, Martinsried, Germany) at 10,000 hKs/cm^2 for media conditions as per 2a were evaluated for immunofluorescence staining with cytokeratin 10 and 14 on Day 5. Figure 4.4.

Experiment 3. Keratinocyte expansion and subculture, – involved the use of two of the media conditions (SEL-KGM and EpiLife™) and cells in larger culture vessels (T75/T175 flasks or cell factories). The fold-increase in cell number, population doubling time (hrs) and day of harvest were assessed for each media type. Four biological replicates were tested for passage one. Figure 4.5.

Digital photographs – phase contrast images were photographed using a Olympus digital camera with adapter (Olympus C5060-ADUS) to an inverted microscope (Olympus, CK40 microscope). Images were taken to assess cellular morphology. Photos were taken at multiple magnifications with a micrometre calibration optical glass slide to assist with measurements using ImageJ (https://imagej.nih.gov/ij/).

Cell counting – Cells were resuspended in the appropriate media, and a small sample, 20-40μL, was removed for counting. Generally, equal volumes of 0.4% trypan blue solution (Sigma-Aldrich, T8154) were gently mixed. Cells were counted using a Neubauer haemocytometer (Weber, UK) and recorded for calculating cell concentrations, viability, and total cell numbers.

Statistical Analyses – Data analysis and charting was performed using GraphPad PRISM version 8 for windows GraphPad Software, San Diego, California USA, www.graphpad.com. Comparisons among multiple groups utilised one-way analysis of variance (ANOVA) with further post-hoc analysis using the Tukey test. Comparisons between two groups utilised paired t-tests. Data are presented with the mean variables and standard deviation. Differences were considered statistically significant at $*p < 0.05$.

4.2.2 Results

4.2.2.1 Cost analysis of keratinocyte medium

A cost analysis for modifying media was required for consideration to support a change. The supplemented media cost per 500mL bottle are, SEL-KGM AU$59.75, EpiLife™ AU$375.00 and dKGM AU$257.00. The cost of SEL-KGM preparation is significantly reduced with bulk production capabilities. The accompanying co-culture costs, i.e., coating matrix, feeder cells, etc., are not built into these prices and warrant inclusion. The coating matrix was costed at ~$0.11/cm^2, iHFbs at 0.50/cm^2 and the Mimetic cultureware at $1.67/cm^2. Based on these costs, calculations to estimate the total keratinocyte media expense for cell expansion per cm^2 of CCS are in Table 4.2.

Table 4.2 The estimated cost of media for the fabrication per cm^2 of CCS with the different keratinocyte media and associated coating substrate. iHFbs – irradiated human fibroblasts, CM – Coating matrix, CCS – Composite cultured skin. Note this is not an estimated unit cost as it does not include reagents, consumables, facilities, labour, or quality assurance (QA) testing costs.

SEL-KGM/iHFbs	EpiLife™/CM	dKGM/CM
$6.09	$7.66	$6.38

4.2.2.2 Keratinocyte primary culture with media ± serum and coating substrates

The proliferative capacity of each medium condition was evaluated in parallel with a new cultureware vessel. Results from three different primary cell lines showed the irradiated human fibroblast feeders provided growth assistance with all three test media (Figure 4.1a), unlike the collagen-coated matrix, which produced few dendritic cells in the SEL-KGM, rounded non-attached cells in EpiLife™ and partial attachment in the dKGM. The Mimetic coated plates with SEL-KGM showed attachment with large differentiated non-viable keratinocytes, and small colonies were sporadic using EpiLife™ with many floating cells by Day 8 of culture. The use of dKGM and mimetic growth plates showed larger cells and elongated keratinocyte morphology, indicating a migratory phenotype with limited proliferating capabilities. The phenotype of oversized flattened cells, enlarged cytoplasm volume, and multinucleate cells indicated senescence in some cells.

Keratinocytes grown in EpiLife™ and dKGM with a feeder layer also showed this phenotype and a reduction of the typical characteristic cobblestone appearance not like that observed in the keratinocytes grown in SEL-KGM + feeders (Figure 4.1B).

Expansion using larger vessels investigated primary culture for the three test media with the corresponding feeder layer or coating matrix. The keratinocytes in dKGM presented with many floating non-attached cells, and the cell morphology was large and flat. Preliminary observations quickly eliminated the dKGM; although cells appeared to attach well within the first days of culture, there was significant cell detachment and apparent loss approaching sub-confluence. This reduction in cell growth correlated with cells counts. For example, cells isolated per cm^2 for the dKGM condition were 11,428/cm^2, EpiLife™ 63,809/cm^2 and SEL-KGM 140,419/cm^2 (n=3) (Figure 4.2). From biopsy isolation to harvest, cells in SEL-KGM (20,000 cells/cm^2) were ready for harvest within 7 days with a higher cell yield compared to media with coating matrix, 9 days (Figure 4.2). Primary keratinocytes grown in SEL-KGM/feeders had a 0.7 ± 0.2-log fold increase in cell growth compared to -0.3 ± 0.7-fold change in EpiLife™/CM and -1.4 ± 0.05-fold change for dKGM (Figure 4.3a). On average human keratinocytes grown with SEL-KGM/feeders from primary isolation took 7.9 days to harvest compared to 12.4 days for cells grown with EpiLife™/CM and 10 days for dKGM (Figure 4.3b). From these observations, a feeder layer for primary keratinocyte cell culture was still optimal, and for further media testing on subcultured cells, keratinocytes were established using SEL-KGM/feeders.

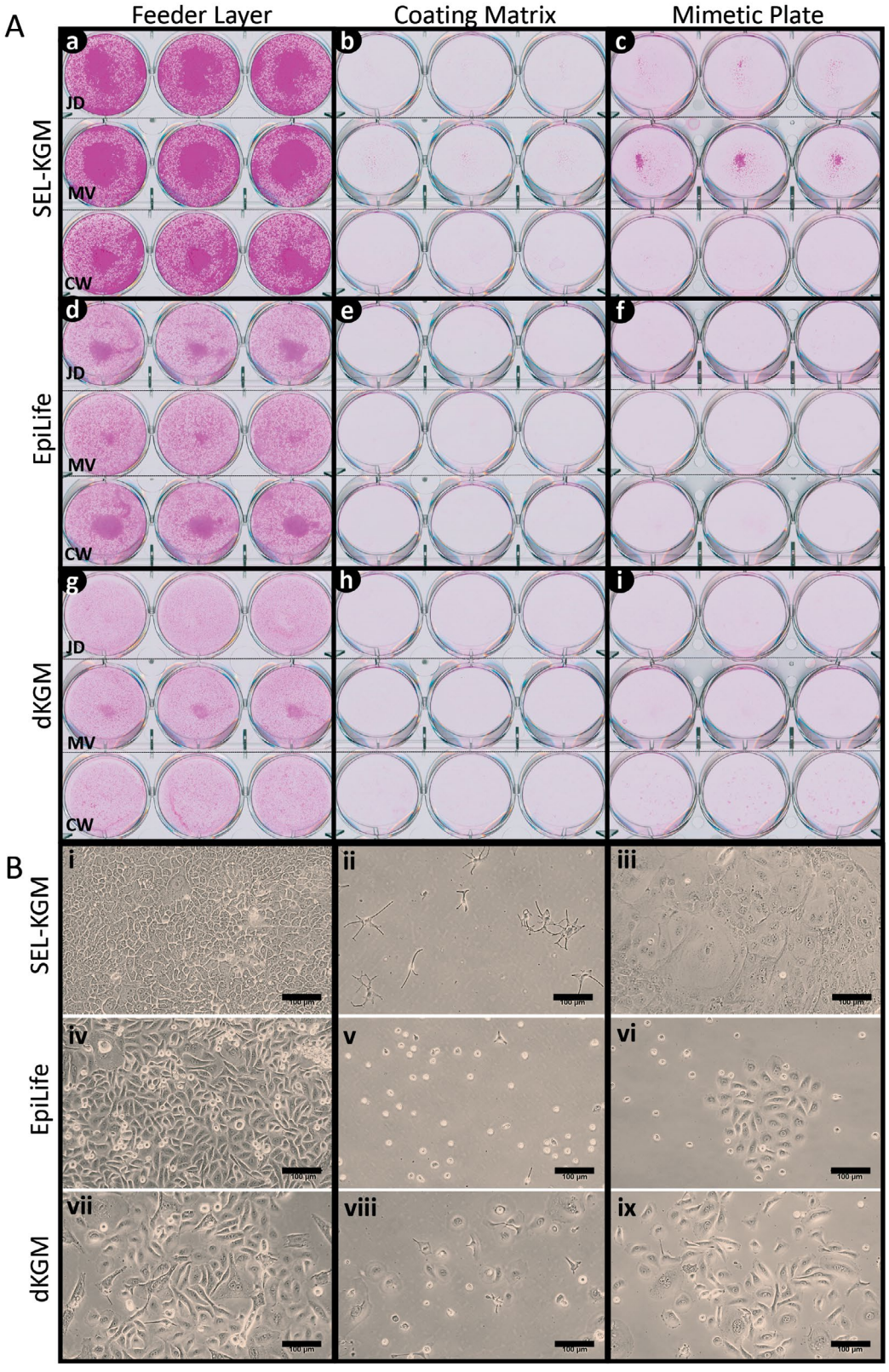

Figure 4.1 Testing of serum-free media and removal of the feeder layer. Panel A shows 6-well plates stained with Rhodamine B for keratinocyte culture (P0), Day 8, using three types of media, SEL-KGM, EpiLife™ and dKGM, with the different methods of culturing support, i.e., feeder layers (a, d, g), coating matrix (b, e, h), or Mimetic coated plates (c, f, i). Panel B shows representative phase-contrast micrograph images for the named conditions on Day 8. The feeder layers display superior growth compared to either of the coated vessels (Figure Bi). Three biological replicates were tested. Scale bar: 100µm.

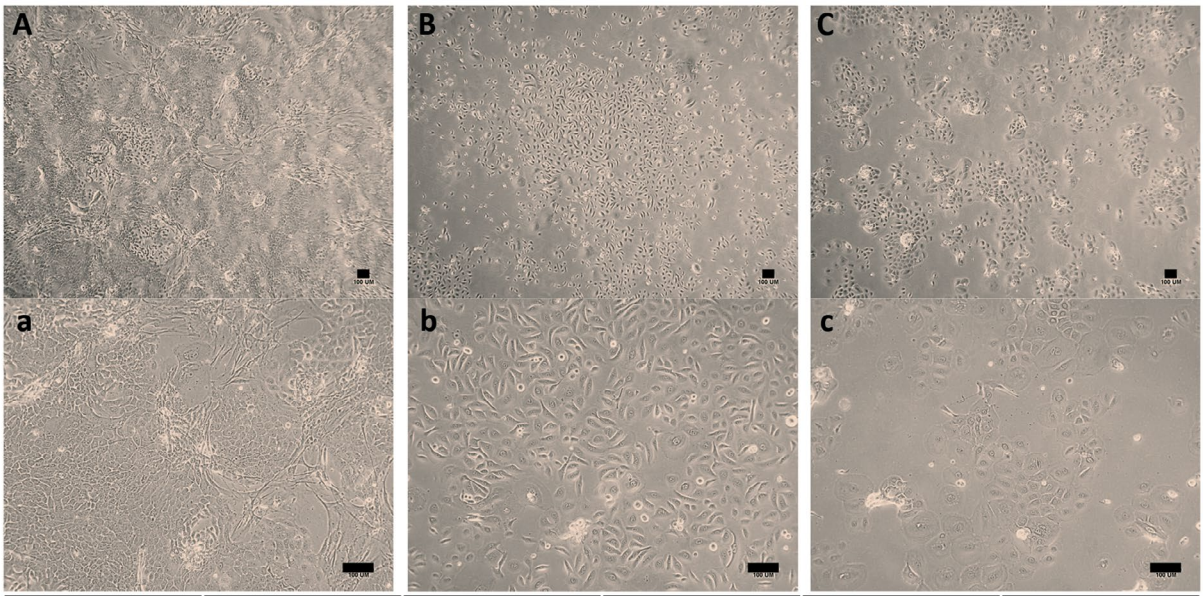

Condition	Day of Harvest	No. of replicates	Flask size	Cells/cm ^{2}	Viability
SEL-KGM + Feeders	7	3	175	140, 419	98
EPILIFE	9	3	175	63, 809	93
dKGM	9	3	175	11, 428	75

Figure 4.2 Representative phase-contrast images of primary keratinocytes grown in A. SEL-KGM/Feeders, B. EpiLife™/CM, and C. dKGM/CM. (A-C) x4 (a-c) x10 magnification. Cells were inoculated at 20,000 cells/cm^2. Harvesting was performed on Days 7 and 9, respectively. Keratinocytes grown in dKGM were large and flat. Cell detachment was represented in the isolated cells/cm^2 (11,428). CM, Collagen Matrix. Scale bar: 100µm.

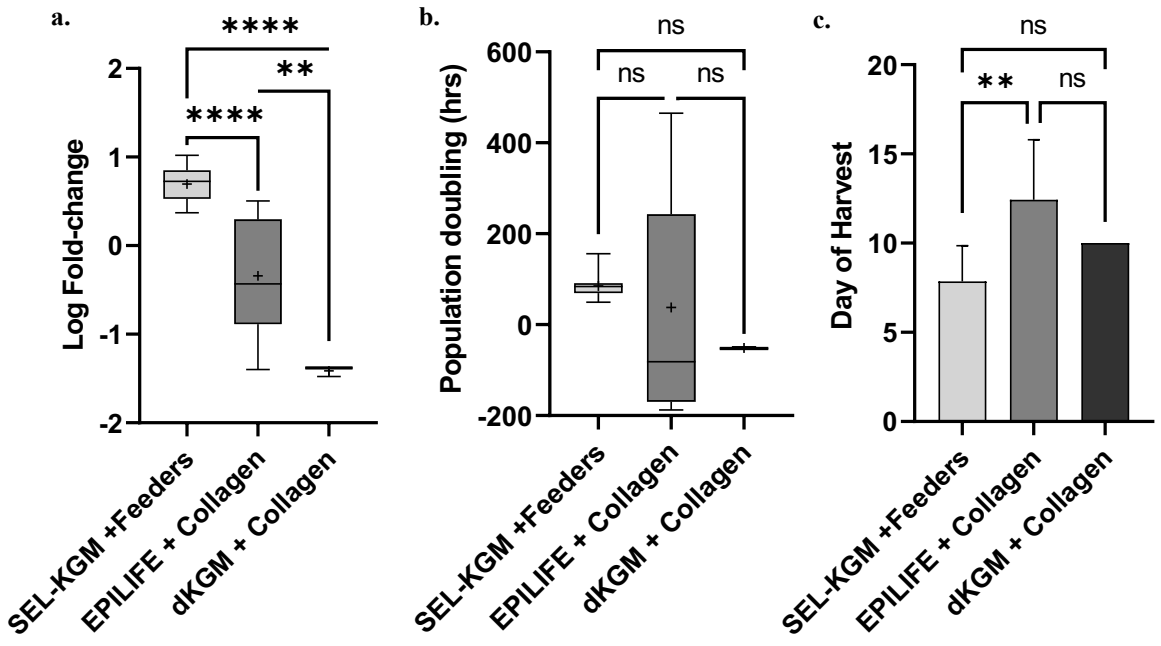

Figure 4.3 Growth of human keratinocytes in SEL-KGM/feeders, EpiLife™/CM and dKGM/CM. Primary cells were assessed for growth potential in different media. The horizontal line in the middle of the box is the median value of the scores, with the mean shown as '+' and the lower and upper boundaries indicate the 25th and 75th percentiles, respectively. Whiskers extend to the minimum and maximum values. a. Log Fold-change in cell number, b. Population doubling time in hours and c. Day of harvest shows the mean SD represented as a column graph. One-way ANOVA with Tukey post-hoc comparison was used to analyse among the groups. * Denotes statistical significance, **p <0.01, ****p < 0.0001, ns is not significant. CM, Collagen matrix.

4.2.2.3 Keratinocyte subculture with media ± serum

Serum-free media and CM were further assessed with SEL-KGM subcultured cells to reduce the use of animal-origin products. Further cell characterisation of cultured keratinocytes by flow cytometry and immunofluorescence were performed for intracellular expression of cytokeratins 14 (basal cell marker) and 10 (suprabasal cell marker). Viable cells isolated per cm^2 were tabulated (Figure 4.4a) for each medium condition showing a greater yield for cells grown in SEL-KGM. Keratinocyte morphology was assessed prior to harvest and flow cytometry (Figure 4.4b-f). The presence of large flat cells was apparent with both EpiLife™ and dKGM. SEL-KGM at Day 5 were confluent in areas with smaller cuboidal shape cells with interspersed iHFbs. Gating and doublet discrimination was performed for flow cytometry data to isolate the subset of cells positively stained for K14 or K10. All media conditions presented with a higher percentage of positive K14 basal keratinocytes than K10. SEL-KGM had 43% positive for K14, 61.9% for EpiLife™ and 76.3% for dKGM. The percentage of K10 positive cells was low in SEL-KGM (0.9%), and EpiLife™ (0.3%) with a slight increase observed in dKGM (2.3%). Immunofluorescence confirmed this increase in K10 cells with positive staining in the dKGM culture compared to the minimal staining in EpiLife™ and only background iHFbs staining with SEL-KGM (Figure 4.4f). A degree of apoptotic debris/artifact was also noted within all samples.

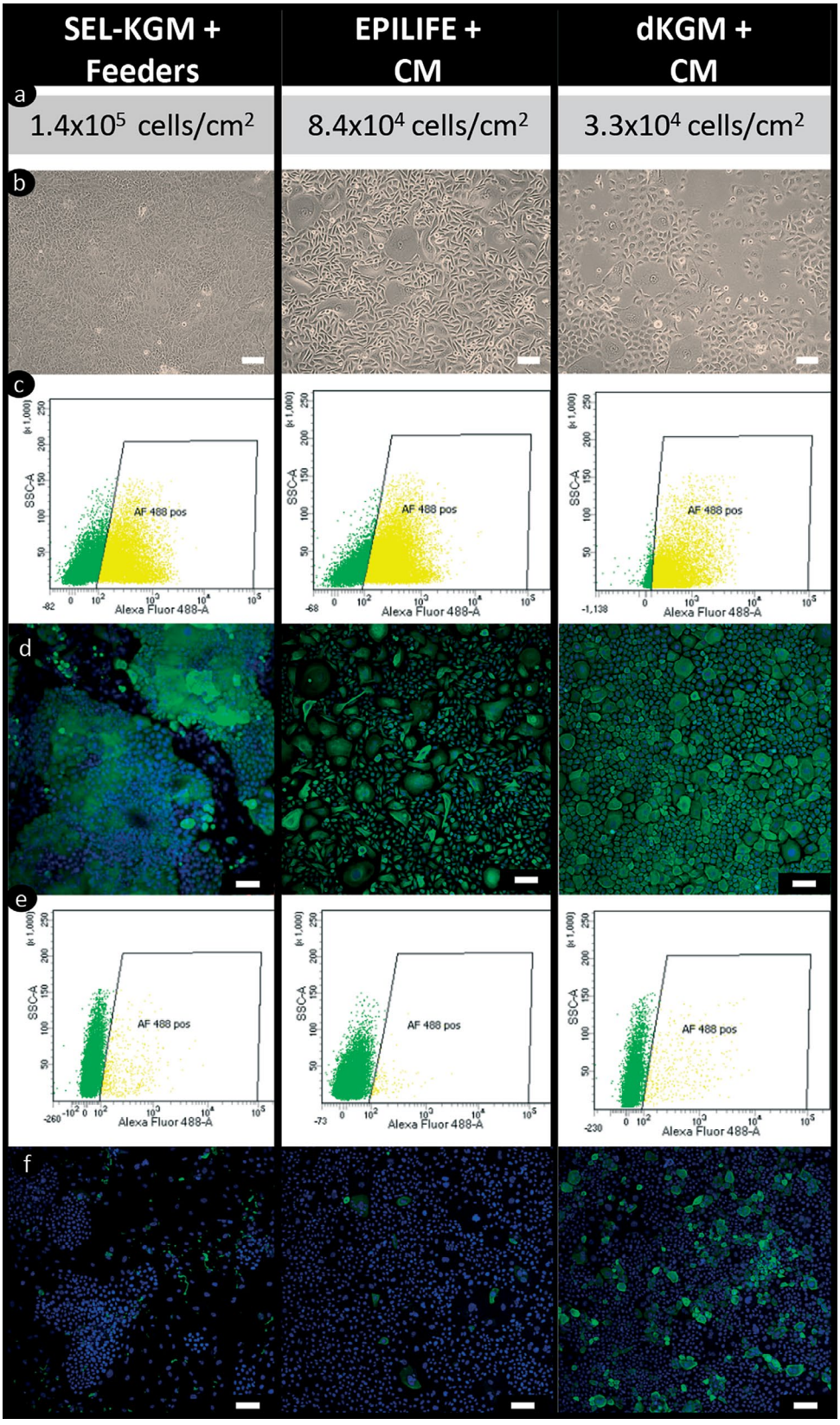

Figure 4.4 Keratinocyte characterisation of cells grown in SEL-KGM + feeders, EpiLife™ + CM and dKGM + CM, row a. Cell counts of harvested keratinocytes prior to analysis, row b. Cell morphology of cells and confluence achieved at Day 5, row c and e Flow cytometry labelling (highlighted yellow) of K14 (c) and K10 (e), and row d and f Immunofluorescence of cultured keratinocytes stained with the corresponding cytokeratins (K14, K10- green, respectively). Blue (DAPI) staining for nuclei. Scale bar: 100µm.

Further evaluation between SEL-KGM/feeders and EpiLife™/CM showed significant differences in the cell number between the two conditions ($p < 0.001$) (Figure 4.5). In keratinocytes grown with SEL-KGM, cells displayed a 3.4 ± 0.25-log fold change compared to 2.3 ± 0.56-log fold change for EpiLife™. However, there were no significant differences in regard to the mean population doubling time (32.51 ± 6.6 vs 36.39 ± 12.9). Interestingly, the keratinocytes in EpiLife™ were ready for harvest 1.5 days sooner than with SEL-KGM (3.15 ± 1.14 vs 4.69 ± 0.85 respectively).

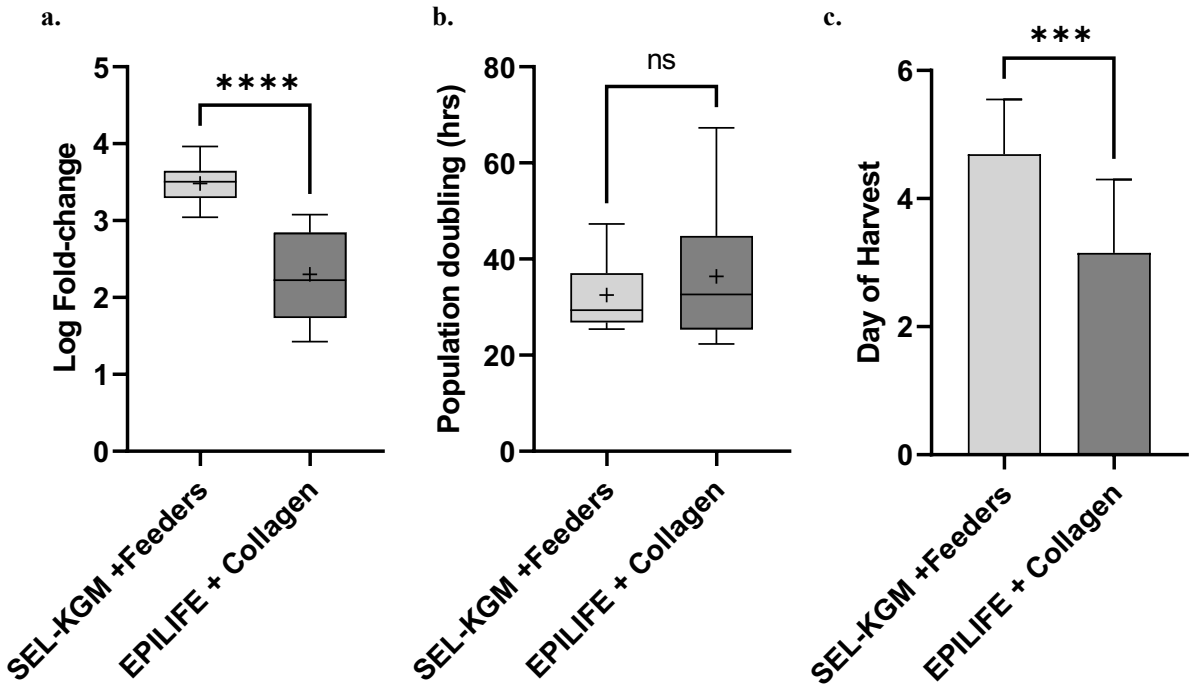

Figure 4.5 Growth of human keratinocytes subcultured with SEL-KGM/feeders, or EpiLife™/CM. Passage one cells were assessed for growth potential in different media, The horizontal line in the middle of the box is the median value of the scores, with the mean shown as '+', and the lower and upper boundaries indicate the 25th and 75th percentiles, respectively. With whiskers extending to the minimum and maximum values. a. Log Fold-change in cell number, b. Population doubling time in hours and c. Day of harvest shows the mean SD represented as a column graph. An unpaired t-test was used to compare the two media conditions. * Denotes statistical significance, ****$p < 0.0001$ and ns is not significant. CM, Collagen matrix.

4.3 Optimisation of Fibroblast Media

Traditional fibroblast culture media contains 5-10% foetal bovine serum and is still widely used today. To increase fibroblast cell yields and obtain animal component-free requirements, a serum-free alternative, TheraPEAK™ Chemically defined fibroblast cell growth medium (FGM-CD), was attempted to be sourced. Unfortunately, this product had a 6-8 week wait period with the potential for discontinuation. Other options from Lifeline cell technology, FibroLife Xeno-free complete cell culture medium, ATCC Fibroblast basal medium (ATCC PCS-201-030), and a basal medium 106 (M-106-500) with low serum growth supplement (LSGS) (S-003-K) from GIBCO Invitrogen was investigated. Due to local accessibility issues of the TheraPEAK™ and ATCC, these were not pursued, and an in-house fibroblast medium with low-serum was formulated (SEL-Fbs). This medium was aligned with the testing of the standard DMEM-5% serum and the available Medium 106 with a low serum growth supplement (Thermo Fisher Scientific, Grand Island, NY, USA).

4.3.1 Materials and Methods

4.3.1.1 Fibroblast culture media

A standard fibroblast medium contains a basal medium supplemented with FBS. The current SEL fibroblasts media contains, Dulbecco's Modified Eagle Medium (DMEM) (1X) + GlutaMAX high glucose pyruvate (Thermo Fisher Scientific, 10569 or 73898) supplemented with 5% (v/v) FBS (CellSera, AU-FBS/PG) and 1% (v/v) Antibiotic solution (Sigma-Aldrich, A5955-100ML). The newly formulated fibroblast medium (SEL-Fbs) contained 2% (v/v) FBS, supplemented with 1µg/mL hydrocortisone, 50µ g/mL Ascorbic acid 2-phosphate (L-AA-2P) (Sigma-Aldrich, A8960), 5.4µg/mL Insulin Actrapid, 10ng/mL EGF, 3ng/mL basic fibroblast growth factor (bFGF) (PeproTech, AF-100-18B-100). The basal medium was either Medium 106 (M106-500) or DMEM (1X) + GlutaMAX high glucose pyruvate (Thermo Fisher Scientific, 10569 or 73898). The third medium was a commercial Human Fibroblast Expansion Basal Medium (Formerly "Medium 106"), supplemented with LSGS kit (S-003-K). The kit components were 2% v/v FBS, 1µg/mL hydrocortisone, 10ng/mL human epidermal growth factor, 3ng/mL basic fibroblast growth factor and 10µg/mL heparin.

The gentamicin was substituted with 1% (v/v) Antibiotic solution (Sigma-Aldrich, A5955-100ML) for consistency with the other fibroblast media. Table 4.3 summarises the above listed fibroblast media and the different reagent composition.

Table 4.3 Overview of the fibroblast media compositions tested for each media type.

Fibroblast Media				
Component	**DMEM + 5% FBS**	**SEL-Fbs (DMEM)**	**SEL-Fbs (Medium 106)**	**Medium 106 + LSGS**
DMEM + GlutaMAX™	✓	✓	×	×
Medium 106	×	×	✓	✓
FBS	5% (v/v)	2% (v/v)	2% (v/v)	2% (v/v)
Insulin Actrapid	×	✓	✓	×
Hydrocortisone	×	✓	✓	✓
bFGF	×	✓	✓	✓
hEGF	×	✓	✓	✓
L-AA-2P	×	✓	✓	×
Heparin	×	×	×	✓
Antibiotic antimycotic	✓	✓	✓	✓

4.3.1.2 Cell culture and experimental design

Normal human dermal fibroblasts were isolated from donated skin samples or current laboratory cryopreserved stocks and pre-cultured using the laboratories standard operating procedure for fibroblast culture (Appendix IV). The use of discarded skin samples and human cells was approved by the Royal Adelaide Hospital ethics committee, HREC/18/CALHN/539 and R20180811. In brief, cells were grown in the corresponding fibroblast mediums (see section 4.3.1.1) until 90% confluence. The medium was exchanged every two to three days. The fibroblast cultures were then passaged with 0.05% Trypsin - EDTA for experimental use, cryopreservation or subculture. Phase contrast images were taken, and cell counting was performed according to section 4.2.1.4. Initial experiments using freshly isolated fibroblasts and a highly supplemented growth medium encouraged the growth and proliferation of a second cell type. Therefore, fibroblasts were established with DMEM-5% FBS for subsequent testing.

Experiment 1a. A CellTiter 96® AQueous One Solution Cell Proliferation Assay (MTS) (Promega, G3581) was performed using the three media conditions, SEL-Fbs, Medium 106 + LSGS and DMEM-5% FBS. 96-well plates with three biological replicates and technical triplicates were set up. This assay was duplicated and discontinued for primary cell investigations. Cell number and viability were determined and plated at $1x10^4$ cells/cm^2. Cells were incubated and maintained at 37°C, 5% CO_2 in a humidified chamber and refeed every two days. The MTS assay was performed on Day 7 of culture with 20µL of CellTiter 96® AQueous One Reagent added to 100µL of media per well. Plates were incubated for 2-3 hours, and absorbance was recorded at 490nm using a plate reader (FLUOstar OPTIMA microplate reader, BMG Labtech). Triplicate control wells (media only - without cells) were prepared for each media condition. The absorbance values from the media-only wells were averaged and subtracted from the test values to obtain corrected absorbance.

Experiment 1b. This assay was performed as per 1a with additional changes. Passage one human dermal fibroblast cells were tested with the three media conditions above, and a different media, SEL-Fbs (DMEM), replaced the Medium 106 basal media with DMEM-GlutaMAX. This assay was repeated three times, with three biological replicates and technical triplicates. Subcultured cells were plated at 3100 cells/$cm^{2,}$ and the assay was performed on Day 4 of culture.

Experiment 2 – The phenotypic characteristics of fibroblasts were assessed and confirmed with immunofluorescence staining for fibroblast marker (1B10, Abcam, ab11333) and collagen I (Abcam, ab34710). Human fibroblasts were grown on 8-well chamber slides (Ibidi GmbH, Martinsried, Germany, 80841) at 3,100 cells/cm^2 with the preferred medium and standard culture conditions as described. A negative control (secondary antibody only) was aligned with this testing. For antibodies and dilutions and a detailed protocol of IF, see Appendix III and VI.

Experiment 3 – To compare expansion potential, experiments 1 and 2 determined the most favourable medium condition to continue evaluation alongside the standard DMEM-5%. Cells were subcultured and expanded between 3,100 - 4,000 cells/cm^2 until a condition reached 80-90% confluence. Cell viability and cell number were determined to calculate the fold-change in cell number, population doubling and day to harvest.

Statistical analyses - Data analysis and charting were performed using GraphPad PRISM version 8 for windows GraphPad Software, San Diego, California USA, www.graphpad.com. Comparisons among multiple groups utilised repeated one-way analysis of variance (ANOVA) or one-way factor ANOVA with further post-hoc analysis using Tukey's multiple comparisons test. Data are presented with the mean variables and standard deviation (SD). Differences were considered statistically significant at $*p < 0.05$.

4.3.2 Results

4.3.2.1 Analysis of fibroblast medium and primary culture

The cost analysis of the fibroblast cell culture media to purchase and or produce per 500mL identified the basal medium with FBS was AU$40.60, SEL-Fbs (106) - AU$218.60, SEL-Fbs (DMEM) - AU$86.13 and supplemented Medium 106 - AU$364.00. Initial experimentation with freshly isolated dermal fibroblasts and the highly supplemented media with growth factors supported the growth of a second cell type. These cells were flat, polygonal-shaped monolayer suggestive of endothelial-like cells. They were not all the typical spindle-shaped fibroblastic morphology and appeared to dominate the culture (Figure 4.6). The results of the cell proliferation assay showed a significant increase ($p < 0.0001$) in growth with the highly supplemented media when compared to the DMEM-5% FBS (Figure 4.7). Taken together, this indicated it was not a pure fibroblast population. Therefore, primary fibroblasts were established in DMEM-5% FBS for further media comparisons on subcultured cells.

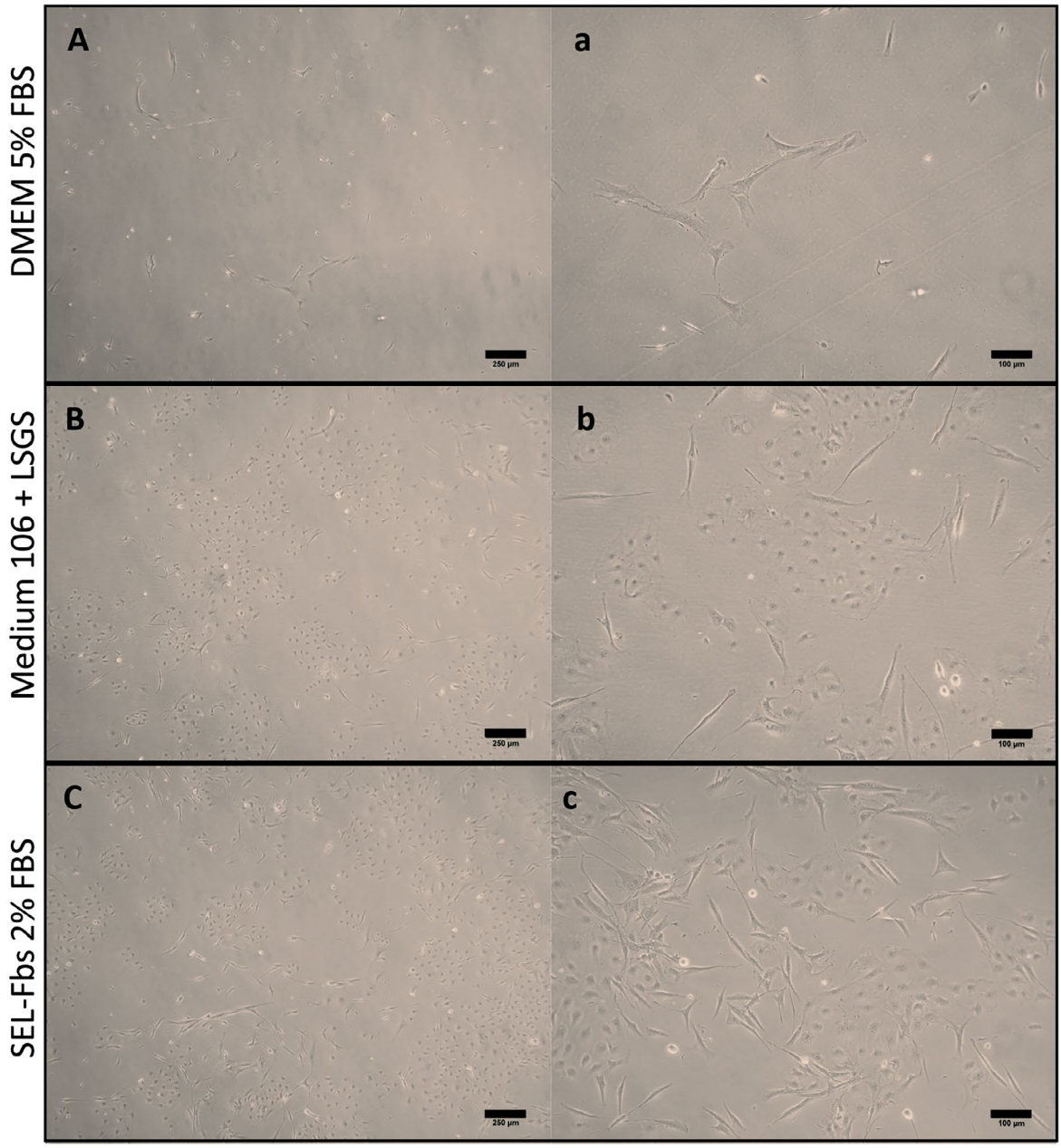

Figure 4.6 Representative phase contrast images of freshly isolated human dermal fibroblasts with different media conditions at low magnification x4 (A-C) and higher magnification x10 (a-c). Aa, DMEM 5% FBS. Bb, Medium 106 + LSGS and Cc, SEL-Fbs 2% FBS. Note the growth of a second cell type in the supplemented media conditions b-c. DMEM- Dulbecco's Modified Eagle Medium, FBS-foetal bovine serum, hFbs – human dermal fibroblasts LSGS – low serum growth supplement, SEL – Skin Engineering Laboratory. Scale bar: A-C 250µm, a-c 100µm.

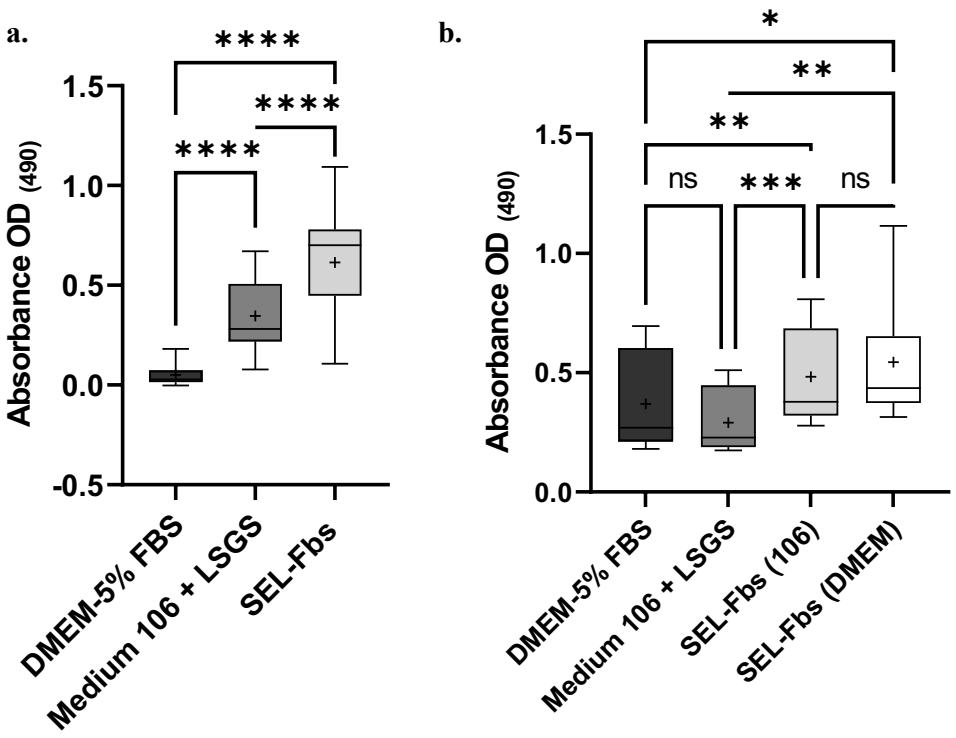

Figure 4.7 Cell proliferation analysis by MTS assay for primary (a) and passaged (b) fibroblasts. Fibroblast growth with DMEM-5% FBS, Medium 106 + LSGS and SEL-Fbs (106 or DMEM). The horizontal line in the middle of the box is the median value of the scores, with the mean shown as '+' and the lower and upper boundaries indicate the 25th and 75th percentiles, respectively. Whiskers extend to the minimum and maximum values. Statistical analysis was performed by repeated measures one-way analysis of variance with pairwise post hoc comparisons by Tukey test. * Denotes statistical significance, * $p < 0.05$, ** $p < 0.01$, ***$p < 0.001$ and ****$p < 0.0001$. ns is not significant.

4.3.2.2 Fibroblast culture and cell characterisation

Subcultured fibroblasts were analysed with the MTS assay with a fourth comparison of culture media. DMEM-GlutaMAX replaced Medium 106 as the basal media for SEL-Fbs. These results showed a significant increase among the media conditions (Figure 4.7b). SEL-Fbs (with either basal media) had superior proliferation to DMEM-5% FBS or Medium 106 + LSGS ($p < 0.05$). No significant differences were observed between SEL-Fbs basal mediums (106 or DMEM) or DMEM-5% FBS and Medium 106 + LSGS. Indicating the basal medium (Medium 106) can be successfully substituted for a traditional DMEM.

The growth potential of the fibroblast cultures with different media was then assessed with larger vessels for culture. Comparing the SEL-Fbs and Medium 106-established cells with slender, more defined nuclei and DMEM-5% FBS-established cells revealed a larger and flatter morphology (Figure 4.8). Cell counts confirmed the difference in cell growth during culture. The isolated cells numbers from figure 4.8a-d were 28,343 cm^2, 42,857 cm^2, 82,371 cm^2, respectively. SEL-Fbs media promotes 66% more cells on day five post isolation compared with traditional basal media-FBS and 46% more than Medium 106 in this example. With SEL-Fbs supplemented media, the mean growth rate was significant 1.3 ± 0.13-log fold change compared to DMEM-5% FBS 0.8 ± 0.2 and 1.0 ± 0.08 for Medium 106 + LSGS, as shown in figure 4.9a. As an additional result of growth in DMEM-5%, population doubling time increased on average every 48 hours for fibroblasts in comparison with SEL-Fbs of 26 hours (Figure 4.9b). The days of harvest for any of the media conditions were not significantly different (Figure 4.9c). The increased serum concentration in the media also prolonged the trypsinisation up to 10 minutes.

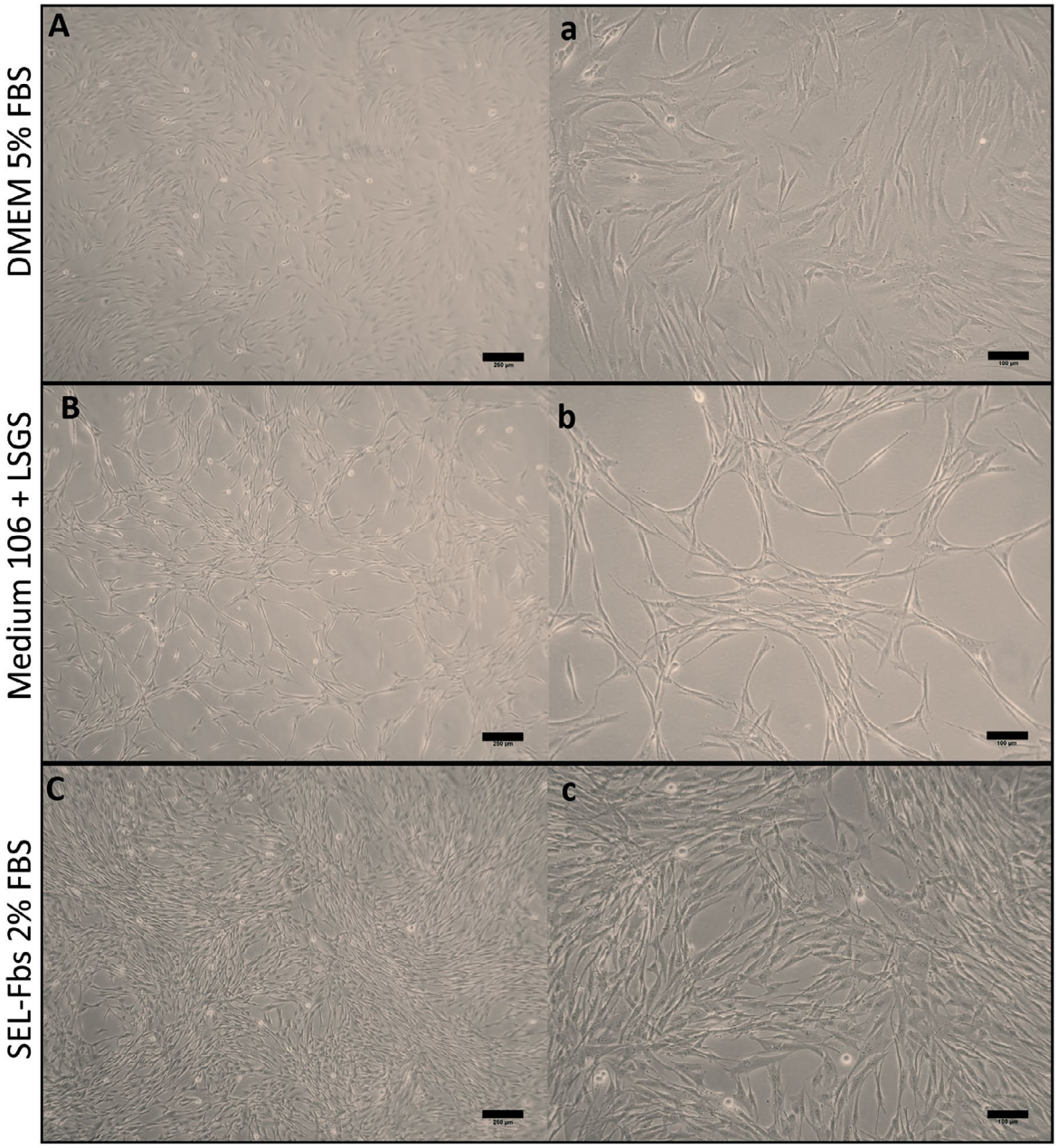

Figure 4.8 Representative phase contrast images of subcultured human dermal fibroblasts in different media conditions at low magnification x4 (A-C) and higher magnification x10 (a-c) Day 5, inoculated at 4000 cells/cm². Aa, DMEM 5% FBS. Bb, Medium 106 + LSGS and Cc, SEL-Fbs 2% FBS. Note the morphology and cell confluence changes of the supplemented media. DMEM- Dulbecco's Modified Eagle Medium, FBS- foetal bovine serum, Fbs – fibroblasts LSGS – low serum growth supplement, SEL – Skin Engineering Laboratory. Scale bar: A-C 250µm, a-c 100µm.

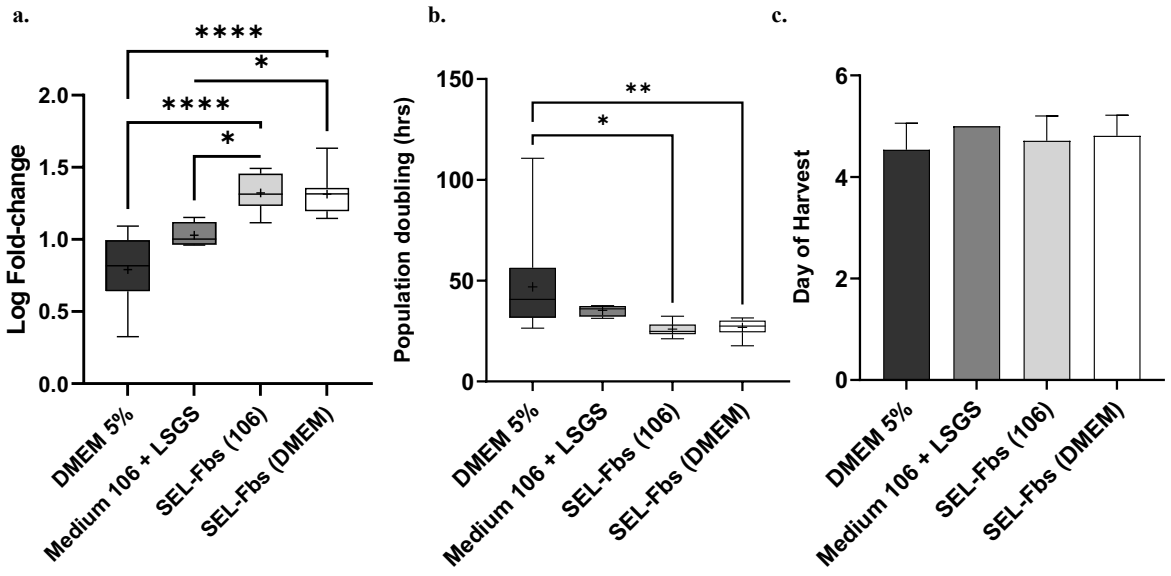

Figure 4.9 Growth of human dermal fibroblasts in DMEM-5% FBS, Medium 106 + LSGS, SEL-Fbs (106) and SEL-Fbs (DMEM). Subcultured cells were assessed for growth potential in different mediums. The horizontal line in the middle of the box is the median values of the scores, with the mean shown as '+' and the lower and upper boundaries indicate the 25th and 75th percentiles, respectively. Whiskers extend to the minimum and maximum values. a. Log Fold-change in cell number, b. Population doubling time in hours and c. Day of harvest shows the mean SD represented as a column graph. One-way ANOVA with Tukey post-hoc comparison was used to analyse among the groups. * Denotes statistical significance, *$p < 0.05$, **$p < 0.01$, and ****$p < 0.0001$.

The anti-human collagen I antibody was used to identify collagen I in the cultured human dermal fibroblasts cells grown with DMEM-5% and SEL-Fbs (Figure 4.10A). Specific staining was localised to the cytoplasm of the cells. The fibroblasts grown in DMEM-5% showed an increase in cytoplasmic staining due to increased cell size. In SEL-Fbs media, the fibroblasts are much smaller, and when confluent, deposited fibres are heavily stained with collagen (Figure 4.10 Ac). In addition to being positive for anti-fibroblast surface protein antibody (1B10) (Figure 4.10 B). The perinuclear region of the 1B10 stained cells grown in both media types displayed strong granular staining, with SEL-Fbs exhibiting an increased staining intensity.

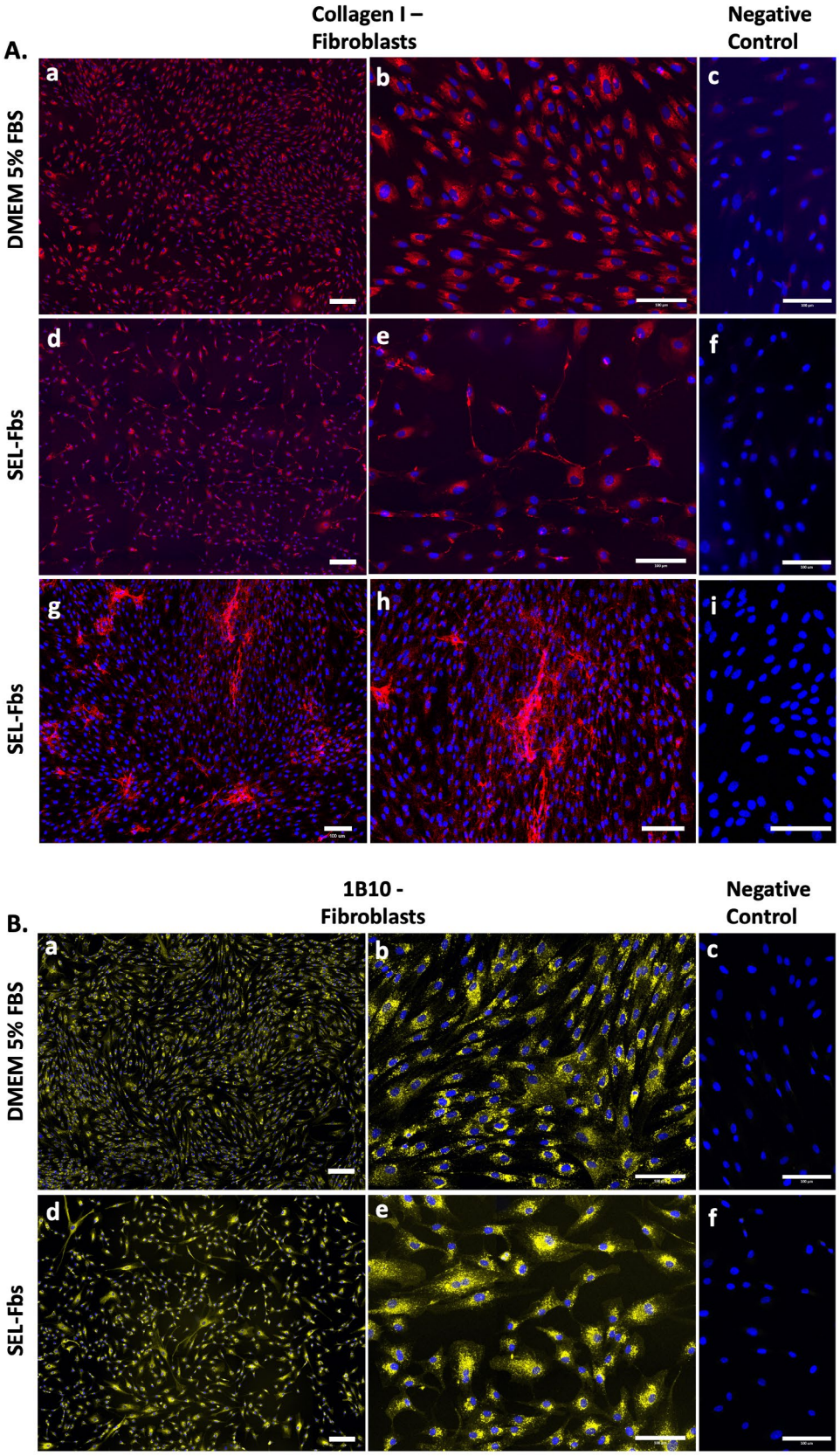

Figure 4.10 Immunofluorescence cytochemistry of human dermal fibroblasts cultured with DMEM-5% FBS and SEL-Fbs (DMEM), A. Shows detection of collagen I (red) with subconfluent cells (d, e, f) and near confluent cells (g, h, i) and B. 1B10 antigen-positive fibroblasts (designated yellow). c, f, i Negative controls. Nuclei are visualised with DAPI (blue). Scale bars: a, d, g 200µm, and b, c, e, f, h, i 100 µm.

4.4 Porcine Cell Culture

4.4.1 Optimised Media Conditions Tested with Porcine Keratinocytes and Fibroblasts

Porcine keratinocytes were grown using the commercially available serum-free media (EpiLife™) with collagen-coated vessels for passage one. Replication of the results was carried out three times. Cell viability and number were significantly lower than those grown previously using SEL-KGM + Feeders, with only a mean 0.4 ± 0.1-log fold increase in comparison to 1.08 ± 0.1-log fold increase in SEL-KGM (Figure 4.11). The population doubling was also significantly different ($p < 0.05$) with SEL-KGM + feeders doubling 40.9 ± 8.8 hrs compared to EpiLife™ at 68.6 ± 23. As an example, on a particular harvest, EpiLife™ only obtained 34,000 cells/cm^2 while SEL-KGM obtained 204,000 cells/cm^2. In the EpiLife™ medium, the morphological discrepancy was significantly different with larger, flatter cells (Figure 4.12a). The highly supplemented fibroblast media (human-derived) also produced atypical morphology (Figure 4.12c). In contrast to the normal bi-polar spindle elongation (Figure 4.12d), the cells were more dendritic to spreading, with a myofibroblastic type morphology. For future expansion, media that produced cells with typical fibroblast morphology were used to fabricate the skin substitutes.

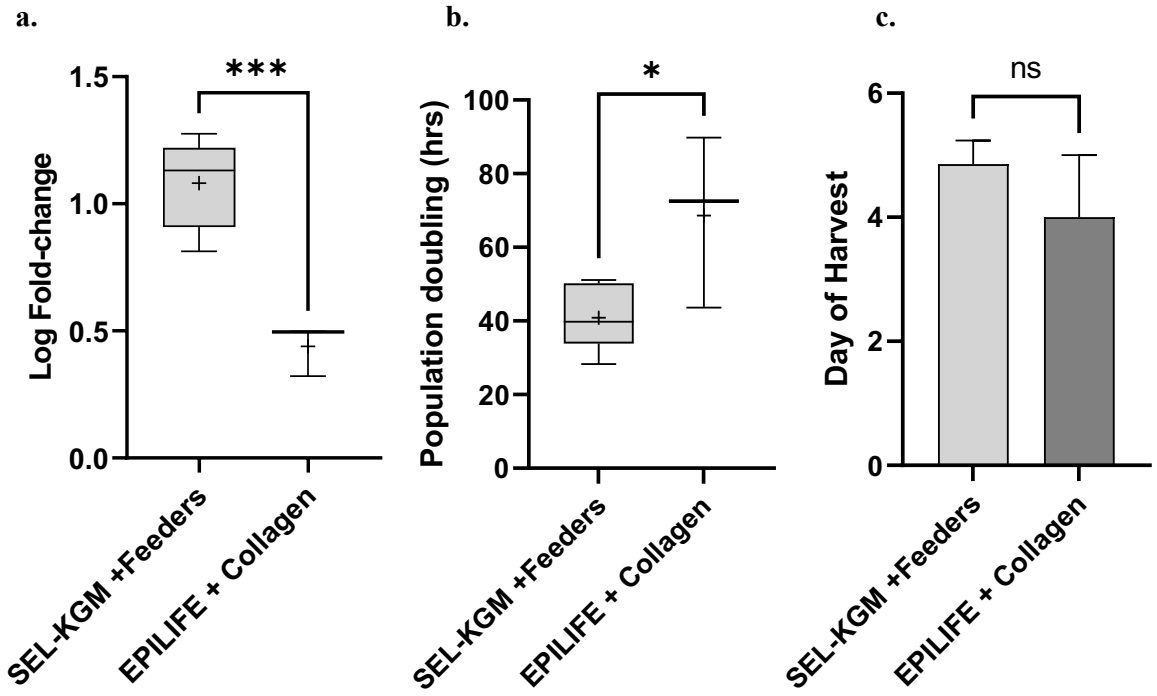

Figure 4.11 Growth of porcine keratinocytes subcultured with SEL-KGM/feeders, or EpiLife™/CM. The horizontal line in the middle of the box is the median value of the scores, with the mean shown as '+' and the lower and upper boundaries indicate the 25th and 75th percentiles, respectively. Whiskers extend to the minimum and maximum values. a. Log Fold-change in cell number, b. Population doubling time in hours and c. Day of harvest shows the mean SD represented as a column graph. Unpaired t-test was used to compare between the two media conditions. Significance is indicated by * $p < 0.05$ and ***$p < 0.001$. ns is not significant. CM, Collagen matrix.

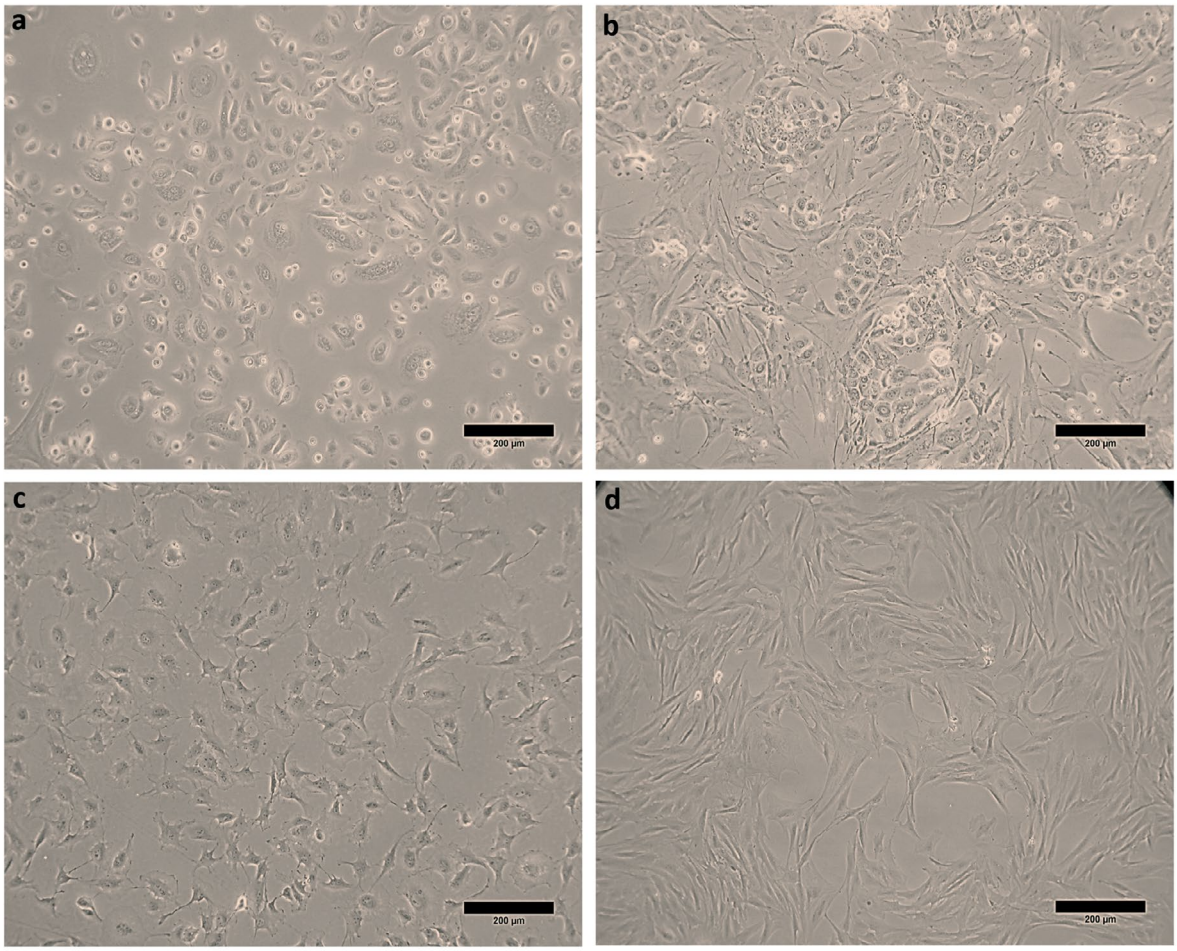

Figure 4.12 Porcine skin cell culture. Representative phase contrast images displaying porcine keratinocytes inoculated at 19,654 cells/cm^2 on Day 2 grown in - a, EpiLife™/CM and b, SEL-KGM/Feeders. c, displays porcine fibroblasts established in SEL-Fbs media on Day 3 and d, pFbs in DMEM-5% FBS on Day 4 at 5000 cells/cm^2. Scale bar: 200µm.

4.5 Discussion

Currently, ancillary materials (media, supplements, growth factors) and methods used for skin culture include human, - and animal-derived products and may be considered to present risks. Foetal bovine serum, and porcine trypsin, are such examples that require assessment and substitution [62, 68, 69]. The original method of keratinocyte culture involves a 'feeder' layer, and although human-derived fibroblast feeder layers can replace the traditional methods of murine (mouse 3T3 fibroblast) feeders [65], these similarly pose a risk of disease transmission [70]. The commercial availability of serum-free media for both keratinocytes and fibroblasts is expanding. Bovine pituitary extract for keratinocyte culture was initially a major substitute for serum-free, and although still available, there are now defined formulations without BPE. This chapter has evaluated the availability and cost of serum-free media and compared their growth potential to the standard low serum-co-cultured irradiated fibroblast method for keratinocytes and a low-serum based medium for fibroblasts.

Purchasing the media pre-made or making the media in-house may be considered when the scale-up of reagents is required. The cell number and turn-around time are critical when fabricating large-scale engineered skin for a patient with extensive burns >50%. One 25cm x 25cm piece would require 6 x 10^8 keratinocytes and 3 x 10^8 fibroblasts, times that by 25 to approximately cover a 95% TBSA burn patient, requires over 1.5 x 10^{10} keratinocytes and 7.5 x 10^9 fibroblasts equates to a significant amount of growth media. Although it is not the primary determinant, the cost is an important factor. Additionally, in-house preparations must meet quality control measures that can be labour intensive and expensive. All ancillary materials should be of Good Manufacturing Practice (GMP) quality. If prepared in-house, they require sterility testing following British Pharmacopoeia guidelines [71]; they must be stored under appropriate controlled conditions and expiry dates established with established quarantine measures before releasing for use. Therefore, an accurate cost analysis must consider these additional factors to ensure a comprehensive analysis when comparing the overall costs.

Prior to accounting for the total number of cells required, the cost of fabricating the CCS per cm^2 appeared similar for the different types of keratinocyte media. EpiLife™ requires increased culture vessels/media to equate, thus directly raising the cost. In comparison,

SEL-KGM involves iHFbs, which require significant pre-work and culture prior to expansion but can be scaled up to produce large batches for cryopreservation and later use. Each medium protocol requires a growth assistant method with associated costs. Both the EpiLife™ and the dKGM media suggest a collagen coated surface, which needs preparation before use and is inconsistent for large vessel plating at the recommended volume ratios. The concept of pre-coated vessels is optimal, with no pre-handling and are temperature stable. Unfortunately, the Mimetic collagen-coated plates did not show optimal growth as observed by Thompson et al., who confirmed similar keratinocyte growth potential and morphology as the collagen I matrix, albeit those were neonatal cells [67]. At the time of testing, larger vessels were not readily available, and if scalable, the cost of mimetic vessels may be excessive, even accounting for the additional manual handling requirements of both the coating matrix and the feeder layer. However, alternative products that are ready to use are necessary to achieve a streamlined animal origin-free process for the future.

The investigation and availability of serum-free media for keratinocyte growth have long been established [61]. This chapter aimed to identify media and reagents that reduce or eliminate serum and feeder layers for keratinocyte growth, to decrease culturing time proving highly beneficial for clinical applications. Commercially available serum-free media, EpiLife™ and dKGM, were analysed alongside the SEL-KGM + feeders for growth potential and cell characterisation. Primary isolated keratinocytes yielded the highest proliferation grown in SEL-KGM + feeders. However, comparing serum-free media (low calcium) with an irradiated feeder layer demonstrated potential, eliminating any concern regarding serum. Although, previous studies have shown that the feeder cells and subcultured keratinocytes are not sustained in subsequent culture unless there is an increase in cell numbers [72] and was therefore not investigated further. The dKGM was also disregarded early in the testing regime as it was substrate-dependent, unable to sustain cultures at low inoculation densities (recommended between 13,333 - 40,000 cells/cm^2), and required 10-20 days to reach target cell numbers. One advantage is its availability as a regulated and accepted medium, a factor lacking for many other media formulations. For the reasons mentioned above, cells were maintained in SEL-KGM + feeders for primary cultures.

Continuing investigations for serum-free and feeder-free conditions, subcultured cells were further tested with the media and coating surfaces. These results also suggested the optimal conditions were SEL-KGM + feeders. However, the EpiLife™ serum-free, low calcium regulated condition should not be dismissed for serial cultivation with further investigations into a switch of calcium concentration (60μM to 0.2M), potentially optimising keratinocyte phenotype by increasing cell-cell contacts [73]. Cells in both media maintained *in vivo* characteristics with positive identification of K14 basal marker for keratinocytes and low levels of differentiation marker, K10. The percentage of K10 cells was increased with keratinocytes grown in dKGM.

In conclusion, the optimal media condition for keratinocyte cell expansion cultures were the SEL-KGM + feeder method. Previous reports also suggest this technique is optimal for cellular growth [74] particularly due to the production of large cell numbers in a short turn-around, a consideration for clinical application. On the other hand, serum and feeders are still undefined growth stimulators, but the risks are not more than tissue or blood products. Similarly, the media testing for porcine keratinocytes produced the same results. Even though previous studies have successfully cultured porcine keratinocytes from piglets using EpiLife™ media, these authors acknowledged the differences between piglet, adult porcine and human keratinocytes [75]. Comparatively, the generation time (hours) reached in the study was 40.5 ± 5.7, which was similar to the SEL-KGM in this study at 40.9 ± 8.8, but not the EpiLife™ at 68.6 ± 23.3.

Typically, human dermal fibroblasts are expanded with a basal medium containing serum; however, changes in morphology and diminished cell growth prompted further research into the composition of the media. Sourcing commercially available serum-free options for fibroblast growth were limited. Together with commercially available fibroblast media, an in-house low serum fibroblast medium was formulated to assess growth. Human dermal fibroblast cell proliferation was significantly increased with the in-house SEL-Fbs media. The increase is reflected by the addition of exogenous agents that have the potential to stimulate proliferation. Although this formulation is not serum-free, a low serum alternative (2% v/v) could sustain growth and replace the currently used DMEM-5% FBS. A suggested

alternative is supplementation with autologous serum at 2% v/v [76], which was previously tested within this laboratory. However, the quantity needed for the total number of cells is limiting.

This growth supplemented medium also promoted a second cell type, endothelial-like cells. The tissue samples were from elective surgery operations where the use of a dermatome or Watson skin graft knife was limited. Therefore, the skin was thicker with additional fat tissue, and the possibility of isolating other contaminating cell types increased through processing. It was concluded that freshly isolated fibroblasts would continue establishment in basal media and serum (which do not support these other cell types). However, future investigations of this media formulation may have endothelial cell isolation and growth potential. The importance of isolating the correct fibroblast population from the dermis is highlighted here. Previous work has shown that fibroblasts isolated from the lower reticular dermis do not support basement membrane formation in generating skin substitutes [77]. Cells were positively characterised as fibroblasts with 1B10 fibroblast marker and collagen I, indicating isolation and growth of functional fibroblasts.

In contrast, the porcine fibroblasts were unable to maintain typical morphology grown in this medium. Further morphological and characterisation studies are necessary to investigate porcine fibroblasts grown in this highly supplemented media. Other considerations include exchanging the human-derived components for either bovine-derived or recombinant growth factors. Although serum volumes were low for keratinocytes (1%) and fibroblasts (2%), the risk of transmitting diseases or immune reactions to bovine proteins still exists due to serum's undefined nature and are still of concern for clinical applications. Autologous and pooled donated AB serum are alternatives but limiting when large volumes are required for fabrication of engineered skin for extensive burn injuries. Although both culturing strategies have their limitations, when introducing new technologies for therapeutic use, regulatory bodies and a biological framework are consulted and followed, ensuring the base requirements and critical raw materials, along with a projected cost analysis, have rigorous quality assurance before clinical application [78].

CHAPTER 5:
Scaffold Optimisation for the *in vitro* Fabrication of Skin Substitutes

5.1 Overview

Chapter 4 defined the culturing parameters for cultivating keratinocytes and fibroblasts required to fabricate skin substitutes and Chapter 3 described the first use of a polyurethane based skin composite in a 95% burn patient. The production of CCSs for this patient exhausted all PUR foam supplies, so a new supply of foams was sourced in preparation for the next patient. This new batch underwent quality assurance testing to ensure CCS repeatability before implementation, but unfortunately it was not equivalent due to excessive porosity. Although there had been no procedural changes in batch production, and the product was deemed within tolerance levels by the company. This meant several different CCS production methods with the new batch were tested; all with unsatisfactory results. There was substantial loss of fibroblasts, minimal retention of superficial keratinocytes, and discontinuous viable epithelium. A redesign of the CCS method (layer-by layer approach) was needed to reduce the inherent porosity issues. In addition, other potential biomaterials were also considered to alleviate these concerns. A hybrid combination scaffold was constructed using the polyurethane (PUR) foam and a collagen-glycosaminoglycan (C-GAG). This chapter describes the *in vitro* establishment and refinement of these protocols prior to the *in vivo* study in Chapter 6.

5.2 Materials and Methods

5.2.1 Preparation of Pooled Fresh Frozen Plasma (FFP)

Human Fresh Frozen Plasma (hFFP) was supplied from the Transfusion Department in the Royal Adelaide Hospital, sourced from the Australian Red Cross Lifeblood. FFP was obtained by apheresis, and rapidly frozen. As a universal donor compatible with all blood types, AB +ve FFP were sourced (ARCL, AUS). A minimum of 4 bags of ~250mL each, were pooled to reduce variability. FFP can be stored at minus 25°C or below for up to 36 months. The FFP was thawed at 37°C for a maximum of 30 minutes.

If a delay is unavoidable before filtering and use, it can be stored for up to 4 hours at 22 ± 2°C or for 24 hours if stored at 4 ± 2°C. Bags of FFP were pooled and filtered using Rapid-flow 0.45µm filter units (Thermo Scientific Nalgene, USA) and Rapid-flow 0.2µm filter units (Thermo Scientific Nalgene, USA) prior to being aliquoted (100mL) and re-frozen ready for use in CCS fabrication or thrombin preparation.

5.2.2 Thrombin Preparation from hFFP

A method for preparing human thrombin from FFP is described here. Pre-filtered and aliquoted FFP was thawed in the waterbath at 37ºC for a maximum of 30 minutes. A dilute acetic acid solution was prepared by adding 175mL of sterile water for injection, 35mL of 0.25% acetic acid (Baxter Healthcare) and 25mL of FFP to a 250mL tube (x4) (Corning, New York, NY, USA). In order to allow precipitation to occur, the tubes were mixed well and allowed to sit for at least 10 seconds. After centrifuging at 3200rpm for 5 minutes at 4ºC using a low brake set at 2, the supernatant was removed to ensure no liquid remained. During centrifugation, a bicarbonate buffer (100mL) was prepared. To 100mL of sodium chloride (saline) (Baxter Healthcare), 0.5mL of 8.4% sodium bicarbonate (Pfizer Pty Ltd) and 5mL of 10% calcium chloride were added. The pellet was dissolved in 9mL of bicarbonate buffer in the 250mL centrifuge tube and mixed by scraping the sides of the tube using a 10mL syringe and cannula. Once into solution, this was transferred to two red top blood tubes (2 per 25mL plasma) and collected in a 50mL centrifuge tube. Two 250mL tubes were pooled, i.e., 18mL of the buffer. These tubes were then incubated at 37ºC for up to 1hour or until coagulation. If there was no coagulum, the samples were then incubated for further 15-30 minutes and regularly checked. A clotting test was performed once the coagulum was observed. Thrombin solution was then collected and filtered (0.2µm), ready for use or storage at -20°C.

5.2.3 Cell Culture – Keratinocytes/Fibroblasts

Cells were isolated from discarded skin tissue from elective surgery operations. The cell culture methods were performed in a Class II biological safety cabinet (BSC) (Email Air Handling, Clyde Apac, AES Environmental, Wacol, QLD) under aseptic conditions. Keratinocytes and fibroblasts were isolated for expansion and maintained at 37°C, 5% CO_2 in a humidified environment. For serial cultivation, keratinocytes were grown with SEL-KGM + feeders and fibroblasts with SEL-Fbs (Chapter 4). Cells for future applications were cryopreserved. The use of discarded skin samples and human cells was approved by the Royal Adelaide Hospital Research Ethics Committee (HREC/18/CALHN/539 and R20180811) (Appendix I).

5.2.4 Skin Substitute Maturation Medium

A specialised formulation based on the University of Cincinnati Dermatology Medium 1 (UCDM1) was used [79]. This medium has been referred to as MM - Maturation Medium for this study, see Table 5.1 for components. It consisted of Dulbecco's Modified Eagle's Medium/F12 GlutaMAX (Gibco, Grand Island, NY, USA), supplemented with 0.3% foetal bovine serum (CellSera, Invitrogen), 1mM strontium chloride, 1% v/v insulin-transferrin-selenium (ITS), 9.4µg/mL linoleic acid (LA), 0.1mM ascorbic acid-2-phosphate (L-AA-2P), 20-pM tri-iodothyronine, 0.5µg/mL hydrocortisone, 1% v/v AA (Sigma-Aldrich, St. Louis, MO, USA), 1ng/mL basic fibroblast growth factor (bFGF), and 5ng/mL keratinocyte growth factor (KGF) (LONZA/PeproTech, VIC, AUS).

Table 5.1 Maturation media supplement components and concentrations

Maturation Media (MM)				
Component	**Concentration**	**Catalogue #**	**Company**	**Location**
DMEM/F12 + GlutaMAX™	1:1	1065-018	GIBCO™, Thermo Fisher Scientific	Grand Island, NY, USA
FBS	0.3% (v/v)	1608A	CellSera	NSW, AUS
Basic fibroblast growth factor (bFGF)	1ng/mL	AF-100-18B-100	LONZA, PeproTech	VIC, AUS
Keratinocyte growth factor (KGF)	5ng/mL	AF-100-19-10	Sigma-Aldrich	St. Louis, MO, USA
Hydrocortisone	0.5µg/mL	H0396		
Insulin transferrin-selenium (ITS)	1% (v/v)	I3146		
Linoleic acid (LA)	9.4µg/mL	L9530		
Ascorbic acid-2 -phosphate (L-AA-2P)	0.1mM	A8960		
tri-iodothyronine	20-pM	T5516		
Strontium chloride (SrCl2)	1mM	255521		
Antibiotic antimycotic	1% (v/v)	A5955-100ML		

5.2.5 Air-Liquid Interface (ALI) Platform

Stainless steel lifting frames were manufactured to ensure sufficient numbers for *in vitro* and *in vivo* use. Thirty frames from 316-grade stainless steel, 3mm height, 9.5cm x 9.5cm with bevelled corners, and 50% punched open holes were produced. These were inspected for levelness, washed and sterilised, and the approximated media-level was determined for ALI.

To maintain an air-liquid interface, a cotton wicking sheet was cut to size and sterilised (Whatman filter paper, USA) with a piece of translucent non-absorbent polyethylene netting (N-Terface®, Richardson, TX). The cotton and frames were then submerged and soaked with media to allow complete absorption. Before transferring the skin substitute (SS), these levels were maintained below ALI and re-established post-transfer.

5.2.6 PUR Foam Preparation

The scaffold material used for the CCS fabrication was a 1-mm thick PUR (NovoSorb®) foam. This new batch consisted of an increased number of irregular pore sizes >1mm. The incorporation of the plasma gel, previously used in Chapter 2 and 3 and published in Dearman et al 2013, 2014 [1, 2], was insufficient to produce a well-developed epithelium. In an attempt to decrease this porosity, other gelation methods were tested. A layer-by-layer technique (LBL) of plasma-thrombin-plasma was employed to retain sufficient fibroblast cells to form a supportive network for keratinocyte stratification and epidermal layer formation. The layer-by-layer approach followed the same three day incubation in plasma and then thrombin, in addition a supplementary layer of plasma was further added to fill in the larger open pores. Following the LBL technique the fibroblast cells were inoculated in media (see 5.2.9).

5.2.7 C-GAG Preparation

The fabrication method for the collagen engineered skin was based on a previously described protocol Boyce et al. 1988 [80]. This protocol previously utilised a polyvinyl alcohol (PVA) product – Merocel (Medtronic-Xomed, USA) to aid with the cell inoculation by capillary action onto the C-GAG dermal template. This product required numerous washes to reduce cell cytotoxicity and overnight incubation for rehydration. Discontinuation of the Merocel product by the company required a new material to be sourced and tested. Ramer Ltd and Carwild Corp were two companies contacted that produce PVA foams with similar properties to Merocel. The foams required cytotoxicity testing before implementation into the skin substitute fabrication method. Initial bench testing and comparisons to Merocel (texture, absorption properties) eliminated the Carwild foams. PVA is known to be cytotoxic to cells (as is untreated Merocel), and elution and cytotoxicity tests were mandatory prior to method incorporation [81].

5.2.7.1 Cytotoxicity testing and preparation of RAMER inoculation platform

Large sheets of Ramer PVA foam, FS grade, were supplied. It was essential to pre-wet the non-sterile foam before cutting out circular discs to fit in the 150mm Petri dishes. Following this, the discs were packed and sterilised with ethylene oxide. For this assay, human dermal fibroblasts were used. T75 flasks were established until 85-90% confluence in DMEM-5% FBS. This elution procedure tests the leachable chemicals extracted from the material. Three pre-wash conditions were evaluated (Table 5.2) in triplicates with an untreated Ramer foam. The washing regime included a one-hour incubation at 37°C with Hanks Balanced Salt Solution (HBSS) + 1% Human Serum Albumin (HSA), followed by 1-3, 10-minute washes with 50mL HBSS + 1% HSA. Discs were then incubated at 37°C, 5% CO_2 in a humidified atmosphere for 24 hours in Maturation Medium. The foam was well-drained with each wash, and at the end of the incubation period, the media was extracted and inoculated onto the established monolayer fibroblast cell line for incubation and reactivity evaluation at 24 and 48 hours. Controls included a negative control (treated with 1% SDS), and HDPE plastic – media only and positive (no treatment). Microscopic observations were recorded after 24- and 48-hour incubation periods for cytotoxic effects.

Morphological changes and biological reactivity are described and graded on a scale (0-4) as per Table.5.3. Test samples graded as a "3" or "4" are considered toxic and "0-2" non-toxic [81].

Table 5.2 Detailed description of conditions with various washes. All cut discs were designated a number and weighed for volume calculation. Note: the absorption + media O/N refers to the raw material. O/N, overnight.

Condition	Designated Foam #	Weight (g)
HBSS+1%HSA 1HR + 1 wash 50mL + MEDIA O/N	1	5.78
	2	5.50
	3	5.48
HBSS+1%HSA 1HR + 2 wash 50mL + MEDIA O/N	5	6.69
	7	6.16
	9	6.42
HBSS+1%HSA 1HR + 3 wash 50mL + MEDIA O/N	4	6.72
	8	6.90
	6	7.24
Absorption + MEDIA O/N	10	4.32

Table 5.3 Description of the morphological changes and biological reactivity and grade (0-4) for the elution testing [81].

Grade	Reactivity	Conditions of all Cultures
0	None	Discrete intracytoplasmic granules; no cell lysis
1	Slight	Less than or equal to 20% of the cell are round, loosely attached, and without intracytoplasmic granules; occasional lysed cells are present
2	Mild	Greater than 20% to less than or equal to 50% of the cells are round and devoid of intracytoplasmic granules; no extensive cell lysis and empty areas between cells
3	Moderate	Greater than 50% to less than 70% of the cell layers contain rounded cells or are lysed
4	Severe	Nearly complete destruction of the cell layers

5.2.7.2 C-GAG hydration

The C-GAG was cut to the desired size prior to hydration or manipulation. To a 150mm dish, a piece of sterile N-Terface® (9.5 x 9.5cm) was aseptically transferred, and the C-GAG was placed on top. To the petri dish, 50mL of 70% sterile isopropanol was dispensed and briefly soaked and aspirated. The piece of C-GAG was measured with a sterile surgical ruler, and width and height recorded to determine contraction during the hydration preparation. The C-GAG was then washed with 50mL of HBSS for 10 minutes at room temperature (RT). This wash step was repeated another 3x for 15 minutes with incubation. The final HBSS rinse was aspirated and replaced with 50mL of MM at RT in the BSC for 20 minutes. The media was aspirated and then incubated for 20 minutes at 37°C in 50mL of media ready for use. The C-GAG was measured at all critical steps.

5.2.8 HYBRID Preparation

The fabrication of the hybrid (PUR/C-GAG) scaffold was performed in collaboration with Boyce and colleagues in Cincinnati, USA. The PUR was wet with 50% isopropanol for 30-60 seconds and was exchanged with 0.5M acetic acid (HAc) x2. A 1:2 dilution (50% v/v) of liquid C-GAG:0.5M HAc replaced the HAc. The residual air bubbles were extracted from the PUR foam and incubated overnight at 4°C. After incubation, a 1:1 C-GAG homogenate was incubated for 5-10 minutes with repeated expression of air from the foam. The PUR/C-GAG were then transferred to a casting frame and filled with C-GAG to freeze and lyophilise overnight. Samples were supplied pre-packed and gamma sterilised. Standard methods of thermal hydration were attempted (125°C), which demonstrated melting of the PUR structure unable to withstand the high temperature. The cross-linking step of thermal hydration was replaced by direct chemical cross-linking in 30mM 1-Ethyl-3-(3-dimethylaminopropyl) carbodiimide hydrochloride (EDC) as per Powell and Boyce [82].

5.2.8.1 Hybrid scaffold – cross-linking

The cross-linking method was based on the protocol previously described [82]. Hybrid scaffolds were pre-cut to the required size prior to cross-linking and placed in a 150mm dish. Solutions were then prepared for use; a 95% ethanol solution, a 50mM MES Hydrate solution in 40% ethanol (pH 5.5) and a 30mM EDC/NHS. The resultant solution was then

sterile filtered (0.2µm) prior to use. First, the hybrid scaffold was briefly wet with 95% ethanol and aspirated. The cross-linking solution was added at 1mL/cm^2 to ensure the hybrid was submerged and all surfaces were in contact with this solution. Dishes were placed in 37°C incubator, 5% CO_2 for 6 hours. After cross-linking was complete, the scaffold was rinsed five times with appropriate buffer (HBSS or PBS) at 1mL/cm^2 for 10 minutes per rinse. A final two rinses were performed using Maturation Media, at 1mL/cm^2 for 10 minutes per rinse and then incubated until ready for cellular inoculation.

5.2.9 Skin Substitute Fabrication – Cell Inoculation

The inoculation platform was required for fibroblast and keratinocyte cell inoculation onto the C-GAG template and for the Hybrid template it was only necessary for the keratinocyte inoculation. Pre-prepared PVA foams (section 5.2.7.1) were used to aid cell inoculation of the C-GAG (Fbs and Ks) and the Hybrid (Ks). All scaffolds were transferred to a separate dish for cell inoculation. The Fbs target density was 5x10^5 cells/cm^2 to inoculate at 3x10^6 Fbs/mL in MM. The inoculated suspension was added at 0.167mL/cm^2. Half the cell suspension was added and then rotated 90°C for the remainder of the suspension. Cell volume was left to soak in before transferring to a new dish with a lifting frame (section 5.2.5). For the hybrid scaffold, the PVA foam was not necessary for the inoculation of fibroblasts, and only half the volume was necessary for cell inoculation. Media were exchanged daily for two days prior to keratinocyte inoculation. The keratinocyte target density was 1.0x10^6 cells/cm^2, resuspending at 1.2x10^7 keratinocytes/mL in MM. The cells were resuspended at 0.083mL/cm^2. All the cell inocula were applied in a single application. They remained in the BSC for 10 minutes after seeding or until full absorption and then were gently transferred to the lifting frame. MM was added to the ALI and incubated at 37°C, 5% CO_2 for the desired culture period, i.e., 14-days of co-culture. The PUR foams did not utilise the PVA foam for cell inoculation and were fabricated with the LBL method as described in 5.2.6. Fibroblasts were inoculated at 0.039mL/cm^2 and keratinocytes at 0.031mL/cm^2. The seeding and experimental duration were the same for the C-GAG and hybrid. The medium was exchanged daily, and all SSs were measured with digital photographs and biopsies at regular intervals (Days 7, 10, 12 and 14) for histological analysis and immunohistochemical staining (Appendix III, VI and VII).

5.3 Results

5.3.1 Cytotoxicity Testing of New PVA Ramer Foam for Cell Inoculation

The negative control displayed complete cytotoxic effects with rounding of cells and a score of 4. The positive control maintained healthy cell morphology and normal appearance throughout the test duration, score of 0. Table 5.4 displays the test conditions scores, with the raw Ramer foam (no pre-wash) being moderately cytotoxic to the cells, causing rounding, detachment, and inhibition of growth, scoring a 3-4 moderate to severe reactivity grade for the elution test. Initial soaking to cut the Ramer foam to size and rinsing 4x in a media solution proved to have no toxic outcomes to the cells tested, with a reactivity scoring of 0 and within acceptable parameters (Figure 5.1). Test conditions were valid, and although 1-2 pre-washes were considered non-toxic, there appeared to be less growth at 24 hrs. Therefore, 3x washes was the regime chosen.

Table 5.4 Graded results for the wash conditions of Ramer foam and controls.

Condition	Grade	Reactivity
HBSS + 1%HSA + 1 wash + MEDIA O/N	1	Slight
HBSS + 1%HSA + 2 wash + MEDIA O/N	1	Slight
HBSS + 1%HSA + 3 wash + MEDIA O/N	0	None
Absorption + MEDIA O/N	3	Moderate
Negative control (1% SDS treatment)	4	Severe
Positive control (no treatment)	0	None

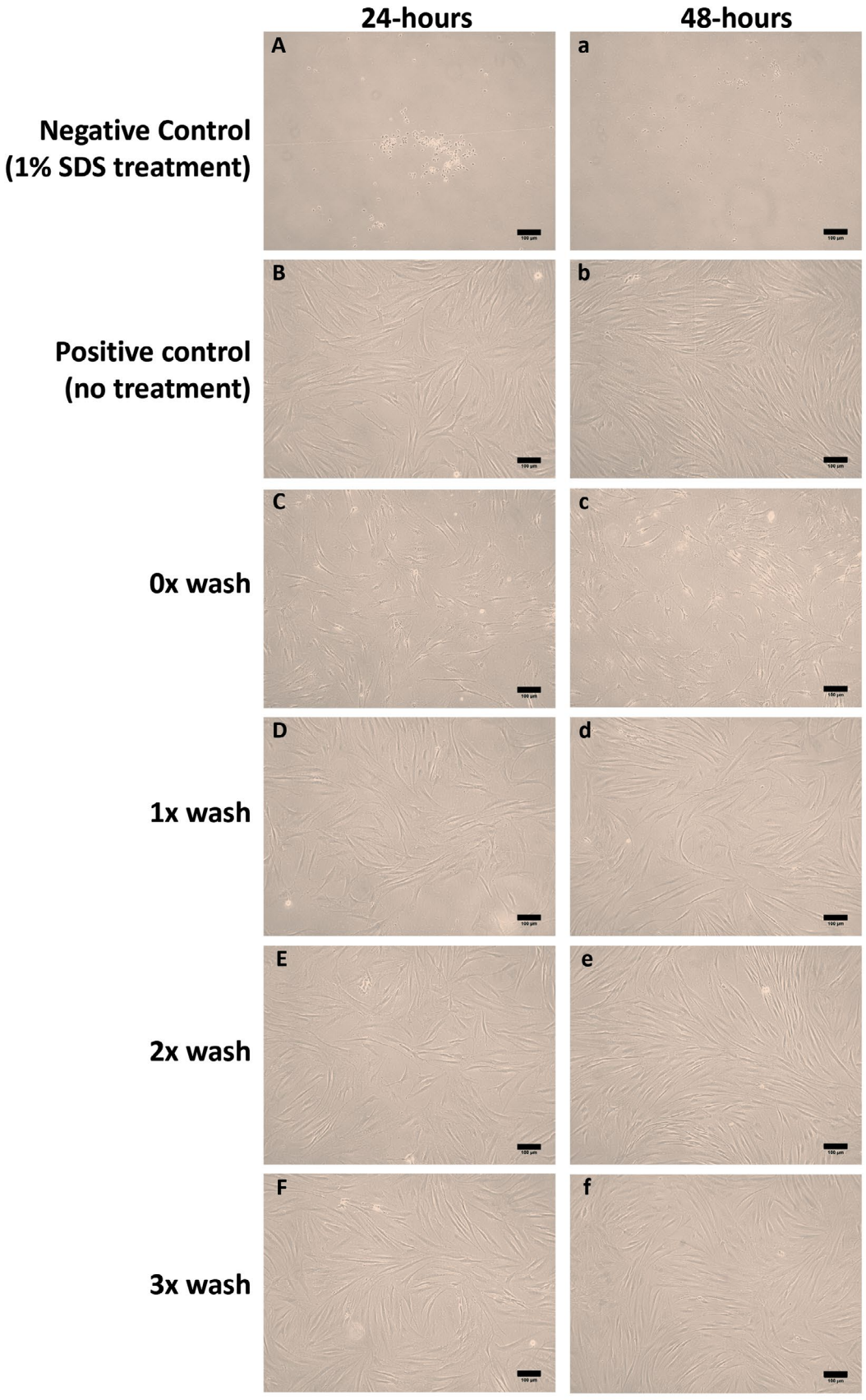

Figure 5.1 Representative phase-contrast images displaying cell cytotoxicity of Ramer foam with controls at 24 and 48 hours (Aa-Ff). Raw Ramer foam (i.e., no wash) displayed rounding cells with dark nuclei and cell loss with detachment. One to two washes showed slight reactivity, and three had no reactivity. Scale bar: 100µm.

5.3.2 Fabrication of Skin Substitutes Utilising PUR, C-GAG and a Hybrid Scaffold

5.3.2.1 Scaffold structure

Figure 5.2 shows the variability of NovoSorb® PUR foam from different batches. Notably larger pores >1.5mm were evident in the second batch received (Figure 5.2b). After the *in vivo* study, optimisation refined the pore consistency with a batch selection process (Figure 5.2 c-d). Although the PUR is infiltrated with plasma and thrombin to form a fibrin network of smaller pores, large pores >1mm are not filled to the surface and do not sustain the adjacent pores' level. The major differences noted between the biopolymers were the thickness; the C-GAG ranged from 240-300µm, the PUR 750-950µm and PUR/C-GAG 919µm -1019µm (Figure 5.3). Additionally, hybrid porosity varied by the degree of C-GAG infiltration with non-uniform collagen distribution and cross-linking regions.

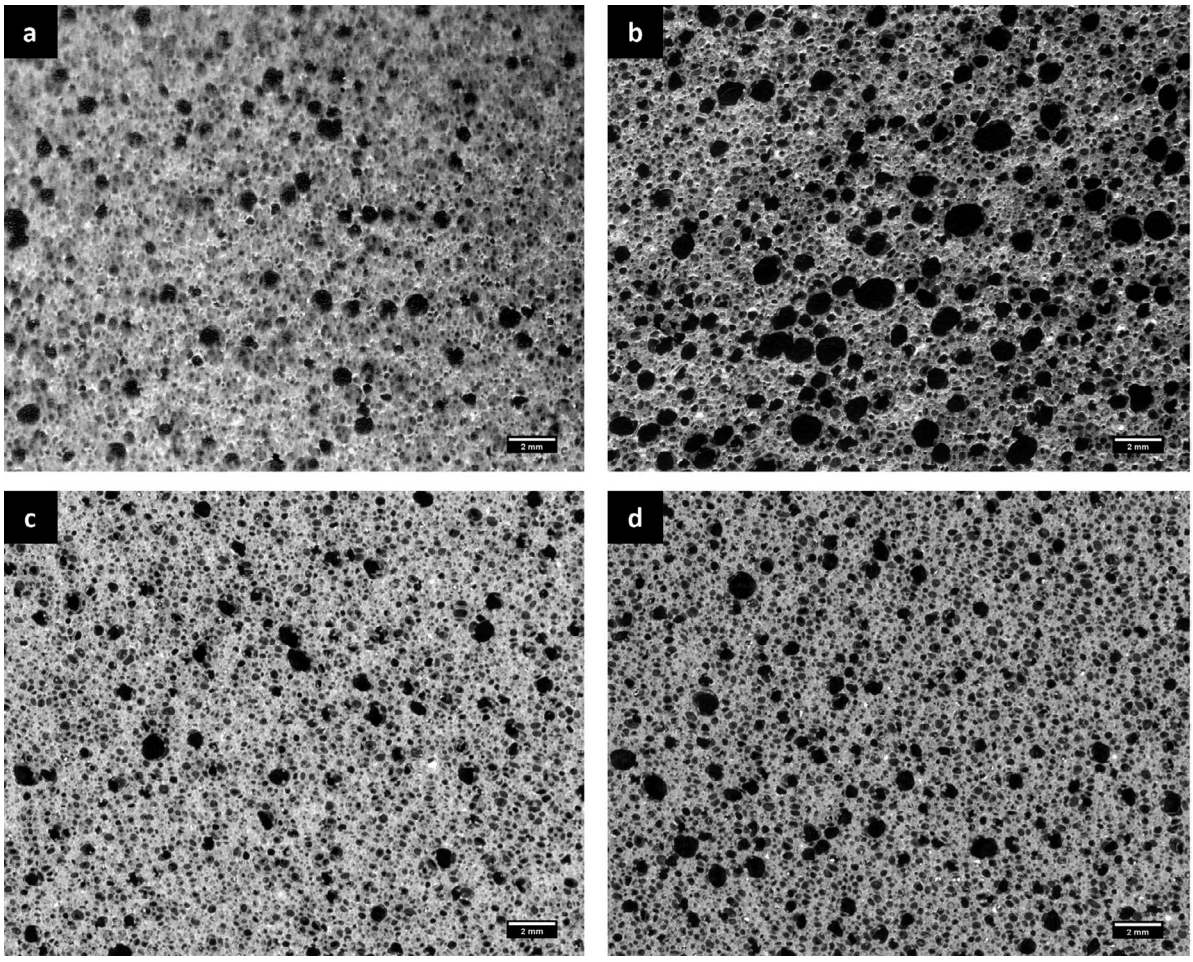

Figure 5.2 NovoSorb PUR Foam showing the variability within batch production, a. 1mm Original batch-A b. 1mm batch-B with unsatisfactory pores > 1mm c. Optimised 1mm batch-C and d. 0.8mm batch-d. Note this is an unsealed PUR foam. Scale bar: 2mm.

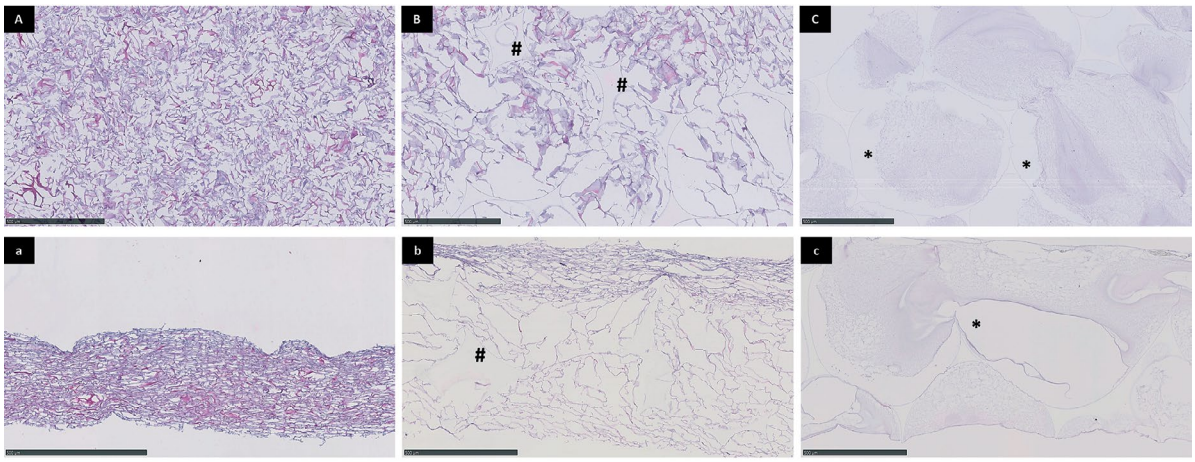

Figure 5.3 Shows representative histological H&E stained sections of the biopolymers with no cells. A-C horizontal cut sections, and a-c vertical cut sections. A, a. C-GAG, B,b. PUR/C-GAG crosslinked, C,c. PUR. # denotes PUR and * shows edge detachment of the fibrin network from the PUR with paraffin-embedded cut sections. Scale bar: 500µm

5.3.2.2 *In vitro* skin substitutes

The skin substitutes were fabricated at an air-liquid interface, scaffolds were inoculated with fibroblasts for three days, followed by the application of keratinocytes and co-cultured for 14 days. Histological staining shows epidermal stratification similar to native tissue for all SS conditions (Figure 5.4). Collagen production was confirmed with Masson's Trichrome staining. The PUR-fibrin filled fibroblast scaffold displayed keratinocytes lining the sides of polymer foam within this structure. Although the hybrid epidermis was not as thick, it was supported by a dermal structure populated with fibroblasts actively producing collagen. The C-GAG scaffold supported a thick, well-developed epidermis with collagen-producing fibroblasts. All engineered substitutes lacked the rete ridges present in native human skin.

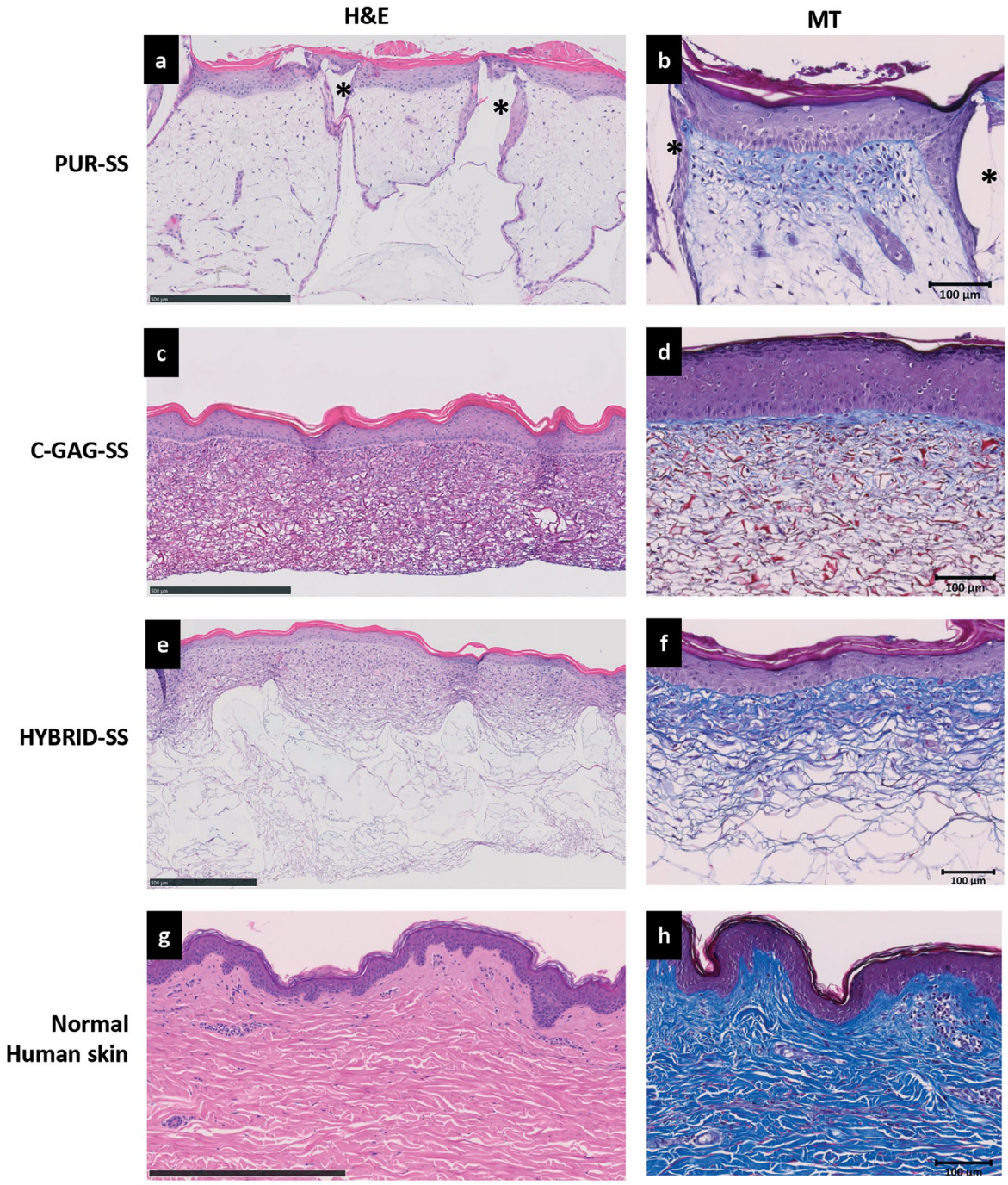

Figure 5.4 Haematoxylin & Eosin (H&E) and Masson's Trichrome (MT) staining of human fabricated skin substitutes (SS) with the different biopolymer scaffolds, a-b. PUR-SS, c-d. C-GAG-SS, e-f. Hybrid-SS and g-h. Native human skin control. * Denotes PUR with infiltration. Scale bar: a, c, e, g 500µm and b, d, f, h 100µm.

Further, immunofluorescence analysis was performed to identify normal skin keratins and basement membrane markers (Figure 5.5). The epidermal layers showed transitioning positivity for cytokeratin 14 compared to normal skin's confined positive basal layer. However, staining of cytokeratin 10 revealed the basal layer (only blue DAPI-positive nuclei) was not positive for the differentiating marker K10 compared with the other layers (Figure 5.5). Laminin confirmed basement membrane formation, and Ki67 positive proliferating cells were within the SS.

Similarly, the porcine skin substitutes employed the same technique devised for the *in vitro* human substitutes. As shown in Figure 5.6, histological staining of the substitutes have well-developed stratified epidermal layers and a thick stratum corneum layer. The basal layer shows typical columnar epithelium adjacent to a layer of collagen producing fibroblasts (Figure 6 column 2). Immunohistochemistry stain for Ki67 proliferative cells showed a normal distribution within the basal layer as per native skin, with no hyperproliferation observed.

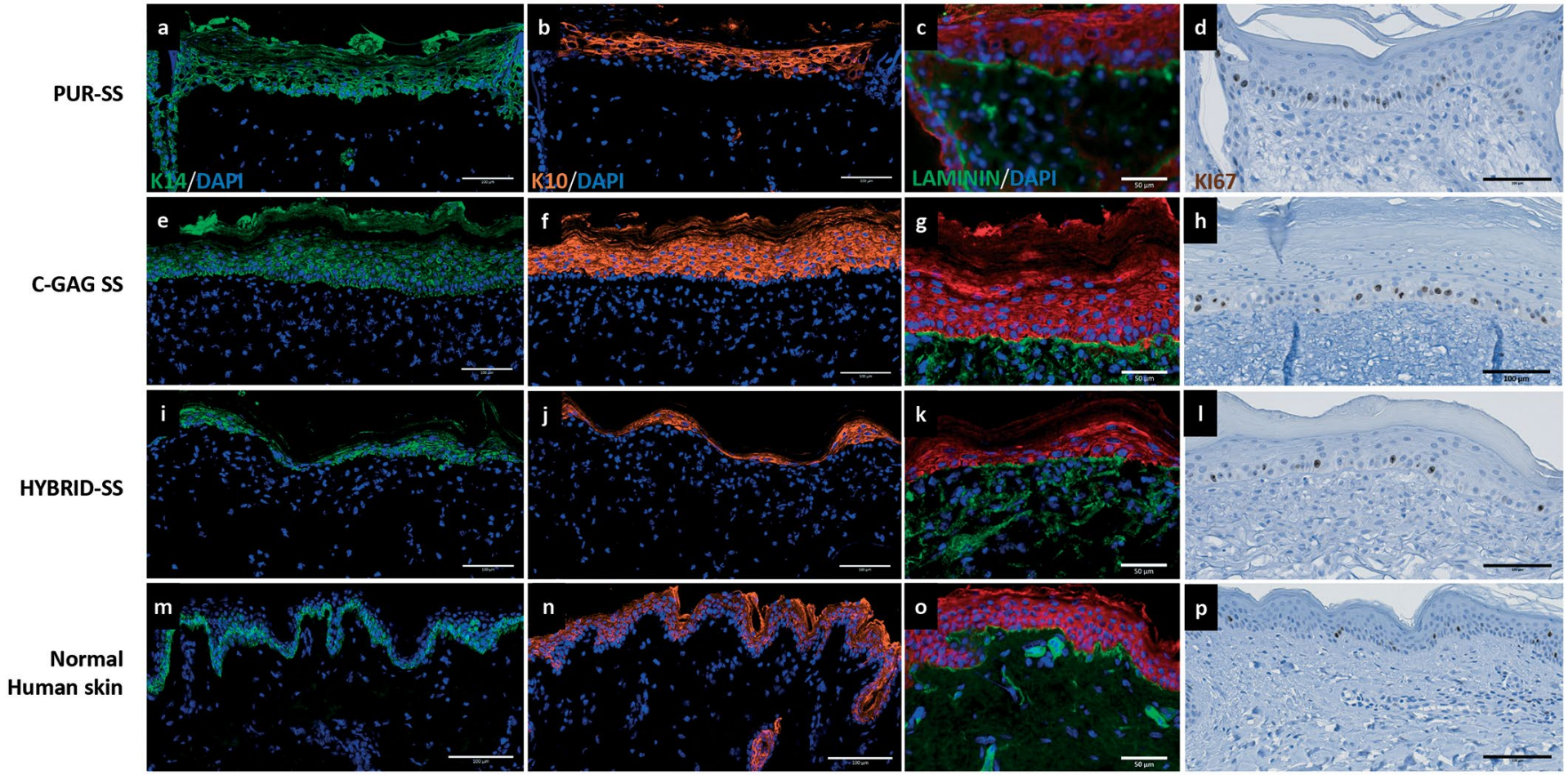

Figure 5.5 Skin substitutes (SS) – human-derived with different biopolymer scaffolds, Row 1. PUR-SS, Row 2. C-GAG-SS, Row 3. Hybrid-SS and Row 4. Native human skin control. Column a cytokeratin 14 (green), column b cytokeratin 10 (depicted orange), Column c laminin (green) and column d Ki67 (brown DAB). Blue (DAPI) counterstained nuclei. Scale bar: 100µm except for c, g, k, o 50µm.

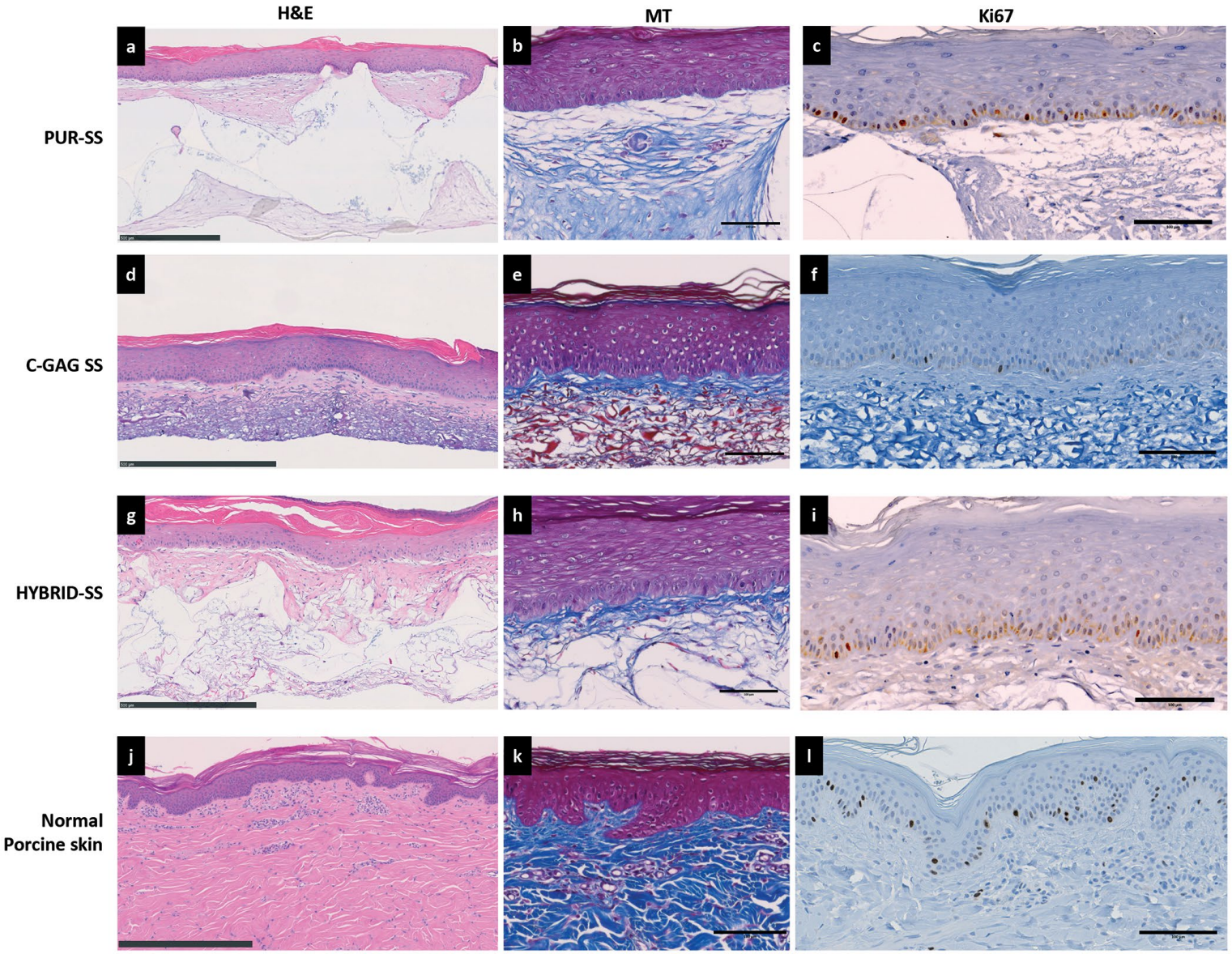

Figure 5.6 Porcine fabricated skin substitutes with PUR, C-GAG, and Hybrid scaffolds. Normal porcine skin is shown as a control. Representative images for H&E stained sections, column a. Masson's Trichrome (MT) stained sections, column b and Ki67 immunohistochemistry, column c. SS – Skin substitute. Scale bar: 100µm, except a, d, g, j 500µm.

5.4 Discussion

This chapter established fabrication methods for bioengineered skin substitutes for human and porcine models. The skin substitutes were constructed with blended scaffold materials with good biocompatibility and morphologically similar structures. All scaffolds were populated with dermal fibroblasts and endogenous collagen, enabling the development of stratified epidermal layers. The porcine epidermis appeared thicker in all groups compared to the human model. As noted in Chapter 4, porcine keratinocytes established using the feeder layer technique and Green's medium exhibit exceptionally high proliferation, fabrication of future grafts may consider an inoculation decrease from the $1x10^6/cm^2$ keratinocytes. Whereas the fibroblast cell inoculation numbers were increased for the porcine fibroblasts, as they are a more difficult population to establish. Previous studies have observed a 28-day growth period for porcine skin fibroblasts grown in a DMEM 15% FBS [83], and others have noted typical fibroblast morphology (spindle elongation) beyond passage two fibroblasts [84]. It is worth noting that these cells were also grown on a collagen coating and with high concentrations of foetal bovine serum [84].

The blending of natural and synthetic polymers achieves both the physical and chemical characteristics of a dermal scaffold. The combinational 3D scaffolds, PUR/plasma and PUR/C-GAG, provided physical support for the growth of fibroblasts and extracellular matrix proteins. These results are similar to other mixed dermal scaffolds that have shown increased biocompatibility and mechanical properties [85-88]. In an attempt to generate bi-layered substitutes, the previously mentioned studies used corresponding pure synthetic polymers as controls which showed decreased cellular affinity and limited morphogenesis, while collagen only hydrogels have shown increased contraction. However, the hybrid approach increases the degree of complexity, and a stand-alone scaffold is desirable. Unlike most synthetic polymers, the biocompatibility of polyurethane has been shown to support cell growth of fibroblasts and keratinocytes [89-92]. Its flexible biodegradability and modifiable properties make it an attractive biomedical alternative.

The first step in constructing a skin substitute akin to human skin involves the isolation and rapid growth of these cells in monolayer *in vitro* to enable re-population into a chosen scaffold. Having sufficient fibroblasts to support the development of the epidermal layer within the skin substitute is crucial to tissue organisation [93, 94]. In addition, providing an interface between the medium and air stimulates stratification and cornification of the epidermal layers [95]. The human PUR-SS was found to have keratinocyte infiltration within the fibroblast dermal scaffold. Cells descended the edge of the polymer pores during transfer post-inoculation to ALI when the pores of the scaffold are stretched. This infiltration leads to epidermal disorganisation and possible cyst formation, which would not produce an epithelium ideal for transplantation.

An engineered skin analogue has yet to replace the anatomy and physiology of skin autografts, much less native skin. However, to promote stable engraftment and skin functionality, the expression of epidermal and dermal markers are fundamental. The presence of basal keratinocytes expressing keratin 14 was evident in all groups of the skin substitutes, although to some extent, this was observed in the suprabasal layer suggesting hyperproliferation that returns to normal with engraftment over time [86, 96]. The keratin 10 marker indicated normal differentiation of the suprabasal stratum spinosum and stratum granulosum in the skin substitutes, as shown in Figure 5.5. While the skin substitutes clearly show prominent stratum corneum on histological sections, a positive marker for terminal differentiation would have confirmed the complete keratinisation process. Anti-filaggrin antibodies that have been used in previous studies were found to be non-reactive on porcine skin [97].

In vitro epidermal maturation, as described above, and the establishment of barrier function are important features for a bioengineered construct. The interaction between keratinocytes and fibroblasts is fundamental for *in vivo* wound healing and an essential interface to establish prior to transplant. The formation of the connecting basement membrane was confirmed by immunohistochemistry staining for laminin. This protein was expressed along the junction between the epidermis and dermis, indicating partial barrier function [98]. Additional laminin staining was observed in the dermal portion of the collagen-based skin substitutes. In line with these findings, Mahjour et al. also found positive laminin infiltrate in

the lower portion of the dermal domain in the cultured skin substitutes suggesting secretion of laminin into this space prior to DEJ establishment [99]. Native human skin also showed positive laminin staining related to the microvascular membranes in the dermal region.

Normal skin anatomy has a microstructure affiliation of rete ridges that increase the surface area and physical attributes of the DEJ, providing niches for keratinocyte stem cells [100]. These structures were not present in the current skin substitute fabrications. While this lack of formation is inherent with *in vitro* engineered constructs [101-103], recent studies have attempted laser micropatterning of dermal templates to mimic rete ridges with varied results. Shen et al. infiltrated a micropatterned template with fibroblasts and keratinocytes with no basement membrane evident [104]. In contrast, Blackstone et al. used fractional CO_2 laser ablation in an established engineered skin model with successful BM formation pre- and post-transplantation [105]. The same group applied cultured epithelial autograft (CEA) to electrospun laser micropatterned dermal templates with narrow and deep invaginations in immunodeficient mice, resulting in rete ridge formation 2-weeks post grafting when compared to a flat DEJ template [103].

Immunohistochemical staining with proliferation marker Ki67 showed the *in vitro* skin substitutes had a similar distribution pattern to native skin. These Ki67-positive keratinocytes resided in the basal epidermal layer with no distribution throughout the upper layers or evidence for keratinocyte hyperproliferation or neoplastic transformation. The next phase consisted of evaluating the histogenesis of these skin substitutes based on the results obtained from the *in vitro* studies. The following chapter explores how the three scaffolds engraft in a porcine model of excisional wounds.

CHAPTER 6:
Comparison of Biopolymer Scaffolds for the Fabrication of Skin Substitutes in a Porcine Wound Model

Dearman BL, Boyce ST, Greenwood JE

Submitted to

Wound Repair and Regeneration

2022

6.1 Overview

The COVID-19 pandemic resulted in a significant delay to the *in vivo* study. From the *in vitro* studies performed in Chapter 5, this study investigated the novel hybrid (PUR/C-GAG) formulation with the layer-by-layer PUR composite cultured skin and a well-established collagen-glycosaminoglycan (C-GAG) skin substitute model. The three test conditions were compared to a meshed skin autograft in a porcine wound model. The results have been reported in a manuscript submitted to *Wound Repair and Regeneration* presented as a revised draft version, for full size images of the paper figures refer to Appendix X.

Statement of Authorship

Title of Paper	Comparison of Biopolymer Scaffolds for the Generation of Skin Substitutes in a Porcine Wound Model.
Publication Status	☐ Published ☐ Accepted for Publication ☑ Submitted for Publication ☐ Unpublished and Unsubmitted work written in manuscript style
Publication Details	Dearman BL, Boyce ST & Greenwood JE 2022, 'Comparison of Biopolymer Scaffold for the Generation of Skin Substitutes in a Porcine Wound Model'. *Submitted to Wound Repair and Regeneration*

Principal Author

Name of Principal Author (Candidate)	Bronwyn Dearman
Contribution to the Paper	Conceptualisation of project. Study design, methodology execution and analysis of all samples. Manuscript writing, editing and review for submission. Corresponding author.
Overall percentage (%)	85%
Certification:	This paper reports on original research I conducted during the period of my Higher Degree by Research candidature and is not subject to any obligations or contractual agreements with a third party that would constrain its inclusion in this thesis. I am the primary author of this paper.
Signature	Date: 5TH APRIL 2022

Co-Author Contributions

By signing the Statement of Authorship, each author certifies that:

i. the candidate's stated contribution to the publication is accurate (as detailed above);
ii. permission is granted for the candidate to include the publication in the thesis; and
iii. the sum of all co-author contributions is equal to 100% less the candidate's stated contribution.

Name of Co-Author	Professor John Greenwood
Contribution to the Paper	Project participation. Manuscript review and editing.
Signature	Date: 5TH APRIL 2022

Name of Co-Author	Professor Steven Boyce
Contribution to the Paper	Project advice, manuscript review and editing.
Signature	Date: 30 April 2022

Please cut and paste additional co-author panels here as required.

WOUND REPAIR AND REGENERATION

Comparison of Biopolymer Scaffolds for the Fabrication of Skin Substitutes in a Porcine Wound Model

Journal:	*Wound Repair and Regeneration*
Manuscript ID	WRR-22-03-0075.R2
Manuscript Type:	Original Article – Basic Science
Date Submitted by the Author:	n/a
Complete List of Authors:	Dearman, Bronwyn; Royal Adelaide Hospital, Skin Engineering Laboratory; Royal Adelaide Hospital, Adult Burns Centre; The University of Adelaide Faculty of Health and Medical Sciences Boyce, Steven; University of Cincinnati, Surgery Greenwood, John; Royal Adelaide Hospital, Adult Burns Centre
Key Words:	Scaffolds, Skin substitutes, Burns, Porcine wound model, Biopolymers
Abstract:	This study compared three acellular scaffolds as templates for the fabrication of skin substitutes. A collagen-glycosaminoglycan (C-GAG), a biodegradable polyurethane foam (PUR) and a hybrid combination (PUR/C-GAG) were investigated. Scaffolds were prepared for cell inoculation. Fibroblasts and keratinocytes were serially inoculated onto the scaffolds and co-cultured for 14 days before transplantation. Three pigs each received four full-thickness 8cm x 8cm surgical wounds, into which a biodegradable temporising matrix (BTM) was implanted. Surface seals were removed after integration (28 days), and three laboratory-generated skin analogues and a control split-thickness skin graft (STSG) were applied for 16 weeks. Punch biopsies confirmed engraftment and re-epithelialisation. Biophysical wound parameters were also measured and analysed. All wounds showed greater than 80% epithelialisation by day 14 post-transplantation. The control STSG displayed 44% contraction over the 16 weeks, and the test scaffolds, C-GAG 64%, Hybrid 66.7% and PUR 67.8%. Immunohistochemistry confirmed positive epidermal keratins and basement membrane components (Integrin alpha-6, collagens IV and VII). Collagen deposition and fibre organisation indicated the degree of fibrosis and scar produced for each graft. All scaffold substitutes re-epithelialised by four weeks. The percentage of original wound area for the Hybrid and PUR was significantly different than the STSG and C-GAG, indicating the importance of scaffold retainment within the first three months post-transplant. The PUR/C-GAG scaffolds reduced the polymer pore size, assisting cell retention and reducing the contraction of in vitro collagen. Further investigation is required to ensure reproducibility and scale-up feasibility.

Original Research Article

Comparison of Biopolymer Scaffolds for the Fabrication of Skin Substitutes in a Porcine Wound Model

Bronwyn L Dearman [1,2,3*], Steven T Boyce [4], John E Greenwood [2]

[1]Skin Engineering Laboratory, Adult Burns Centre, Royal Adelaide Hospital, Adelaide, SA, Australia

[2]Adult Burns Centre, Royal Adelaide Hospital, Adelaide, SA, Australia

[3]The University of Adelaide, Faculty of Health and Medical Science, Adelaide, SA, Australia

[4]University of Cincinnati, Department of Surgery, Cincinnati, OH, United States

*** Correspondence:**

Bronwyn Dearman

Royal Adelaide Hospital, 1 Port Road, Adelaide, SA, 5000

+61 419 811 887

bronwyn.dearman@sa.gov.au

Short running title: Comparison of Biopolymer Scaffolds for Skin Substitutes

Keywords: Scaffolds, Biopolymers, Burns, Porcine wound model, Skin substitutes.

This project was supported by Lifetime Support Authority.

Abstract

This study compared three acellular scaffolds as templates for the fabrication of skin substitutes. A collagen-glycosaminoglycan (C-GAG), a biodegradable polyurethane foam (PUR) and a hybrid combination (PUR/C-GAG) were investigated.

Scaffolds were prepared for cell inoculation. Fibroblasts and keratinocytes were serially inoculated onto the scaffolds and co-cultured for 14 days before transplantation. Three pigs each received four full-thickness 8cm x 8cm surgical wounds, into which a biodegradable temporising matrix (BTM) was implanted. Surface seals were removed after integration (28 days), and three laboratory-generated skin analogues and a control split-thickness skin graft (STSG) were applied for 16 weeks. Punch biopsies confirmed engraftment and re-epithelialisation. Biophysical wound parameters were also measured and analysed.

All wounds showed greater than 80% epithelialisation by day 14 post-transplantation. The control STSG displayed 44% contraction over the 16 weeks, and the test scaffolds, C-GAG 64%, Hybrid 66.7% and PUR 67.8%. Immunohistochemistry confirmed positive epidermal keratins and basement membrane components (Integrin alpha-6, collagens IV and VII). Collagen deposition and fibre organisation indicated the degree of fibrosis and scar produced for each graft.

All scaffold substitutes re-epithelialised by four weeks. The percentage of original wound area for the Hybrid and PUR was significantly different than the STSG and C-GAG, indicating the importance of scaffold retainment within the first three months post-transplant. The PUR/C-GAG scaffolds reduced the polymer pore size, assisting cell retention and reducing the contraction of *in vitro* collagen. Further investigation is required to ensure reproducibility and scale-up feasibility.

1 Introduction

In the last decade, transformative technologies have emerged and expanded the interest in tissue engineered skin substitutes. However, a cost-effective, clinically available, dermal-epidermal tissue-engineered skin substitute still remains elusive due to the complexity, high cost and time-consuming nature of production (1). Several limitations exist with the current dermal scaffold models used to generate engineered skin substitutes. Most experience since 1975 has been with utilising animal-derived collagens and combinations such as collagen/glycosaminoglycan (C-GAG) (2-4). Since the dermis lost to burn injury is composed of these biopolymers, replacement with like as a scaffold for autologous cellular delivery seems intuitive, although xenogeneic collagens are costly and have potential immunogenicity and concerns of disease transmission. Despite clinical success (5), these scaffolds and subsequent grafts have been shown to contract to 50% of their original area *in vitro*, and have the potential to alter mechanical properties (6). Recently, experience with synthetic polymers as scaffolds has been published, demonstrating successful incorporation into a skin substitute model (7), even indicating apparent advantages over collagen-based scaffolds (8), albeit with limitations. There are few substitutes that constitute only a scaffold without additional materials. Some synthetic polymers' degradation products and residual additives are cytotoxic or fail to degrade completely (9). Polyethylene glycol, polyurethanes (PUR), polyvinyl alcohol (PVA), polylactic acid (PLA), polycaprolactone (PCL) (10, 11), polyvinylpyrrolidone (PVP) (12), poly(lactide-co-glycolide) (PLGA) (13) and polystyrene (14) have all received attention. Whether consisting of electrospun or woven fibres or having a foam structure, the pores are not uniform and have a broad range of sizes and an unpredictable proportion of open or closed cells. Pore size variability, mainly if they are large, decreases the mechanical stability of the overall structure and cell retention (15), although diameters of greater than 500µm might aid rapid vascularisation (16). If the pores are too small, they inhibit cellular ingrowth and collagen

deposition. Some iterations of tissue scaffolds use a combination of biological and synthetic polymers to generate an extracellular matrix that mimics the dermal fibrous structure by increasing cellular recognition and tissue compatibility. These have included fibrin hydrogels, gelatin, sodium alginate, hyaluronic acid (HA), amniotic membrane, and silk (17) (8) (18-24). These can assist with porosity whilst providing a microenvironment that supports epidermal integrity.

The potential of a PUR generated composite cultured skin (CCS) in a porcine wound model in small and large wounds has been demonstrated (7, 25, 26). However, PUR batch consistency has plagued production with an unacceptable proportion of pores exceeding 1mm diameter. The CCS consists of a PUR foam scaffold soaked in fresh frozen plasma and human thrombin to produce a fibrin network, reducing the polymer pore sizes. This gelation reduces fibroblast loss and increases keratinocyte retention on an external surface during and after inoculation. Although this method has shown clinical success with previous PUR foam iterations, the additives inherently introduce variability and batch to batch inconsistency. A ready-to-use, off-the-shelf product is desirable. Since collagen-GAG has an experimental and clinical history, it was postulated that a PUR/C-GAG hybrid might provide advantages from both materials - simultaneously filling the oversized pores of the PUR foam with C-GAG to afford greater cellular retention post-inoculation and promotion of epidermal morphogenesis. The PUR scaffold provides additional structural support to reduce C-GAG contraction. This report describes a comparison among these three scaffolds against each other and a skin-graft control to generate a bi-layered skin substitute for extensive full-thickness burns. The investigators believe this is the first hybrid scaffold composed of PUR foam and collagen-GAG scaffold that has been evaluated in a large animal model.

2 Materials and Methods

2.1 Scaffolds

The biodegradable polyurethane (PUR) NovoSorb® foam is 1mm thick for CCS production. PUR scaffolds for both *in vitro* and *in vivo* experiments were cut to size from sterile 24.5cm x 24.5cm ± 0.3cm sheets. The collagen-glycosaminoglycan (C-GAG) scaffolds were bovine dermal collagen and chondroitin-6-sulfate from shark cartilage and fabricated as per Boyce et al. 1988 (kindly provided from the Boyce Lab, Cincinnati). These were dry-packed, sterile ~8cm x 8cm pieces. The hybrid (PUR/C-GAG) was formulated using 1mm PUR sheets and liquid C-GAG. The C-GAG permeated the PUR overnight and was then processed as per Boyce et al. 1988 (3). The cross-linking step of thermal hydration was replaced by direct chemical cross-linking in 30mM 1-Ethyl-3-(3- dimethylaminopropyl) carbodiimide hydrochloride (EDC) as per Powell and Boyce (27). All scaffolds were sterilised by gamma-irradiation.

2.2 Animal Model

Three large white x Landrace pigs were used, average weight 27kg upon BTM implantation. Approval was granted by the South Australian Health and Medical Research Institute (SAHMRI) Animal Ethics Committee (Approval number SAM282v4). Due to the use of bovine collagen from the USA, additional approval from the Australian Government Department of Agriculture, Water and the Environment (DAWE) was necessary for the *in vivo* use of a restricted imported biological material (Approval #2019/081). All animals were humanely treated and were acclimatised for 11 days. Four days prior to surgery, one unit of blood (~400mL) was collected from each pig by jugular venipuncture to isolate autologous porcine fresh frozen plasma (pFFP) for PUR substitute fabrication. On the day of surgery, general anaesthesia was induced with intramuscular Ketamine-Xylazine (Ketamine 10mg/kg, Xylazine 2mg/kg) 30 minutes before intubation with IM Noroclav (amoxicillin/clavulanic acid

- 1ml/20kg) administered once anaesthetised. Post-operative pain was managed with 1mL of Buprenorphine Hydrochloride (324µg) administered subcutaneously on anaesthetic recovery and for the next three days with a single 2µg/kg/hr Fentanyl patch.

2.3 Wound Administration (BTM implantation)

The wounds were generated, prepared, and dressed according to our previous studies (7, 25-26). In brief, four full-thickness 8cm x 8cm surgical wounds were created to the level of the panniculus adiposus. The excised skin provided the source of autologous cells for individual substitute fabrication. NovoSorb™ Biodegradable Temporising Matrix (BTM) was cut to size and implanted, affixed with staples and allowed to integrate for 28 days. The wounds were monitored, measured, photographed and re-dressed twice weekly.

2.4 Fabrication of Skin Substitutes

On the day of BTM implantation, the four pieces of excised skin per pig were processed for autologous cell isolation. On average, this totalled 195cm^2 per pig. Porcine fibroblasts (pFbs) and porcine keratinocytes (pKs) were cultured as per Dearman et al. 2013, 2014, 2021 (7, 25, 26). Cells were expanded and then cryopreserved (Coolcell, Corning, Australia) until required for pending skin substitute setup. Duplicate substitutes were established for each pig, except C-GAG (where triplicates were required). Three days prior to pFbs inoculation, PUR foams were soaked in autologous pFFP. One day prior, the C-GAGs underwent pre-washing along with hybrid cross-linking. A double-layering method (LBL) of plasma/thrombin was used for the PUR. pFbs were inoculated on day 0 at 7.5x10^5/cm^2 and pKs three days later at 1x10^6/cm^2. All substitutes were cultured at an air-liquid interface, and media were exchanged daily as previously described (28). The skin substitutes were incubated at 37ºC, 5% CO_2, saturated humidity for 14 days until their application 28 days after the implanted BTMs. To prepare the sites for graft transplantation, BTM seals were delaminated and lightly dermabraded to

generate punctate bleeding. The skin substitutes were then cut to size and applied with a piece of Mepitel-one cut 1cm larger than the graft to aid transfer to the wound site.

Split-thickness skin graft (STSG), meshed 1:3, were used as controls to replicate a typical mesh size employed for extensive burns. A Zimmer® Electric Dermatome (kindly loaned by Zimmer Pty Ltd), set at 0.012inches, enabled a clean ~5cm x 9cm graft from the top right shoulder area. This graft was meshed, applied to wounds and secured with staples.

2.5 Qualitative Wound Analysis

Wounds were maintained and dressed as previously described (7). The DermaLab Combo (Cortex, Hadsund, Denmark) readings were performed at weeks 2, 4, 8, 12 and 16. Three-mm punch biopsies were collected and fixed in 10% neutral buffered formalin for paraffin embedding. Fresh frozen samples were placed in cryoprotectant OCT™ embedding medium (ProSciTech, QLD, Australia) in plastic moulds, frozen in isopentane cooled to freezing point, and stored at -80°C. The wound area and biopsy locations was traced onto sterile acetate sheets for map tracing. ImageJ analysis of wound area was performed by taking two ruler measurements top and bottom of the wound, averaging them, scale set and area determined. Epithelialisation and engraftment were defined by a visible epidermal matte layer on the wound surface. The percentage of re-epithelialisation and original wound area were determined over time.

2.5.1 Histological Evaluations

Post fixation, paraffin-embedded biopsies were processed for routine histology, cut at 5-7µm, and stained with haematoxylin and eosin (H&E). Three biopsies were taken for each condition at each timepoint for histological analysis. Immunohistochemical (IHC) staining on paraffin and frozen sections confirmed the epidermal and dermal anatomy. Frozen sections were air-dried at room temperature for 1hour before a 10minute acetone fixation step followed by

standard immunofluorescence. Paraffin sections were processed using a Mouse and Rabbit specific HRP/DAB IHC micro polymer detection kit (ab236466, Abcam) or a streptavidin-biotinylated immunoperoxidase technique (29). For immunofluorescence, primary and secondary antibodies are detailed in supplementary data tables. Images were captured with an Olympus FV3000 confocal microscope and scanned with a Zeiss Axio Scan.Z1 slide scanner (Carl Zeiss, Germany). Control tissues were normal human skin from donors undergoing elective surgery procedures, or normal porcine skin from healthy, species matched pigs. Picrosirius red (PSR) stain (ab150681, Abcam) was used to determine and visualise collagen deposition, fibre orientation and organisation. Samples were taken on days 10, 21, 56 and 112 for each condition. Representative slides were imaged using polarising light microscopy (Zeiss, Axio Scan.Z1 slide scanner, Germany) to detect birefringence. Collagen Type 1 (thick fibres) stains yellow/orange birefringence, and Collagen III (thin fibres) stain green birefringence. Microvascular density (MVD) was assessed for endothelial cell marker CD31, positive neovessels were stained with 3,3'-diaminobenzidine (DAB), and Ki67 was used as a cellular marker to assess Ki67+ expression and proliferation.

2.6 Ordinal and Quantitative Wound Assessment

2.6.1 Observer Scar Assessment Scale (OSAS)

The POSAS (30) observer scale was modified as a scar assessment tool for the final study time point. This scale measures the overall vascularity, pigmentation, thickness, relief, pliability, and site surface area. These were scored on a scale ranging from 1 ('like normal skin') to 10 ('very different from normal skin'), with an overall observer opinion. The total score was calculated for each condition. Ratings from animal subjects could not be recorded.

2.6.2 DermaLab

The Transepidermal Water Loss (TEWL) probe is an open chamber method based on Nilsson's Vapor Pressure gradient (Cortex, DermaLab). Light to moderate pressure was applied against the skin. In addition to measuring TEWL, the other DermaLab probes evaluated skin elasticity, skin colour and skin thickness. Measurements were performed in triplicate, except for the skin elasticity probe (single sample), as this requires a 45-minute rest period between each measurement cycle. Environmental temperature and humidity were recorded for all measurements. Viscoelasticity (VE - MPa), Melanin Index (MI) and Erythema Index (EI) were parameters chosen for evaluation. The DermaLab calculates the VE by combining the elasticity modulus and the retraction phase. The same investigator performed all the measurements at all timepoints.

2.7 Statistical Analyses

Wound area percentage over time was assessed using linear mixed-effects modelling, with fixed effects for test conditions (STSG, C-GAG, PUR, PUR/C-GAG), time in days and the reciprocal of time in days. Two-way interactions between condition and time and the reciprocal of time were included to enable the effect of time on wound area to vary according to condition. A random effect for each animal was specified to account for repeated measurements made on the same pigs. Mean wound percentage for each condition at selected time points were estimated post-hoc, and pairwise comparisons of wound area percentage between and among conditions were conducted at 14, 28 and 112 days. The Bonferroni adjustment for multiple comparisons was applied, a p-value of < 0.05 was considered statistically significant. The charts displayed show the observed values with mean and standard deviation for each outcome. In addition, a Friedman test was conducted on three pigs to examine the effect of condition on OSAS score. Each pig was subjected to each of five conditions. Pairwise comparisons of

interest were assessed using Wilcoxon matched-pairs signed-rank tests, adjusted for multiple comparisons using the Bonferroni correction. All analyses were performed using Stata v15 (College Station, TX, USA).

3 Results

3.1 In vitro Observations of Skin Substitutes

Prior to the commencement of the *in vivo* study, PUR, C-GAG and hybrid models showed histological evidence of an organised epidermal-dermal composite suitable for transplant (Supplementary Figure S1). *In vitro* contraction of C-GAG scaffolds showed a mean percentage decrease of 55% from dry state to cellular inoculation (n = 9). The hybrid (PUR/C-GAG) and PUR scaffold resulted in no contraction. A decrease of cross-linked C-GAG in hybrid scaffolds was observed in histological sections, causing non-homogenous epidermal integrity.

3.2 Macroscopic Observations

The BTM integrated into wounds with minimal delamination of the surface seals and only contracted 3.6% of the original wound area until transplantation. Biopsies post-delamination and pre-dermabrasion showed well-integrated polymer adjacent to the subcutaneous fat with a small granulation layer supra.

The C-GAG grafts were fragile and thin to manipulate, requiring multiple staples to piece together and achieve wound area coverage. The hybrid graft was the easiest to cut, handle, and apply, followed closely by the PUR scaffold graft. There was no evidence of gross infection in any conditions with minimal scratching observed; all pigs were healthy for the entirety of the study, and upon complete healing, all wounds remained closed for the observation period. Representative images of wounds and conditions from selected time points post-transplantation

at days 0, 14, 28, 56 and 112 (2, 4, 8, 16 weeks) are shown in Figure 1 columns a-d. The final percentage of wound contraction from original is tabled in Figure 1e for each condition.

The 1:3 meshed STSG engrafted by day 14 with 100% wound re-epithelialisation. The PUR substitute displayed a dry superficial crust-like appearance over a large percentage of the wound, and with gentle removal, the wound was fully re-epithelialised below with a developed epidermal barrier. Hybrid grafts showed initial engraftment with small areas of PUR scaffold extrusion two weeks post-transplant with secondary re-epithelialisation assisting complete closure. The C-GAG substitutes displayed interstitial healing. A small area of graft detachment and loss was observed, and a serous collection was extracted to enable reattachment.

The percentage of wound area from the original showed significant differences ($p < 0.05$) for all skin substitute conditions compared with the STSG for all time points measured. No differences ($p > 0.05$) were observed among the three test conditions by study end (Figure 2a). On day 28 post-transplant, the percentage of original wound area was estimated to be 22.2% smaller for the C-GAG relative to STSG (95% CI: 15.2 to 29.2). PUR/C-GAG was 26% (95% CI: 19.2 to 33.2) smaller, and PUR was 28% (95% CI: 21.9 to 35.9) smaller. From day 28 onwards, the wounds were considered 'closed' and stabilised to day 112 with no significant change for any condition.

Epithelialisation was measured from day 14 until completely healed (Figure 2b). The wound area and degree of contraction observed within the first 14 to 28 days relate to the percentage of epithelialisation and wound stabilisation. Within the test conditions, C-GAG and PUR/C-GAG substitutes showed on average the greatest percentage of epithelialisation at day 14 (87% and 88%, respectively). In reviewing conditions separately, two out of the three wounds for the polymer-based scaffolds were >90% healed at day 14. By day 112, most wound edges were indistinct and fused with the normal edge tissue.

An experienced burn surgeon performed the POSAS scoring system to assess the wound appearance by ordinal scoring. Due to a single reading and low numbers, results showed that the overall effect of condition on OSAS score was not significant ($Q(4) = 7.45$, $p = 0.113$). Table 1 shows the mean observer score outcomes. The STSG displayed the meshed graft pattern and contraction in all four corners with the beginning of a stellate appearance and a contour defect. The skin graft had a matte appearance and was more mature as it lacked colouration (pale) and had returned to uninjured skin colour. Although it was thinner, with less relief and supple, it had contracted in the head to tail perspective and expanded in the spine/flank with pig growth. The C-GAG substitute contracted quite markedly compared with the skin graft, and the majority was flush with the surface of the surrounding wound with small, raised contours and relatively pliable residual scar. They appeared redder, and the colour centrally indicated a wound not as mature, with capillary blanching and a shiny appearance. The PUR/C-GAG had a more matte appearance, less contraction and reduced scar thickness. There were minimal contour defects, and two out of the three displayed near full maturity with the least vascular pattern of pigmentation. The PUR wounds were flush with minimal contour defects; however, they were the most contracted with central bands of thickened scar and shiny mid-pink pigmentation.

3.3 DermaLab Results

The non-invasive multi-parameter skin analysis system, the DermaLab Combo, was used to relate the subjective observations noted above and provided more objective observations (Figure 3). At day 17, statistically significant differences in transepidermal water loss were found between the control STSG and all test conditions, the STSG did not differ from normal skin, (mean differences: STSG vs C-GAG 15.54g/m^2/h (95% CI: 1.94 to 29.15), STSG vs PUR/C-GAG 39.56g/m^2/h (95% CI: 25.95 to 53.16) and STSG vs PUR 29.11g/m^2/h (95% CI:

15.50 to 42.72), respectively). However, the PUR site showed no difference from the C-GAG and PUR/C-GAG. All test conditions displayed higher values than normal skin at this early time point. With complete healing from day 28, all wound TEWL readings showed no changes among the groups for the study duration (Figure 3a). Additionally, the evaporative water loss decreased over time (day 17 to 112) for all skin substitute conditions ($p < 0.05$). The STSG showed no change over time as the site was re-epithelialised by day 14, with complete barrier function. For wound pigmentation (Figure 3b), melanin and erythema values differed significantly from normal skin and STSG to all test conditions on days 17, 28 and 56 for melanin and days 17 and 28 for erythema. By day 84, only the PUR containing scaffolds mean values (PUR, 30.57 ± 2.03 and PUR/C-GAG, 33.8 ± 6.13) differed with a higher melanin index than normal skin (23.68 ± 1.87). There were significant differences from day 17 to day 112 for each graft condition ($p < 0.05$), representing a shift over time from dark to light (i.e., higher to lower MI). No differences were noted among the three test conditions for any time points for Melanin or Erythema Indices (Figure 3b and c). However, the Erythema Index (i.e., redness/vascularity) of the PUR containing skin substitutes remained higher compared to the other conditions from day 17 (PUR/C-GAG 9.99 ± 2.85 and PUR 7.64 ± 2.4) through to day 84 for the PUR (PUR 4.22 ± 2.42), by endpoint at day 112, no differences were observed among all conditions.. The EI for all conditions decreased over time similarly to intact normal skin.

Measuring Young's Modulus on days 17, 28, 56, 84 and 112 confirmed wound parameters, i.e., viscoelastic stretch under load, visco-elastic recovery after release of load and unrecovered deformation normalised by day 56 (Figure 3d). The PUR/C-GAG and PUR were the only conditions that differed from normal skin and STSG at d17, VE 51.61 (95% CI: 29.57 to 73.66) and 29.67 (95% CI: 3.1 to 51.72) respectively. Subsequent time points did not display this difference with STSG. Interestingly, all scaffolds showed an increase in VE readings on day 28. From this point, all test conditions displayed decreasing values, indicating some

improvement of skin pliability over time. The ultrasound probe used to measure skin thicknesses only showed differences compared to normal skin and not within test conditions ($p > 0.05$) (data not shown).

3.4 Microscopic Evaluations

Biopsies post-delamination confirmed BTM integration (n = 12). The 2mm inserted BTM after 28 days of integration with seal delamination decreased in thickness on average by half (964.5µm ± 207.3). The BTM polymer layer resides below the surface of the skin at the interface between the connective tissue and the subcutaneous fat, with 21.5% remaining of the original polymer at 4.5 months post-implantation.

3.4.1 Evaluation of Histochemical Staining

The structure of the wounds was evaluated by stained sections using Haematoxylin and Eosin (H&E). In Figure 4, row 1, representative images show normal epidermal morphology at day 112 post-transplant. Extrusion of the PUR was evident microscopically at day 10. An initial thick double epidermal layering effect with central PUR was evident within the PUR and PUR/C-GAG wounds at day 10, accentuating a very thick hyperproliferative epidermis. By day 112, the stratified epidermal layers for all test conditions appeared similar to STSG (Figure 4). All wounds presented with typical epidermal morphology, well-defined rete ridges, columnar basal cells and keratin layers by day 112.

The hyperproliferative epidermal phenotype observed at day ten was resolved by day 112, displaying a regular expression of Ki67 within the basal keratinocytes (Figure 4, row 2. Revascularisation of the tissue was confirmed by staining with CD31 endothelial cell marker (Figure 4, row 3). Blood vessel density increased at the early stages of healing for all test conditions compared with normal skin.

The initial granulation layer was highly cellular, populated with numerous vessels and inflammatory cells. The dermal structure was then assessed for collagen deposition and morphology using picrosirius red stain (Figure 4, row 4). Type I collagen predominates in all sections (red/yellow staining), shown as thick, dense bundles in the control tissues (Figure 4, row 4). At early time points for the test conditions, the collagen fibres were thin with minimal collagen deposition (i.e., reduced red). The C-GAG presented thin, compact/dense bundles compared to the PUR and hybrid, which contained a less dense, looser, randomly organised fibre orientation. The three test scaffolds illustrated black areas within the tissue, consistent with a lower density of collagen fibres (Figure 4, row 4 c-e) compared with either the control STSG or normal porcine skin (Figure 4, row 4a-b) at day 112. The degree of collagen deposition increased over time for all wound conditions, with fibroblasts actively depositing and producing new collagen. All comprised qualitatively less collagen than normal skin, donor site and STSG control site.

At day 112 post-transplant epidermal structural integrity was confirmed by staining for keratin marker, cytokeratin 14 (K14), this showed K14 positive cells for all test and control conditions within the basal layers (Figure 5, row 1). Basement membrane markers indicated epidermal-dermal structure integrity with positive staining for collagen IV, collagen VII and integrin α6 (CD49f) (Figure 5, row 2-4).

4 Discussion

The hybrid scaffold was successfully fabricated to fill the pores of the PUR with collagen-GAG. It provided and facilitated a surface that promoted morphogenesis of the cells into a dermal-epidermal skin substitute, with good *in vitro* and handling properties. Data presented in this study demonstrates all three test scaffolds, and subsequent skin substitutes allowed for tissue integration and enabled stable wound closure. This study, in addition, confirms the advantages and disadvantages of these materials. The split-thickness skin autograft is

considered the prevailing standard of care for wound coverage in extensive full-thickness injuries. The meshed 1:3 skin autograft was a control condition and resulted in a superior outcome over the test skin substitutes regarding wound size and resemblance to intact, normal skin. However, the limitations of this treatment option is its paucity and aesthetics (characteristic mesh interstices and concave appearance) (31), not unlike those observed in this study.

The second-largest wound (C-GAG) and the largest of the three test conditions re-epithelialised early, with an apparent thicker dermis but a loose, 'wrinkling' appearance by study end. The inherent contraction of the C-GAG template during skin substitute fabrication increased the quantities required, potentially increasing handling and future set up costs for clinical use (32). In an attempt to reduce contraction a previous study by Powell and Boyce demonstrated a combination C-GAG with a PCL component improving its mechanical properties (33). The PUR/C-GAG hybrid also reduced *in vitro* contraction with superior thickness and handling properties. Conversely, the *in vivo* PUR loss and extrusion reduced mechanical support and resulted in smaller wounds with increased contraction. This PUR 'crusting' phenomenon has been reported previously (25). The hybrid inconsistencies noted with the C-GAG fabrication and cross-linking produced non-contiguous epithelium *in vitro* attributing to areas showing delayed post-polymer 'spitting'.

The patient observer scar assessment scale (POSAS) is becoming the accepted measure of scar quality (34). Using this method enabled valuable subjective observations of the wounds, and for future studies, increased observer scores may allow for data correlation with the DermaLab, enabling multiple assessments and conclusions of the wound/scar (35, 36). TEWL confirmed wound closure and barrier function which could be associated with the percentage of re-epithelialisation and closure rates. The TEWL values stabilised to normal skin values from day 31 to day 112, demonstrating continual epidermal barrier function with the outermost layer,

the stratum corneum (37). Immunohistochemical staining confirmed that the major constituents of the basement membrane which are fundamental in attaching the epidermal cells to the underlying extracellular matrix are present. All conditions demonstrated, collagen IV (BM stability), collagen VII (BM anchoring fibrils), and CD49f (binding of integrin α-6 to BM), markers essential to maintain basement membrane formation-function and skin homeostasis (38).

The skin's viscoelasticity is mainly determined by the ECM and the presence of collagen and elastin fibres, enabling the skin to return to its prior shape after stretch. An increase in viscoelasticity values- high MPa was initially observed for all grafts at early time points (day 17-28), presenting a stiffer, less pliable graft. The increase in PUR and PUR/C-GAG elasticity values may be related to the proportion of collagen III at this early time point. In common with a previous study (39), a peak in collagen type III alpha chain (COL3A1) expression was observed at 28 days in a hypertrophic scar porcine wound model for >1.9mm deep dermatome injuries (39), suggesting PUR containing substitutes initiated a similar healing process. Once in the remodeling phase, the VE values decreased over time, improving the pliability of the skin. Although they never achieved intact skin values, they also did not differ from STSG by study end. This has previously been noted when autograft and bilayered skin substitutes were evaluated in 14 burned patients (40). Furthermore, Boyce and colleagues reported the scar pliability of skin substitutes (collagen-based) were similar to autograft one year after treatment in burn patients (41). In this study the C-GAG presented increased collagen content organised into thinner, more compact fibres with an apparent thicker dermis, suggesting the C-GAG grafts matured earlier (8) with similar viscoelastic properties to skin autograft.

Since the skin of dominant white pigs lack melanocytes (42) the pigmentation observed in the porcine wounds reflect the degree of inflammation and erythema of a skin injury. Therefore, the elevated melanin index and vascularity values at early time points were consistent with

neovascularisation and the proliferation phase of wound healing (43), restoring to baseline with graft stabilisation by study end for all except the PUR grafts. All biomaterial implants are considered foreign bodies. The minimal change in erythema in the PUR grafts from transplant to the study end, suggests the wound remained (red) in an active inflammatory state from a retention of polymer (foreign body), thus prolonging maturation (43). The expression of CD31+ vessels confirmed an ingrowth of vascular supply with an increase in MVD during the early inflammatory and proliferative phases for all wounds. An increase in matrix deposition with a decrease in vascularisation at day 112 suggests regulation of angiogenesis in the remodeling phase. It has been previously reported that engineered skins *in vitro* have a hyperproliferative phenotype and, within weeks, is normalised after grafting (17, 44). The present study also showed this characteristic, normalising to control STSG levels by study end with no detrimental effect on engraftment and no overexpression of Ki67.

Several limitations of this study are noteworthy; the DermaLab-ultrasound provided some difficulties. The probe has a limiting penetration capacity of 3.4mm, and considering post histological sections showed greater than this, Young's Modulus elasticity values may have been affected (36). Using the mean of repeated measurements to interpret the DermaLab results correctly is highly recommended where feasible (45). The requirement of a time delay between each repetition, the curvature of the animal and wound shape and size, only enabled the collection of one measurement with the elasticity probe. The use of the DermaLab has shown potential for its use in large animal cutaneous wound healing models providing a non-invasive, standardised technique for multiple wound parameters and, with repetition, is a promising all-in-one instrument. Another study constraint includes sample size. Porcine wound studies are limited to the number of wounds per pig, handling capacity and cost (46, 47). Histological variability can be produced upon processing, staining and analysing sections and the heterogeneity within the field of graft upon sampling is a consideration.

Overall, based on these data, the three biopolymer scaffolds used to fabricate engineered skins produced a permanent skin replacement, promoting wound closure with epithelialisation and vascularisation with similar biophysical properties to the skin autograft. Therefore, taking into consideration their disadvantages and advantages, any one of these formulations would reduce the requirement for skin autografts, and the plausibility of laboratory-based skin as a replacement is feasible (5, 48). A trending effect was observed in this preliminary study, with prospective studies being required to decrease conditions to allow greater sample sizes in order to provide stronger statistical analysis and conclusions. However, the PUR/C-GAG hybrid has shown potential as a suitable biomaterial scaffold for fabricating skin substitutes, resolving the inherent concerns with collagen (i.e. contraction) and PURs (i.e. porosity). This material would significantly impact extensive burns and other acute and chronic wounds that would benefit therapeutically to reduce donor site harvesting, numbers of skin autografting procedures, and long-term morbidity from scars.

5 Acknowledgements

This project was supported by Lifetime Support Authority. The authors thank LARIF SAHMRI Animal facility technicians, The University of Adelaide Histology, Microscopy and Statistician Departments. We gratefully acknowledge the Skin Engineering Laboratory and Renal laboratory personnel for assistance with culturing and staining techniques. Thanks and much appreciation to the Engineered Skin Laboratory at the University of Cincinnati for assistance and advice with the hybrid scaffold fabrication.

6 Footnotes and Abbreviations

BM	Basement membrane
BTM	Biodegradable temporising matrix
CCS	Composite cultured skin
C-GAG	Collagen- glycosaminoglycan scaffolds
DAB	3,3'-diaminobenzidine

DAWE	Australian Government Department of Agriculture, Water and the Environment
EI	Erythema index
H&E	Haematoxylin and eosin
HRP	Horseradish peroxidase
IHC	Immunohistochemistry
LBL	Layer by layer
MI	Melanin index
MVD	Microvessel density
OCT	Optimal cutting temperature embedding medium
pFbs	Porcine fibroblasts
pFFP	Porcine fresh frozen plasma
pKs	Porcine keratinocytes
PSR	Picrosirius red stain
PCL	polycaprolactone
PLA	polylactic acid
PLGA	poly(lactide-co-glycolide)
PUR	Polyurethane
PVA	polyvinyl alcohol
PVP	polyvinylpyrrolidone
SAHMRI	South Australian Health and Medical Research Institute
STSG	Split-thickness skin graft
TEWL	Transepidermal water loss
VE	Viscoelasticity

Author Contributions: BD wrote the manuscript. All authors provided critical feedback and reviewed and approved the final version of the manuscript. Data are available upon request from the first author.

7 References

1. Dearman BL, Boyce ST, Greenwood JE. Advances in Skin Tissue Bioengineering and the Challenges of Clinical Translation. *Front Surg* 2021;8:640879.

2. Yannas IV, Burke JF, Huang C, Gordon PL. Correlation of in vivo collagen degradation rate with in vitro measurements. *Journal of Biomedical Materials Research* 1975;9(6):623-8.

3. Boyce ST, Christianson DJ, Hansbrough JF. Structure of a collagen-GAG dermal skin substitute optimized for cultured human epidermal keratinocytes. *Journal of Biomedical Materials Research* 1988;22(10):939-57.

4. Yannas IV, Burke JF. Design of an artificial skin. I. Basic design principles. *Journal of Biomedical Materials Research* 1980;14(1):65-81.

5. Boyce ST, Simpson PS, Rieman MT, Warner PM, Yakuboff KP, Bailey JK, et al. Randomized, Paired-Site Comparison of Autologous Engineered Skin Substitutes and Split-Thickness Skin Graft for Closure of Extensive, Full-Thickness Burns. *J Burn Care Res* 2017;38(2):61-70.

6. Vaissiere G, Chevallay B, Herbage D, Damour O. Comparative analysis of different collagen-based biomaterials as scaffolds for long-term culture of human fibroblasts. *Medical & biological engineering & computing* 2000;38(2):205-10.

7. Dearman BL, Greenwood JE. Scale-up of a Composite Cultured Skin Using a Novel Bioreactor Device in a Porcine Wound Model. *J Burn Care Res* 2021;42(6):1199-209.

8. Banakh I, Cheshire P, Rahman M, Carmichael I, Jagadeesan P, Cameron NR, et al. A Comparative Study of Engineered Dermal Templates for Skin Wound Repair in a Mouse Model. *Int J Mol Sci* 2020;21(12).

9. Harley BAC, Gibson LJ. In vivo and in vitro applications of collagen-GAG scaffolds. *Chemical Engineering Journal* 2008;137(1):102-21.

10. Eskandarinia A, Kefayat A, Agheb M, Rafienia M, Amini Baghbadorani M, Navid S, et al. A Novel Bilayer Wound Dressing Composed of a Dense Polyurethane/Propolis Membrane and a Biodegradable Polycaprolactone/Gelatin Nanofibrous Scaffold. *Sci Rep* 2020;10(1):3063.

11. Anjum F, Agabalyan NA, Sparks HD, Rosin NL, Kallos MS, Biernaskie J. Biocomposite nanofiber matrices to support ECM remodeling by human dermal progenitors and enhanced wound closure. *Sci Rep* 2017;7(1):10291.

12. Sadeghi-Avalshahr AR, Nokhasteh S, Molavi AM, Mohammad-Pour N, Sadeghi M. Tailored PCL Scaffolds as Skin Substitutes Using Sacrificial PVP Fibers and Collagen/Chitosan Blends. *Int J Mol Sci* 2020;21(7).

13. Sadeghi AR, Nokhasteh S, Molavi AM, Khorsand-Ghayeni M, Naderi-Meshkin H, Mahdizadeh A. Surface modification of electrospun PLGA scaffold with collagen for bioengineered skin substitutes. *Mater Sci Eng C Mater Biol Appl* 2016;66:130-7.

14. Knight E, Murray B, Carnachan R, Przyborski S. Alvetex®: Polystyrene Scaffold Technology for Routine Three Dimensional Cell Culture. *3D Cell Culture* 2010;695:323-40.

15. Khalili S, Nouri Khorasani S, Razavi M, Hashemi Beni B, Heydari F, Tamayol A. Nanofibrous scaffolds with biomimetic structure. *Journal of biomedical materials research Part A* 2018;106(2):370-6.

16. Dehghani F, Annabi N. Engineering porous scaffolds using gas-based techniques. *Current opinion in biotechnology* 2011;22(5):661-6.

17. Paul M, Kaur P, Herson M, Cheshire P, Cleland H, Akbarzadeh S. Use of Clotted Human Plasma and Aprotinin in Skin Tissue Engineering: A Novel Approach to Engineering Composite Skin on a Porous Scaffold. *Tissue Eng Part C Methods* 2015;21(10):1098-104.

18. Solovieva EV, Teterina AY, Klein OI, Komlev VS, Alekseev AA, Panteleyev AA. Sodium alginate-based composites as a collagen substitute for skin bioengineering. *Biomed Mater* 2020;16(1):015002.

19. Solovieva EV, Fedotov AY, Mamonov VE, Komlev VS, Panteleyev AA. Fibrinogen-modified sodium alginate as a scaffold material for skin tissue engineering. *Biomed Mater* 2018;13(2):025007.

20. Chanda A, Adhikari J, Ghosh A, Chowdhury SR, Thomas S, Datta P, et al. Electrospun chitosan/polycaprolactone-hyaluronic acid bilayered scaffold for potential wound healing applications. *International Journal of Biological Macromolecules* 2018;116:774-85.

21. Kim H, Son D, Choi TH, Jung S, Kwon S, Kim J, et al. Evaluation of an amniotic membrane-collagen dermal substitute in the management of full-thickness skin defects in a pig. *Arch Plast Surg* 2013;40(1):11-8.

22. Türkkan S, Atila D, Akda An, Tezcaner Ae. Fabrication of functionalized citrus pectin/silk fibroin scaffolds for skin tissue engineering. *Journal of biomedical materials research Part B, Applied biomaterials* 2018.

23. Sierra-Sanchez A, Fernandez-Gonzalez A, Lizana-Moreno A, Espinosa-Ibanez O, Martinez-Lopez A, Guerrero-Calvo J, et al. Hyaluronic acid biomaterial for human tissue-engineered skin substitutes: Preclinical comparative in vivo study of wound healing. *J Eur Acad Dermatol Venereol* 2020;34(10):2414-27.

24. Kim JW, Kim MJ, Ki CS, Kim HJ, Park YH. Fabrication of bi-layer scaffold of keratin nanofiber and gelatin-methacrylate hydrogel: Implications for skin graft. *Int J Biol Macromol* 2017;105(Pt 1):541-8.

25. Dearman BL, Stefani K, Li A, Greenwood JE. "Take" of a polymer-based autologous cultured composite "skin" on an integrated temporizing dermal matrix: proof of concept. *J Burn Care Res* 2013;34(1):151-60.

26. Dearman BL, Li A, Greenwood JE. Optimization of a polyurethane dermal matrix and experience with a polymer-based cultured composite skin. *J Burn Care Res* 2014;35(5):437-48.

27. Powell HM, Boyce ST. EDC cross-linking improves skin substitute strength and stability. *Biomaterials* 2006;27(34):5821-7.

28. Supp DM, Hahn JM, Lloyd CM, Combs KA, Swope VK, Abdel-Malek Z, et al. Light or Dark Pigmentation of Engineered Skin Substitutes Containing Melanocytes Protects against Ultraviolet Light-Induced DNA Damage In Vivo. *J Burn Care Res* 2020.

29. Hassiotis S, Manavis J, Blumbergs PC, Hattersley KJ, Carosi JM, Kamei M, et al. Lysosomal LAMP1 immunoreactivity exists in both diffuse and neuritic amyloid plaques in the human hippocampus. *Eur J Neurosci* 2018;47(9):1043-53.

30. Draijers LJ, Tempelman FRH, Botman YAM, Tuinebreijer WE, Middelkoop E, Kreis RW, et al. The patient and observer scar assessment scale: a reliable and feasible tool for scar evaluation. *Plastic and reconstructive surgery (1963)* 2004;113(7):1960-5.

31. Shevchenko RV, James SL, James SE. A review of tissue-engineered skin bioconstructs available for skin reconstruction. *J R Soc Interface* 2010;7(43):229-58.

324. Powell HM, Boyce ST. Wound closure with EDC cross-linked cultured skin substitutes grafted to athymic mice. *Biomaterials* 2007;28(6):1084-92.

335. Powell HM, Boyce ST. Engineered human skin fabricated using electrospun collagen-PCL blends: morphogenesis and mechanical properties.(Original Article). *Tissue Engineering, Part A: Tissue Engineering* 2009;15(8):2177.

346. Carriere ME, Kwa KAA, de Haas LEM, Pijpe A, Tyack Z, Ket JCF, et al. Systematic Review on the Content of Outcome Measurement Instruments on Scar Quality. *Plast Reconstr Surg Glob Open* 2019;7(9):e2424.

357. Gankande TU, Duke JM, Danielsen PL, DeJong HM, Wood FM, Wallace HJ. Reliability of scar assessments performed with an integrated skin testing device - the DermaLab Combo®. *Burns* 2014;40(8):1521-9.

368. Peperkamp K, Verhulst AC, Tielemans HJP, Winters H, van Dalen D, Ulrich DJO. The inter-rater and test-retest reliability of skin thickness and skin elasticity measurements by the DermaLab Combo in healthy participants. *Skin Res Technol* 2019;25(6):787-92.

379. Suetake T, Sasai S, Zhen Y-X, Ohi T, Tagami H. Functional Analyses of the Stratum Corneum in Scars: Sequential Studies After Injury and Comparison Among Keloids, Hypertrophic Scars, and Atrophic Scars. *Archives of dermatology* 1996;132(12):1453-8.

4380. Supp DM, Hahn JM, Combs KA, McFarland KL, Schwentker A, Boissy RE, et al. Collagen VII Expression Is Required in Both Keratinocytes and Fibroblasts for Anchoring Fibril Formation in Bilayer Engineered Skin Substitutes. *Cell Transplant* 2019;28(9-10):1242-56.

39. Blackstone BN, Kim JY, McFarland KL, Sen CK, Supp DM, Bailey JK, et al. Scar formation following excisional and burn injuries in a red Duroc pig model. *Wound Repair Regen* 2017;25(4):618-31.

40. Germain L, Larouche D, Nedelec B, Perreault I, Duranceau L, Bortoluzzi P, et al. Autologous bilayered self-assembled skin substitutes (SASSs) as permanent grafts: a case series of 14 severely burned patients indicating clinical effectiveness. *Eur Cell Mater* 2018;36:128-41.

41. Boyce ST, Supp AP, Wickett RR, Hoath SB, Warden GD. Assessment with the Dermal Torque Meter of skin pliability after treatment of burns with cultured skin substitutes. *Journal of burn care & rehabilitation* 2000;21(1):55-63.

42. Müller, Wanke, Distl. Inheritance of melanocytic lesions and their association with the white colour phenotype in miniature swine. *Journal of animal breeding and genetics* 2001;118(4):275-83.

43. Landen NX, Li D, Stahle M. Transition from inflammation to proliferation: a critical step during wound healing. *Cell Mol Life Sci* 2016;73(20):3861-85.

44. Smiley AK, Klingenberg JM, Boyce ST, Supp DM. Keratin expression in cultured skin substitutes suggests that the hyperproliferative phenotype observed in vitro is normalized after grafting. *Burns* 2006;32(2):135-8.

45. Anthonissen M, Daly D, Fieuws S, Massage P, Van Brussel M, Vranckx J, et al. Measurement of elasticity and transepidermal water loss rate of burn scars with the Dermalab®. *Burns* 2013;39(3):420-8.

46. Sami DG, Heiba HH, Abdellatif A. Wound healing models: A systematic review of animal and non-animal models. *Wound Medicine* 2019;24(1):8-17.

47. Pastar I, Liang L, Sawaya AP, Wikramanayake TC, Glinos GD, Drakulich S, et al. Preclinical models for wound-healing studies. In: Marques AP, Pirraco RP, Cerqueira MT, Reis RL, editors. *Skin Tissue Models for Regenerative Medicine*: Elsevier, 2018:223-53.

48. Schiestl C, Meuli M, Vojvodic M, Pontiggia L, Neuhaus D, Brotschi B, et al. Expanding into the future: Combining a novel dermal template with distinct variants of autologous cultured skin substitutes in massive burns. *Burns Open* 2021;5(3):145-53.

8 Tables

Table 1. Showing the OSAS mean total score results for normal skin and all test conditions. No significant differences were observed within the test conditions. SD, standard deviation. N, number. Pairwise comparisons were assessed using Wilcoxon matched-pairs signed-rank tests.

Condition	n	Mean	SD	Median
Normal Skin	3	6.0	0.0	6
PUR	3	23.3	8.0	24
C-GAG	3	25.0	2.7	26
HYBRID	3	22.3	12.1	18
STSG	3	19.3	4.2	18

Figure Captions

Figure 1. Representative macroscopic images showing the progression of graft and skin substitute integration during weeks 0 – 16 post-transplant for each treatment condition. Meshed STSG (1:3) exhibited 44.2% contraction (column a), followed by the C-GAG substitute (63.1% column b), PUR/C-GAG 66.7% (column d) and the PUR substitute was on average the most contracted condition with 67.9% (column c). E, Percentage of contraction from day 0 after transplantation to day 112 endpoint.

Figure 2. Wound percentage of original area and re-epithelialisation of the four test conditions over time shows the observed values and mean with standard deviation. (a) At 14 days post-transplant >80% of all wounds were re-epithelialised and by 28 days complete closure was obtained by secondary re-epithelialisation. At 28 days (dotted line) to 112 days, wound areas stabilised, and significant differences (**$p < 0.05$) were noted for all three skin substitutes compared to the STSG site at day 112, however there were no differences within each skin substitute condition (*$p > 0.05$). **(b)** Mean percentage of re-epithelialisation of test

conditions over time until complete healing. No significant differences were found among the graft types after 14 days post-transplant ($p > 0.05$). Three biological replicates (n=3) for each condition were analysed using a linear mixed effects model with Bonferroni correction.

Figure 3. Results from the DermaLab with each biophysical wound assessment parameter graphed for all treatment conditions over time post-transplant. (**a)** Transepidermal water loss- TEWL ($g/m^2/h$), (**b)** Melanin Index (MI), (**c)** Erythema Index (EI), and (**d)** Viscoelasticity (VE). The observed values represent the means and standard deviations at respective time points. The mean differences were compared among conditions and over time. *$p < 0.05$ for comparisons among PUR/C-GAG, PUR, and C-GAG **$p < 0.05$ Normal skin compared to all conditions including STSG. ***$p < 0.05$ for comparisons of PUR/C-GAG, and normal skin, STSG, C-GAG. ****$p < 0.05$ PUR and normal skin. ^$p < 0.05$ Normal skin, STSG and both PUR-containing conditions. ^^$p < 0.05$ Normal skin, STSG and all test conditions. #$p < 0.05$ for comparisons among all test conditions at the indicated time points from day 17 to day 112. Three biological replicates (n=3) for each condition were analysed using a linear mixed effects model with Bonferroni correction.

Figure 4. Representative histological images on day 112 post-transplantation. Haematoxylin and Eosin (H&E) row 1, Ki67- proliferative marker row 2, CD31- endothelial cell marker row 3 and Picrosirius red (PSR) stain row 4 for normal porcine skin (column a), and the four test conditions, skin graft (STSG-column b), C-GAG (column c), PUR (column d) and hybrid PUR/C-GAG (column e). The collagen structure was visualised using PSR under polarised light. Scale bar: 200µm row 1, 50µm row 2, 100µm row 3 and 4.

Figure 5. Representative immunohistological images of normal porcine skin and test conditions at 112 days post-transplantation showing epidermal and basement membrane confirmation. Cytokeratin 14 row 1, Collagen IV row 2, Collagen VII row 3 and Integrin α6 (CD49f) row 4. Column a represents porcine normal skin, column b STSG, column c C-GAG,

column d PUR and column e PUR/C-GAG. Red staining for wide spectrum cytokeratin, Green staining depicts relevant maker, DAPI nuclei stain. Scale bar: 50µm.

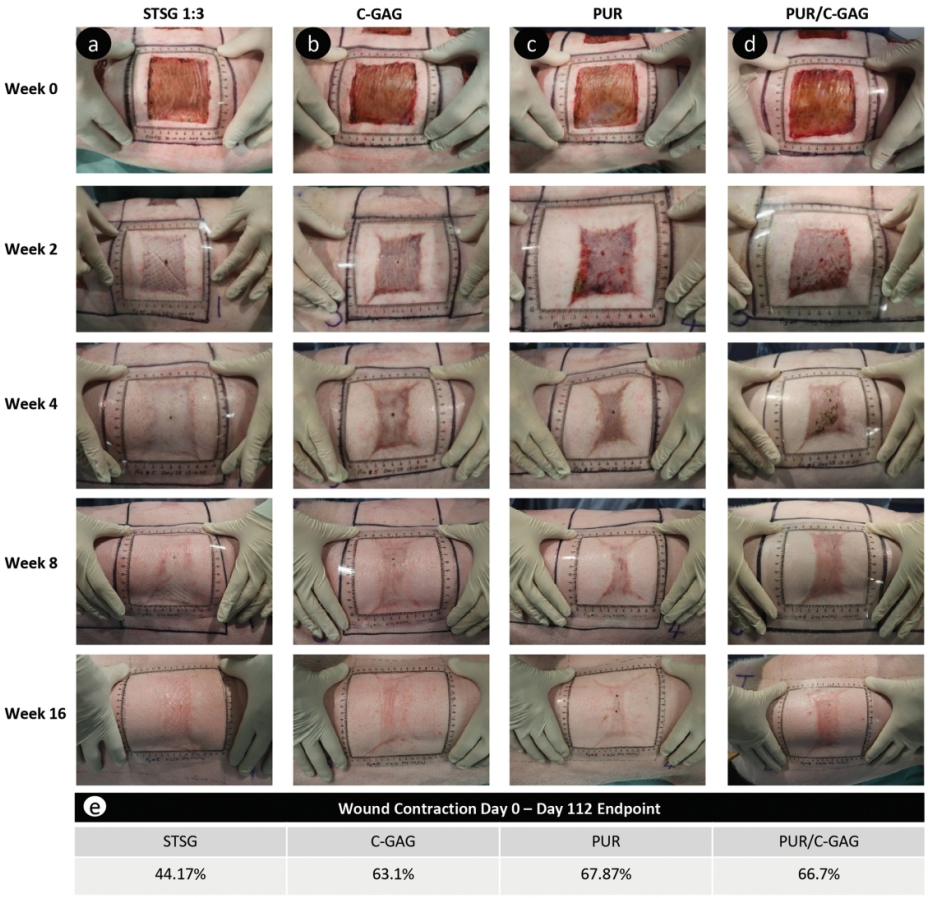

e Wound Contraction Day 0 – Day 112 Endpoint

STSG	C-GAG	PUR	PUR/C-GAG
44.17%	63.1%	67.87%	66.7%

Figure 1. Representative macroscopic images showing the progression of graft and skin substitute integration during weeks 0 – 16 post-transplant for each treatment condition. Meshed STSG (1:3) exhibited 44.2% contraction (column a), followed by the C-GAG substitute (63.1% column b), PUR/C-GAG 66.7% (column d) and the PUR substitute was on average the most contracted condition with 67.9% (column c). E, Percentage of contraction from day 0 after transplantation to day 112 endpoint.

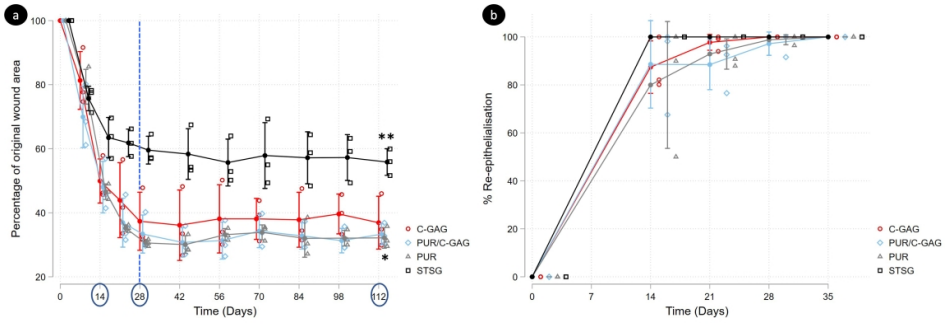

Figure 2. Wound percentage of original area and re-epithelialisation of the four test conditions over time shows the observed values and mean with standard deviation. (a) At 14 days post-transplant >80% of all wounds were re-epithelialised and by 28 days complete closure was obtained by secondary re-epithelialisation. At 28 days (dotted line) to 112 days, wound areas stabilised, and significant differences (**p < 0.05) were noted for all three skin substitutes compared to the STSG site at day 112, however there were no differences within each skin substitute condition (*p > 0.05). (b) Mean percentage of re-epithelialisation of test conditions over time until complete healing. No significant differences were found among the graft types after 14 days post-transplant (p > 0.05). Three biological replicates (n=3) for each condition were analysed using a linear mixed effects model with Bonferroni correction.

338x119mm (288 x 288 DPI)

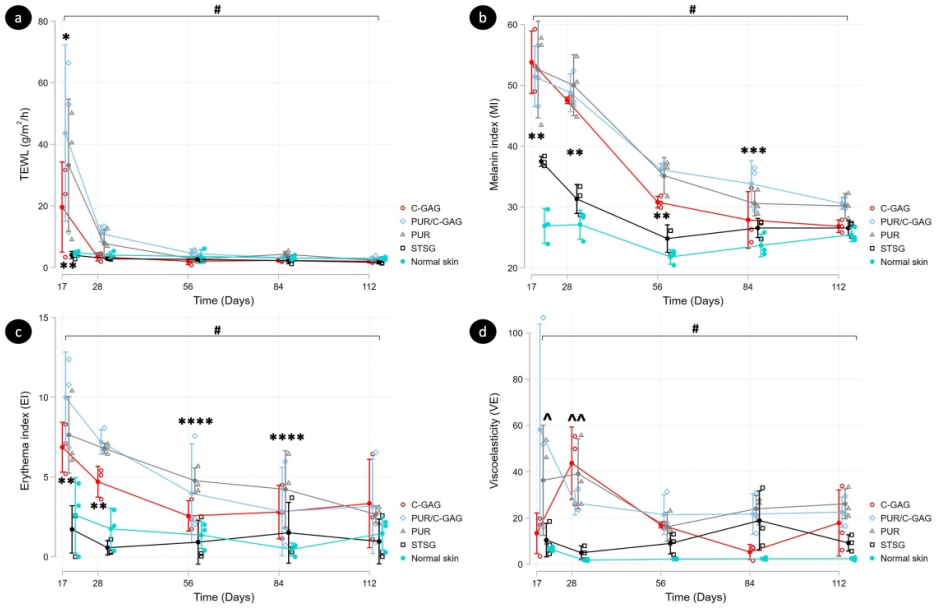

Figure 3. Results from the DermaLab with each biophysical wound assessment parameter graphed for all treatment conditions over time post-transplant. (a) Transepidermal water loss- TEWL (g/m2/h), (b) Melanin Index (MI), (c) Erythema Index (EI), and (d) Viscoelasticity (VE). The observed values represent the means and standard deviations at respective time points. The mean differences were compared among conditions and over time. *p < 0.05 for comparisons among PUR/C-GAG, PUR, and C-GAG **p < 0.05 Normal skin compared to all conditions including STSG. ***p < 0.05 for comparisons of PUR/C-GAG, and normal skin, STSG, C-GAG. ****p <0.05 PUR and normal skin. ^p < 0.05 Normal skin, STSG and both PUR-containing conditions. ^^p < 0.05 Normal skin, STSG and all test conditions. #p < 0.05 for comparisons among all test conditions at the indicated time points from day 17 to day 112. Three biological replicates (n=3) for each condition were analysed using a linear mixed effects model with Bonferroni correction.

292x190mm (288 x 288 DPI)

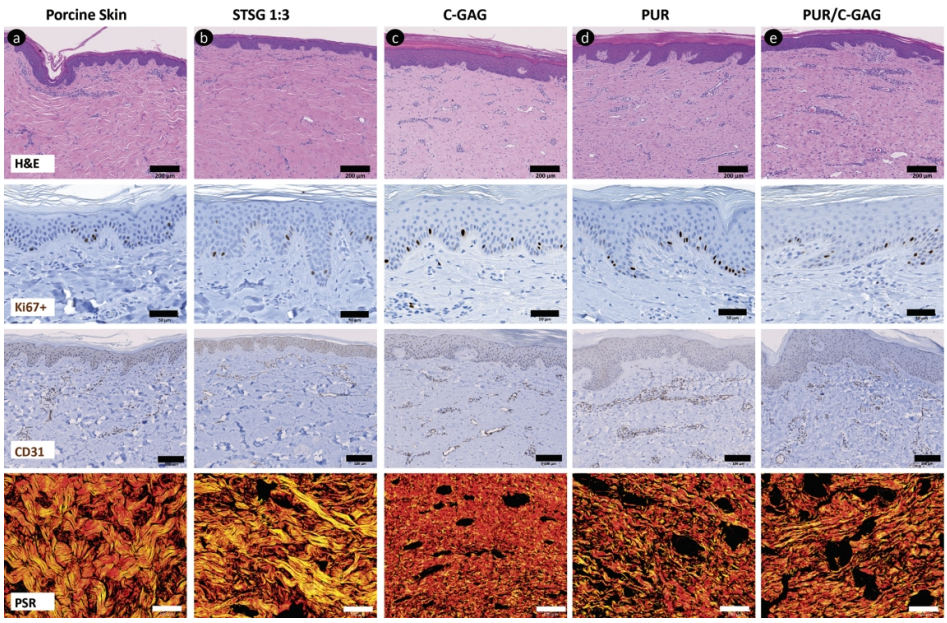

Figure 4. Representative histological images on day 112 post-transplantation. Haematoxylin and Eosin (H&E) row 1, Ki67- proliferative marker row 2, CD31- endothelial cell marker row 3 and Picrosirius red (PSR) stain row 4 for normal porcine skin (column a), and the four test conditions, skin graft (STSG-column b), C-GAG (column c), PUR (column d) and hybrid PUR/C-GAG (column e). The collagen structure was visualised using PSR under polarised light. Scale bar: 200μm row 1, 50μm row 2, 100μm row 3 and 4.

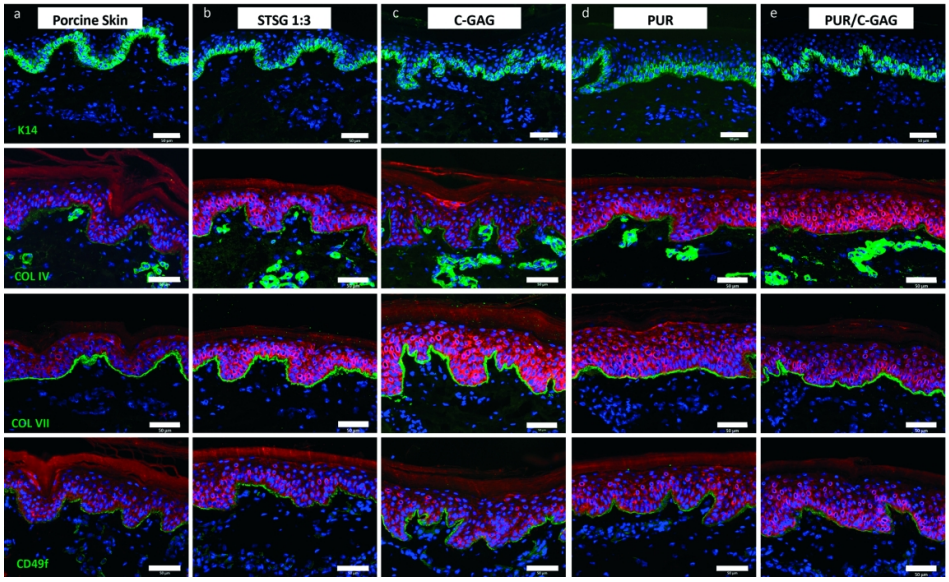

Figure 5. Representative immunohistological images of normal porcine skin and test conditions at 112 days post-transplantation showing epidermal and basement membrane confirmation. Cytokeratin 14 row 1, Collagen IV row 2, Collagen VII row 3 and Integrin α6 (CD49f) row 4. Column a represents porcine normal skin, column b STSG, column c C-GAG, column d PUR and column e PUR/C-GAG. Red staining for wide spectrum cytokeratin, Green staining depicts relevant maker, DAPI nuclei stain. Scale bar: 50μm.

Comparison of Biopolymer Scaffolds as Skin Substitutes

1 Supplementary Data – Dearman et al

Supplementary S1. Representative histology images of skin substitutes using different scaffolds in a porcine *in vitro* model. a. Hybrid - PUR/C-GAG, b. PUR and c. C-GAG substitute. Scale bar: 250µm.

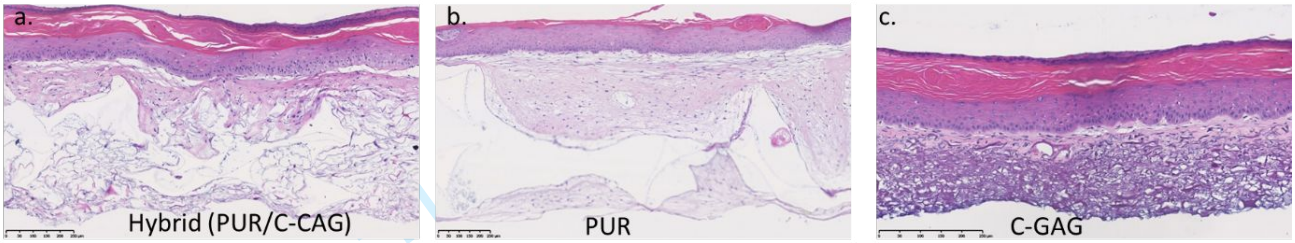

Supplementary S2 Table 2. Primary antibodies listed for staining techniques. Abbreviations used, DAB – diaminobenzidine, FF - Fresh Frozen section, IF – Immunofluorescence, P - Paraffin section.

Antibody Name/ Catalogue #	Host species	Source	Detection method	Clone/Dilution
Collagen IV (MA5-13437)	Mouse monoclonal	Invitrogen	IF - FF	1:50 CIV22
COL7A1 (MA5-13432)	Mouse monoclonal	Invitrogen	IF - FF	1:100 LH7.2
CD49f (Integrin alpha-6) (MA5-16884)	Rat monoclonal	Invitrogen	IF - FF	1:100 NKI-GoH3
Anti-wide spectrum Cytokeratin (ab9377)	Rabbit polyclonal	Abcam	IF - FF	1:500
Anti-cytokeratin 14 (MA1-06323)	Mouse monoclonal	Invitrogen	IF - FF	1:500 RCK107
Anti-CD31 (ab28364)	Rabbit polyclonal	Abcam	DAB Kit - P	1:50
Recombinant Anti-KI67 (ab16667)	Rabbit monoclonal	Abcam	DAB - P	1:250 SP6

Comparison of Biopolymer Scaffolds as Skin Substitutes

Supplementary S3 Table 3. a. Secondary antibodies listed for staining techniques and b. methods. AF- Alexa Fluor.

a Antibody Name/ Catalogue #	Host species	Source	AF/Dilution
Goat-anti-Rabbit IgG (ab150086)	Goat polyclonal	Abcam	AF 555 1:500
Goat-anti-Rabbit IgG (ab150079)	Goat polyclonal	Abcam	AF 647 1:500
Goat-anti-Mouse IgG (ab150113)	Goat polyclonal	Abcam	AF 488 1:500
Goat-anti-rat IgG2a (NB7124)	Goat polyclonal	Novus Biologicals	AF FITC 1:500
Goat-anti-rat IgG (ab150157)	Goat polyclonal	Abcam	AF 488 1:500
Biotinylated horse anti-mouse IgG (BA-2000)	Horse polyclonal	Vector Laboratories	1:250
Biotinylated horse anti-rabbit IgG (BA-1100)	Horse polyclonal	Vector Laboratories	1:250

b Staining Methods	Catalogue #	Source
Mouse and Rabbit specific HRP/DAB Detection IHC micropolymer Kit	ab236466	Abcam
Streptavidin-biotinylated immunoperoxidase technique	21127	ThermoFisher-Pierce
Cell nuclei – Fluoroshield with DAPI	F6057-20ml	Sigma
Picrosirius red stain kit	ab150681	Abcam

6.2 Supplementary Figures (unpublished)

The original data from the microscopic evaluations of the BTM are shown in an additional figure (Figure S4) below. This shows triplicate measurements to obtain the mean residual BTM polymer layer with digital photographs and H&E stained sections from biopsies before and after dermabrasion. In addition, the hyperproliferative state of the epidermis at early biopsy timepoints is shown in Figure S5 for all test conditions.

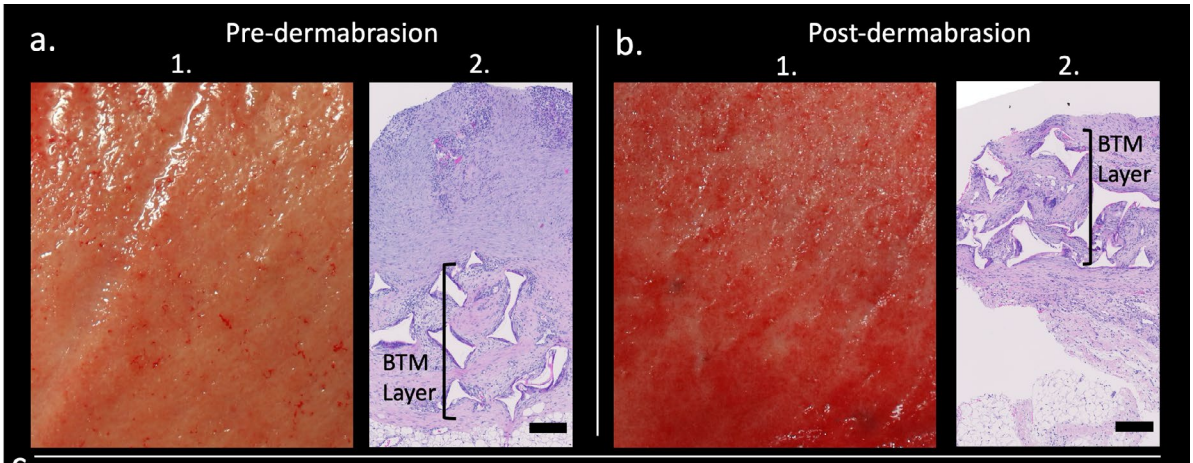

c.

Pig - site	Day	M1 (µm)	M2 (µm)	M3 (µm)	Pig - site	Day	M1 (µm)	M2 (µm)	M3 (µm)
1-1	28	1012	1234	1109	1-1	112	346	253	234
2-2	28	785	1017	816	2-2	112	387	471	316
3-3	28	798	892	800	3-3	112	526	482	324
1-4	28	1358	1095	1267	1-4	112	628	539	486
2-5	28	921	1169	1051	2-5	112	767	451	750
3-6	28	830	946	636	3-6	112	360	453	682
1-7	28	875	1301	1101	1-7	112	541	551	482
2-8	28	979	768	766	2-8	112	537	534	500
3-9	28	609	536	641	3-9	112	255	187	185
1-10	28	1127	757	1134	1-10	112	256	185	262
2-11	28	923	1212	1039	2-11	112	298	255	308
3-12	28	983	1160	1077	3-12	112	560	484	673

Supplementary S4. Shows a representative wound bed (1) with corresponding histology (2) prior to CCS transplant. (a), Displays the residual BTM post seal removal and pre-dermabrasion and (b.) shows the residual BTM post-dermabrasion before CCS transplant c. Tables the measurement data in trip-licate per wound (n =12) of BTM thickness from histological sections at Day 0 pre-CCS transplant and Day 112 study endpoint. CCS-Composite cultured skin, BTM- biodegradable temporising matrix. Scale bar 200µm.

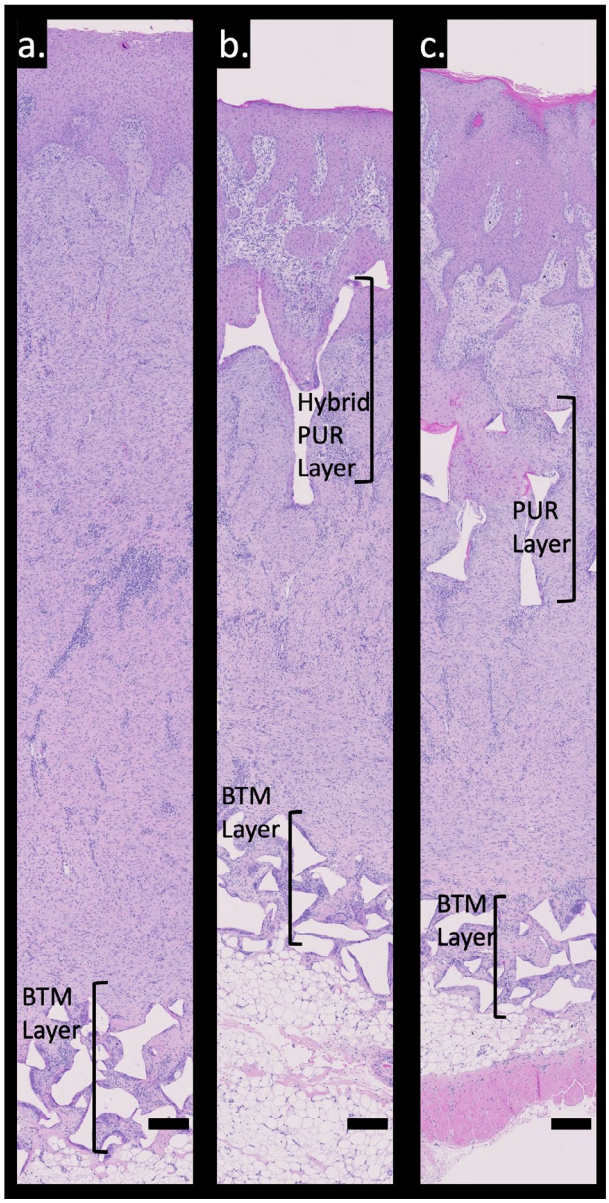

Supplementary S5. Haematoxylin and Eosin stained sections from biopsies of treatment conditions on Day 10 post-transplantation. (a) C-GAG skin substitute (b) Hybrid skin substitute and (c) PUR skin substitute. Note the thickened epidermis at this early timepoint. Scale bar 200µm.

CHAPTER 7:
Validation of Automated Bioreactor in a Cleanroom Environment

7.1 Overview

Chapter two describes the use of a novel bioreactor for the generation of large composite cultured skins (25cm x 25cm). This study investigated the 1mm PUR material in a submerged culture system using the automated bioreactor. Further optimisation, described in **Chapters 4, 5, and 6,** has elucidated essential modifications to be incorporated to both the culturing parameters and bioreactor device to support the morphogenesis of a composite skin. These changes included lifting the large pieces to an air-liquid interface (ALI) and cell transfer and inoculation methods. In addition, the second *in vivo* porcine study (**Chapter 6**) revealed a PUR scaffold less than 1mm in thickness would be advantageous for complete engraftment. Therefore, a 0.8mm thick foam with refined consistency and pores < 2mm was formulated for testing with the bioreactor. The primary aim of this study incorporated all the CCS optimisation changes to test with the automated bioreactor device in an ISO 7 environment to produce large pieces of CCS for the purposes of manufacture and clinical use.

7.2 Bioreactor System and Design

7.2.1 Bioreactor preparations

New incubators were sourced with a greater internal volume to accommodate the bioreactor fixtures. The Heracell™ CO_2 incubator (250i) features complete contamination control with a steri-cycle system containing an in-chamber HEPA air filtration system. The HEPA filter provides quality-controlled conditions (Class 100). With a polished stainless-steel interior, sturdy reinforced stainless-steel shelving, and the use of cell factories, the Heracell can support six 10-layer factories for cell expansion. The footprint is 2.1m x 1m. Bespoke software directs computer-controlled pumps for media fill and waste management (Figure 7.1). The initial bioreactor layout (used in Chapter 2) consisted of a spigot system with 6.4mm internal diameter (ID) tubing, which produced intermittent, unsteady flow. The spigot was thus re-designed to fit 4.8mm ID tubing and tested for flow rate and consistency. Input and output flow were measured with different media volumes at various flow rates.

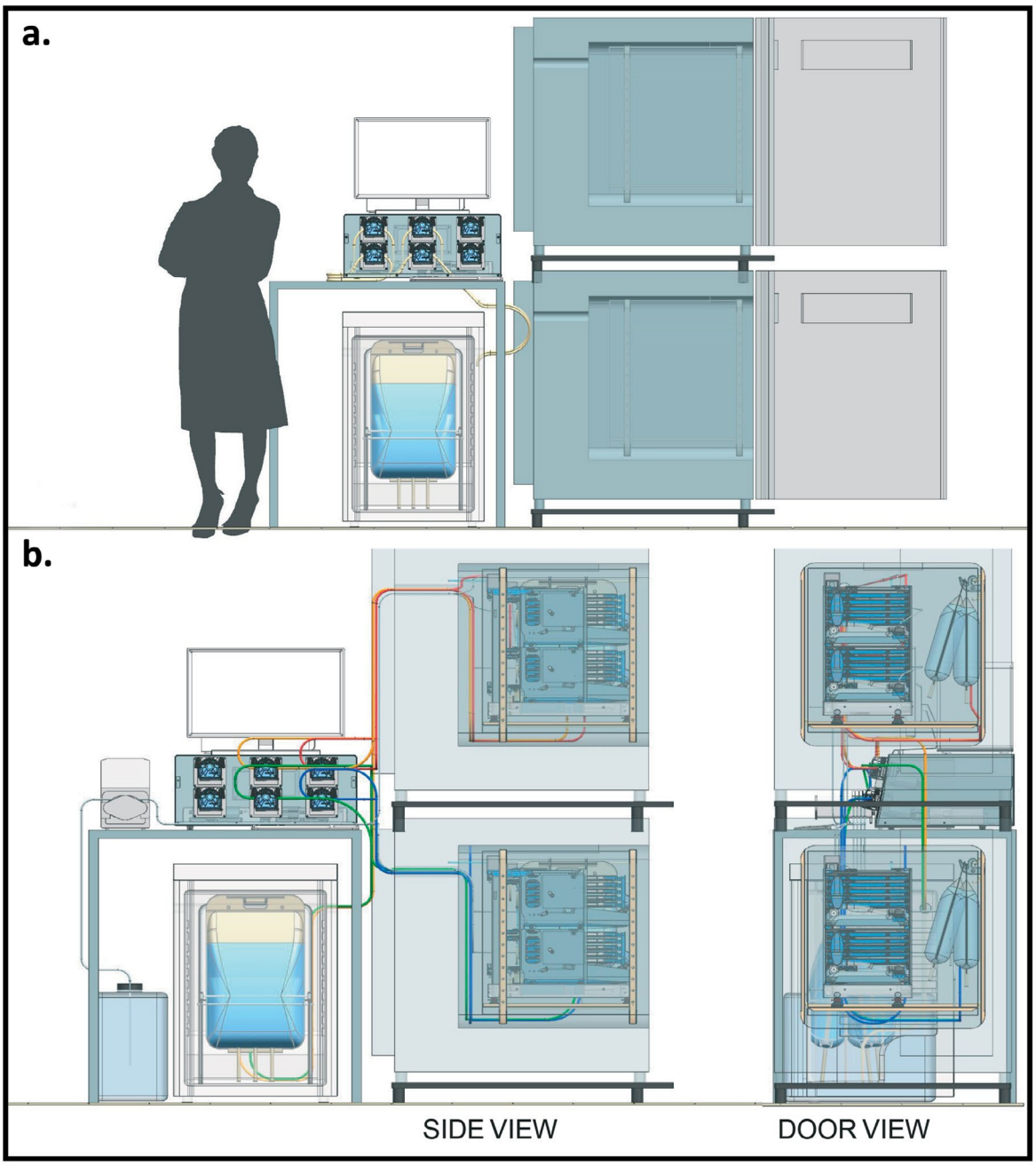

Figure 7.1 Bioreactor footprint a. 2.1m x 1m overview layout, b. Side and door views of the internal workings of the bioreactor, showing the media input from the refrigerator bag to the incubator bag (yellow and green tubing) and the feed hose from the incubator bag to the spigot (blue and red tubing).

Figure 7.2 displays the tubing framework for two bioreactor incubators. The feed hose travels from the warmed media bag within the incubator, via a dedicated media pump, to the spigot head enabling warm media to be exchanged in the cassettes. Another hose, the reservoir hose, is attached to the male outlet of the incubator media bag. It passes through a second pump to the refrigerator media bag. Fresh media can then be replenished and warmed in the incubator media bag. Two waste hoses (one for each 5-array assembly) extract waste media via a smaller pump system into an external waste vessel. An additional waste hose is connected to a purge bag within the incubator via the smaller pump system to extract purged media externally. The tubing system is replicated for the second incubator. All tubes were measured to the required length, cut, and autoclaved in preparation for assembly.

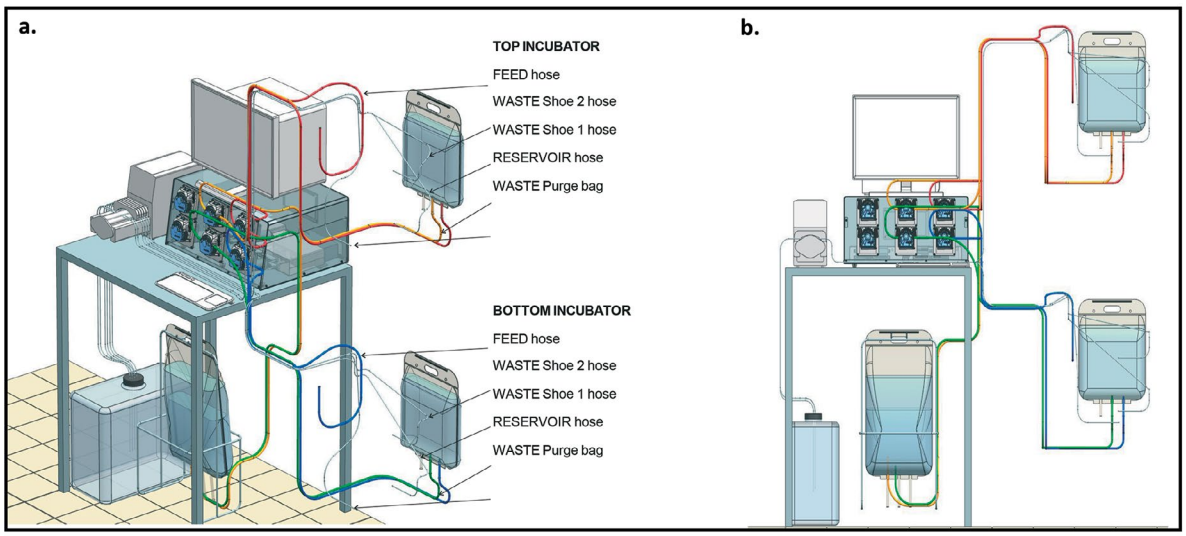

Figure 7.2 Tubing overview a. Schematic detailing the tubing length and workings within the incubator and processing pump systems. The waste tubing and collection mechanism is shown to the left of the computer system (small grey tubing) with the media bag (refrigerator) below, b. shows the tubing run from the refrigerator bag (yellow/green) to the incubator bag and the feed hose from the incubator bag to the spigot head (red/blue).

The manifold incorporated a new design feature to decrease the flow rate and media build-up in the bottom of the manifold during cassette tipping (media exchange). Cassette tipping allows spent media to be transferred into the waste vessel. Build-up of media in the manifold can result in leaking from the manifold-cassette junction. A food-grade grease was sourced and applied to seal this junction after being pre-packaged and gamma sterilised. The grease was applied with a sterile cotton tip to the outlets of the cassette and manifold during assembly.

New cassettes were produced overseas with the current bioreactor tooling. They required washing, assembly, and gamma sterilisation before use. A rigorous washing procedure was developed and implemented for all cassettes and accessories to decrease the bioburden from manufacture. They were air-dried within a biological safety cabinet, assembled, and double bagged in preparation for sterilisation. All parts were labelled and catalogued. To achieve ALI within the cassettes, a lifting frame was required. Four prototype designs were tested, varying in thickness and material type (plastic vs stainless steel).

7.3 Methodology

7.3.1 CCS Fabrication and Bioreactor Operation

7.3.1.1 Cell expansion

Cell expansion methods are described in earlier chapters and appendices. In brief, keratinocytes were co-cultured with iHFbs in SEL-KGM, and human matched dermal fibroblasts were expanded in SEL-Fbs and cryopreserved. In total, $3.032x10^9$ keratinocytes and $1.74x10^9$ fibroblasts were established at passage two in preparation for CCS/bioreactor testing. The pre-cultured cells were tested for microbiological contamination before use within the cleanrooms.

7.3.1.2 CCS fabrication and culture

Three large 25cm x 25cm CCS replicates (designated for bioreactor) and matched small 8cm x 8cm controls (designated for standard incubator) were established and cultured for 14 days at ALI. The CCS layer-by-layer method was employed. hFFP and in-house thrombin were prepared prior to use as described in Chapter 5 (sections 5.2.1 and 5.2.2).

In brief, hFFP was pooled and pre-filtered before the PUR was 'wet' and soaked for three days in large dishes. It was then transferred to cassettes for fibroblast inoculation. On Day 3, fibroblasts were thawed and inoculated at $5x10^5$cells/cm^2 and established for three days at ALI before keratinocyte addition at $1x10^6$ cells/cm^2. Maturation media (detailed in Chapter 5) was exchanged daily with microbiological testing of pooled, spent culture media. Pooled media was purged on Days 3, 7, 10, 12 and 14. Endotoxin samples were collected on Days 3 and 14 for testing on Day 14, and pH levels were also monitored at these time points.

7.3.1.3 Histological analysis

Multi-quadrant biopsies of CCS samples were taken on Day 14. These were cut and divided for fixation in 10% buffered formalin, SEM/TEM fixative, and snap-frozen in isopentane. SEM and TEM samples were processed as per Appendix VIII. Paraffin-embedded sections were processed for routine histology and cut at 5-7µm for haematoxylin and eosin (H&E), Periodic acid-Schiff (PAS) or Masson's Trichrome staining. Frozen sections were cut and air-dried at room temperature for 1 hour before a 10-minute acetone fixation step, followed by standard immunofluorescence. Paraffin sections were de-waxed using xylene and rehydrated through alcohols. Sections were then processed using a streptavidin-biotinylated immunoperoxidase technique (Appendix VII). Heat-induced antigen retrieval was performed using citrate buffer (pH 6). For immunofluorescence, matched secondary antibodies were Alexa fluor 488 (ab150113 or ab150157), Alexa fluor 647 (ab150079) or 555 (ab150086) purchased from Abcam. FITC goat-anti-rat (NB7124) was purchased from Novus Biologicals. The antibodies and detection methods used are detailed in supplementary data tables (Appendix III). In brief, anti-wide pan-cytokeratin (ab9377) and anti-cytokeratin (K14 MA1-06323/K10 ab9025) were used for positive keratin identification. Basement membrane structure and markers for Collagen IV (MA5-13437), Collagen VII (MA5-13432), Laminin (ab11575), Integrin alpha-6 (MA5-16884), and Ki67 (ab16667) proliferation marker were used. AE1/AE53 pan keratin (ab86734) was co-stained with Collagen I (ab233080). Images were captured with an Olympus FV3000 confocal microscope and scanned with a Zeiss Axio Scan Z1 slide scanner (Carl Zeiss, Germany). Control tissues were normal human skin from donors undergoing elective surgery procedures.

7.4 Results

7.4.1 Bioreactor Performance Prior to Cleanroom Testing

Consistent flow is integral to establishing precise media liquid levels within the cassette. The substitution of the 6.4mm ID tube for a smaller 4.8mm ID tube and re-design of the spigot outlet enabled a reduction in flow from 110mL/min to 100mL/min with a steady stream. Flow from the spigot was accurate with no intermittent stopping. Repeated testing resulted in a mean 34% tolerance level from the software input and output volumes ranging between 100-200mL.

Test prototype parts were manufactured from acrylic plastic to attain an ALI within the 25cm x 25cm cassette. These featured perforations (50% open area) and were desirable as a single-use disposable plate. The resultant plastic sheets exhibited a degree of distortion due to the mechanically formed perforations causing material stretching. Therefore, a 25cm x 25cm stainless steel lifting frame with >50% open area perforations was designed and manufactured (Figure 7.3b). The 0.9mm thick sheet was chosen for stability and made from SS grade 316, enabling repetitive autoclaving and high corrosion resistance. To assist with the prototype testing, and achieve an accurate 3mm lifting height, multiple stainless steel 316 spacers were used. The addition of the SS lifting frame presented several issues within the cassette. With the 7-degree tip for media extraction, a volume remained within the cassette trapped by a meniscus against the cassette lid (Figure 7.3c). A sealing tab on the cassette lid was removed, and a rocking regime for the tipping process was incorporated to mix any remaining media with fresh.

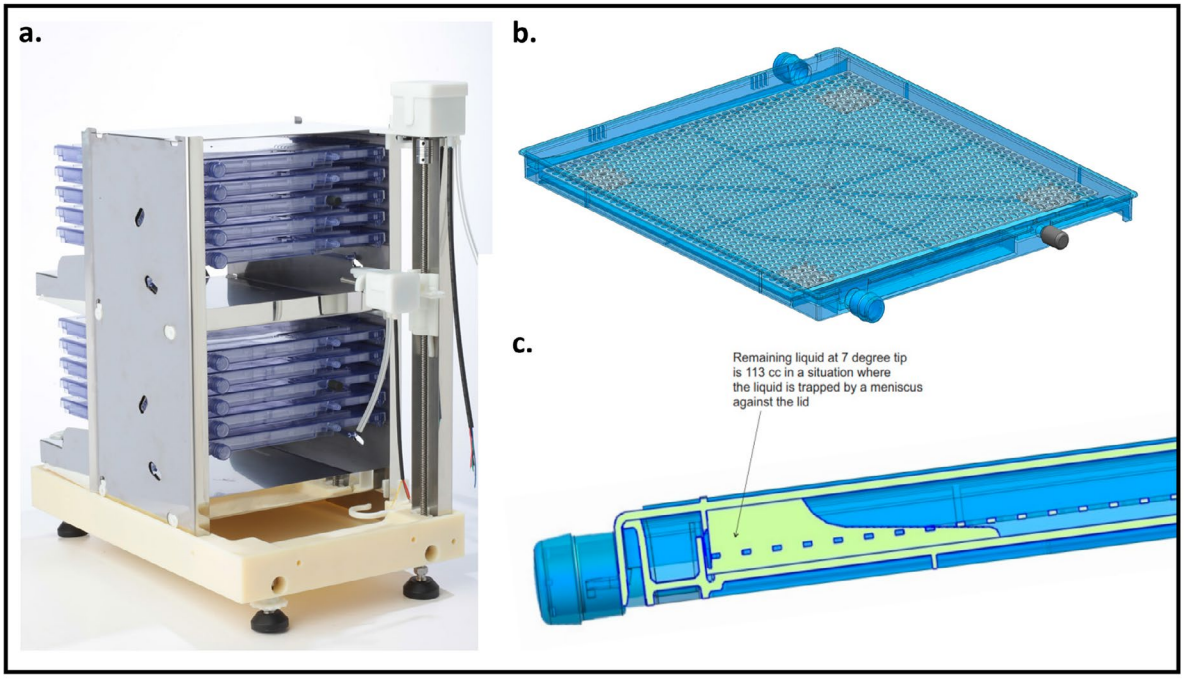

Figure 7.3 Bioreactor cassette arrangement a. Shows a tower setup with ten cassettes, five in each array. The mechanical driver assembly for spigot control and media exchange and waste tipping, b. Displays the internal cassette with the stainless-steel lifting frame to achieve an air-liquid interface and c. demonstrates the residual liquid build-up from the incorporation of the frame.

7.4.2 Bioreactor Performance During Cleanroom Testing

Technical issues were encountered when moving the bioreactor equipment into the cleanroom, delaying the initial setup of the pump and computer systems. After removing equipment from the cleanroom and reinstallation, the issue was determined to be loose internal wires within the computer/hard drive caused by physically moving the system.

For media set-up and fill, 200mL was primed and purged from the tubing to ensure new media was available for each exchange. With the first media change (post keratinocyte inoculation), a small volume (estimated 50mL) had leaked from the cassettes and pooled in the bottom of the shoe. The leak appeared to be coming from the cassette lid and wicking down the sides. Media underneath the purge bag at the bottom of the tower was also evident. Careful assessment of the mechanical process for the automated media changes determined the spigot tubing knocked the purge bag vent out of alignment, causing the spigot to misalign with the purge inlet.

A fabricated stainless-steel lifting frame created the air-liquid interface for the CCS. There were no air bubbles visible beneath these lifting grids. However, media frothing from the spigot outlet was visible from occasional trapped air within the pump lines. This may have been due to the unclamping and re-clamping of the pump lines post media change which was required for initial start-up, and would not occur if the system was operational for the entirety of the campaign. Another concern was the tubing being compressed, inhibiting the flow of media. Fortunately, this was captured before media change with no deleterious effects. The mixing and rocking of the media in the cassettes set at 11°C tilt functioned sufficiently to mix the residual media with fresh. It also assisted with the removal of any air bubbles trapped underneath the grids during the tipping process.

Media changes were straightforward (~1hour per day), and if not for the small manual handling of the control CCSs, the media changes would have mainly been observational with minimal to no physical manipulation by personnel required. On the other hand, the cell inoculation days were lengthy and required a minimum of two personnel with an intense procedural regime. A temperature data logger was affixed to the side of the bag within the incubator to assess the time taken for the cold media to warm to 37°C. The results showed it took ~10 hours from the flow-in of the ~800mL refrigerated media to reach the 37°C internal incubator temperature suitable for media change.

7.4.3 CCS Evaluation

7.4.3.1 Microbiological, endotoxin and pH testing

Microbes were not detected in the extracted spent media in any collection bags for any time points (Appendix IX). Environmental sampling performed throughout the campaign showed no positive results in the critical processing areas (Appendix IX). The anterooms (Area 7A-2) did have a positive count (1 colony-forming unit (CFU)) towards the end of the period on Day 9 (21-169-08836), identified as Staph spp (1 CFU) and Day 10 (21-170-09229) identified as a gram +ve rod. The first anteroom (Area 7-2) on the last day of processing (on exit), d14 (21-174-16329), also showed a positive with 1 CFU, identified as a gram-positive rod. The first anteroom has an acceptance criterion of 200 CFUs, and the second has 10 CFUs and is therefore within the acceptable parameters. The organisms noted are of environmental nature. A quarterly clean and shutdown post-campaign was scheduled.

Endotoxin testing was performed on spent media from each CCS culture on Day 14, with archive samples stored for Day 3. All tests were completed and passed, indicating the validity of the result. High endotoxin levels were detected in all CCSs compared to the freshly prepared maturation media, and control CCS values were half the bioreactor CCSs (Table 7.1).

Table 7.1 Endotoxin results of spent culture media for all test conditions and control maturation media at Day 14 endpoint.

ID	Mean Sample Value	Result
Maturation media (unused)	<0.25 EU/mL	PASS
Control-CCS	0.643 EU/mL	PASS
Bioreactor-CCS	1.27 EU/mL	PASS

The pH of the spent culture media was tested on Days 3 and 14 for each test condition, showing no deviations from the freshly prepared maturation media (Table 7.2) and, on average, there was no significant shift in pH from Day 3 to Day 14.

Table 7.2 pH readings of spent media from the control and bioreactor CCS and unused maturation medium (MM) on Days 3 and 14.

pH	Control-CCS	Bioreactor-CCS	MM
Day 3	7.4	7.4	7.6
Day 14	7.7	7.5	7.3

7.4.3.2 Histological analysis

Biopsies from day three of fibroblasts only, i.e., prior to keratinocyte inoculation, showed a layer of fibroblast cells superficial to the hFFP-impregnated PUR foam. However, histological sections and H&E staining at Day 14 endpoint revealed fibroblast deposition and integration within the PUR pores. This effect enabled keratinocytes to fall through the sides of the pores upon cell inoculation. Only small sections, i.e., <50% of the total surface area of the bioreactor CCSs, showed structural morphology and integrity. These areas had promoted morphogenesis of a stratified epithelium with dermal elements *in vitro* in both the control CCSs and bioreactor CCSs (Figure 7.4). In addition, Ki67, a cell proliferation marker showed clear positive staining of DAB-brown stain in the nuclei of the basal cells in the epidermis of the test conditions, indicating the proliferative capacity of the CCS to produce a stratified squamous epithelium.

7.4.3.3 Immunohistochemical staining

The CCSs were positive for wide-spectrum epidermal cytokeratin and specific keratins, K14 and K10 (Figure 7.5a-b). However, there was weak expression of cytokeratin 10. Basement membrane (BM) markers identified laminin, collagen IV, collagen VII and integrin α6 (CD49f) (Figure 7.5 c-f). Collagen VII was only dominant with an established epidermal-dermal, cell-cell interaction of fibroblasts and keratinocytes. Transmission Electron Microscopy (TEM) and Scanning Electron Microscopy (SEM) were performed to identify the presence of hemidesmosomes and the CCSs basement membrane integrity with dermal collagen deposition (Figure 7.6). However, the BM was intermittent and difficult to assess due to the inconsistency of the epidermal/dermal structure. Figure 7.7 additionally depicts the cell fall through and discontinuity with heterogeneous deposition of cells throughout the bioreactor CCSs, particularly noted with pores > 500µm.

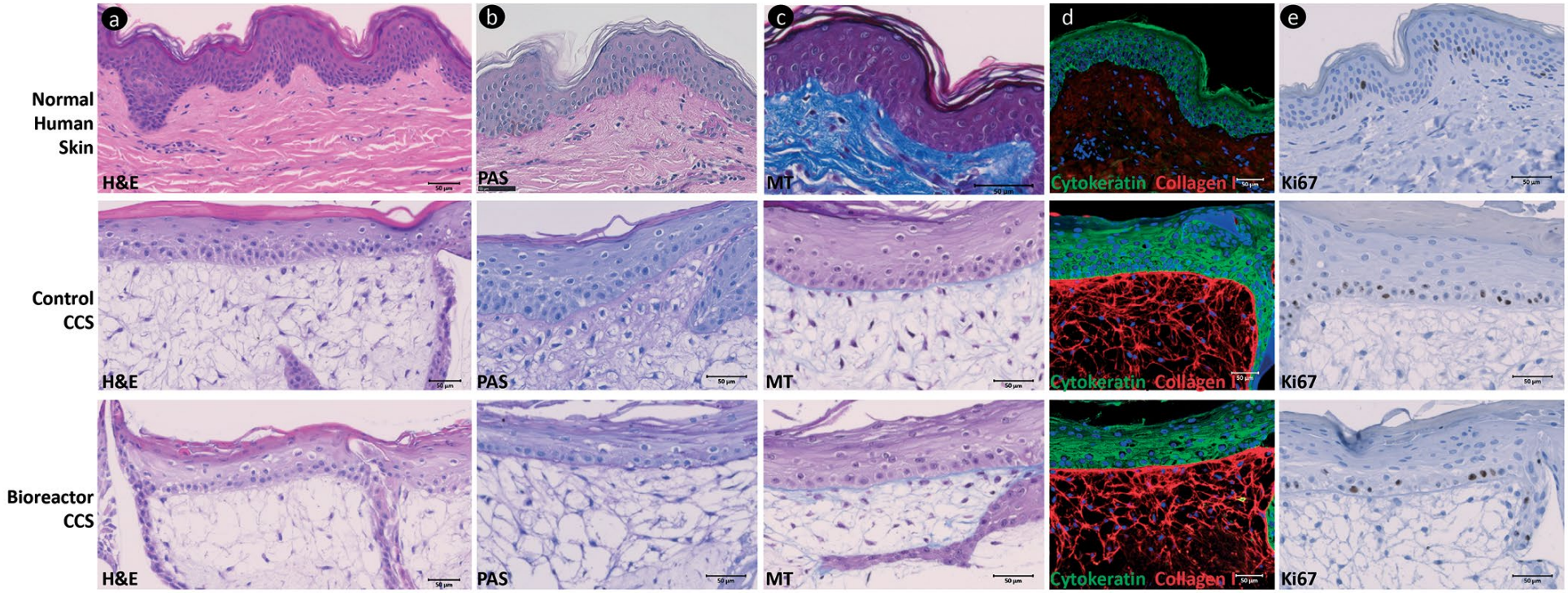

Figure 7.4 Representative histology images of normal human skin and Day 14 of CCS show epidermal-dermal morphology similar to normal human skin. H&E-stained sections in column a. of normal human skin first row, small control CCS second row, a CCS established in the bioreactor third row. PAS staining identified basement membrane (column b.) with MT (column c.), also identifying positive collagen deposition (blue staining). Immunohistochemical staining for cytokeratin (green) showed stratified epidermal layers and collagen I (red) staining in the dermal scaffold. Blue (DAPI) counterstained for nuclei, and solid blue is the PUR scaffold (column d.). Proliferating cells were positively identified with DAB (brown) and the Ki67 proliferation marker (column e.). H&E – Haematoxylin and eosin stain, PAS – Periodic acid-Schiff, MT- Masson's trichrome, CCS – Composite cultured skin, PUR- Polyurethane. Scale bar: 50µm.

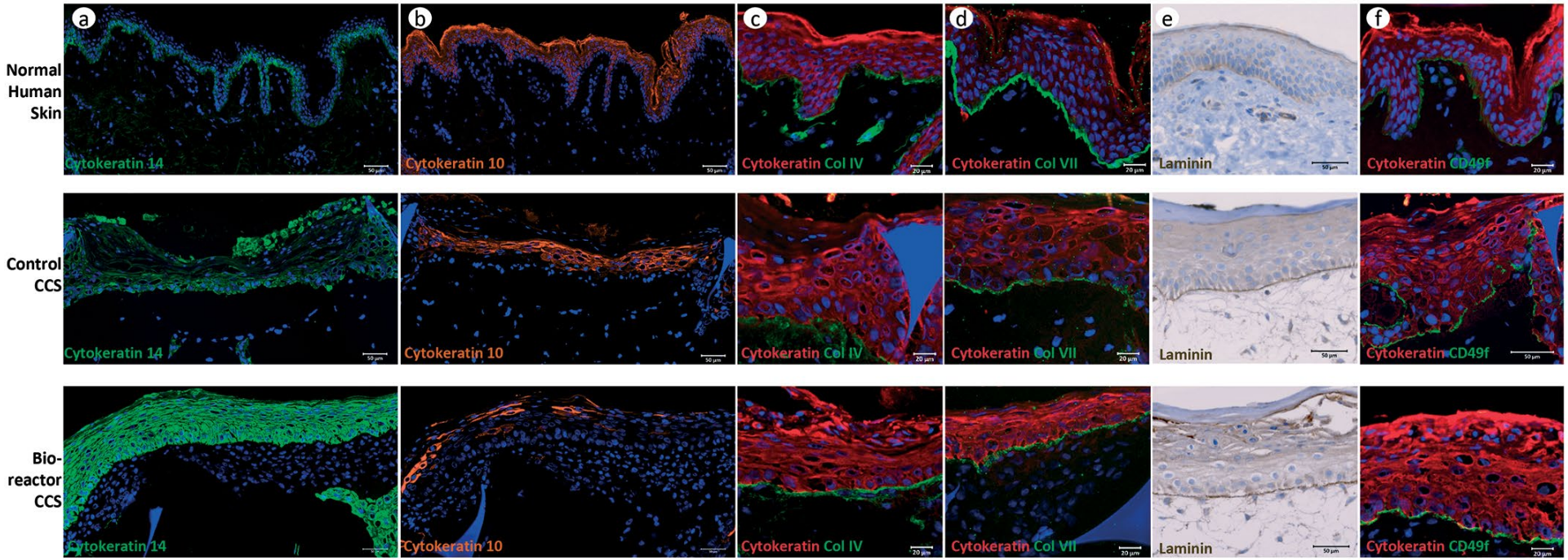

Figure 7.5 Representative immunohistological images for control normal human skin sections, small control CCS and bioreactor generated CCS on Day 14 of co-culture. The majority of cells were positive for cytokeratin 14 staining (green) in column a. and minimal cytokeratin 10 (column b. – designated orange). Basement membrane structure was confirmed by staining for multiple BM markers, collagen IV (column c. - green), collagen VII (column d. - green), Laminin (column e. - brown), and Integrin α6 (CD49f- green) in column f. These were co-stained with pan-cytokeratin (red) for epidermal integrity. BM – basement membrane. Note: columns = Ca-f and rows = R1-3. Scale bar for CcR1-3, CdR1-3 and CfR1&3 is 20µm and CaR1-3, CbR1-3, CeR1-3 and CfR2 is 50µm.

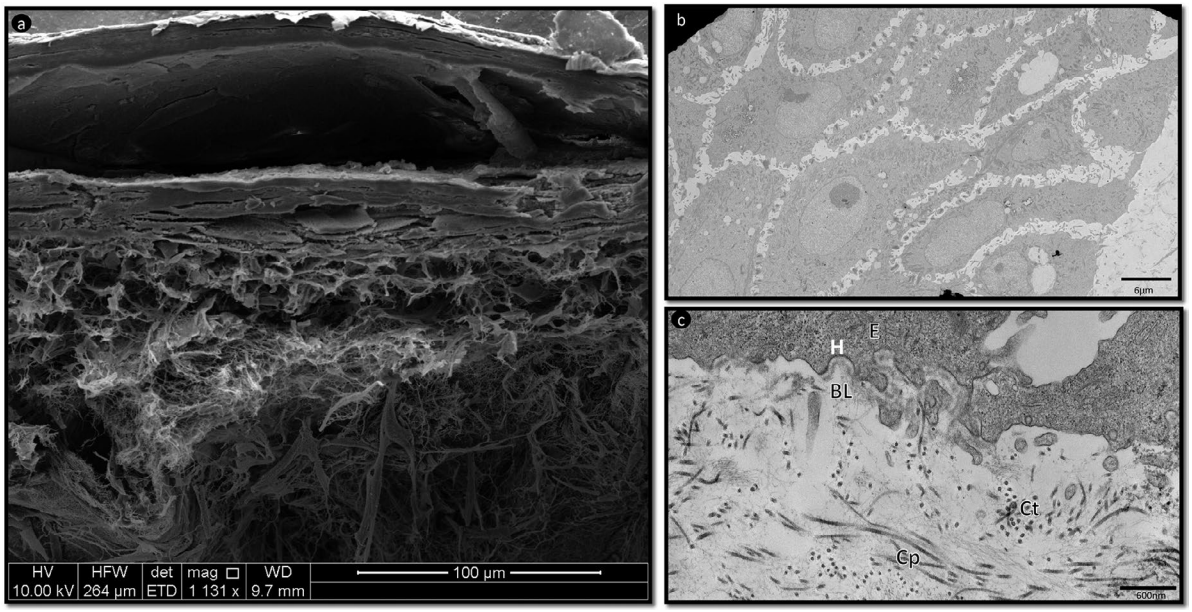

Figure 7.6 Representative SEM and TEM images from a CCS, a. Shows an SEM image with fibrous collagen network and fibroblasts within the PUR scaffold with superficial epidermal structure and a keratinising detached squamous epithelium, b. Epidermal layers with interconnecting keratinocyte cell structure, c. Magnified image showing deposited collagen with striated fibres running parallel directions (Cp) and dots, transverse (Ct). E - epithelial cell, H – hemidesmosome, BL- basal lamina. Scale bar for a is 100µm, b is 6µm and c is 600nm.

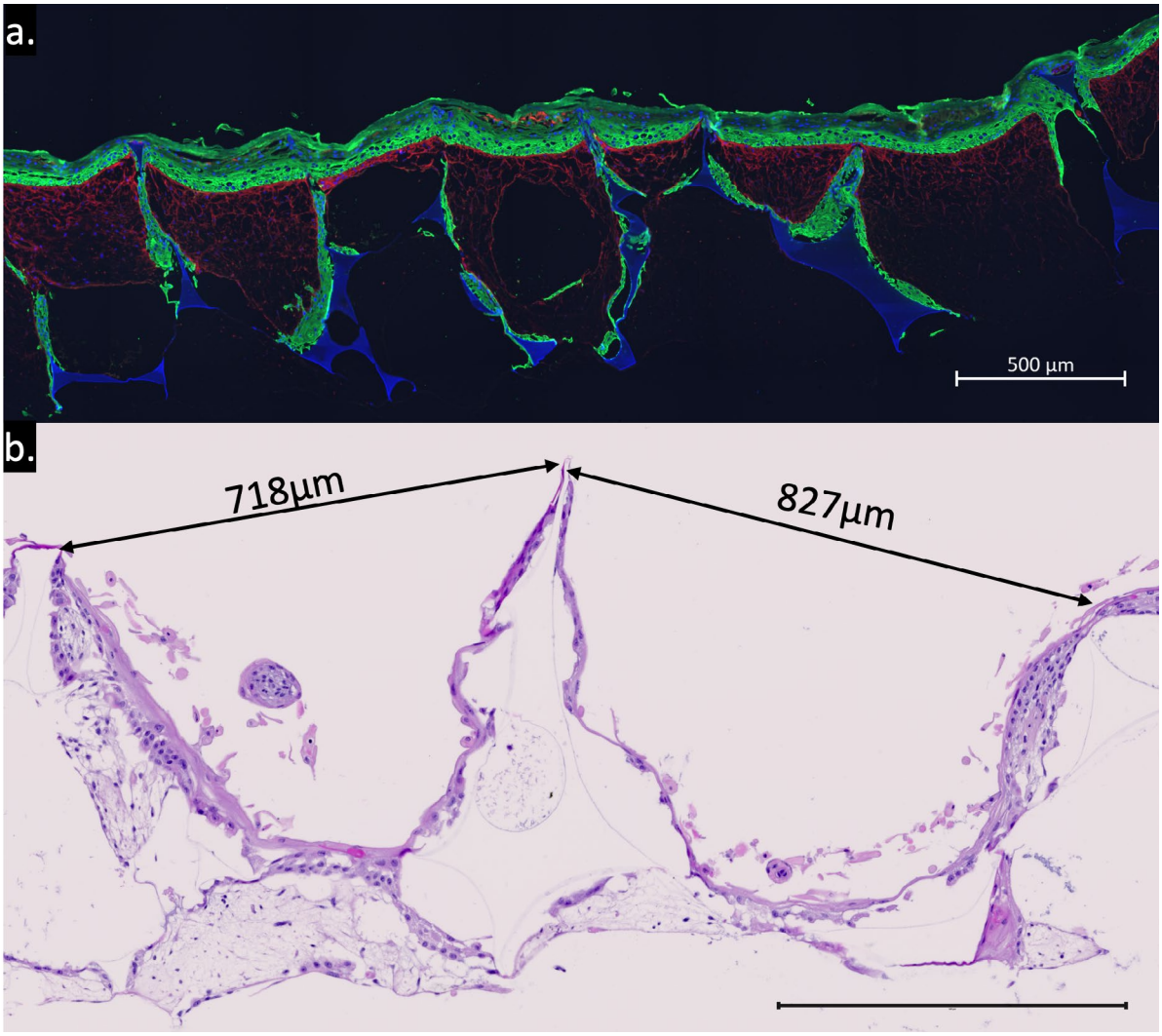

Figure 7.7 Variability of the bioreactor CCS displaying the (a) cell infiltration and (b) heterogeneous strucutre with pores larger than 500µm. Scale bar 500µm.

7.5 Discussion

Compared to small 8cm x 8cm CCSs, the automated bioreactor was not able to produce a consistent 24.5cm x 24.5cm CCS. However, areas that showed promise had viable thick, stratified epidermis with basement membrane, collagen deposition and proliferating cells (Figure 7.4-6). The cell fall-through still appears to be an issue where the PUR surface segments meet the superficial side of the skin, enabling cells to infiltrate the edges and grow within the middle of the CCS. This effect is due to the manipulation, and transfer of the large plasma filled PUR scaffold for cell inoculation, causing the material to stretch.

A complete cassette change at the time of cell inoculation would overcome the wicking and leakage of media from the cassettes. Although this change slightly increases the costs, the cassettes made and purchased in bulk would outweigh this and be insignificant in the overall costs. The high endotoxin levels may be attributed to the components used in the culturing system, i.e., the stainless-steel grid, the wicking agent, and the transfer sheet. These components are considerably larger in the bioreactor CCS cultures and could explain the higher endotoxin levels detected. Although these items were autoclaved-sterilised, testing endotoxin levels prior to use would give baseline levels. pH levels remained stable, with no indication of bacteria (acidic shift), and sufficient media performance.

The nutritional requirements for a scaled bioengineered skin substitute are critical [106]. The increased cell density within these substrates leads to a depletion of nutrients and accumulation of growth inhibitory metabolites [107]. An unbalanced medium environment can have deleterious cytotoxic effects on graft morphogenesis [108, 109]. Additionally, overfeeding can also create an unsuitable medium environment for the growth of cells. Standard media exchange methods for monolayer cultures and tissue-engineered constructs are via a static batch-feed technique at set time points. There is evidence that static cultures and even rotating vessel bioreactors do not adequately nourish the centre of tissue-engineered constructs [110]. Therefore, investigations with flow-perfusion culture have improved the transfer of required nutrients and provided mechanical stimulation to tissue-engineered constructs [109, 110]. However, these are flow-rate dependent, and for engineered skin constructs, a relatively low flow is generally employed to ensure sufficient oxygen exchange and air-liquid interface requirements are maintained [111].

The majority of bioengineered tissues and bioreactors are small compared to 25 cm x 25cm, with no reference to further testing of spent media over the course of the perfusion culture. Analysing the media should be extended to determine when stability, growth, and productivity are optimal. These will improve consistency and reduce batch-to-batch variability while potentially reducing media costs and should be considered for future testing. The ability of automation and independent control within the bioreactor enables a fed-batch approach with timed media exchange at any time of day and a mixing mechanism designed to suit the required feeding strategy for optimal yield.

Scale-up of the CCS and use of the bioreactor are feasible within a cleanroom environment. The bioreactor's workflow and design as single-use equipment were completed and achieved success for up to 14 days of use. The current methods used for cell inoculation days was extensive for two personnel, although with technological advances, approaches of bio-printing and/or automated seeding devices are areas for further investigation that will increase reproducibility. In addition, automated closed systems for cell expansion (for example, Quantum cell expansion system, Terumo BCT) reduce labour-intensive culture requirements, albeit initially prohibitive cost. The process for media exchange was straightforward, with future automation protocols requiring even less manual handling. Environmental, microbiological, and other media parameters were all within acceptable criteria, demonstrating that the scale-up procedure and bioreactor can produce results that meet a quality management and control system that complies with cGMP guidelines.

The CCS generated from the bioreactor apparatus within a cleanroom environment was comparable to the control CCSs in small sections, and although inhomogeneous distribution, further refinement of the foam porosity is predicted to produce reliably consistent CCSs. The scale-up process proved challenging when manipulating large pieces for cell inoculation. A factory-made moving device/tool may assist and reduce the stretching and pulling of the scaffold during this step. This validation study has confirmed the presence of essential skin substitute components, i.e., proliferating basal keratinocytes, collagen-producing fibroblasts with intermittent anchoring basement membrane structure positive for essential basal lamina elements such as collagen IV, collagen VII, and integrin α6.

The basement membrane staining of collagen VII was patchy due to a non-uniform fibroblast population and sparse matrix deposition. This lack of uniformity prevented the paracrine keratinocyte-fibroblast interactions essential for basement membrane structure and fibril formation [112].

The automated bioreactor has the potential to produce large-capacity skin substitutes for patients requiring extensive wound coverage. The preceding chapters demonstrate that a highly manipulated autologous therapy with a point-of-care approach results in expensive production costs. Nonetheless, automating these therapies improves batch-to-batch reproducibility and reduces overall costs by decreasing the labour-intensive requirements, and length of stay in the intensive care unit by the accomplishment of earlier wound closure.

CHAPTER 8:
Long-term Follow-up of a Major Burn Treated Using a Composite Cultured Skin

Dearman BL and Greenwood JE

Published in

Burns Open

2022

8.1 Overview

Translation of research from ‘bench to bedside’ demonstrates a significant achievement for this candidature. More gratifying is long-term follow-up, enabling assessment of the patient’s outcome over subsequent years. Traditionally, a burn of this Total Body Surface Area (TBSA) and depth (complicated by severe lower airway inhalation injury) would likely have been a non-survivable injury. With the availability of a composite cultured skin (CCS), this patient not only survived but lives independently with a reasonable outcome from a functional perspective. The following chapter consists of a case report for The Journal of Burns (Open) and elucidates some of the challenges, lessons learned and conclusions arising from use of a bioengineered skin during the treatment of extensive full-thickness burns.
It has been published in *Burns Open*, for additional high quality images of the manuscript figures refer to Appendix XI.

Statement of Authorship

Title of Paper	Long-term Follow-up of a Major Burn treated using a Composite Cultured Skin.
Publication Status	☑ Published ☐ Accepted for Publication ☑ Submitted for Publication ☐ Unpublished and Unsubmitted w ork w ritten in manuscript style
Publication Details	Dearman BL and Greenwood JE 2022, 'Long-term Follow-up of a Major Burn treated using a Composite Cultured Skin'. *Submitted to Burns Open and published on 23/6/2022*

Principal Author

Name of Principal Author (Candidate)	Bronwyn Dearman		
Contribution to the Paper	Study design, methodology execution and data collation/analysis. Writing, editing and review for submission. Corresponding author.		
Overall percentage (%)	90%		
Certification:	This paper reports on original research I conducted during the period of my Higher Degree by Research candidature and is not subject to any obligations or contractual agreements with a third party that would constrain its inclusion in this thesis. I am the primary author of this paper.		
		Date	03/05/2022

Co-Author Contributions

By signing the Statement of Authorship, each author certifies that:

i. the candidate's stated contribution to the publication is accurate (as detailed above);

ii. permission is granted for the candidate to include the publication in the thesis; and

iii. the sum of all co-author contributions is equal to 100% less the candidate's stated contribution.

Name of Co-Author	Professor John Greenwood		
Contribution to the Paper	Review and editing.		
Signature		Date	03/05/22

.

Burns Open 6 (2022) 156–163

Contents lists available at ScienceDirect

Burns Open

journal homepage: www.sciencedirect.com/journal/burns-open

Case Report

Long-term follow-up of a major burn treated using composite cultured skin

Bronwyn L. Dearman [a,b,c,*], John E. Greenwood [b]

[a] Skin Engineering Laboratory, Adult Burns Centre, Royal Adelaide Hospital, Adelaide, SA, Australia
[b] Adult Burns Centre, Royal Adelaide Hospital, Adelaide, SA, Australia
[c] The University of Adelaide, Faculty of Health and Medical Science, Adelaide, SA, Australia

ARTICLE INFO

Keywords:
Skin
Burns
Composite cultured skin
Skin substitute
NovoSorb® BTM
DermaLab

ABSTRACT

In 2020, we reported the first human use of a polyurethane composite cultured skin (CCS) in a large wound in our burn centre. Whilst we acknowledge that this is a single case, we believe that this patient's long-term outcomes would interest the burns community. To recap, the patient suffered 95 % TBSA (predominantly full-thickness) burns and underwent the inaugural 'two-stage' therapy treatment. The first stage involved total escharectomy and application of Biodegradable Temporising Matrix (BTM) to 85 % TBSA. The second stage was the serial application of Composite Cultured Skin. As per Burn Service protocols and standard operating regimens, the small available donor site was serially harvested to provide cover for highly functional areas, in this case, the hands. The case has been reported previously with initial patient outcomes described up to 1 year; Greenwood JE, Damkat-Thomas L, Schmitt B, Dearman B. Successful proof of the "two-stage strategy" for major burn wound repair. Burns Open. 2020;4(3):121–31. We now present a long-term follow-up of the patient three years after his injury. It illustrates the patient's mobility and confirms the biophysical properties of the CCS.

1. Introduction

Recent years have seen bioengineered skin substitutes at the forefront of medical advances [1–4]. Skin tissue engineering is not a new concept [5], however, the challenges for clinical translation are stringent and costly, but striving for a heightened functional outcome and meaningful quality of life is paramount for the survivors of significant burn injury. The following elucidates the feasibility and potential strategy for improving the survival of patients with extensive burn injury and presents the long-term follow-up on the first polyurethane skin substitute for the treatment of massive full-thickness burn injury.

2. Case presentation

2.1. Admission and surgical treatment modalities

A 32-year-old male was admitted to the Royal Adelaide Hospital with a significant burn injury to 95 % TBSA. Several treatment modalities were used for complete wound coverage. The two-stage strategy involved the application of BTM to 85 % TBSA followed by serial application of a laboratory-based composite cultured skin (CCS) and available autograft (Sheet, meshed and Meek) [1]. Fig. 1 summarises and charts the patient burn, treatment sites and management pathway with an 8-month discharge from hospital.

2.2. Method for composite cultured skin

The CCS journey has been described in the preceding manuscripts and a body of work since 2010 with pre-clinical trials of small and large pieces of CCS in a large animal model [1]. The CCS was initially designed prior to the development of BTM to incorporate a synthetic polyurethane (PUR) scaffold. To a 1 mm-thick polyurethane scaffold, 25 cm × 25 cm, a plasma gel is incorporated with the patient isolated dermal fibroblasts and sequential inoculation of keratinocytes, cultured for a total of 14 days prior to transplantation to the patient.

3. Results

3.1. Clinical outcomes from 1-year post-burn date (PBD)

The video shows the patient walking with no assistance at 380 PBD (Fig. 2 -Video 1). Preceding 1-year, supplementary functional surgeries included left hand and left elbow release. Since then, the patient has undergone additional surgeries with recent procedures for a Z-plasty

* Corresponding author at: Royal Adelaide Hospital, 1 Port Road, 7G 451-469, Adelaide, SA 5000, Australia.
E-mail address: Bronwyn.dearman@sa.gov.au (B.L. Dearman).

https://doi.org/10.1016/j.burnso.2022.07.002
Received 26 May 2022; Received in revised form 23 July 2022; Accepted 26 July 2022
Available online 29 July 2022

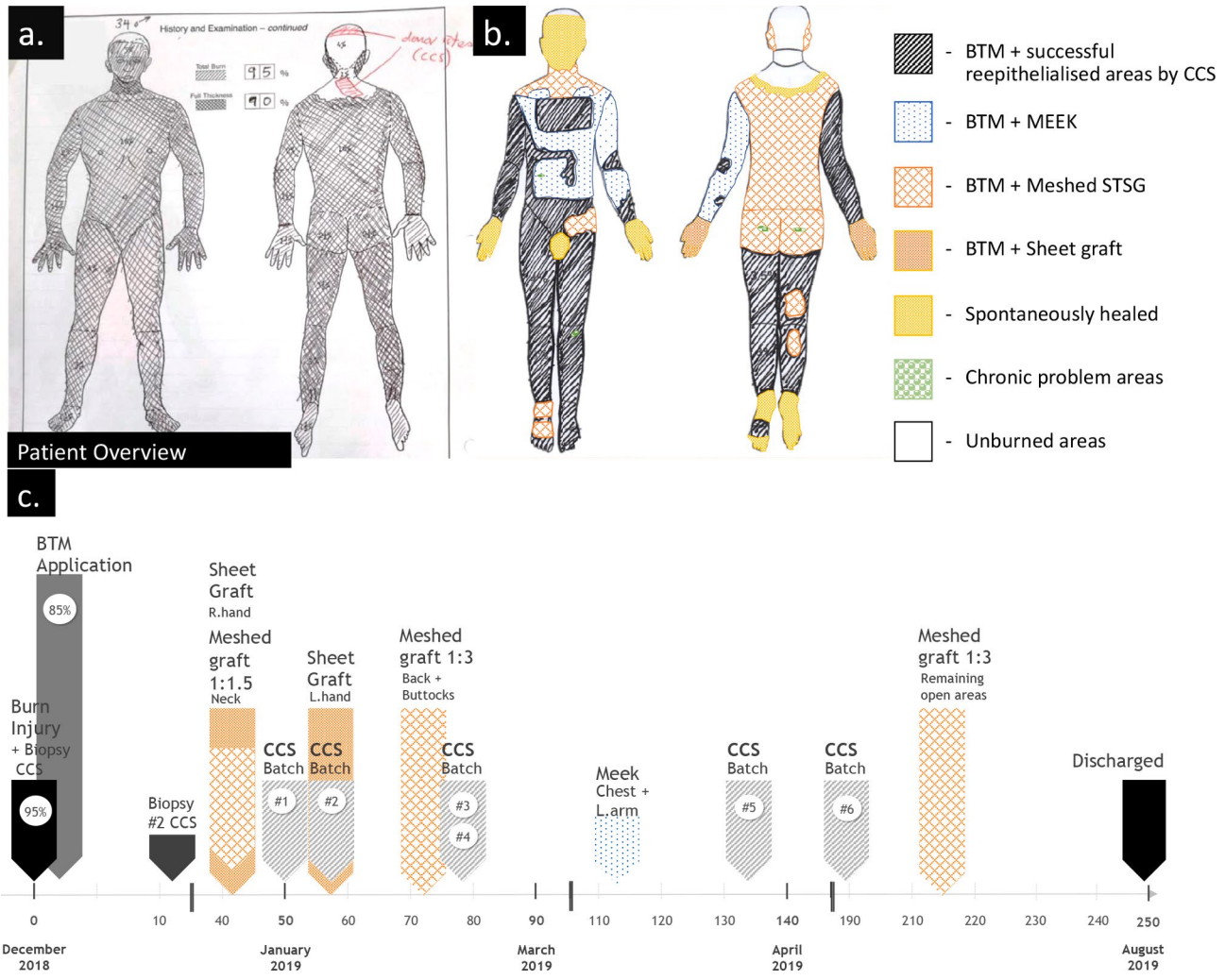

Fig. 1. Patient burn assessment and treatment modalities with timeline until discharge, a. Initial burn assessment was recorded using the Lund and Browder burn chart modified from Greenwood 2020, b. Schematic overview showing the alternative therapy treatments, and c. Outlines the treatment timeline from December 2018 to 8-months post burn injury with discharge to the rehabilitation centre.

release to the left and right axilla. Other scar and non-healing areas included the right foot, right iliac region of the abdomen, areas on each side of the gluteal fold, sole of the left foot and currently the left knee. These have recently been treated with laser therapy around the chronic non-healing wounds to release areas of surrounding tension across the wound to facilitate improved healing. Some sites mentioned above, particularly over joints or pressure areas, have necessitated ongoing dressing regimes and are self-managed. Small incidental injuries to the healed skin post-1-year have generally healed with conservative measures. The major mobility problems affecting the patient are the soles of his feet, with contracture releases and additional release of left hand webspaces. In retrospect, if an alternative treatment option was available during the initial burn assessment this might have yielded a different outcome, although during these early stages, his feet were less of a priority in the overall picture of a massive burn injury. The soles of the feet largely healed spontaneously. To date, the CCS presents with no hair or sweat glands. Occasional hair is seen on the left arm where Meek grafting had been performed using scalp graft. There is no hypertrophic scarring at any CCS sites compared to the autografted left arm. Areas healed by secondary intention are hypopigmented, and some have a tight scar band (e.g., right lateral thigh).

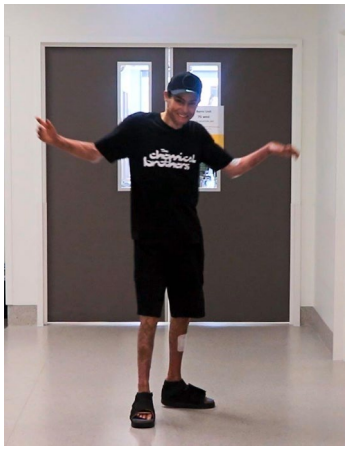

Video 1.

At two years, PBD photographs and measurements were obtained to demonstrate the differences between the treatment sites (Fig. 3). The range of motion (ROM) at 2 and 3 years PBD, for major flexor and extensor joints were assessed and compared to pooled normal ROM values [6] and burns treated with BTM and graft [7] (Table 1 and Fig. 4). Minimal to no change was observed with a slight reduction in the left

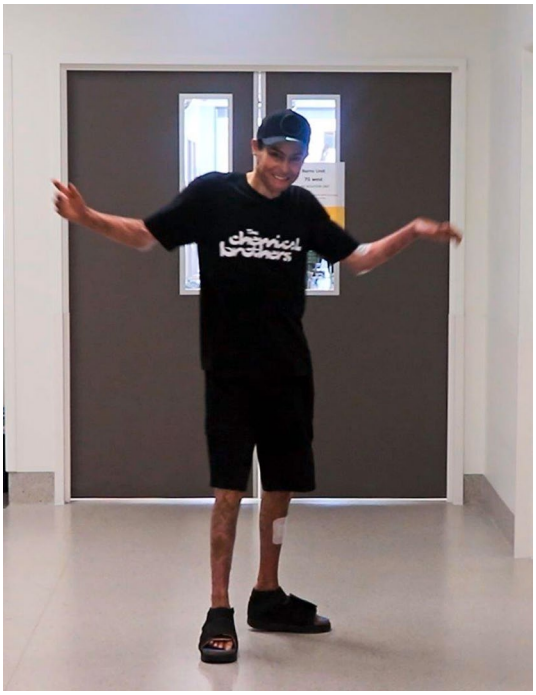

Fig. 2. Video of patient discharged and walking independently at 380 PBD (12.4 months).

knee, elbow, and right elbow mobility. The left and right shoulder ROM increased with the assistance of surgical releases. However, no active patient therapy is pursued to maintain or assist functionality. Skin maintenance is minimal with infrequent moisturiser application. The patient was not always fully compliant with his pressure garments and splints. Although, sun exposure is now currently kept to a minimum, early overexposure led to hyperpigmented areas. Assessment of scar quality with the Patient and Observer Scar Assessment Scale (POSAS) revealed no major change or variability over the years from the observers' scores, although a worsening of the patient scores was noted between 1 year and 3 year review (Table 2). Despite this change in his scores, on discussion he accepts his skin as his 'new normal' skin. Fig. 5 represents anterior and posterior overview photos at 3.3 years PBD. The patient continues independent living and now has the capability to drive a modified vehicle.

3.2. Histological analysis Day 21 to 19-months post-CCS application

Biopsies were obtained and stained for haematoxylin and eosin (H&E) on Days 21, 3-months, 6-months and 19-months. Fig. 6 shows the two-stage strategy with visible PUR layers that decreased over time (Fig. 6a-c), and none observed at 19-months (Fig. 7b-d). Laminin staining depicts the basement membrane of the epidermis and abundant membrane of the blood vessels at Day 21, with the density decreasing over time at 6-months (Fig. 6d-f).

Biopsies at 19-months were taken from areas that were perceived as clinically pigmented (Meek, CCS treated) and hypopigmented (CCS treated), these were stained with H&E, Masson's Trichrome (MT), Masson's Fontana (MF) and Melan-A (Fig. 7). An additional biopsy from uninjured skin (Fig. 7a, e, i) shows well-formed rete-ridges and the presence of sebaceous glands indicating a section of untouched skin. The treated sites that were pigmented also demonstrated rete-ridges similar to normal skin, but a flatter basal layer and less epidermal involution

Table 1
Range of motion (ROM) flexion and extension joint measurements at 2 and 3 years post-burn date (PBD) compared to normal ROM values[6] for the sites and values from BTM and autograft treated sites[7].

Joint Motion	2-Yr PBD Left	3-Yr PBD Left	2-Yr PBD Right	3-Yr PBD Right	BTM ranges[7]	Normal ROM values [6]
Knee flexion	123	119	126	127	135	137.7
Elbow extension	−14	−11	−6	−6	0	0.8
Elbow flexion	146	144	142	138	145	144.6
Shoulder flexion	142	148	132	139	180	168.8

Fig. 3. Photo images at 2.1 years PBD, a. Uninjured skin (marked), b. Donor site, c. Mesh 1:3 graft, d. Sheet graft, e. Meek (dotted area) with adjacent CCS and f. CCS, R arm, g. CCS, L leg (posterior), h. CCS L leg (anterior). R- right, L-Left.

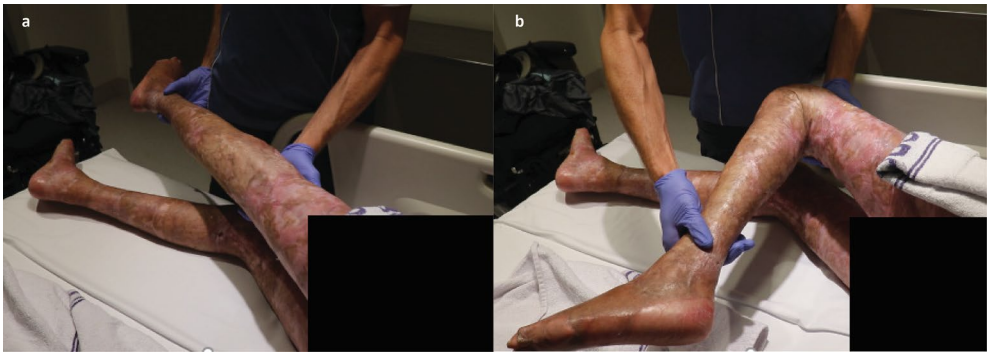

Fig. 4. Extension (a) and flexion (b) of left knee joint showing range of motion at 13-months post-burn.

Table 2
The Patient and Observer Scar Assessment Scale (POSAS) at approximately 1[(1)] and 3 years PBD for the different wound closure techniques at various treatment sites.

Wound closure technique	Site	POSAS observer		POSAS observer overall		POSAS patient		POSAS patient overall	
		1 yr	3 yr	1 yr	3 yr	1 yr	3 yr	1 yr	3 yr
CCS	L)Abdo	12	15	2	2	8	15	1	5
	L)Knee	19	13	3	2	12	14	1	5
	R)Calf	17	17	2	3	10	15	2	5
	L)Chest	15	12	2	2	18	14	1	5
	R) Forearm	16	15	2	2	8	14	1	5
	R)Arm	11	15	2	3	8	14	1	6
SSG sheet	R)Hand dorsum	17	19	2	4	8	14	2	6
Meek 1:4	L)Forearm	24	19	3	3	10	14	2	6
SSG meshed 1:3	Back	18	15	3	4	10	16	1	6

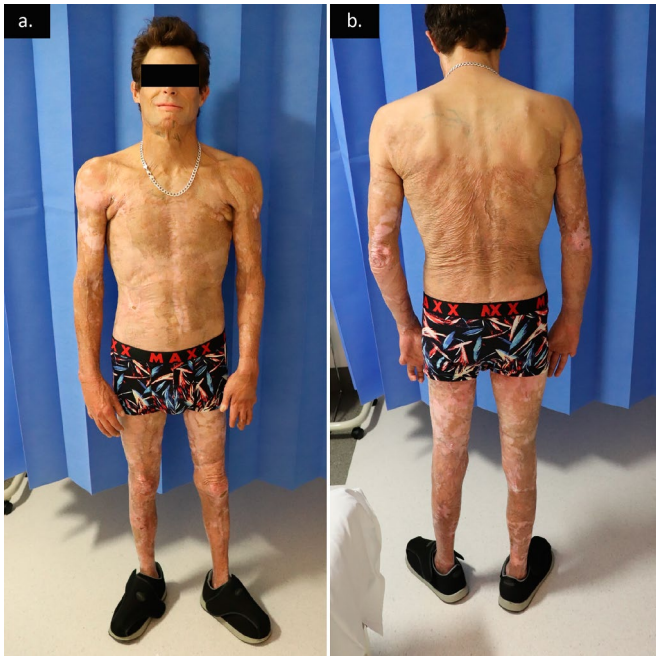

Fig. 5. Photo images at 3.3 years PBD, a. Anterior full-body overview, b. Posterior full-body overview.

were noted in the non-pigmented site (Fig. 7b-d). Masson's trichrome staining of the collagen defines the papillary and reticular dermal layers with thick loose irregular collagen bundles in the uninjured skin (Fig. 7e) compared to the treated areas showing thin, dense dermal fibrosis and parallel aligned collagen fibres (Fig. 7f-h).

Before the burn injury, the patient described when exposed to the sun, he burnt moderately and tanned brown in skin colour, classified with a Fitzpatrick skin type III [8]. Pigmentation in the 'normal' skin was apparent with melanin stained black with MF and positive melanocytes stained with Melan-A (Fig. 7i, m). The degree of black melanin staining appeared to increase with the pigmented treated sites (Fig. 7j, k), showing positive Melan-A melanocytes in the basal layer (Fig. 7n-o). In contrast, the hypopigmented areas showed no such melanin staining or melanocytes observed in the non-pigmented CCS site (Fig. 7l, p). This lack of melanocytes may be from secondary healing or from later CCS batches with potentially fewer passenger melanocytes, as melanocytes were not actively incorporated into the CCS.

3.3. *Non-invasive analysis of wound parameters*

The DermaLab Combo (Cortex, Hadsund, Denmark) was utilised to measure the biophysical parameters of the CCS, autograft (AG), donor site and uninjured skin. Baseline transepidermal water loss (TEWL) is difficult in this patient group, and the only available unharvested, 'normal' skin, was near the hairline/neck, three readings were obtained for each site (Fig. 8). Different anatomical regions for TEWL values can vary, even between closely related sites [9], and the data collected for the treated areas show variability within those locations. Uninjured skin values were 15.4 ± 2.52 g/m^2/h, which was comparable to reference samples from other studies for that location [9]. All treated areas, including sheet graft, Meek, CCS and donor areas, were generally in the lower range, indicating a protective barrier but not a normal functional barrier. Other anatomically treated sites were measured and can be compared to pooled standard estimates, as shown in Table 3.

Melanin index was measured with higher values for all sun-exposed hyperpigmented areas (e.g., hand, legs, arm) compared to uninjured skin (neck). Non-pigmented areas had a lower erythema index than uninjured and autograft skin, with other CCS treated areas within the range of donor site and normal skin values. The patient's observation of the pigmentation on his right forearm represents his 'normal' tanned colouring. The autograft's viscoelastic (VE) properties (apart from the Meek on the chest) and the CCS arm treated sites were similar to the uninjured skin on the neck. The chest and the leg sites displayed higher mean VE readings indicating less pliable skin in these regions, which was noted with the thinner skin thickness measurements of the chest sites. The thickness of normal healthy skin varies at each anatomical site. On average, skin ranges from 0.5 mm to 4 mm thick. For example, the average thickness of a healthy forearm (posterior) skin from previous

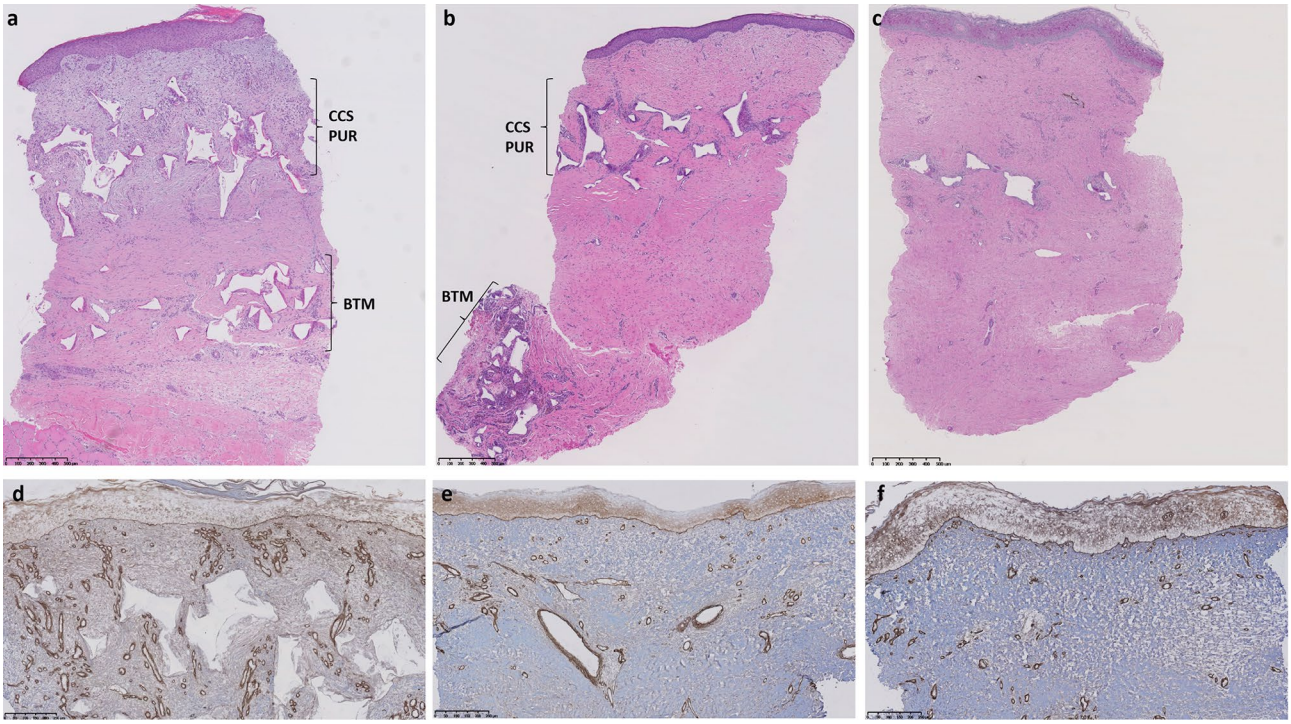

Fig. 6. Histological sections stained with H&E (a-c) and Laminin (d-f). a, d - Day 21. b, e 3 - months, and c, f – 6 months. Note: The abundant laminin staining of the basement membrane of prominent blood vessels beneath the epidermis at Day 21, this vascularity decreased by 6-months. CCS PUR resides in the upper region of the section at 21 days and 3 months with the BTM layer present in the lower dermis. At 6-months minimal polymer remains in this section. Scale bar: a-c 500 μm, d-f 250 μm.

studies has shown to be 1.49 mm for males [10]. The overall thickness of the treatment sites from ultrasound ranged between 0.948 mm (chest) to 1.746 mm (CCS arm). Other variables contribute to skin thickness, namely gender and the possible effects of smoking [11]. This patient is a moderate smoker and was of a slender stature before the burn.

To non-invasively monitor the skin post-19-months, the VivaScope® 1500 (Caliber Imaging and Diagnostics, Rochester, NY, USA), 830 nm laser, was used as an *in vivo* tool. The maximum penetration depth of this machine is limited to ~ 250 μm. Images were acquired for the CCS treated forearm at the 3-year time point showing the layers of the skin are well defined, depicting the honeycomb pattern with junctions and bright refractile pigmented keratinocytes distributed at one level throughout the basal layer instead of forming rings around the dermal papillae. The dermal papillae in the treated grafts are absent due to the complete removal and culture of the skin cells only.

4. Discussion

The use of engineered tissues to treat full-thickness extensive injuries where donor sites are limited are areas of ongoing investigations. This patient was treated with CCS and autograft, and at three years post-burn is driving, living independently and appears generally happy. Where CCS sheets were applied there is no discernible seamed junctions between each applied graft apart from the patchy colouration. This disparity between graft applications has been noted with the use of engineered skins of smaller size [3]. The meshed autograft and Meek autograft pattern remains visible at the 3-year follow-up visit, but its application on NovoSorb® BTM appears subjectively better than previous reports on allografted or fat bed [12,13]. The biophysical parameters of the CCS were similar to autograft with varying pigmentation, with further investigations required to increase the sample size to support the validity of these results. Post-discharge, patient follow-up was intermittent, there was non-compliance with the wearing of therapy garments, and minimal skin maintenance was observed, in addition to being a smoker, the skin appeared dry and thin over joints. These areas posed difficult to heal from initial timepoints PBD, possibly due to the early mobilisation and repetitive tension, assisting areas of breakdown over time.

5. Conclusion

Bioengineered skin substitutes have been shown to reduce donor site harvesting, numbers of skin autografting procedures, and assist with the long-term morbidity from scars [4]. Without the use of this treatment modality, this patient would have been unlikely to survive. The treatment was necessitated due to the depth of burn and the small percentage of harvestable donor skin. The early extubation of this patient with serial delamination and staged reconstruction advocates the next paradigm

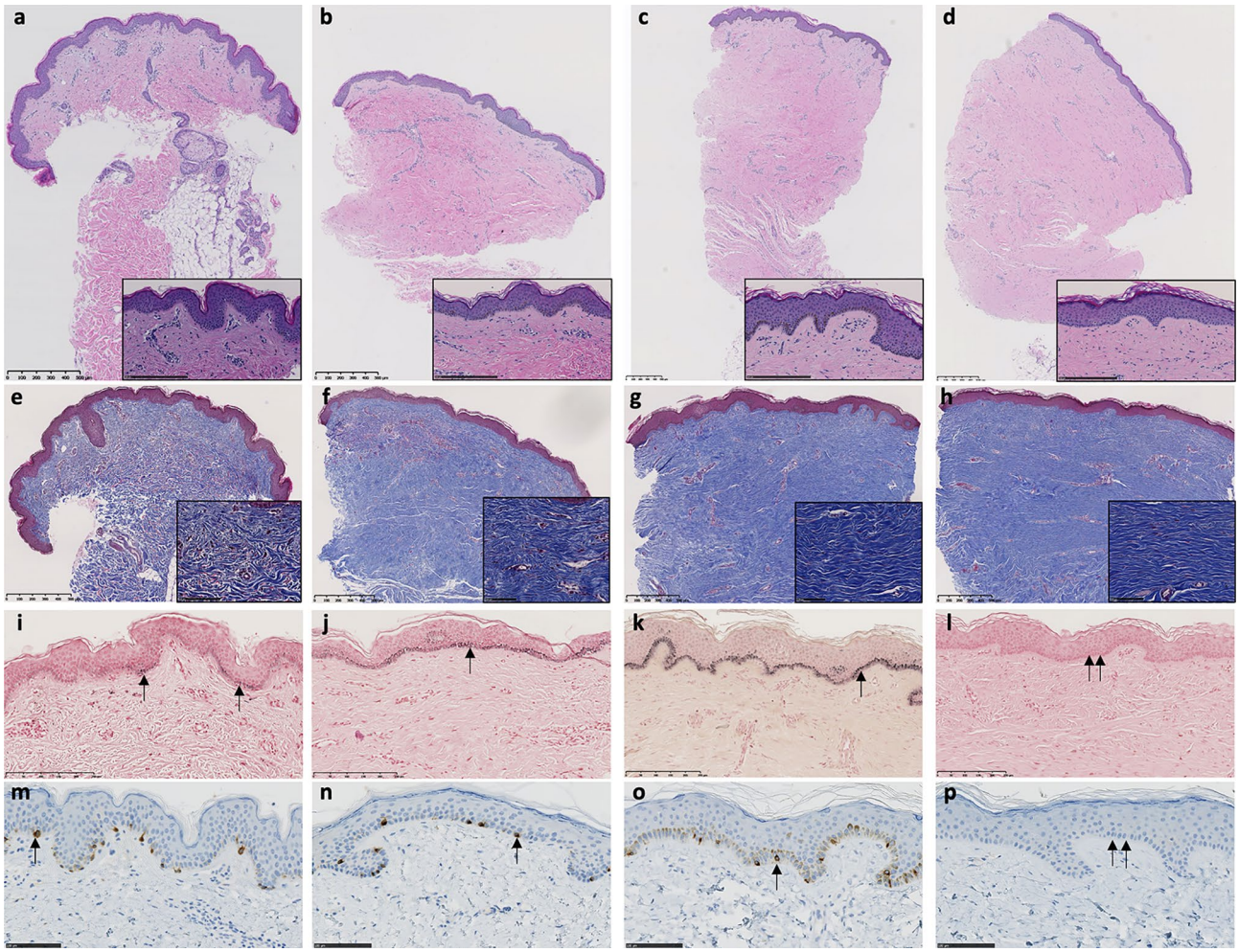

Fig. 7. Representative histological sections and immunohistochemical staining (row 1H&E, row 2 Masson's trichrome, row 3 Masson's Fontana and row 4 Melan-A) at 582 PBD. a, e, i, m uninjured skin. b, f, j, n, Meek treated. c, g, k, o, CCS treated -Pigmented. d, h, l, p, CCS treated –non-pigmented site. Inset images, a-d show defined or lack of epidermal rete ridges of the uninjured skin to treated sites for the H&E sections and inset e-h show the varying collagen density in the MT sections. A single arrow indicates positive Melanin or Melan-A stained melanocytes in the pigmented sections and double arrows depict no staining along the basal layer in the non-pigmented section. Scale bar a-h 500 μm, i-l and a-d inset 250 μm, m-p and e-h inset 100 μm. H&E – Haematoxylin and eosin, MT – Masson's trichrome, MF – Masson's Fontana, PBD – post burn date.

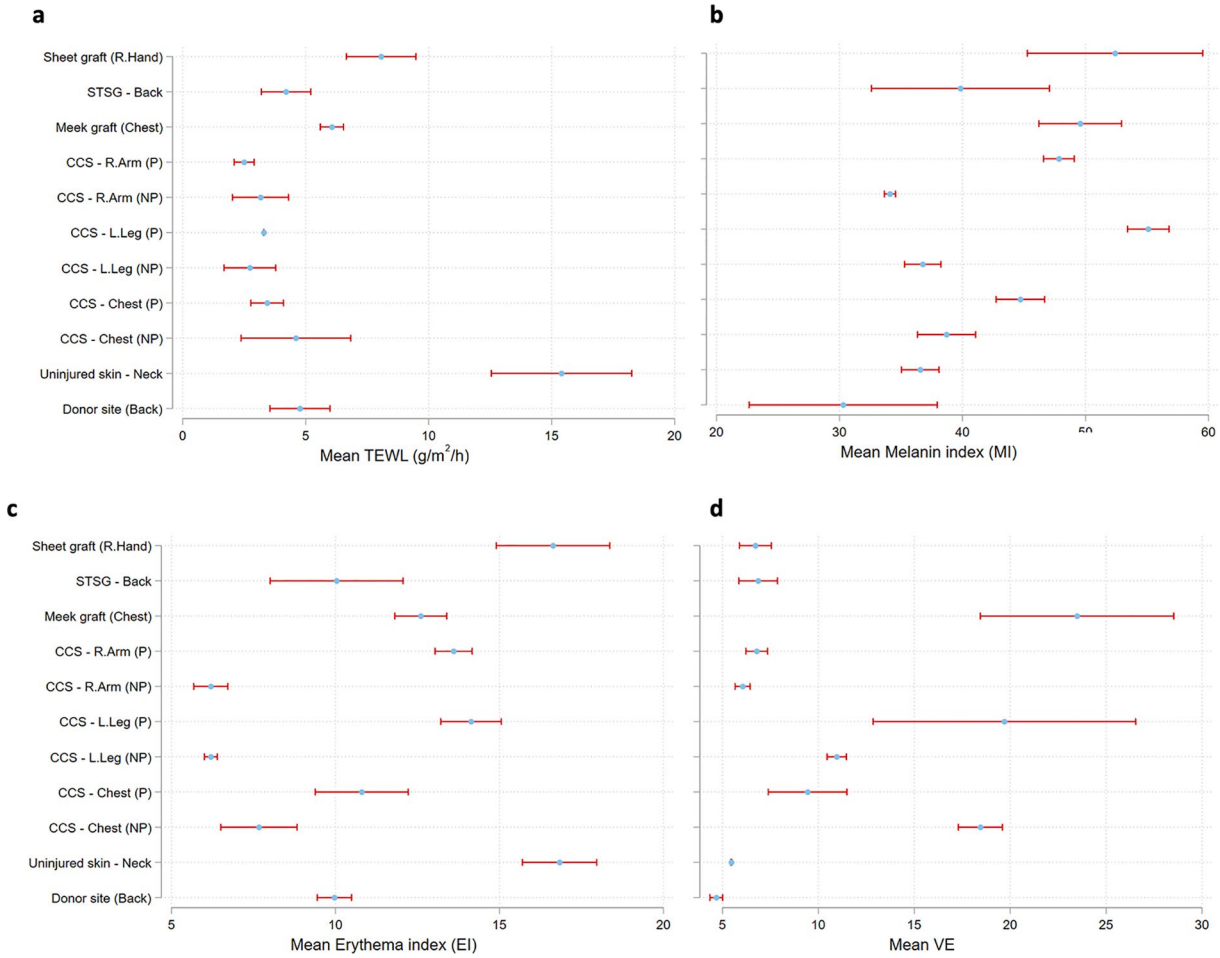

Fig. 8. DermaLab Wound Parameters, at 2 years post-burn, a. Transepidermal water loss (TEWL), b. Melanin, c. Erythema, and d. ViscoElasticity (VE). Mean measurements are represented graphically for uninjured normal skin, meshed 1:3 autograft on the back, Meek graft on the chest, CCS on the arm, leg and chest and donor site on the back.

Table 3
Transepidermal waterloss (TEWL) measurements for treated sites compared to pooled reference estimates (Akdeniz et al. 2018[9]). CCS – composite cultured skin, STSG – Split-thickness skin graft, NP - non-pigmented, P – pigmented, L- left, R- right.

Mesure	Donor site Back	Uninjured skin Neck	CCS Chest (NP)	CCS Chest (P)	CCS L. Leg (NP)	CCS L. Leg (P)	CCS R. Arm (NP)	CCS R. Arm (P)	Meek graft Chest	STSG Back	Sheet graft. Hand
TEWL	**4.77 (1.08)**	**15.40 (2.52)**	**4.60 (1.97)**	**3.43 (0.59)**	**2.73 (0.93)**	**3.30 (0.00)**	**3.17 (1.01)**	**2.50 (0.36)**	**6.07 (0.42)**	**4.20 (0.89)**	**8.07 (1.25)**
Reference estimates[9]	6.5 (4.8–8.2)	8.3 (7.4–9.3)	8.6 (6.8–10.5)	8.6 (6.8–10.5)	5.1 (4.1–6.1)	6.6 (2.2–11.0)	5.1 (4.4–5.8)	3.9 (2.9–5.0)	8.6 (6.8–10.5)	6.5 (4.8–8.2)	12.4 (10.7–14.2)

shift in burn practice for extensive burns [13]. Further studies with CCS on smaller areas will allow a comparative analysis of AG and uninjured skin. However, this procedure is used for extensive skin loss conditions where there are extremely limited options to facilitate wound healing. Understandably this study is 'n = 1', and site-matched control studies are required to objectively validate the biophysical properties of CCS long-term, compared with skin autograft or other definitive wound closure mechanisms.

6. Ethics approval and consent to participate

Special Access Scheme approval via the Therapeutic Goods Administration (TGA) was granted. The patient gave informed consent to use photographs and discuss this case.

Declaration of Competing Interest

The authors declare the following financial interests/personal relationships which may be considered as potential competing interests: At the time of this patients treatment, Professor John Greenwood was a major shareholder in PolyNovo Biomaterials Pty Ltd, the company that produced the NovoSorb® Polyurethane material. Professor John Greenwood and Bronwyn Dearman were stakeholders in Skin Tissue Engineering Pty Ltd. Professor Greenwood retired in 2020 and has no further clinical practice.

Funding Source and Acknowledgements

This was supported by Lifetime Support Authority grant #GA00061. The authors thank The University of Adelaide Histology, Microscopy and Statistician Departments. We gratefully acknowledge the Skin

Engineering Laboratory and CCET personnel for assistance with culturing and staining techniques. Senior physiotherapist Brad Schmitt for the follow-up ROM measurements and POSAS scoring. Dr Patrick Coghlan and Dr Christopher Wearn for final review of the manuscript.

References

[1] Greenwood JE, Damkat-Thomas L, Schmitt B, Dearman B. Successful proof of the 'two-stage strategy' for major burn wound repair. Burns Open 2020;4(3):121–31. https://doi.org/10.1016/j.burnso.2020.06.003.

[2] Schiestl C, Meuli M, Vojvodic M, Pontiggia L, Neuhaus D, Brotschi B, et al. Expanding into the future: Combining a novel dermal template with distinct variants of autologous cultured skin substitutes in massive burns. Burns Open 2021;5(3):145–53.

[3] Germain L, Larouche D, Nedelec B, Perreault I, Duranceau L, Bortoluzzi P, et al. Autologous bilayered self-assembled skin substitutes (SASSs) as permanent grafts: a case series of 14 severely burned patients indicating clinical effectiveness. Eur Cell Mater 2018 Sep;36:128–41.

[4] Boyce ST, Simpson PS, Rieman MT, Warner PM, Yakuboff KP, Bailey JK, et al. Randomized, paired-site comparison of autologous engineered skin substitutes and split-thickness skin graft for closure of extensive, full-thickness burns. J Burn Care Res 2017;38(2):61–70.

[5] Hansbrough JF, Boyce ST, Cooper ML, Foreman TJ. Burn wound closure with cultured autologous keratinocytes and fibroblasts attached to a collagen-glycosaminoglycan substrate. JAMA 1989;262(15):2125–30. https://doi.org/10.1001/jama.1989.03430150093032.

[6] Soucie JM, Wang C, Forsyth A, Funk S, Denny M, Roach KE, et al. Range of motion measurements: reference values and a database for comparison studies. Haemophilia 2011 May;17(3):500–7. https://doi.org/10.1111/j.1365-2516.2010.02399.x.

[7] Schmitt B, Heath K, Kurmis R, Klotz T, Wagstaff MJD, Greenwood J. Early physiotherapy experience with a biodegradable polyurethane dermal substitute: Therapy guidelines for use. Burns 2021 Aug;47(5):1074–83. https://doi.org/10.1016/j.burns.2020.10.023.

[8] Fitzpatrick TB. The validity and practicality of sun-reactive skin types I through VI. Arch Dermatol 1988;124(6):869–71. https://doi.org/10.1001/archderm.1988.01670060015008.

[9] Akdeniz M, Gabriel S, Lichterfeld-Kottner A, Blume-Peytavi U, Kottner J. Transepidermal water loss in healthy adults: a systematic review and meta-analysis update. Br J Dermatol 2018 Nov;179(5):1049–55. https://doi.org/10.1111/bjd.17025.

[10] Van Mulder TJS, de Koeijer M, Theeten H, Willems D, Van Damme P, Demolder M, et al. High frequency ultrasound to assess skin thickness in healthy adults. Vaccine 2017;35(14):1810–5.

[11] Ortiz A, Grando SA. Smoking and the skin. Int J Dermatol 2012;51(3):250–62. https://doi.org/10.1111/j.1365-4632.2011.05205.x.

[12] Wagstaff MJD, Salna IM, Caplash Y, Greenwood JE. Biodegradable Temporising Matrix (BTM) for the reconstruction of defects following serial debridement for necrotising fasciitis: A case series. Burns Open 2019;3(1):12–30. https://doi.org/10.1016/j.burnso.2018.10.002.

[13] Greenwood JE. A paradigm shift in practice-the benefits of early active wound temporisation rather than early skin grafting after burn eschar excision. Anaesth Intensive Care 2020 Mar;48(2):93–100. https://doi.org/10.1177/0310057X19895788.

Click here to access/download
e-Component
Figure 2_video 1.mp4

Inactive link above. Click here to view video.

Click here to view larger images in Appendix XI

CHAPTER 9:
Thesis Conclusion and Future Directions

This thesis highlights the feasibility of translational research in this field and has shown that this approach has the potential to provide an alternative treatment for life-threatening burns. The studies included in this thesis provide insights into the challenges of clinical translation and demonstrate the importance of incorporating automation and scalability into a tissue-engineered skin product. Although further refinement of the novel synthetic PUR scaffold with reduced pore size is required to sustain consistent skin morphogenesis within the bioreactor, the data obtained suggest that the polyurethane can support a functional skin substitute with engraftment and biophysical properties similar to native skin. Additionally, the investigated fabrication of a hybrid blend to assist with PUR porosity and collagen contraction has shown potential in an *in vivo* animal model. These findings will aid with the development of future mixed scaffolds to support the dermal ECM environment and epidermal stratification with barrier function.

Clinically fabricated bioengineered skin, until recent years, have been small manual laboratory-based substitutes. Cutiss, a Swiss skin tissue engineering company, has just launched the denovoCast, a closed machine capable of generating multiple pieces of personalised human tissue. The current design for one machine incorporates four multi controlled media supplied chambers for skin pieces, each ~10 x 20cm. There is no mention of exact size measurements, and have therefore been extrapolated from published findings and online features. The ability to generate multiple large pieces of skin tissue is paramount for patients who suffer extensive skin loss, such as deep burn injuries and was the first fundamental principle of the candidature. There was no comparable bioreactor on the market to grow skin when the project began, so an in-house device was developed. Previous work from the Skin Engineering Laboratory had established small 8cm x 8cm CCSs, and the design of the bioreactor enabled the CCS to be scaled up (25cm x 25cm) and tested in a large porcine wound model. These results ultimately led to the translation and first-in-man use of this composite skin and novel bioreactor in a patient who had suffered 95% burns. The current laboratory facilities only enabled the CCSs to be produced in 5-piece batches.

Batches 1-4 successfully covered 42% TBSA, with 5 and 6 used for touch-ups—totalling 26 CCSs to cover 1.6m^2 TBSA. Although initial engraftment rates were not similar to Boyce et al., Schiestl et al., or Germain et al. [54, 56, 113], the following applications showed a 94% success rate, as with any innovation or first-in-man, learning curves are to be expected. This single case report was permitted through the Special Access Scheme on compassionate terms through the TGA. The CCS was not dissimilar to skin autograft, although CCS application over joints and bone presented as problematic areas noted at long term follow-up. Pigmented CCS areas were apparent, similar to the original Fitzpatrick III skin type, with a heavy degree of Fontana-Masson stain in the pigmented skin areas lining the basal layer with positive melanocyte presentation. The Melan-A staining for melanocytes originated from the CCS as there was no adjacent normal skin for edge reepithelialisation.

Post clinical treatment with CCS, new batches of PUR underwent QA to ensure reproducibility, these were unsuccessful, and new methods were required to be established to overcome the pore size and distribution. In addition, the CCSv1 was submerged culture, and with the aim of epidermal stratification and graft robustness, ALI within the bioreactor was desired. Cell proliferation and characterisation were conducted with keratinocytes and fibroblasts to optimise the CCS methods further and explore the serum-free approach. Supplemented human dermal fibroblast media showed superior growth compared to a basal DMEM with serum only. These cells appeared to have less collagen production, a feature noted by other investigators [114], but they were still able to sustain 3D culture in a scaffold and support the generation of a stratified epidermis. This medium contained 2% serum, and although a complete serum-free approach is desirable, at this stage, the addition of serum is still a necessity, albeit these concentrations have dramatically reduced, and it will only be a matter of time before it can be eliminated. Xeno-free culture and its substitution with human-derived elements (human serum or platelet lysate) have shown potential for the culture of individual cell types, [66] but volume and supply may be the limiting factor for these replacements.

Media for three-dimensional skin substitute maturation similarly utilises serum (0.3% v/v), and to date, this has been of bovine origin. The culture medium and the ALI increase the morphogenesis of the epidermis and the basement membrane structure prior to transplant. The addition of ALI to the CCS method presented challenges, and a hybrid with C-GAG was explored to fill the pores. Although the plasma gel fills the pores and has many beneficial complements providing growth factors and natural clotting mechanisms, it also produces variability and ultimately is an allogenic product with some risk of unknown disease transmission not unlike blood banked products. The investigation of a hybrid resolved the issue of PUR pore size and collagen contraction. *In vitro* fabrication methods were devised for these scaffolds and were subsequently tested *in vivo* in a porcine excised wound model, showing similar biophysical properties to the control meshed skin autograft. The hybrid scaffold with amendments to collagen incorporation and cross-linking approaches for scale-up will produce a more robust non-contractile support for the dermal-epidermal organisation.

Furthermore, the layer-by-layer procedural changes to the CCS assisted epidermal morphogenesis on a small scale, but with bioreactor testing and scale-up, this method proffered manipulation and set up challenges producing inhomogeneous areas. The inclusion of an automated cell inoculation method and an assisted device for scale-up and the refinement of PUR pore size will produce a homogeneous substitute suitable for transplantation. In conclusion, this thesis supports the clinical potential of CCS for assisting the treatment of extensive full-thickness burns using a bioreactor device.

9.1 Emerging Next-Generation Skin Substitutes

9.1.1 What is the Right Blend?

The PUR design is improving with each iteration and has the potential to progress further with a newly appointed research and development team. Other methods for material blends may be viable options to assist with the evolution of the CCS to reduce variability and eliminate xenogeneic or allogenic properties. The ultimate goal is a synthetic scaffold with biocompatible and bioabsorbable properties that can mechanically support the development of an exogenous ECM with a stratified epidermis and connecting basement membrane. Recent investigations for skin tissue engineering applications include combination based hydrogels with platelet lysate and gelatin methacryloyl [115] and sodium alginate-fibrinogen [116]; however, these formulations require further *in vivo* animal testing prior to clinical translation.

9.1.2 Colour, Vascularisation, and Skin Appendages

As the need arises to produce distinct anatomical substitutes by incorporating complex cell subpopulations and potential growth factors, so does the timeframe for clinical translation. The first goal of a bioengineered skin substitute is to provide wound closure and barrier function, and it has been successfully used clinically to save patients' lives with life-threatening burns [54, 56-58]. However, restoring additional features to align with native skin poses potentially limiting challenges within the field of tissue engineering thus far. Pigmentation alongside vascularisation are attributes being refined for a bioengineered skin substitute. Extensive investigations are continuing for the inclusion of melanocytes into these grafts as the associated stigma from hypopigmentation is a major socio-economic isolator for some ethnicities, and the lack of pigment in burn scars impacts the quality of life [117] in addition to compromised protection when exposed to ultraviolet radiation. The pigmentation of clinically available or investigative skin substitutes is unpredictable and generally results in hypopigmentation or patchy isolated pigmentation from passenger melanocytes [118].

Nonetheless, significant success has been shown for pigmented cutaneous wound healing in various preclinical models where melanocytes have been expanded and inoculated into skin substitutes [79, 119-121]. Scuderi et al. have clinically used the three cell combination with varying success and minimal long-term follow-up. This study [122, 123], and original melanocyte culture media required phorbol esters - a tumor-promoting agent. A melanocyte growth medium without this additive has been formulated [124], and others contain bovine pituitary extract. Although there is still some risk of prions with these products, this is relatively small as it is obtained from bovine spongiform encephalopathy-free herds. The major concern with melanocyte manipulation is possible tumour formation and needs consideration for therapeutic transplants to ensure melanomas do not eventuate. A study investigating such potential injected melanocytes subcutaneously into mice for 24 weeks with no tumour formation [125] and has since shown the incorporation of melanocytes (originated from dark or light skin) into ESSs have shown no malignancy tendency during the study period [79].

Adequate vascularisation is another primary goal as it is essential to supply nutrients and oxygen for the survival of a graft, either an autograft or a skin substitute. In the field of skin tissue engineering, vascularization strategies are being used, including proangiogeneic growth factors, bioinductive scaffolds, and cell-based incorporation techniques [126].
As endothelial cells are immunogenic, the incorporation of an endothelial source to a bioengineered tissue needs consideration for clinical translation. It should be autologous and can be isolated from a skin biopsy at the same time as the other cell types [114]; however, the isolated cell numbers may be a limiting factor [127]. Pre-vascularised tissue promotes the inosculation between host and graft, potentially shortening the time period of avascularity, promoting earlier graft stabilisation. However, a well-vascularised dermal bed is just as critical, and the two-stage strategy using a novel polyurethane as the dermal template has shown (Chapter 6) that autograft and skin substitutes can engraft within ten days of application. The leading collagen dermal templates vascularisation is decreased and can take up to 3 weeks for host vessel ingrowth [128], causing a delay in graft take. Therefore, a question may be raised regarding the validity of *in vitro* endothelial cell addition if an

adequate dermal bed is produced. There are still unknown variables related to endothelial cell inoculation (cell density, ability to form blood vessels *in vitro*, homogenous distribution and VEGF expression) that need further research before clinically applicable. A vasculature source from adipose-derived fractions addresses the quantity issue and may provide *in vivo* signalling factors from other cell types [129-131] and are areas for further investigation.

To replicate native skin, restoring cutaneous appendages are features that pose challenges for tissue engineering. These include hair follicles, sebaceous and sweat glands. Hair follicle regeneration knowledge is based on embryonic hair generation and hair cycling interactions. Several experimental strategies have been put forward to elucidate hair follicle neogenesis from adults that have shown trichogenic feasibility [132-135], but none to date have been successfully translated for clinical use in large skin defects. The elimination of hair follicles in deep burns reduces the guidance cues required for sensory structures and results in a permanent loss of sensation or decreased axonal migration (especially where there is no adjacent normal skin). The depth of the skin defect (or fascial excision), degree of neuronal damage, and fibrotic scar can determine the regenerative sensory innervation and even report abnormal sensation or hypersensitivity [136]. The plausibility of reinnervation of skin substitutes and restoration of skin sensitivity has been shown [137-139], but a recovery to full sensation is yet to be determined. Schwann cells and neurons (derived from human iPSCs) have been incorporated into tissue-engineered skin models showing enhanced nerve regeneration capacity with potential as a disease model but a long way to a personalised medicine approach [140].

Nerve regeneration aligns with revascularisation [141]. If a scaffold with the principle wound closing properties can support regeneration and ingrowth of both of these structures, is there a need to complicate a skin substitute with extra cell populations (i.e., Schwann cells, endothelial cells), confounding the *in vitro* practice [142]. As multiple cell populations are mixed with matrix scaffolds, further research is required to understand the effects and interactions of multiple growth factors in an *in vitro* environment.

9.2 Automated Fabrication for Three-Dimensional Regeneration of Tissues

Technology advancements over the last decade have directed the fabrication of 3D native tissues to cell-laden scaffolds or hydrogels using computer-aided design and manufacturing methods [143]. The terminology bioprinting and bioink have become 'buzz terms' within tissue and organ regeneration fields, requiring delineation and standardisation [144]. Nonetheless, the combination of an automated device(s) that assists with a layer-by-layer approach for the fabrication of a skin substitute with a scaled media assisted program will further advance the skin bioengineering field to enable a straightforward translation for therapeutic use. This progression will primarily assist major wound loss conditions such as extensive burns but additionally has clinical potential for reconstructive surgery, and with continuing advancements and inclusion of other cell types, correction of pigmented defects, reduction of scar revisions and elimination of blistering skin diseases. Although the field has come so far, there is still much work to be done, and the next generation of skin substitutes will undoubtedly be a transformative accomplishment.

REFERENCES

1. Dearman BL, Stefani K, Li A, Greenwood JE. “Take” of a polymer-based autologous cultured composite “skin” on an integrated temporizing dermal matrix: proof of concept. J Burn Care Res. 2013 Jan-Feb;34(1):151-60. DOI: 10.1097/BCR.0b013e31828089f9.
2. Dearman BL, Li A, Greenwood JE. Optimization of a polyurethane dermal matrix and experience with a polymer-based cultured composite skin. J Burn Care Res. 2014 Sep-Oct;35(5):437-48. DOI: 10.1097/BCR.0000000000000061.
3. Weinstein GD, McCullough JL, Ross P. Cell proliferation in normal epidermis. J Invest Dermatol. 1984 Jun;82(6):623-8. DOI: 10.1111/1523-1747.ep12261462.
4. Cuono C, Langdon R, McGuire J. Use of cultured epidermal autografts and dermal allografts as skin replacement after burn injury. Lancet (London, England). 1986;1(8490):1123.
5. Fuchs E. Keratins and the skin. Annu Rev Cell Dev Biol. 1995;11(1):123-53. DOI: 10.1146/annurev.cb.11.110195.001011.
6. Elias PM. Lipids and the epidermal permeability barrier. Arch Dermatol Res. 1981;270(1):95-117. DOI: 10.1007/BF00417155.
7. Scheuplein RJ. Permeability of the skin: A review of major concepts and some new developments. J Invest Dermatol. 1976;67(5):672-6. DOI: 10.1111/1523-1747.ep12544513.
8. Serre G, Mils V, Haftek M, Vincent C, Croute F, Reano A, et al. Identification of late differentiation antigens of human cornified epithelia, expressed in re-organized desmosomes and bound to cross-linked envelope. J Invest Dermatol. 1991 Dec;97(6):1061-72. DOI: 10.1111/1523-1747.ep12492589.
9. Aleemardani M, Trikic MZ, Green NH, Claeyssens F. The importance of mimicking dermal-epidermal junction for skin tissue engineering: A review. Bioengineering 2021 Oct 20;8(11). DOI: 10.3390/bioengineering8110148.
10. Uitto J, Has C, Vahidnezhad H, Youssefian L, Bruckner-Tuderman L. Molecular pathology of the basement membrane zone in heritable blistering diseases: The paradigm of epidermolysis bullosa. Matrix Biol. 2017 Jan;57-58:76-85. DOI: 10.1016/j.matbio.2016.07.009.
11. Riley PA. Melanin. Int J Biochem Cell Biol. 1997 Nov;29(11):1235-9. DOI: 10.1016/s1357-2725(97)00013-7.
12. Woo SH, Ranade S, Weyer AD, Dubin AE, Baba Y, Qiu Z, et al. Piezo2 is required for Merkel-cell mechanotransduction. Nature. 2014 May 29;509(7502):622-6. DOI: 10.1038/nature13251.
13. Sorrell JM, Caplan AI. Fibroblast heterogeneity: more than skin deep. J Cell Sci. 2004 Feb 15;117(Pt 5):667-75. DOI: 10.1242/jcs.01005.

14. Driskell RR, Lichtenberger BM, Hoste E, Kretzschmar K, Simons BD, Charalambous M, et al. Distinct fibroblast lineages determine dermal architecture in skin development and repair. Nature. 2013 Dec 12;504(7479):277-81. DOI: 10.1038/nature12783.

15. Vig K, Chaudhari A, Tripathi S, Dixit S, Sahu R, Pillai S, et al. Advances in skin regeneration using tissue engineering. Int J Mol Sci. 2017 Apr 7;18(4). DOI: 10.3390/ijms18040789.

16. Auger FA, Lacroix D, Germain L. Skin substitutes and wound healing. Skin Pharmacol Physiol. 2009;22(2):94-102. DOI: 10.1159/000178868.

17. Gurtner GC, Werner S, Barrandon Y, Longaker MT. Wound repair and regeneration. Nature. 2008;453(7193):314-21. DOI: 10.1038/nature07039.

18. Versteeg HH, Heemskerk JW, Levi M, Reitsma PH. New fundamentals in hemostasis. Physiol Rev. 2013;93(1):327-58.

19. Li JP, Chen JMD, Kirsner RP. Pathophysiology of acute wound healing. Clin Dermatol. 2007;25(1):9-18.

20. Harvey C. Wound healing. Orthop Nurs. 2005;24(2):143-57.

21. Plotczyk M, Higgins C. 1 - Skin biology. In: García-Gareta E, editor. Biomaterials for Skin Repair and Regeneration: Woodhead Publishing; 2019. p. 3-25.

22. Levenson SM, Geever EF, Crowley LV, Oates rJF, Berard CW, Rosen H. The Healing of Rat Skin Wounds. Annals of surgery. 1965;161(2):293-308.

23. Jarbrink K, Ni G, Sonnergren H, Schmidtchen A, Pang C, Bajpai R, et al. The humanistic and economic burden of chronic wounds: a protocol for a systematic review. Syst Rev. 2017 Jan 24;6(1):15. DOI: 10.1186/s13643-016-0400-8.

24. McCosker L, Tulleners R, Cheng Q, Rohmer S, Pacella T, Graves N, et al. Chronic wounds in Australia: A systematic review of key epidemiological and clinical parameters. Int Wound J. 2019 Feb;16(1):84-95. DOI: 10.1111/iwj.12996.

25. Gauglitz GG, Korting HC, Pavicic T, Ruzicka T, Jeschke MG. Hypertrophic scarring and keloids: pathomechanisms and current and emerging treatment strategies. Mol Med. 2011 Jan-Feb;17(1-2):113-25. DOI: 10.2119/molmed.2009.00153.

26. Tomasek JJ, Gabbiani G, Hinz B, Chaponnier C, Brown RA. Myofibroblasts and mechano-regulation of connective tissue remodelling. Nat Rev Mol Cell Biol. 2002;3(5):349-63.

27. Bhardwaj N, Chouhan D, Mandal BB. Tissue engineered skin and wound healing: Current strategies and future directions. Curr Pharm Des. 2017;23(24):3455-82. DOI: 10.2174/1381612823666170526094606.

28. Jeschke MG, van Baar ME, Choudhry MA, Chung KK, Gibran NS, Logsetty S. Burn injury. Nat Rev Dis Primers. 2020 Feb 13;6(1):11. DOI: 10.1038/s41572-020-0145-5.

29. Burns BF, McCauley RL, Murphy FL, Robson MC. Reconstructive management of patients with greater than 80 per cent TBSA burns. Burns. 1993;19(5):429-33. DOI: 10.1016/0305-4179(93)90068-J.

30. Spronk I, Polinder S, van Loey NEE, van der Vlies CH, Pijpe A, Haagsma JA, et al. Health related quality of life 5-7 years after minor and severe burn injuries: a multicentre cross-sectional study. Burns. 2019 Sep;45(6):1291-9. DOI: 10.1016/j.burns.2019.03.017.

31. Spronk I, Legemate CM, Dokter J, van Loey NEE, van Baar ME, Polinder S. Predictors of health-related quality of life after burn injuries: a systematic review. Crit Care. 2018 Jun 14;22(1):160. DOI: 10.1186/s13054-018-2071-4.

32. Janzekovic Z. A new concept in the early excision and immediate grafting of burns. J Trauma. 1970 Dec;10(12):1103-8.

33. Burke JF, Bondoc CC, Quinby WC. Primary burn excision and immediate grafting: a method shortening illness. J Trauma. 1974 May;14(5):389-95. DOI: 10.1097/00005373-197405000-00005.

34. Skalak, R. and Fox, C. 1988 NSF Workshop, UCLA Symp. Molecular and Cellular Biology, 1988. New York, NY: Alan R. Liss.

35. Langer R, Vacanti JP. Tissue engineering. (Methods of replacing or substituting for damaged or diseased tissues). Science. 1993;260(5110):920. DOI: 10.1126/science.8493529.

36. Billingham RE, Medawar PB. The technique of free skin grafting in mammals. J Exp Biol. 1951;28(3):385-402. DOI: 10.1242/jeb.28.3.385.

37. Rheinwald JG, Green H. Serial cultivation of strains of human epidermal keratinocytes: the formation of keratinizing colonies from single cells. Cell. 1975;6(3):331.

38. Barrandon Y, Green H. Three clonal types of keratinocyte with different capacities for multiplication. PNAS. 1987;84(8):2302-6. DOI: 10.1073/pnas.84.8.2302.

39. O'Connor N, Mulliken J, Banks-Schlegel S, Kehinde O, Green H. Grafting of burns with cultured epithelium prepared from autologous epidermal cells. The Lancet. 1981;317(8211):75-8. DOI: 10.1016/s0140-6736(81)90006-4.

40. Chua AW, Khoo YC, Tan BK, Tan KC, Foo CL, Chong SJ. Skin tissue engineering advances in severe burns: review and therapeutic applications. Burns Trauma. 2016;4:3. DOI: 10.1186/s41038-016-0027-y.

41. Böttcher-Haberzeth S, Biedermann T, Reichmann E. Tissue engineering of skin. Burns. 2010 Jun;36(4):450-60. DOI: 10.1016/j.burns.2009.08.016.

42. Oberweis CV, Marchal JA, Lopez-Ruiz E, Galvez-Martin P. A worldwide overview of regulatory frameworks for tissue-based products. Tissue Eng Part B Rev. 2020 Apr;26(2):181-96. DOI: 10.1089/ten.TEB.2019.0315.

43. MacNeil S. Progress and opportunities for tissue-engineered skin. Nature. 2007 Feb 22;445(7130):874-80. DOI: 10.1038/nature05664.

44. Burke JF, Yannas IV, Quinby WC, Bondoc CC, Jung WK. Successful use of a physiologically acceptable artificial skin in the treatment of extensive burn injury. Annals of surgery. 1981;194(4):413. DOI: 10.1097/00000658-198110000-00005.

45. Stojic M, Rodenas-Rochina J, Lopez-Donaire ML, Gonzalez de Torre I, Gonzalez Perez M, Rodriguez-Cabello JC, et al. Elastin-plasma hybrid hydrogels for skin tissue engineering. Polymers 2021 Jun 28;13(13). DOI: 10.3390/polym13132114.

46. Herndon DN, Parks DH. Comparison of serial debridement and autografting and early massive excision with cadaver skin overlay in the treatment of large burns in children. J Trauma. 1986 Feb;26(2):149-52. DOI: 10.1097/00005373-198602000-00009.

47. Delvoye P, Pierard D, Noel A, Nusgens B, Foidart JM, Lapiere CM. Fibroblasts induce the assembly of the macromolecules of the basement membrane. J Invest Dermatol. 1988;90(3):276-82. DOI: 10.1111/1523-1747.ep12456042.

48. Desai MH, Mlakar JM, McCauley RL, Abdullah KM, Rutan RL, Waymack JP, et al. Lack of long-term durability of cultured keratinocyte burn-wound coverage : A case report. J burn care rehabil. 1991;12(6):540-5. DOI: 10.1097/00004630-199111000-00009.

49. Meek CP. Successful microdermagrafting using the Meek-Wall microdermatome. Am J Surg. 1958;96(4):557–8. DOI.org/10.1016/0002-9610(58)90975-9.

50. Hansbrough JF, Boyce ST, Cooper ML, Foreman TJ. Burn wound closure with cultured autologous keratinocytes and fibroblasts attached to a collagen-glycosaminoglycan substrate. JAMA. 1989;262(15):2125-30. DOI: 10.1001/jama.1989.03430150093032.

51. Boyce ST, Goretsky MJ, Greenhalgh DG, Kagan RJ, Rieman MT, Warden GD. Comparative assessment of cultured skin substitutes and native skin autograft for treatment of full-thickness burns. Ann surg. 1995;222(6):743. DOI: 10.1097/00000658-199512000-00008.

52. Boyce ST, Supp AP, Wickett RR, Hoath SB, Warden GD. Assessment with the Dermal Torque Meter of skin pliability after treatment of burns with cultured skin substitutes. J burn care rehabil. 2000;21(1):55-63. DOI: 10.1097/00004630-200021010-00011.

53. Boyce ST, Kagan RJ, Yakuboff KP, Meyer NA, Rieman MT, Greenhalgh DG, et al. Cultured skin substitutes reduce donor skin harvesting for closure of excised, full-thickness burns. Ann Surg. 2002 Feb;235(2):269-79. DOI: 10.1097/00000658-200202000-00016.

54. Boyce ST, Simpson PS, Rieman MT, Warner PM, Yakuboff KP, Bailey JK, et al. Randomized, paired-site comparison of autologous engineered skin substitutes and split-thickness skin graft for closure of extensive, full-thickness burns. J Burn Care Res. 2017 Mar/Apr;38(2):61-70. DOI: 10.1097/BCR.0000000000000401.

55. Vacanti CA. The history of tissue engineering. J Cell Mol Med. 2006 Jul-Sep;10(3):569-76. DOI: 10.1111/j.1582-4934.2006.tb00421.x.

56. Germain L, Larouche D, Nedelec B, Perreault I, Duranceau L, Bortoluzzi P, et al. Autologous bilayered self-assembled skin substitutes (SASSs) as permanent grafts: a case series of 14 severely burned patients indicating clinical effectiveness. Eur Cell Mater. 2018 Sep 13;36:128-41. DOI: 10.22203/eCM.v036a10.

57. Greenwood JE, Damkat-Thomas L, Schmitt B, Dearman B. Successful proof of the 'two-stage strategy' for major burn wound repair. Burns Open. 2020;4(3):121-31. DOI: 10.1016/j.burnso.2020.06.003.

58. Schiestl C, Meuli M, Vojvodic M, Pontiggia L, Neuhaus D, Brotschi B, et al. Expanding into the future: Combining a novel dermal template with distinct variants of autologous cultured skin substitutes in massive burns. Burns Open. 2021;5(3):145-53. DOI: 10.1016/j.burnso.2021.06.002.

59. Leigh I, Watt FM. The culture of human epidermal keratinocytes. In: Leigh I, Lane EB, Watt FM, editors. The keratinocyte handbook. Cambridge [England] ;: Cambridge University Press; 1994. p. 43-51.

60. Henrot P, Laurent P, Levionnois E, Leleu D, Pain C, Truchetet ME, et al. A method for isolating and culturing skin cells: Application to endothelial cells, fibroblasts, keratinocytes, and melanocytes from punch biopsies in systemic sclerosis skin. Front Immunol. 2020;11:566607. DOI: 10.3389/fimmu.2020.566607.

61. Boyce ST, Ham RG. Calcium-regulated differentiation of normal human epidermal keratinocytes in chemically defined clonal culture and serum-free serial culture. J Invest Dermatol. 1983;81(1):S33-S40. DOI: 10.1111/1523-1747.ep12540422.

62. Boyce ST, Ham RG. Cultivation, frozen storage, and clonal growth of normal human epidermal keratinocytes in serum-free media. Journal of Tissue Culture Methods. 1985;9(2):83-93. DOI: 10.1007/bf01797779.

63. Rheinwald JG, Green H. Epidermal growth factor and the multiplication of cultured human epidermal keratinocytes. Nature. 1977 Feb 3;265(5593):421-4. DOI: 10.1038/265421a0.

64. Limat A, Hunziker T, Boillat C, Bayreuther K, Noser F. Post-mitotic human dermal fibroblasts efficiently support the growth of human follicular keratinocytes. J Invest Dermatol. 1989;92(5):758-62.

65. Bisson F, Rochefort E, Lavoie A, Larouche D, Zaniolo K, Simard-Bisson C, et al. Irradiated human dermal fibroblasts are as efficient as mouse fibroblasts as a feeder layer to improve human epidermal cell culture lifespan. Int J Mol Sci. 2013 Feb 26;14(3):4684-704. DOI: 10.3390/ijms14034684.

66. Cheshire P, Zhafira AS, Banakh I, Rahman MM, Carmichael I, Herson M, et al. Xeno-free expansion of adult keratinocytes for clinical application: the use of human-derived feeder cells and serum. Cell Tissue Res. 2019 Jun;376(3):389-400. DOI: 10.1007/s00441-018-02986-5.

67. Thompson K, Partridge J, Abraham E, Flaherty P, Qian S, Saxena D. Corning® purecoat™ ECM mimetic cultureware collagen I peptide: Novel synthetic, animal-free surface for culture of human keratinocytes. Corning Incorporated, Tewksbury, MA, USA2012 [cited 2018]. Available from: https://www.corning.com/catalog/cls/documents/application-notes/an_DL_008_PureCoat_ECM_Mimetic_Cultureware_Collagen_I_Peptide_Culture_of_Human_Keratinocytes.pdf

68. van der Valk J, Mellor D, Brands R, Fischer R, Gruber F, Gstraunthaler G, et al. The humane collection of fetal bovine serum and possibilities for serum-free cell and tissue culture. Toxicol In Vitro. 2004;18(1):1-12. DOI: 10.1016/j.tiv.2003.08.009.

69. Karnieli O, Friedner OM, Allickson JG, Zhang N, Jung S, Fiorentini D, et al. A consensus introduction to serum replacements and serum-free media for cellular therapies. Cytotherapy. 2017 Feb;19(2):155-69. DOI: 10.1016/j.jcyt.2016.11.011.

70. Zheng MH, Pembrey R, Niutta S, Stewart-Richardson P, Farrugia A. Challenges in the evaluation of safety and efficacy of human tissue and cell based products. ANZ J Surg. 2006 Sep;76(9):843-9. DOI: 10.1111/j.1445-2197.2006.03880.x.

71. Appendix XVI A: Test for sterility, in: The British Pharmacopoeia, 2022.

72. Watt FM, Hudson DL, Lamb AG, Bolsover SR, Angus Silver R, Aitchison MJ, et al. Mitogens induce calcium transients in both dividing and terminally differentiating keratinocytes. J Cell Sci. 1991;99:397-405.

73. Bikle DD, Xie Z, Tu CL. Calcium regulation of keratinocyte differentiation. Expert Rev Endocrinol Metab. 2012 Jul;7(4):461-72. DOI: 10.1586/eem.12.34.

74. Tenchini ML, Ranzati C, Malcovati M. Culture techniques for human keratinocytes. Burns. 1992;18:S11-S6. DOI: 10.1016/0305-4179(92)90104-3.

75. Ponce L, Heintz F, Schäfer I, Klusch A, Holloschi A, Schmelz M, et al. Isolation and cultivation of primary keratinocytes from piglet skin for compartmentalized co-culture with dorsal root ganglion neurons. J Cell Biotech. 2017;2(2):93-115. DOI: 10.3233/jcb-15030.

76. Morimoto N, Takemoto S, Kanda N, Ayvazyan A, Taira MT, Suzuki S. The utilization of animal product-free media and autologous serum in an autologous dermal substitute culture. J Surg Res. 2011 Nov;171(1):339-46. DOI: 10.1016/j.jss.2009.11.724.

77. Ghetti M, Topouzi H, Theocharidis G, Papa V, Williams G, Bondioli E, et al. Subpopulations of dermal skin fibroblasts secrete distinct extracellular matrix: implications for using skin substitutes in the clinic. Br J Dermatol. 2018 Aug;179(2):381-93. DOI: 10.1111/bjd.16255.

78. Rayment EA, Williams DJ. Concise review: mind the gap: challenges in characterizing and quantifying cell- and tissue-based therapies for clinical translation. Stem Cells. 2010 May;28(5):996-1004. DOI: 10.1002/stem.416.

79. Supp DM, Hahn JM, Lloyd CM, Combs KA, Swope VB, Abdel-Malek Z, et al. Light or dark pigmentation of engineered skin substitutes containing melanocytes protects against ultraviolet light-induced DNA damage *in vivo*. J Burn Care Res. 2020 Jul 3;41(4):751-60. DOI: 10.1093/jbcr/iraa029.

80. Boyce ST, Christianson DJ, Hansbrough JF. Structure of a collagen-GAG dermal skin substitute optimized for cultured human epidermal keratinocytes. J Biomed Mater Res. 1988 Oct;22(10):939-57. DOI: 10.1002/jbm.820221008.

81. United States Pharmacopeia (2020). Chapter 87, Biological Reactivity Tests, In Vitro. USP 43-NF 38. Rockville, MD: United States Pharmacopeia.

82. Powell HM, Boyce ST. EDC cross-linking improves skin substitute strength and stability. Biomaterials. 2006 Dec;27(34):5821-7. DOI: 10.1016/j.biomaterials.2006.07.030.

83. Tondato F, Zeng H, Goodchild T, Ng FS, Chronos N, Peters NS. Autologous dermal fibroblast injections slow atrioventricular conduction and ventricular rate in atrial fibrillation in swine. Circ Arrhythm Electrophysiol. 2015 Apr;8(2):439-46. DOI: 10.1161/CIRCEP.114.001536.

84. Richter A, Kurome M, Kessler B, Zakhartchenko V, Klymiuk N, Nagashima H, et al. Potential of primary kidney cells for somatic cell nuclear transfer mediated transgenesis in pig. BMC Biotechnol. 2012 Nov 9;12:84. DOI: 10.1186/1472-6750-12-84.

85. Powell HM, Boyce ST. Engineered human skin fabricated using electrospun collagen-PCL blends: morphogenesis and mechanical properties. Tissue Eng Part A. 2009 Aug;15(8):2177-87. DOI: 10.1089/ten.tea.2008.0473.

86. Paul M, Kaur P, Herson M, Cheshire P, Cleland H, Akbarzadeh S. Use of clotted human plasma and aprotinin in skin tissue engineering: A novel approach to engineering composite skin on a porous scaffold. Tissue Eng Part C Methods. 2015 Oct;21(10):1098-104. DOI: 10.1089/ten.TEC.2014.0667.

87. Gentile P, McColgan-Bannon K, Gianone NC, Sefat F, Dalgarno K, Ferreira AM. Biosynthetic PCL-graft-collagen bulk material for tissue engineering applications. Materials 2017 Jun 23;10(7). DOI: 10.3390/ma10070693.

88. Bacakova M, Pajorova J, Broz A, Hadraba D, Lopot F, Zavadakova A, et al. A two-layer skin construct consisting of a collagen hydrogel reinforced by a fibrin-coated polylactide nanofibrous membrane. Int J Nanomedicine. 2019;14:5033-50. DOI: 10.2147/IJN.S200782.

89. Wright KA, Nadire KB, Busto P, Tubo R, McPherson JM, Wentworth BM. Alternative delivery of keratinocytes using a polyurethane membrane and the implications for its use in the treatment of full-thickness burn injury. Burns. 1998;24(1):7-17.

90. Phan TT, Lim IJ, Tan EK, Bay BH, Lee ST. Evaluation of cell culture on the polyurethane-based membrane (Tegaderm™): implication for tissue engineering of skin. Cell Tissue Bank. 2005;6(2):91-7. DOI: 10.1007/s10561-004-3904-8.

91. Greenwood JE, Li A, Dearman BL, Moore TG. Evaluation of novosorb novel biodegradable polymer for the generation of a dermal matrix part 2: *In-vivo* studies. Wound Practice & Research: Journal of the Australian Wound Management Association. 2010;18(1):24, 6, 8, 30, 2-4.

92. Greenwood JE, Li A, Dearman BL, Moore TG. Evaluation of novosorb novel biodegradable polymer for the generation of a dermal matrix part 1: *In-vitro* studies. Wound Practice & Research: Journal of the Australian Wound Management Association. 2010;18(1):14-22.

93. Boyce ST. Methods for the serum-free culture of keratinocytes and transplantation of collagen-GAG-based skin substitutes. Methods Mol Med. 1999;18:365-89. DOI: 10.1385/0-89603-516-6:365.

94. Costello L, Fullard N, Roger M, Bradbury S, Dicolandrea T, Isfort R, et al. Engineering a multilayered skin equivalent: The importance of endogenous extracellular matrix maturation to provide robustness and reproducibility. In: Böttcher-Haberzeth S, Biedermann T, editors. Methods Mol Biol. New York, NY: Springer New York; 2019. p. 107-22.

95. Prunieras M, Regnier M, Woodley D. Methods for cultivation of keratinocytes with an air-liquid interface. J Invest Dermatol. 1983 Jul;81(1 Suppl):28s-33s. DOI: 10.1111/1523-1747.ep12540324.

96. Smiley AK, Klingenberg JM, Boyce ST, Supp DM. Keratin expression in cultured skin substitutes suggests that the hyperproliferative phenotype observed *in vitro* is normalized after grafting. Burns. 2006 Mar;32(2):135-8. DOI: 10.1016/j.burns.2005.08.017.

97. Debeer S, Le Luduec JB, Kaiserlian D, Laurent P, Nicolas JF, Dubois B, et al. Comparative histology and immunohistochemistry of porcine versus human skin. Eur J Dermatol. 2013 Jul-Aug;23(4):456-66. DOI: 10.1684/ejd.2013.2060.

98. Rittié L, Fisher G. Isolation and culture of skin fibroblasts. In: Varga J, Brenner D.A, S.H. P, editors. Fibrosis Research. Totowa, NJ: Humana Press; 2005. p. 83-98.

99. Mahjour SB, Fu X, Yang X, Fong J, Sefat F, Wang H. Rapid creation of skin substitutes from human skin cells and biomimetic nanofibers for acute full-thickness wound repair. Burns. 2015 Dec;41(8):1764-74. DOI: 10.1016/j.burns.2015.06.011.

100. Tumbar T, Guasch G, Greco V, Blanpain C, Lowry WE, Rendl M, et al. Defining the epithelial stem cell niche in skin. Science. 2004 Jan 16;303(5656):359-63. DOI: 10.1126/science.1092436.

101. El Ghalbzouri A, Commandeur S, Rietveld MH, Mulder AA, Willemze R. Replacement of animal-derived collagen matrix by human fibroblast-derived dermal matrix for human skin equivalent products. Biomaterials. 2009 Jan;30(1):71-8. DOI: 10.1016/j.biomaterials.2008.09.002.

102. Klar A, Michalak K, Böttcher-Haberzeth S, Reichmann E, Meuli M, Biedermann T. The expression pattern of keratin 24 in tissue-engineered dermo-epidermal human skin substitutes in an *in vivo* model. Pediatric Surgery International. 2018;34(2):237-44. DOI: 10.1007/s00383-017-4198-9.

103. Malara MM, Blackstone BN, Baumann ME, Bailey JK, Supp DM, Powell HM. Cultured epithelial autograft combined with micropatterned dermal template forms rete ridges *in vivo*. Tissue Eng Part A. 2020 Nov;26(21-22):1138-46. DOI: 10.1089/ten.TEA.2020.0090.

104. Shen Z, Cao Y, Li M, Yan Y, Cheng R, Zhao Y, et al. Construction of tissue-engineered skin with rete ridges using co-network hydrogels of gelatin methacrylated and poly(ethylene glycol) diacrylate. Mater Sci Eng C Mater Biol Appl. 2021 Oct;129:112360. DOI: 10.1016/j.msec.2021.112360.

105. Blackstone BN, Malara MM, Baumann ME, McFarland KL, Supp DM, Powell HM. Fractional CO2 laser micropatterning of cell-seeded electrospun collagen scaffolds enables rete ridge formation in 3D engineered skin. Acta Biomater. 2020 Jan 15;102:287-97. DOI: 10.1016/j.actbio.2019.11.051.

106. Boyce ST. Design principles for composition and performance of cultured skin substitutes. Burns. 2001 Aug;27(5):523-33. DOI: 10.1016/s0305-4179(01)00019-5.

107. Moysidou CM, Barberio C, Owens RM. Advances in engineering human tissue models. Front Bioeng Biotechnol. 2020;8:620962. DOI: 10.3389/fbioe.2020.620962.

108. Boyce ST, Warden GD. Principles and practices for treatment of cutaneous wounds with cultured skin substitutes. Am J Surg. 2002 Apr;183(4):445-56. DOI: 10.1016/s0002-9610(02)00813-9.

109. Kalyanaraman B, Supp DM, Boyce ST. Medium flow rate regulates viability and barrier function of engineered skin substitutes in perfusion culture. Tissue Eng Part A. 2008 May;14(5):583-93. DOI: 10.1089/tea.2007.0237.

110. Jaasma MJ, Plunkett NA, O'Brien FJ. Design and validation of a dynamic flow perfusion bioreactor for use with compliant tissue engineering scaffolds. J Biotechnol. 2008 Feb 29;133(4):490-6. DOI: 10.1016/j.jbiotec.2007.11.010.

111. Helmedag MJ, Weinandy S, Marquardt Y, Baron JM, Pallua N, Suschek CV, et al. The effects of constant flow bioreactor cultivation and keratinocyte seeding densities on prevascularized organotypic skin grafts based on a fibrin scaffold. Tissue Eng Part A. 2015 Jan;21(1-2):343-52. DOI: 10.1089/ten.TEA.2013.0640.

112. Supp DM, Hahn JM, Combs KA, McFarland KL, Schwentker A, Boissy RE, et al. Collagen VII expression is required in both keratinocytes and fibroblasts for anchoring fibril formation in bilayer engineered skin substitutes. Cell Transplant. 2019 Sep-Oct;28(9-10):1242-56. DOI: 10.1177/0963689719857657.

113. Meuli M, Hartmann-Fritsch F, Huging M, Marino D, Saglini M, Hynes S, et al. A cultured autologous dermo-epidermal skin substitute for full-thickness skin defects: A phase I, open, prospective clinical trial in children. Plast Reconstr Surg. 2019 Jul;144(1):188-98. DOI: 10.1097/PRS.0000000000005746.

114. Supp DM, Hahn JM, Combs KA, McFarland KL, Powell HM. Isolation and feeder-free primary culture of four cell types from a single human skin sample. STAR Protoc. 2022 Mar 18;3(1):101172. DOI: 10.1016/j.xpro.2022.101172.

115. Daikuara LY, Yue Z, Skropeta D, Wallace GG. In vitro characterisation of 3D printed platelet lysate-based bioink for potential application in skin tissue engineering. Acta Biomater. 2021 Mar 15;123:286-97. DOI: 10.1016/j.actbio.2021.01.021.

116. Solovieva EV, Teterina AY, Klein OI, Komlev VS, Alekseev AA, Panteleyev AA. Sodium alginate-based composites as a collagen substitute for skin bioengineering. Biomed Mater. 2020 Nov 27;16(1):015002. DOI: 10.1088/1748-605X/abb524.

117. Oh H, Boo S. Assessment of burn-specific health-related quality of life and patient scar status following burn. Burns. 2017 Nov;43(7):1479-85. DOI: 10.1016/j.burns.2017.03.023.

118. Harriger MD, Warden GD, Greenhalgh DG, Kagan RJ, Boyce ST. Pigmentation and microanatomy of skin regenerated from composite grafts of cultured cells and biopolymers applied to full-thickness burn wounds. Transplantation. 1995;59(5):702-7. DOI: 10.1097/00007890-199503150-00011.

119. Liu Y, Suwa F, Wang X, Takemura A, Fang YR, Li Y, et al. Reconstruction of a tissue-engineered skin containing melanocytes. Cell Biol Int. 2007 Sep;31(9):985-90. DOI: 10.1016/j.cellbi.2007.03.009.

120. Böttcher-Haberzeth S, Klar AS, Biedermann T, Schiestl C, Meuli-Simmen C, Reichmann E, et al. "Trooping the color": restoring the original donor skin color by addition of melanocytes to bioengineered skin analogs. Pediatr Surg Int. 2013 Mar;29(3):239-47. DOI: 10.1007/s00383-012-3217-0.

121. Biedermann T, Klar AS, Böttcher-Haberzeth S, Michalczyk T, Schiestl C, Reichmann E, et al. Long-term expression pattern of melanocyte markers in light- and dark-pigmented dermo-epidermal cultured human skin substitutes. Pediatr Surg Int. 2015 Jan;31(1):69-76. DOI: 10.1007/s00383-014-3622-7.

122. Scuderi N, Onesti MG, Bistoni G, Ceccarelli S, Rotolo S, Angeloni A, et al. The clinical application of autologous bioengineered skin based on a hyaluronic acid scaffold. Biomaterials. 2008 Apr;29(11):1620-9. DOI: 10.1016/j.biomaterials.2007.12.024.

123. Scuderi N, Anniboletti T, Carlesimo B, Onesti M. Clinical application of autologous three-cellular cultured skin substitutes based on esterified hyaluronic acid scaffold: Our experience. In vivo 2009;23(6):991-1003.

124. Swope VB, Medrano EE, Smalara D, Abdel-Malek ZA. Long-term proliferation of human melanocytes is supported by the physiologic mitogens alpha-melanotropin, endothelin-1, and basic fibroblast growth factor. Exp Cell Res. 1995 Apr;217(2):453-9. DOI: 10.1006/excr.1995.1109.

125. Boyce ST, Zimmerman RL, Supp DM. Tumorigenicity testing in athymic mice of cultured human melanocytes for transplantation in engineered skin substitutes. Cell Transplant. 2015;24(8):1423-9. DOI: 10.3727/096368914X683052.

126. Bourland J, Fradette J. Strategies to promote the vascularization of skin substitutes after transplantation. 2018:177-200. DOI: 10.1016/b978-0-12-810545-0.00008-5.

127. Supp DM, Wilson-Landy K, Boyce ST. Human dermal microvascular endothelial cells form vascular analogs in cultured skin substitutes after grafting to athymic mice. FASEB J. 2002 Jun;16(8):797-804. DOI: 10.1096/fj.01-0868com.

128. Debels H, Hamdi M, Abberton K, Morrison W. Dermal Matrices and Bioengineered Skin Substitutes: A Critical Review of Current Options. Plastic and reconstructive surgery Global open. 2015;3(1):e284-e. DOI: 10.1097/GOX.0000000000000219.

129. Klar AS, Guven S, Biedermann T, Luginbuhl J, Böttcher-Haberzeth S, Meuli-Simmen C, et al. Tissue-engineered dermo-epidermal skin grafts prevascularized with adipose-derived cells. Biomaterials. 2014 Jun;35(19):5065-78. DOI: 10.1016/j.biomaterials.2014.02.049.

130. Klar AS, Biedermann T, Simmen-Meuli C, Reichmann E, Meuli M. Comparison of *in vivo* immune responses following transplantation of vascularized and non-vascularized human dermo-epidermal skin substitutes. Pediatr Surg Int. 2017 Mar;33(3):377-82. DOI: 10.1007/s00383-016-4031-x.

131. Frueh FS, Spater T, Lindenblatt N, Calcagni M, Giovanoli P, Scheuer C, et al. Adipose tissue-derived microvascular fragments improve vascularization, lymphangiogenesis, and integration of dermal skin substitutes. J Invest Dermatol. 2017 Jan;137(1):217-27. DOI: 10.1016/j.jid.2016.08.010.

132. Balana ME, Charreau HE, Leiros GJ. Epidermal stem cells and skin tissue engineering in hair follicle regeneration. World J Stem Cells. 2015 May 26;7(4):711-27. DOI: 10.4252/wjsc.v7.i4.711.

133. Wang X, Wang X, Liu J, Cai T, Guo L, Wang S, et al. Hair follicle and sebaceous gland de novo regeneration with cultured epidermal stem cells and skin-derived precursors. Stem Cells Transl Med. 2016 Dec;5(12):1695-706. DOI: 10.5966/sctm.2015-0397.

134. Abaci HE, Coffman A, Doucet Y, Chen J, Jackow J, Wang E, et al. Tissue engineering of human hair follicles using a biomimetic developmental approach. Nat Commun. 2018 Dec 13;9(1):5301. DOI: 10.1038/s41467-018-07579-y.

135. Wang J, Wang X, Xie J, Yao B, Mo M, Ma D, et al. Engineered skin substitute regenerates the skin with hair follicle formation. Biomedicines. 2021 Apr 8;9(4). DOI: 10.3390/biomedicines9040400.

136. Blais M, Parenteau-Bareil R, Cadau S, Berthod F. Concise review: tissue-engineered skin and nerve regeneration in burn treatment. Stem Cells Transl Med. 2013 Jul;2(7):545-51. DOI: 10.5966/sctm.2012-0181.

137. Biedermann T, Böttcher-Haberzeth S, Klar AS, Pontiggia L, Schiestl C, Meuli-Simmen C, et al. Rebuild, restore, reinnervate: do human tissue engineered dermo-epidermal skin analogs attract host nerve fibers for innervation? Pediatr Surg Int. 2013 Jan;29(1):71-8. DOI: 10.1007/s00383-012-3208-1.

138. Biedermann T, Klar AS, Böttcher-Haberzeth S, Reichmann E, Meuli M. Myelinated and unmyelinated nerve fibers reinnervate tissue-engineered dermo-epidermal human skin analogs in an *in vivo* model. Pediatr Surg Int. 2016 Dec;32(12):1183-91. DOI: 10.1007/s00383-016-3978-y.

139. Gingras M, Paradis I, Berthod F. Nerve regeneration in a collagen–chitosan tissue-engineered skin transplanted on nude mice. Biomaterials. 2003;24(9):1653-61. DOI: 10.1016/s0142-9612(02)00572-0.

140. Muller Q, Beaudet MJ, De Serres-Berard T, Bellenfant S, Flacher V, Berthod F. Development of an innervated tissue-engineered skin with human sensory neurons and Schwann cells differentiated from iPS cells. Acta Biomater. 2018 Dec;82:93-101. DOI: 10.1016/j.actbio.2018.10.011.

141. Weng T, Wu P, Zhang W, Zheng Y, Li Q, Jin R, et al. Regeneration of skin appendages and nerves: current status and further challenges. J Transl Med. 2020 Feb 3;18(1):53. DOI: 10.1186/s12967-020-02248-5.

142. Yannas IV. Emerging rules for inducing organ regeneration. Biomaterials. 2013 Jan;34(2):321-30. DOI: 10.1016/j.biomaterials.2012.10.006.

143. Varkey M, Visscher DO, van Zuijlen PPM, Atala A, Yoo JJ. Skin bioprinting: the future of burn wound reconstruction? Burns Trauma. 2019;7:4. DOI: 10.1186/s41038-019-0142-7.

144. Boyce ST. Automated fabrication of human skin substitutes: inherent advantages and fundamental challenges. J 3D Print Med. 2021;5(3):127-32. DOI: 10.2217/3dp-2021-0019.

SUPPLEMENTARY FIGURES

APPENDICES

SUPPLEMENTARY FIGURES

Figure S1: Negative controls corresponds to Chapter 4 Figure 4.4

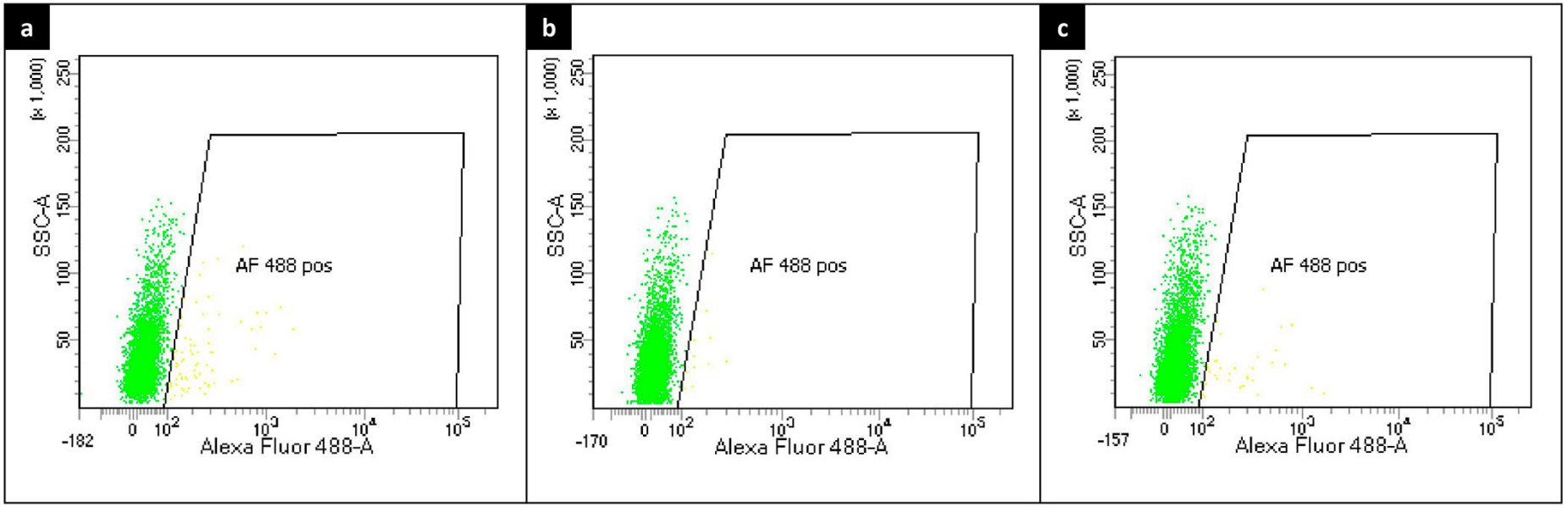

Supplementary Figure S1. Negative controls for the flow cytometry analysis, related figure see Chapter 4 figure 4.4,
a. SEL-KGM + Feeders, b. EpiLife™ + CM, c. dKGM + CM. CM, coating matrix.

SUPPLEMENTARY FIGURES

Figure S2: Negative controls corresponds to Chapter 5 Figure 5.5

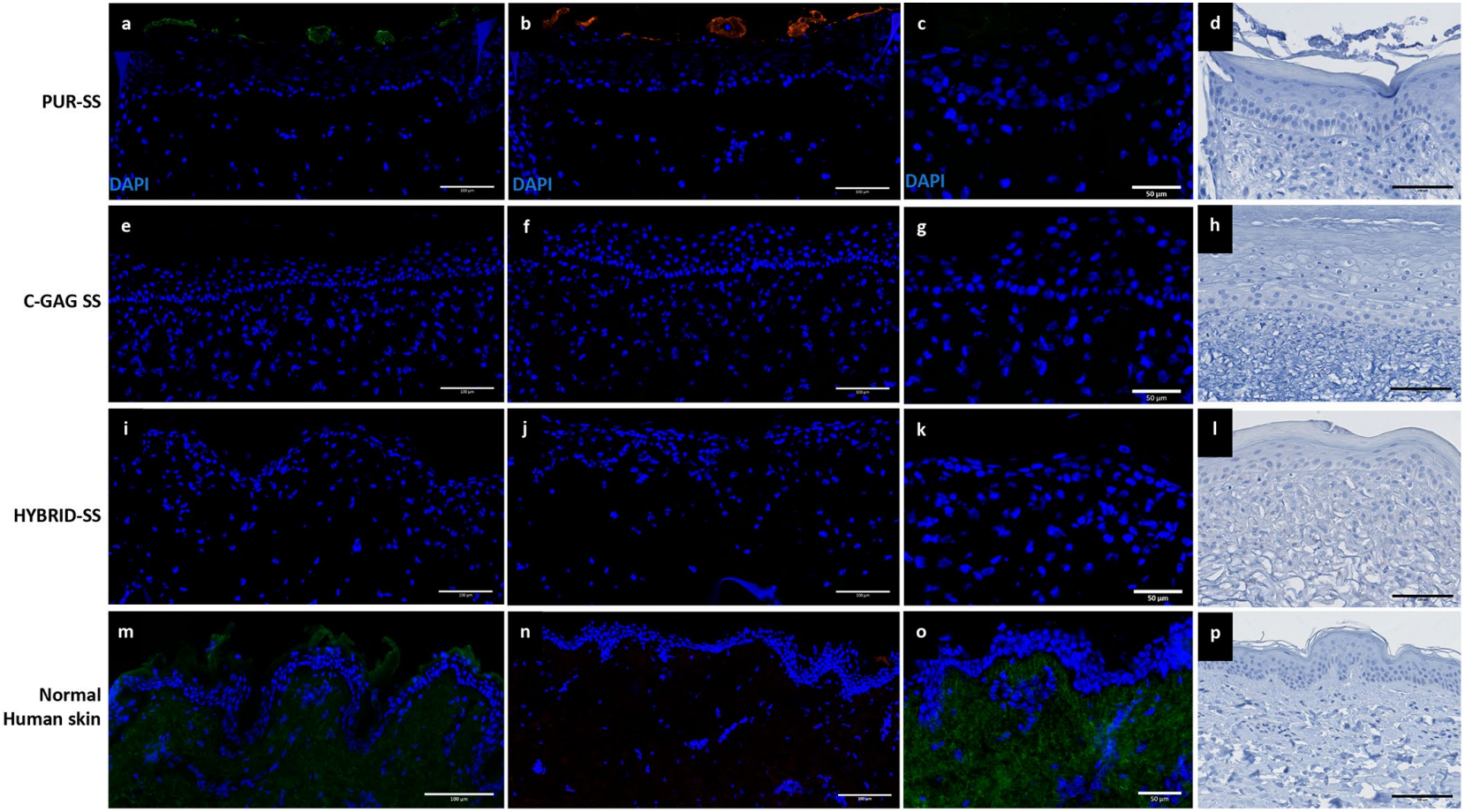

Supplementary Figure S2. Skin substitutes (SS) – human-derived with different biopolymer scaffolds negative controls for Chapter 5 figure 5.5, Row 1. PUR-SS, Row 2. C-GAG-SS, Row 3. Hybrid-SS and Row 4. Native human skin. Column 1 corresponds to cytokeratin 14, column 2 cytokeratin 10, column 3 laminin, and column 4 Ki67. Blue (DAPI) counterstained nuclei. Scale bar: 100µm except for c, g, k, o 50µm.

Figure S3: Negative controls corresponds to Chapter 7 Figure 7.4

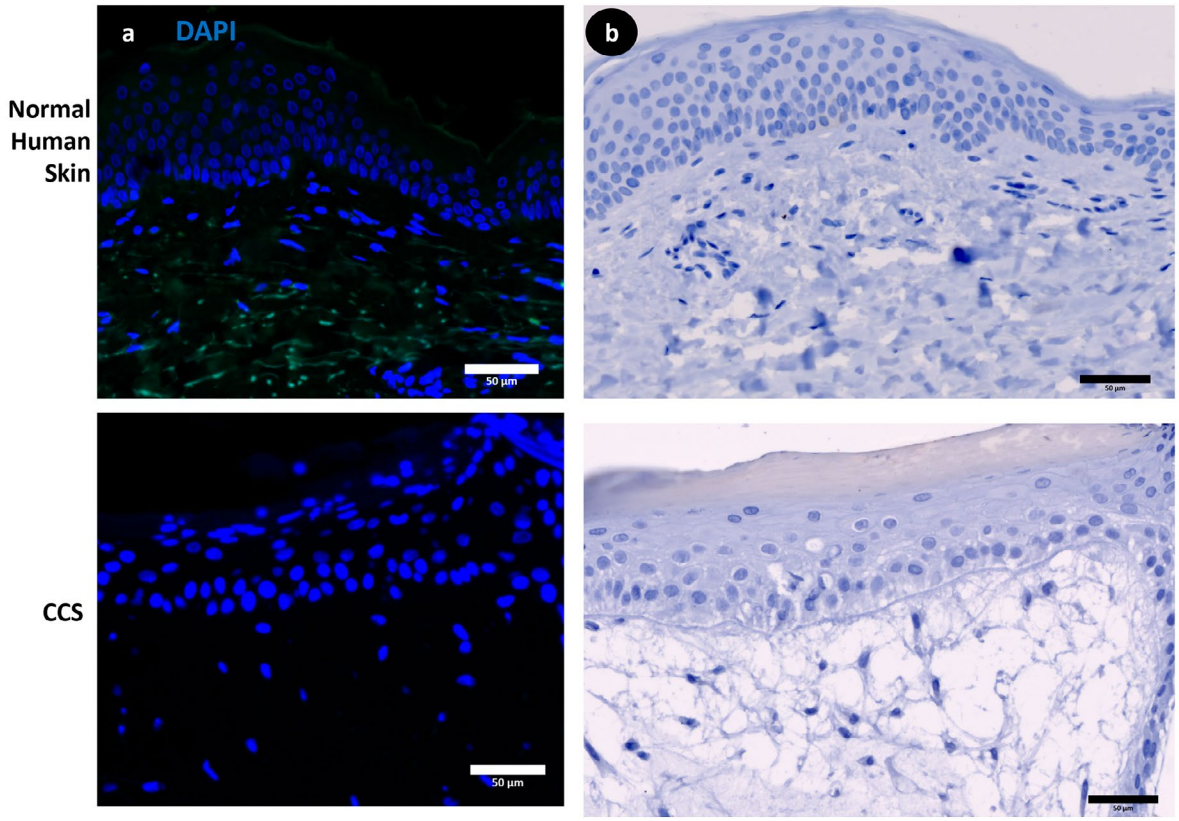

Supplementary Figure S3. Negative controls for Chapter 7 figure 7.4, a. Corresponds to figure 7.4 column d (Cytokeratin-collagen I staining) and b. corresponds to figure 7.4 column e (Ki67 staining). Blue (DAPI) staining depicts cell nuclei. CCS – composite cultured skin. Scale bar: 50µm.

SUPPLEMENTARY FIGURES

Figure S4: Negative controls corresponds to Chapter 7 Figure 7.5

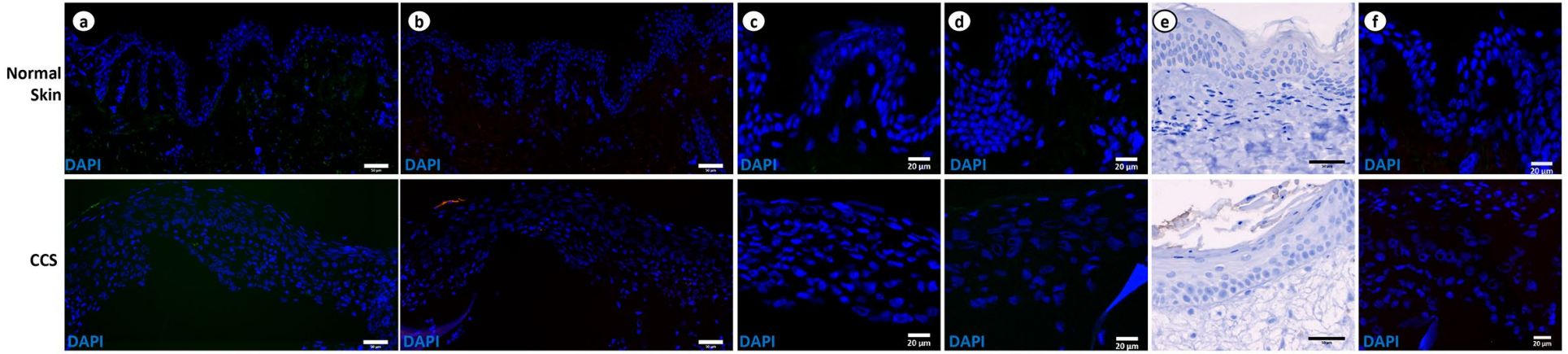

Supplementary Figure S4. Negative controls for Chapter 7 figure 7.5, a. Corresponds to figure 7.5 column (a) cytokeratin 14 staining, column (b) cytokeratin 10, column (c) collagen IV, column (d) collagen VII staining, column (e) laminin and column (f) CD49f. Blue (DAPI) staining depicts cell nuclei. CCS – composite cultured skin. Scale bar: column c, d, f is 20µm and column a, b, e is 50µm.

APPENDIX I: Ethics Approval Letters

Government of South Australia
SA Health

Central Adelaide Local Health Network
CALHN Human Research Ethics Committee
Level 3, Roma Mitchell House
136 North Terrace
Adelaide, South Australia, 5000
Telephone: +61 8 7117 2229
The Queen Elizabeth Hospital, BHI Building
Telephone: +61 88222 684
Email: Health.CALHNResearchEthics@sa.gov.au

Approval Date: 25 September 2018

Prof John Greenwood
Adult Burns Unit
ROYAL ADELAIDE HOSPITAL

Dear Prof Greenwood

Project Title: The ex-vivo expansion of human skin cells for the generation of a composite cultured skin (CCS) for burn patients.

HREC reference number: HREC/18/CALHN/539

CALHN Reference number: R20180811

RE: Ethics Application APPROVAL

Thank you for submitting the above project for ethical and scientific review. The project was first considered by the CALHN Human Research Ethics Committee at its meeting held on 13 September 2018.

The HREC has reviewed all responses, and I am pleased to advise that your protocol has been granted full ethics approval. The study meets the requirements of the *National Statement on Ethical Conduct in Human Research, incorporating all updates*. The documents reviewed and approved include:

Document	Version	Date
LNR Application	AU/15/8CE7310	16 July 2018
Cover Letter	-	16 July 2018
Protocol	1	12 July 2018
Participant Information Sheet and Consent Form	1	12 July 2018
Supporting documents • Wavier of consent for 030516 - Approval for 030516 application May 2003 • Wavier of consent for 030516 - Approval for 030516 to include FG Apr 2006 • Wavier of consent for 030516 - Approval to include CCS study in 030516 Mar 2005 • Wavier of consent for 030516 - ethics application submitted May 2003 • RAH -consent form • WCH - consent form		

Sites covered by this approval:

Site	State	Investigator
The Royal Adelaide Hospital	SA	CPI: Prof John Greenwood

HREC approval is valid for 5 years from **25 September 2018** to **25 September 2023**

GENERAL TERMS AND CONDITIONS OF ETHICAL APPROVAL:

- For all clinical trials, the study must be registered in a publicly accessible trials registry prior to enrolment of the first participant.
- This HREC is certified with the NHMRC for National Mutual Acceptance of Single Ethical and Scientific Review of Multi-centre Clinical Trials. Any study sites that are not listed on this letter are not covered by this ethics approval. Any study-sites that wish to be added must contact the CPI, who must write formally to this HREC requesting the additional study site.
- Adequate record-keeping is important and must be maintained in accordance with GCP, NHMRC and state and national guidelines. If the project involves signed consent, you should retain the completed consent forms which relate to this project and a list of all those participating in the project, to enable contact with them in the future if necessary. The duration of record retention for all clinical research data is 15 years.

- Researchers must notify the HREC of any events which might warrant review of the approval or which warrant new information being presented to research participants, including:
  (a) adverse events which warrant protocol change or notification to research participants;
  (b) changes to the protocol;
  (c) changes to the safety or efficacy of the investigational product, device or method;
  (d) premature termination of the study.
- The HREC must be notified within 72 hours of any Urgent Safety Measures (USMs) occurring at this or any approved sites.
- Confidentiality of the research participants shall be maintained at all times as required by law.
- Approval is valid for **5 years** from the date of this letter, after which an extension must be applied for.
- **Annual Review Reports must be submitted to the HREC, every 12 months on the anniversary of the above approval date**. Each site covered by this HREC must submit a report and it is the responsibility of the Coordinating Principal Investigator to ensure this is provided to the CALHN HREC Executive Officer within 10 working days on each anniversary of the approval date using the Annual Review Report Form available at: https://www.rahresearchfund.com.au/rah-research-institute/for-researchers/human-research-ethics/ and http://www.basilhetzelinstitute.com.au/research/information-for-researchers/human-research-ethics-committee/
- **A final Annual Review Report must be submitted to the HREC on completion of the study.** Each site covered by this HREC must submit a report, and it is the responsibility of the Coordinating Principal Investigator to ensure this is provided to the CALHN HREC Executive Officer using the CALHN Annual Review Report Form available at https://www.rahresearchfund.com.au/rah-research-institute/for-researchers/human-research-ethics/ and http://www.basilhetzelinstitute.com.au/research/information-for-researchers/human-research-ethics-committee/. A copy of any published material must also be provided with the report, or following when available.

You are reminded that this letter constitutes ethical approval only. You must not commence this research project at any site until separate authorisation from the Chief Executive or delegate of that site has been obtained. For any queries, please contact the CALHN Governance Office: Health.CALHNResearchGovernance@sa.gov.au

This Committee is constituted in accordance with the NHMRC's *National Statement on the Ethical Conduct of Human Research (2007)* incorporating all updates.

Should you have any queries about the HREC's consideration of your project, please contact the Executive Officer on 08 7117 2229, or Health.CALHNResearchEthics@sa.gov.au.

The HREC wishes you every success in your research.

Yours sincerely,

Ian Tindall
CHAIR
CALHN HUMAN RESEARCH ETHICS COMMITTEE

cc: Site Research Governance Officer

Government of South Australia
SA Health

Central Adelaide Local Health Network
Level 3, Roma Mitchell House
North Terrace, Adelaide SA
Australia 5000

Basil Hetzel Institute for Translational Research
Ground Floor
28 Woodville Road, Woodville South SA
Australia 5011

T : 08 7117 2231
E : Health.CALHNResearchGovernance@sa.gov.au

20 December 2018

Professor John Greenwood
Royal Adelaide Hospital
Port Rd, Adelaide, SA 5000

Dear Professor Greenwood

HREC reference number: HREC/18/CALHN/322

SSA reference number: SSA/18/CALHN/818

Governance reference number: 11027

Project title: A prospective evaluation of Composite Cultured Skin (CCS) as a definitive closure second stage [where biodegradable polyurethane dermal matrix (BTM) represents the first stage] in the management of extensive deep burn injury.

RE: Site Specific Assessment Review

Thank you for submitting an application for authorisation of this project. I am pleased to inform you that authorisation has been granted for this study to commence at [Royal Adelaide Hospital, SA.

Authorisation is valid from **19 December 2018 to 20 December 2020.** You are reminded that annual reports must be submitted to the reviewing HREC. Failure to do so will result in cessation of both ethical and governance authorisation. Proposed extensions beyond this term must be submitted to the CALHN Research Office as a governance amendment.

In addition to the documents approved by the Central Adelaide Local Health Network HREC as listed in their letter dated 24 July 2018, specific approval is also provided for the following documents:

- Medicines Australia Clinical Trial Research Agreement, dated 19 December 2018
- Medical Technology Association of Australia Form of Indemnity, dated 05 December 2018
- RAH Main PISCF, Version 2, dated 23 July 2018
- RAH PISCF – NOK, Version 2, dated 23 July 2018

The following conditions apply to the authorisation of this research project. These are additional to those conditions imposed by the Human Research Ethics Committee (HREC) that granted ethical approval to this project:

1. Authorisation is limited to the site/s identified in this letter only.
2. Project authorisation is granted for the term specified above.
3. The study must be conducted in accordance with the conditions of ethical approval provided by the lead HREC, SA Health policies, and in conjunction with the standards outlined in the *National Statement on Ethical Conduct in Human Research* (2007) and the *Australian Code for the Responsible Conduct of Research* (*2007).*
4. Proposed amendments to the research protocol or conduct of the research which may affect the ethical acceptability of the project, and which are submitted to the HREC for review, are copied via email to the CALHN Research Office;
5. For all clinical trials, the study must be registered in a publicly accessible trials registry prior to enrolment of the first participant.
6. Proposed amendments to the research protocol or conduct of the research which may affect both the ongoing ethical acceptability of the project and the site acceptability of the project are to be submitted to the CALHN Research Office after a HREC decision is made.

7. Proposed amendments to the research protocol or conduct of the research which may affect both the ongoing ethical acceptability of the project and the site acceptability of the project are to be submitted to the CALHN Research Office after a HREC decision is made.
8. A copy of this letter should also be maintained on file by the Coordinating Principal Investigator as evidence of project authorisation.
9. Notification of completion of the study at this site is to be provided to the CALHN Research Office.

If University personnel are involved in this project, the Principal Investigator should notify the University before commencing their research to ensure compliance with University requirements including any insurance and indemnification requirements.

We wish you every success in your research project.

Yours sincerely

Bernadette Swart
Manager, CALHN Research Office
Email: Health.CALHNResearchGovernance@sa.gov.au

SAHMRI
South Australian Health & Medical Research Institute
ABN 54 141 228 346
P 08 8128 4000
SAHMRI, North Terrace, Adelaide SA 5000 Australia
PO Box 11060, Adelaide SA 5001 www.sahmri.com

Associate Professor John Oliver
Chair, SAHMRI AEC
e: john.oliver@sahmri.com
W: www.sahmri.com

29-Aug-2017

Professor John Greenwood
Burns Unit, Royal Adelaide Hospital
E: john.greenwood@sa.gov.au

Dear Professor Greenwood,

Re: Project No. SAM282v1
Entitled 'Using Composite Cultured Skin (CCS) to provide definitive closure of temporized wounds in a porcine model'.

Thank you for responding to the issues raised by the SAHMRI AEC. **I wish to advise that the project has now been approved.**

This approval is granted subject to the following conditions:

- You have personal responsibility for all matters related to the welfare of the animals you use and you must act in accordance with all requirements of the 8th edition of the *Australian Code for the Care and Use of Animals for Scientific Purposes.* (2013)

- Any adverse or unexpected events that impact on animal wellbeing that occurs during the period of the approved project must be reported promptly to the AEC.

- You must ensure that records of the use and monitoring of animals used in the project are maintained. Records should include the origin and fate of issued animals, how animal welfare was assessed, any unexpected negative impact on animal wellbeing and notation of procedures.

- You must provide an annual report to the AEC – the continuation of all projects is subject to receipt of written annual reports that should advise on:
  - (i) what progress has been achieved;
  - (ii) any problems that may have interfered with progress of the project;
  - (iii) how many animals have been used;
  - (iv) whether the wellbeing of the animals is consistent with that anticipated in the proposal;
  - (v) whether any changes are envisaged;
  - (vi) whether the project is meeting its aims.

- You must inform the Committee when an approved project is completed or discontinued.

It is necessary to apply to the AEC for approval if the project is to continue for a longer period of time, if additional animals are required, or if any change to procedure is proposed.

Any additional conditions are included in the attached Approval Notice.

We wish you well in your research and the AEC will be interested to hear of future developments in your work.

Yours sincerely,

Associate Professor John Oliver
as Chair
and on behalf of
SAHMRI Animal Ethics Committee

APPENDIX II: Flow Cytometry Protocol

Purpose:

This protocol describes a method for flow cytometric staining of keratinocytes for intracellular proteins.

Technical Notes:

- 5 x 10^5 cells per tube are recommended
- Prepare antibody dilution in blocking buffer, include an unstained tube of cells for control
- Use 100µl of antibodies per tube

Materials

Blocking buffer – 0.5% BSA and 2% FBS in 1x PBS (without calcium, magnesium)

HHF-5 – HBSS and 5% FBS

Protocol

1. Harvest keratinocytes as per SOP (do not over trypsinise cells)
2. Wash cells 1x with PBS
3. Fix and permeabilise the cells with a 10-minute incubation in 70% ethanol (-20°C) on ice
    a. Vortex cells gently whilst resuspending cells in ethanol
    b. Set timer for 8 minutes
    c. Spin cells in immufuge (1000g for 2 minutes)
    d. Wash 1x with HHF-5
4. Block the cells with the blocking buffer for 15 minutes
5. Spin and resuspend cells in appropriate dilution of primary antibody (s)
6. Incubate for 1hour on ice
7. Rinse the cells 3x in HHF-5 by centrifugation
8. Incubate cells with secondary antibody(s) for 1 hour on ice
9. Rinse the cells 3x in HHF-5 by centrifugation with minimal light exposure
10. Resuspend cells in 0.4mL of FACS fix
11. Analyse with a flow cytometer

APPENDIX III: List of Antibodies

Antibody Name/ Catalogue #	Host species	Source	Detection method	Clone/Dilution
Anti-Collagen I (ab233080)	Rabbit polyclonal	Abcam	PK, DAB	1:500
Collagen I (ab34710)	Rabbit polyclonal	Abcam	IF	1:500
Collagen IV (MA5-13437)	Mouse monoclonal	Invitrogen	PK, DAB & FF-IF	1:50 CIV22
COL7A1 (MA5-13432)	Mouse monoclonal	Invitrogen	IF - FF	1:100 LH7.2
Laminin beta-1 (MA5-14657)	Rat monoclonal	Invitrogen	IF - FF	1:50 LT3
Anti-Laminin (ab11575)	Rabbit polyclonal	Abcam	DAB Kit - P	1:250
CD49f (Integrin α-6) (MA5-16884)	Rat monoclonal	Invitrogen	IF - FF	1:100 NKI-GoH3
Anti pan-cytokeratin (ab86734)	Mouse monoclonal	Abcam	IF –P/FF	1:500 AE1/AE3 + 5D3
Anti-wide spectrum Cytokeratin (ab9377)	Rabbit polyclonal	Abcam	IF –P/FF	1:250
Anti-cytokeratin 14 (MA1-06323)	Mouse monoclonal	Invitrogen	DAB-P & IF-FF	1:100P-500FF RCK107
Anti-cytokeratin 14 (ab9220)	Mouse monoclonal	Abcam	DAB-P & IF-FF	1:100P-500FF RCK107
Anti-cytokeratin 10 (ab9025)	Mouse monoclonal	Abcam	IF - FF	1:500 RKSE60
Recombinant Anti-KI67 (ab16667)	Rabbit monoclonal	Abcam	DAB-JM	1:250 SP6
Anti-fibroblast surface protein [1B10] (ab11333)	Mouse monoclonal	Abcam	IF	1:50 IB10

APPENDIX III: List of Antibodies

Antibody Name/Catalogue #	Host species	Source	AF/Dilution
Goat-anti-Rabbit IgG (ab150086)	Goat polyclonal	Abcam	AF 555 1:500
Goat-anti-Rabbit IgG (ab150079)	Goat polyclonal	Abcam	AF 647 1:500
Goat-anti-Mouse IgG (ab150113)	Goat polyclonal	Abcam	AF 488 1:500
Goat-anti-rat IgG2a (NB7124)	Goat polyclonal	Novus Biologicals	AF FITC 1:500
Goat-anti-rat IgG (ab150157)	Goat polyclonal	Abcam	AF 488 1:500
Biotinylated horse anti-mouse IgG (BA-2000)	Horse polyclonal	Vector Laboratories	1:250
Biotinylated horse anti-rabbit IgG (BA-1100)	Horse polyclonal	Vector Laboratories	1:250
Cell nuclei – Fluoroshield with DAPI	F6057-20mL	Sigma	NA
Streptavidin-biotinylated immunoperoxidase technique	21127	ThermoFisher-Pierce	NA

Purpose:

This document describes the protocol for the isolation and culture of keratinocytes and fibroblasts from a skin biopsy.

Technical Notes:

Dispase treatment time: Dispase is a neutral protease that cleaves collagen and fibronectin fibres at the basement membrane zone effectively separating the epidermis and the dermis while preserving the viability of the epithelial cells[1]. For split-thickness skin, incubation period of 20 to 60 minutes at 37°C. For thicker skin, incubation time of 1-2 hours may be required. Alternatively, the skin may be incubated overnight in Dispase II at 2-8°C.

Cell numbers required per flask for co-culture: Depending on the cell numbers obtained and the target cell number, co-cultures of keratinocytes and irradiated feeder cells should contain 1-4x10^6 keratinocytes and 2-3.5x10^6 irradiated fibroblast feeder cells per flask. Primary dermal fibroblasts target cell number is 10-11,000 cells/cm^2.

Human dermal fibroblast feeder layer: human dermal fibroblasts are growth arrested to use in co-culture with human keratinocytes. The fibroblasts are isolated from discard donor tissue as per method below and established until 90% confluence in DMEM- 5% FBS. Cells are irradiated at a dose of 60Gy using an RS2000 Series Biological Irradiator (Rad Source, Buford, GA, USA). Vials are then cryopreserved at 7x10^6/vial and stored in vapor phase of liquid nitrogen for future use as a feeder layer at 18-20,000 cells/cm^2.

1.1. Skin Processing - Part 1 - Rinsing and cutting of skin biopsy

1.1.1. Label containers and dishes:

- 2x petri dishes for PBS
- 3x 70mL container for Rinse 1, 2 and 3
- 1 x 70mL container for betadine
- 1 x 70mL container for Gentamicin

1.1.2. Prepare reagents required for washing the biopsy:

- Dispense 20mL of PBS into each petri dish; dispense 30mL of PBS into the 3x Rinse containers; dispense 40mL of PBS into the gentamicin container.
- Dispense 1 vial of betadine into the betadine container.
- Dispense the gentamicin (80mg/2mL) into a 5mL tube. Transfer 250µl of this gentamicin to the designated gentamicin container containing 40mL of PBS, mix gently.

1.1.3. Line up the aliquots of solutions with the 70mL containers in front of the Petri dishes in the following order from left to right: R3, Gentamicin, R2, Betadine and R1.

1.1.4. Introduce forceps and skin biopsy into the cabinet and set up instruments for use on a sterile Petri dish.

1.1.5. Rinse the skin tissue sequentially from R1 through to R3 for 5 minutes each. Periodically during each rinse, dip the skin tissue repeatedly in the solutions to ensure that all area of the tissue is exposed to the solution.

1.1.6. After rinse in R3, transfer skin biopsy into one of the petri dishes with PBS.

1.1.7. Introduce scalpel into cabinet and prepare for use.

1.1.8. Determine the size of the biopsy using the ruler on the scalpel handle or sterile disposable ruler. Calculate the number of dispase dishes required. Record in worksheet.

1.1.9. On the sterile inverted lid of a petri dish, cut the skin biopsy into strips of ~3mm x 15mm. Recommended procedure is to cut the biopsy into large pieces first and divide evenly for the number of dispase dishes required. These pieces may be kept segregated in the same PBS dish or in separate dishes to prevent desiccation. Then cut one piece at a time into strips.

1.1.10. Introduce the Dispase II (6mg/mL) solution and other required materials into the cabinet. Aseptically transfer one entire aliquot of Dispase II into a sterile Petri dish.

1.1.11. Transfer the skin pieces into the Dispase dish using forceps.

1.1.12. Seal the dish with Parafilm. Label appropriately using permanent marker. Place dish in 37°C CO_2 incubator and incubate for 20 minutes - 2 hours.

1.1.13. Record incubation start time on worksheet.

1.1.14. De-clutter cabinet. Remove all used instruments.

1.2. Set up trypsin for epidermal digestion

1.2.1. For each dish of dispase digest, prepare a 70mL container with magnetic flea and 20mL of trypsin-EDTA. Label container. If the skin is <10cm^2 use a 15mL container with 5mL of trypsin/EDTA.

1.2.2. Place container(s) in 37°C incubator to keep warm. De-clutter cabinet.

1.3. Separation of epidermal sheets and dermal pieces

1.3.1. If processing the dermal tissue for fibroblasts, prepare appropriately labelled Petri dish(es) containing 20mL of PBS.

1.3.2. Set up instruments required on a sterile Petri dish.

1.3.3. De-clutter cabinet and transfer the Dispase dish with skin strips from incubator into the cabinet. Remove parafilm.

1.3.4. Transfer some skin pieces onto the sterile petri dish lid, hold the edge of a skin piece and gently tease the epidermal sheet from the dermal tissue with the second pair of forceps. Periodically transfer the dermal pieces into the designated PBS dish(es) if collected. Repeat until all finished.

1.3.5. Place the dish(es) of dermal tissue into the fridge until keratinocytes have been isolated and plated. If dermal tissue is not required then discard appropriately.

1.4. Isolation of keratinocytes

1.4.1. Introduce the pre-warmed trypsin-EDTA into the cabinet and using a pair of forceps, transfer the epidermal strips into the container. Replace the cap and immediately place the container onto the magnetic stirrer at 700rpm. This step is performed as quickly as possible to avoid the trypsin-EDTA from cooling significantly. Trypsinise for exactly 5 minutes. (Set timer).

1.4.2. Continue processing other dishes of skin pieces if time permitting, continue separation of epidermal sheets.

1.4.3. After tryspinisation, add equal amounts of soybean trypsin inhibitor (SBTI) to the trypsin digest. Swirl gently to mix.

1.4.4. Use forceps to pull out the epidermal sheets from the digest then transfer digest OR pass the quenched cell digest through a 70µm cell strainer into a 50mL tube. Rinse strainer with 10mL of SBTI.

1.4.5. Centrifuge cell suspension at 1200rpm for 5 minutes at 15 ± 5°C.

1.4.6. During centrifugation, if other dishes of skin pieces are to be processed, continue separation and trypsinisation of epidermal sheets. If all skin pieces have been processed, proceed with thawing of fibroblast feeder cells.

1.4.7. After centrifugation, remove the supernatant using a 25mL pipette and depending on the size of cell pellet, resuspend in a total of 10-50mL of media. Pool cell suspensions if applicable.

1.4.8. When all isolated keratinocytes have been pooled into one tube, transfer some of the cell suspension into a microcentrifuge tube for viability cell count. Record the cell counts and calculate the number and volume of keratinocytes required per vessel. De-clutter cabinet.

1.5. Thawing of cells (irradiated fibroblast feeder)

1.5.1. Thaw the vials of irradiated fibroblasts at 37°C and resuspend in associated media.

1.5.2. Retrieve samples from liquid nitrogen storage and place into a charged dry shipper (ensure weight >5kg). Do not remove samples from shipper until ready to thaw.

1.5.3. When ready to thaw, 'rapid-thaw' the cells by placing the ampoules into a 36-38ºC waterbath until the majority of media is liquid, leaving a pellet of ice in the ampoule. Ensure this time does not exceed 2 minutes.

1.5.4. Transfer the contents of the ampoules into a tube using a transfer pipette. Rinse the ampoules with 1-2mL of media if desired.

1.5.5. Drop-wise, add warm media to the cells whilst gently agitating the tube to ensure mixing of cells and media. Generally, add 9mL per ampoule of cells up to a total of 50mL. Centrifuge at 1200rpm for 5 minutes at 15 ± 5ºC.

1.5.6. Remove supernatant and resuspend cell pellet by gently flicking/tapping the tube. Add fresh warmed media and perform a cell count to ascertain cell number and viability. Use the cells as required.

1.6. Set up of keratinocytes with irradiated dermal fibroblasts

1.6.1. Add 20mL of keratinocyte media to each T175 flask. Then add the required volume of keratinocytes and irradiated feeder cells.

1.6.2. Mix the cells by gently swirling the flasks and ensure that the growth surface of the flask is covered.

1.6.3. Complete details required on the flask labels and affix to each flask.

1.6.4. Place the flasks in 37ºC CO_2 incubator. De-clutter cabinet.

1.7. Collagenase digestion of the dermal pieces

1.7.1. Transfer the collagenase I (3mg/mL) solution to a labelled tube.

1.7.2. On the inverted lid of the dermal tissue dish, cut the dermis into smaller pieces (~0.5mm -1mm^2) and transfer the pieces into collagenase I solution. Agitate with transfer pipette.

1.7.3. Incubate at 37°C for 30 minutes – 2 hours. Record digest start time and set timer.

1.7.4. Agitate for 1-2 minutes at 20-30 minute intervals during the digestion process.

1.7.5. After digestion with minimal fragments remaining collect and centrifuge 250g for 5 minutes at 4°C.

1.7.6. Aspirate collagenase and resuspend in DMEM- serum. Repeat centrifuge and resuspend for cell count and inoculate 10-11,000 cells/cm^2.

1.7.7. Collect dermal fragments and plate into a pre-coated 10% serum flask at 1cm^2 dermal tissue/50cm^2 flask. 24-hrs post inoculation add 15mL of media.

1.7.8. Media change every 2-3 days until 80-90% confluent.

1- Stenn *et al*. 1989. Dispase, a neutral protease from Bacillus polymyxa, is a powerful fibronectinase and type IV collagenase. *J Invest Dermatol*. 93(2):285-290.

Cascade Biologics™
invitrogen cell culture

GIBCO®
invitrogen cell culture

Coating Matrix Kit

Animal Origin-Free

Cat. no. R-011-K

Product Description

Coating Matrix Kit is an animal origin-free kit containing materials suitable for coating up to 750 cm^2 of tissue culture plasticware. Coating Matrix Kit contains 0.5 ml sterile recombinant human Type-1 collagen as a Coating Matrix (Item # 50-9700) and 50 ml Dilution Medium (Item # 50-9701).

Intended Use

Coating Matrix Kit enhances the growth of human keratinocytes *in vitro*, and is intended for use in conjunction with EpiLife® Medium (cat. no. M-EPI-500-CA, M-EPICF-500, or M-EPICF/PRF-500) supplemented with either Supplement S7 (cat. no. S-017-5) or EDGS (cat. no. S-012-5) for the routine culture of normal human keratinocytes. Coating Matrix Kit may also be used for the primary isolation of keratinocytes in an animal-origin-free environment.

This product is for research use only. Not intended for human or animal therapeutic or diagnostic use.

Caution: If handled improperly, some components of this product may present a health hazard. Take appropriate precautions when handling this product, including the wearing of protective clothing and eyewear. Dispose of properly.

Storage and Stability

Coating Matrix Kit is stored at 2° to 8° C at our facility and is shipped at ambient temperature. When stored at 2° to 8° C, the product is stable until the expiration date on the label. Do not freeze.

Instructions for Coating Flasks

1. Using sterile technique in a laminar flow culture hood, add Dilution Medium (50-9701) to each flask (5 ml per each 75 cm^2 flask, or 1.7 ml per each 25 cm^2 flask).
2. Add Coating Matrix (50-9700) directly to the Dilution Medium in each flask (50 µl per each 75 cm^2 flask, or 17 µl per each 25 cm^2 flask). Rock back and forth vigorously to ensure uniform distribution of the coating matrix over the surface of the flask.
3. Cap the flasks and incubate for 30 minutes at room temperature.
4. Remove excess Coating Matrix/Dilution Medium from each flask. The flasks may be used immediately, or may be stored at 2° to 8° C for short periods.

EpiLife® is a Registered Trademark of Life Technologies.

For research use only.

Life Technologies Corporation • 5791 Van Allen Way • Carlsbad • CA 92008 • Tel: 800.955.6288 • www.invitrogen.com • E-mail: tech_support@invitrogen.com

MAN0001572 Revised: 20 August 2009

APPENDIX VI: Immunohistochemistry and Immunofluorescence Protocol

Purpose

This protocol is for staining paraffin sections with indirect immunofluorescence, primary antibody dependent, using heat mediated antigen retrieval (citrate buffer) and proteinase K for collagens. Secondary antibodies 488, 555 or 647 are used depending on primary antibodies.

Immunohistochemistry method for paraffin sections

1. Label slides with a pencil.
2. Heat section on the heating block at 60ºC for a minimum of 5 minutes (only required if histologist has not performed this step).
3. Prepare a humid chamber using wet tissues in a black plastic box.
4. For antibody calculations, allow ~50µl small section 100µl large section.
5. Take care not to touch sections or allow them to dry out, tip-off excess fluid onto a tissue.

Deparaffinise and Rehydrate sections

SOLUTION	TIME
Xylene*	5 Minutes
Xylene**	5 Minutes
Xylene**	5 Minutes
100% Alcohol* (Prepare citrate buffer)	5 Minutes
100% Alcohol**	5 Minutes
100% Alcohol**	5 Minutes
95% Alcohol*	5 Minutes
70% Alcohol*	5 Minutes
50% Alcohol***	5 Minutes
PBS***	5 Minutes
Circle sections with pap pen	

NOTE: Top up containers as required. *** discard after use. ** rotate after 10th use. *Discard when 10th run.

6. Make sure all buffers and solutions are at RT before starting the experiment.
7. Prepare methanol/ Hydrogen peroxide (H_2O_2) by adding 8.6mL of H_2O_2 (30%) to 500mL methanol (100%).
    a. Pour stock H_2O_2 into a 50mL tube first, then measure.
8. Add enough drops of methanol/H_2O_2 block to cover the sections and incubate for 10 minutes.
9. Pre-heat citrate buffer after the first washing step; see below.
10. Wash 2 times in 1xPBS buffer for 5 minutes.

Pre-treatment Antigen retrieval (heat mediated and citrate buffer)

11. Prepare **0.01 M sodium citrate buffer (freshly prepared on the day).**
    a. Dissolve 1.47g of trisodium citrate in 400mL Milli Q water on a heated stirrer, adjust to pH 6 with 1M HCl and make up to 500mL.
12. Fill the pressure cooker with 500mL RO water.
13. Fill the staining pot to the rim with sodium citrate buffer, place the staining pot into the pressure cooker, and seal tightly.
14. During the 50% ethanol step above, place the pressure cooker in a 1100W microwave oven. Cook on high for 9 minutes – water temperature will reach ~100°C.
15. Remove cooker from microwave, open with care, check the buffer solution level, and top-up if necessary.
16. Place slide rack into buffer solution and seal pressure cooker. Replace in the microwave, select P2 (power level 2) and cook for another 20 minutes – water temperature will be maintained at 100°C.
17. Remove cooker from microwave and allow cooling at room temperature (RT) for 20 minutes. Prepare blocking solution for staining during this time.
18. Remove slides from pressure cooker with care and rinse in PBS 2 x 5min
19. **Post heat-induced enzyme treatment, add proteinase K for 15 minutes at RT. COLLAGEN SLIDES ONLY.**
    a. Prepare 1mL of proteinase K in 9mL of PBS
20. Wash 2x in PBS at 5 minutes each.
21. Apply Protein Block and incubate for 1 hour at RT to block non-specific background staining.
22. Prepare primary antibodies in 3% normal goat serum (GS) in 1xPBS.
23. Rinse with PBS buffer.
24. Tap excess and wipe slides around tissue section.

25. Apply ~50-100µl or 1-3 drops of prepared primary antibody to cover sections and incubate according to the manufacturer's protocol.
26. Ensure negative control receives no antibody.
27. Incubate in humidifying chamber overnight at 4°C.

DAY 2 PROCESS

28. Rinse off primary antibody with PBS and then wash 3 times in PBS buffer, 5mins each.
29. During the wash step, prepare secondary antibodies. See table.
30. Apply 50-100µl of secondary for 1 hour at RT.
31. Rinse off secondary with PBS and then wash 3 times in PBS buffer, 5 minutes each.
32. Counterstain with DAPI and coverslip.

Immunofluorescence method for fresh frozen sections

1. Let thaw and air dry for 5 minutes, and label slides.
2. Circle section with pap pen.
3. Add 100µL of blocking buffer (10% GS in PBS) and incubate in a humidified chamber at RT for 30 minutes.
4. Prepare primary antibodies in 3% GS.
5. Drain blocking buffer and rinse off slides with 1x PBS.
6. Re-circle with pap pen if required.
7. Add primary antibody (diluted in 3% GS) and incubate overnight at 4°C.

DAY 2 PROCESS

8. Rinse slides in PBS, 3x for 5 minutes each.
9. Apply 50-100µL of secondary antibody diluted in 3% GS for 1 hour.
10. Rinse off slides in PBS, then wash 3x for 5 minutes each.
11. Counterstain with DAPI and coverslip.

APPENDIX VII: Streptavidin-Biotinylated Immunoperoxidase Technique

For the immunohistochemical detection of Laminin and Ki67 the following antibodies were used: a rabbit polyclonal against Laminin (Abcam, Cambridge, UK, Code # ab11575), and a rabbit monoclonal against Ki67 (clone SP6, Abcam, Cambridge, UK, Code # ab16667) using a standard streptavidin-biotinylated immunoperoxidase technique. In brief, sections were dewaxed using xylene and then rehydrated through alcohols. Sections were then treated with Methanol/H_20_2 for 30 minutes. The sections were rinsed twice in PBS (pH 7.4) for a further 5 minutes each wash. Heat induced antigen retrieval for Laminin and Ki67 antibodies was performed using citrate buffer (pH 6). Slides were allowed to cool and then washed twice in PBS (pH 7.4). Laminin sections then underwent post heat induced enzyme digestion for 3 minutes at 37^0C (Trypsin type II, 0.0625g in 250ml PBS, Sigma-Aldrich, St Louis MO, Cat No. T-7409 or Proteinase K Cat No. 21627). This was then followed by two washes in PBS (pH 7.4). Non-specific proteins were blocked using normal horse serum for 30 min. The rabbit polyclonal Laminin at 1/200 and the rabbit monoclonal polyclonal Ki67 at 1/250, all at room temperature overnight. Slides minus the primary antibody were also run in parallel. The following day, the sections were given two washes in PBS then a biotinylated anti-mouse secondary (Vector Laboratories, CA, USA, Cat # BA-2000) and biotinylated anti-rabbit secondary (Vector Laboratories, CA, USA, Cat #BA-1100) was applied for 30 minutes at room temperature. Following two PBS washes, the slides were incubated for 1 hour at room temperature with a streptavidin-conjugated peroxidase tertiary (Pierce, MA, USA, Cat # 21127). Sections were then visualised using diaminobenzidinetetrahydrochloride (DAB), washed, counterstained with haematoxylin, dehydrated, cleared and mounted on glass slides.

MATERIALS

- Samples to test in 24-well plate

NOTES:

- Fixative supplied by Adelaide Microscopy
- PBS + 4% sucrose stored in fridge pre-made
- Discard formaldehyde into the appropriate container
- Hexamethyldisilazane (HMDS)
- Samples can float and flip easily be gently when adding reagents

METHOD

1. Fix samples for 30 minutes to 2 hours in EM fixative (4% Paraformaldehyde/1.25% Glutaraldehyde in PBS, + 4% sucrose, pH7.2)
2. Wash in washing buffer (PBS + 4% sucrose) – 5 minutes x1
3. Post–fix in 2% Osmium tetroxide -30 minutes x1 (Note this step is usually performed by authorised personnel) **TOXIC AUTHORISED USE ONLY.**
4. Wash in washing buffer (PBS + 4% sucrose) – 5 minutes x2 (Place waste and used pipettes into appropriate osmium waste container in fume hood)
5. DEHYDRATE
    a. 70% Ethanol – 10 minutes x2
    b. 90% Ethanol – 10 minutes x2
    c. 100% Ethanol – 10 minutes x2
6. Drying samples
    a. Prepare a solution of 1:1, 100% Ethanol:HMDS i.e., 5mL of each should be sufficient
    b. HMDS 1:1 100% Ethanol:HMDS for 20 minutes
    c. 100% HMDS – 20 minutes x1
    d. 100% HMDS – 10 minutes x1
7. Air dry samples
    a. Move samples into a new well and leave samples to dry for at least 1 hour, leave partially covered with the lid of the dish to protect from dust

8. Mounting and cutting samples
    a. Retrieve stubs and carbon tabs (supplied from AHMS)
    b. Cut samples in half and place on edge, cut side facing upwards on sticky carbon tabs (both halves on one tab)
9. Carbon coating
    a. Complete a request form for sample coating
10. Book and view on the Quanta 450 SEM

TEM samples, process as per steps 1 to 5 above then:

1 Intermediate step
    a. Propylene oxide 15 minutes x 2
2 Resin infiltration
    a. Prepare fresh TAAB Epon Araldite 812 epoxy resin
    b. Make up Resin 1:1 100% Ethanol and add to samples 1hour x1
    c. Change samples into pure resin 1hour x1
    d. Change samples into fresh pure resin and leave overnight in fume hood
3 Embedding samples
    a. Place samples into silicon moulds, add resin and place into oven at 60^{o} C for 48hours
4 Sectioning
    a. Cut 0.5micron survey sections on ultramicrotome and stain with 0.05% toluidine blue for viewing with LM
    b. Select small area of interest and reduce the face of the block with a razorblade
    c. Cut 70-90nm sections and collect onto copper grids
5 Staining the section for EM
    a. Grids stained with 4% Uranyl Acetate for 8 minutes
    b. Washed by dipping each grid 20 times in 3 changes of filtered water
    c. Grids stain in lead citrate (Reynolds lead stain) for 8 minutes
    d. Washed by dipping each grid 20 times in 3 changes of filtered water
    e. Grids placed on filter paper to dry
6 Imaging sections
    a. Sections are imaged with the Tecnai G2 Spirit 120kV TEM

ANALYTE	ACCESSION	RESULT VALUE	COLLECTED
Room Details	21-160-16774	Room 2-207C-H	22:00 09/06/2021
Room Grid	21-160-16774	7C-1	22:00 09/06/2021
Bacteria Result	21-160-16774	0	22:00 09/06/2021
Bacteria Result	21-160-16775	0	22:30 09/06/2021
Room Details	21-160-16775	Room 2-207A-H	22:30 09/06/2021
Room Grid	21-160-16775	7A-1	22:30 09/06/2021
Room Details	21-160-16776	Room 2-207-H	02:00 10/06/2021
Room Grid	21-160-16776	7-2	02:00 10/06/2021
Bacteria Result	21-160-16776	0	02:00 10/06/2021
Room Details	21-160-16773	Room 2-207C-H	21:30 09/06/2021
Cabinet Grid	21-160-16773	3	21:30 09/06/2021
Bacteria Result	21-160-16773	0	21:30 09/06/2021
Room Details	21-163-09390	Room 2-207C-H	16:30 12/06/2021
Cabinet Grid	21-163-09390	3	16:30 12/06/2021
Bacteria Result	21-163-09390	0	16:30 12/06/2021
Room Details	21-163-09391	Room 2-207C-H	17:00 12/06/2021
Room Grid	21-163-09391	7C-1	17:00 12/06/2021
Cabinet Grid	21-163-09391	3	17:00 12/06/2021
Bacteria Result	21-163-09391	0	17:00 12/06/2021
Room Details	21-163-09392	Room 2-208A-H	17:30 12/06/2021
Room Grid	21-163-09392	7A-2	17:30 12/06/2021
Bacteria Result	21-163-09392	0	17:30 12/06/2021
Room Details	21-165-03795	Room 2-207C-H	10:35 14/06/2021
Cabinet Grid	21-165-03795	3	10:35 14/06/2021
Bacteria Result	21-165-03795	0	10:35 14/06/2021
Room Details	21-165-03796	Room 2-207C-H	10:55 14/06/2021
Room Grid	21-165-03796	7C-1	10:55 14/06/2021
Bacteria Result	21-165-03796	0	10:55 14/06/2021
Room Details	21-165-03797	Room 2-208A-H	11:15 14/06/2021
Room Grid	21-165-03797	7A-2	11:15 14/06/2021
Cabinet Grid	21-165-03797	3	11:15 14/06/2021
Bacteria Result	21-165-03797	0	11:15 14/06/2021
Room Details	21-165-03797	Room 2-207A-H	11:15 14/06/2021
Room Details	21-166-06872	Room 2-207C-H	10:05 15/06/2021
Cabinet Grid	21-166-06872	3	10:05 15/06/2021
Bacteria Result	21-166-06872	0	10:05 15/06/2021
Room Details	21-166-06873	Room 2-207C-H	10:20 15/06/2021

Room Grid	21-166-06873	7C-1	10:20 15/06/2021
Bacteria Result	21-166-06873	0	10:20 15/06/2021
Room Details	21-166-06874	Room 2-207A-H	10:30 15/06/2021
Room Grid	21-166-06874	7A-2	10:30 15/06/2021
Bacteria Result	21-166-06874	0	10:30 15/06/2021
Room Details	21-167-11552	Room 2-207C-H	10:30 16/06/2021
Cabinet Grid	21-167-11552	3	10:30 16/06/2021
Bacteria Result	21-167-11552	0	10:30 16/06/2021
Room Details	21-167-11553	Room 2-207C-H	10:50 16/06/2021
Room Grid	21-167-11553	7C-1	10:50 16/06/2021
Bacteria Result	21-167-11553	0	10:50 16/06/2021
Room Details	21-167-11554	Room 2-207A-H	11:00 16/06/2021
Room Grid	21-167-11554	7A-2	11:00 16/06/2021
Bacteria Result	21-167-11554	0	11:00 16/06/2021
Room Details	21-168-09276	Room 2-207C-H	10:35 17/06/2021
Cabinet Grid	21-168-09276	3	10:35 17/06/2021
Bacteria Result	21-168-09276	0	10:35 17/06/2021
Room Grid	21-168-09277	7C-1	10:45 17/06/2021
Bacteria Result	21-168-09277	0	10:45 17/06/2021
Room Details	21-168-09277	Room 2-207C-H	10:45 17/06/2021
Room Details	21-168-09278	Room 2-208A-H	10:55 17/06/2021
Room Grid	21-168-09278	7A-2	10:55 17/06/2021
Bacteria Result	21-168-09278	0	10:55 17/06/2021
Room Details	21-169-08834	Room 2-207C-H	10:30 18/06/2021
Cabinet Grid	21-169-08834	3	10:30 18/06/2021
Bacteria Result	21-169-08834	0	10:30 18/06/2021
Room Details	21-169-08835	Room 2-207C-H	10:40 18/06/2021
Room Grid	21-169-08835	7C-1	10:40 18/06/2021
Bacteria Result	21-169-08835	0	10:40 18/06/2021
Room Details	21-169-08836	Room 2-207A-H	10:50 18/06/2021
Room Grid	21-169-08836	7A-2	10:50 18/06/2021
Bacteria Result	21-169-08836	1	10:50 18/06/2021
Bacteria ID	21-169-08836	Staph spp	10:50 18/06/2021
Room Details	21-170-09227	Room 2-207C-H	10:10 19/06/2021
Cabinet Grid	21-170-09227	3	10:10 19/06/2021
Bacteria Result	21-170-09227	0	10:10 19/06/2021

Room Details	21-170-09228	Room 2-207C-H	10:15 19/06/2021
Cabinet Grid	21-170-09228	3	10:15 19/06/2021
Bacteria Result	21-170-09228	0	10:15 19/06/2021
Room Details	21-170-09229	Room 2-207A-H	10:20 19/06/2021
Room Grid	21-170-09229	7A-2	10:20 19/06/2021
Cabinet Grid	21-170-09229	3	10:20 19/06/2021
Bacteria Result	21-170-09229	1	10:20 19/06/2021
Bacteria ID	21-170-09229	Gram +ve rod	10:20 19/06/2021
Room Details	21-170-09231	Room 2-207-H	11:30 19/06/2021
Room Grid	21-170-09231	7-2	11:30 19/06/2021
Bacteria Result	21-170-09231	0	11:30 19/06/2021
Room Details	21-171-03643	Room 2-207C-H	12:30 20/06/2021
Cabinet Grid	21-171-03643	3	12:30 20/06/2021
Bacteria Result	21-171-03643	0	12:30 20/06/2021
Room Details	21-171-03644	Room 2-207C-H	12:40 20/06/2021
Room Grid	21-171-03644	7C-2	12:40 20/06/2021
Cabinet Grid	21-171-03644	3	12:40 20/06/2021
Bacteria Result	21-171-03644	0	12:40 20/06/2021
Room Details	21-171-03645	Room 2-207A-H	12:50 20/06/2021
Room Grid	21-171-03645	7A-2	12:50 20/06/2021
Bacteria Result	21-171-03645	0	12:50 20/06/2021
Room Details	21-172-11115	Room 2-207C-H	11:30 21/06/2021
Cabinet Grid	21-172-11115	3	11:30 21/06/2021
Bacteria Result	21-172-11115	0	11:30 21/06/2021
Room Details	21-172-11116	Room 2-207C-H	11:40 21/06/2021
Room Grid	21-172-11116	7C-2	11:40 21/06/2021
Bacteria Result	21-172-11116	0	11:40 21/06/2021
Room Details	21-172-11117	Room 2-207A-H	11:50 21/06/2021
Room Grid	21-172-11117	7A-2	11:50 21/06/2021
Bacteria Result	21-172-11117	0	11:50 21/06/2021
Room Details	21-173-07681	Room 2-207C-H	12:05 22/06/2021
Cabinet Grid	21-173-07681	3	12:05 22/06/2021
Bacteria Result	21-173-07681	0	12:05 22/06/2021
Room Details	21-173-07682	Room 2-207C-H	12:15 22/06/2021
Room Grid	21-173-07682	7C-2	12:15 22/06/2021
Cabinet Grid	21-173-07682	3	12:15 22/06/2021
Bacteria Result	21-173-07682	0	12:15 22/06/2021

Room Details	21-173-07683	Room 2-207A-H	12:25 22/06/2021
Room Grid	21-173-07683	7A-2	12:25 22/06/2021
Cabinet Grid	21-173-07683	3	12:25 22/06/2021
Bacteria Result	21-173-07683	0	12:25 22/06/2021
Room Details	21-174-16322	Room 2-207C-H	15:15 23/06/2021
Cabinet Grid	21-174-16322	3	15:15 23/06/2021
Bacteria Result	21-174-16322	0	15:15 23/06/2021
Room Details	21-174-16323	Room 2-207C-H	16:30 23/06/2021
Room Grid	21-174-16323	7C-2	16:30 23/06/2021
Cabinet Grid	21-174-16323	3	16:30 23/06/2021
Bacteria Result	21-174-16323	0	16:30 23/06/2021
Room Details	21-174-16324	Room 2-207A-H	17:00 23/06/2021
Room Grid	21-174-16324	7A-2	17:00 23/06/2021
Cabinet Grid	21-174-16324	3	17:00 23/06/2021
Bacteria Result	21-174-16324	0	17:00 23/06/2021
Room Details	21-174-16329	Room 2-207-H	19:40 23/06/2021
Room Grid	21-174-16329	7-1	19:40 23/06/2021
Cabinet Grid	21-174-16329	3	19:40 23/06/2021
Bacteria Result	21-174-16329	1	19:40 23/06/2021
Bacteria ID	21-174-16329	Gram +ve rod	19:40 23/06/2021

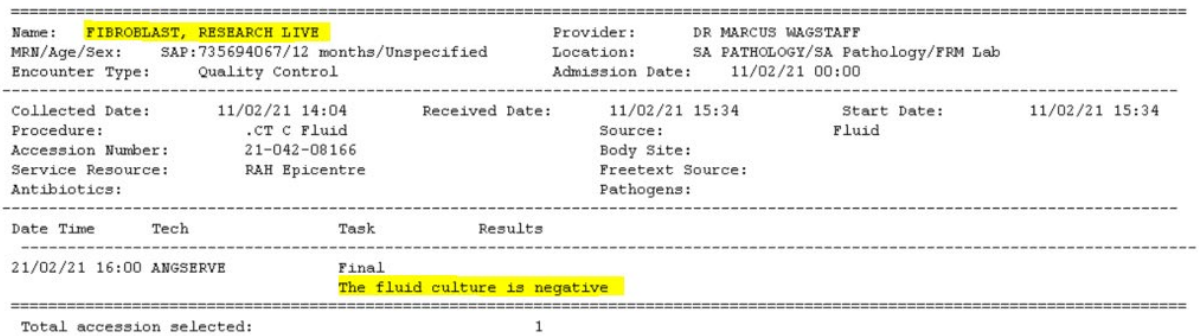

Name: FIBROBLAST, RESEARCH LIVE
MRN/Age/Sex: SAP:735694067/12 months/Unspecified
Encounter Type: Quality Control
Provider: DR MARCUS WAGSTAFF
Location: SA PATHOLOGY/SA Pathology/FRM Lab
Admission Date: 11/02/21 00:00

Collected Date: 11/02/21 14:04
Procedure: .CT C Fluid
Accession Number: 21-042-08166
Service Resource: RAH Epicentre
Antibiotics:
Received Date: 11/02/21 15:34
Source:
Body Site:
Freetext Source:
Pathogens:
Start Date: 11/02/21 15:34
Fluid

Date Time	Tech	Task	Results
21/02/21 16:00	ANGSERVE	Final	The fluid culture is negative

Total accession selected: 1

********** END OF REPORT **********

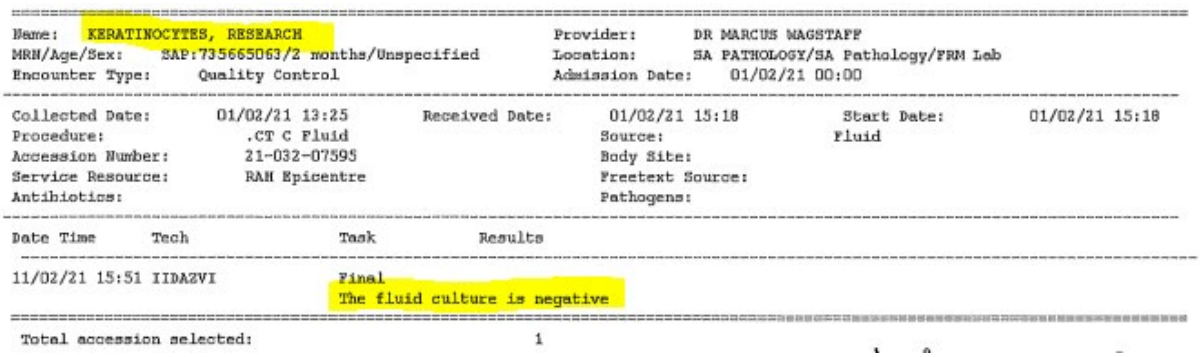

Name: KERATINOCYTES, RESEARCH
MRN/Age/Sex: SAP:735665063/2 months/Unspecified
Encounter Type: Quality Control
Provider: DR MARCUS WAGSTAFF
Location: SA PATHOLOGY/SA Pathology/FRM Lab
Admission Date: 01/02/21 00:00

Collected Date: 01/02/21 13:25
Procedure: .CT C Fluid
Accession Number: 21-032-07595
Service Resource: RAH Epicentre
Antibiotics:
Received Date: 01/02/21 15:18
Source:
Body Site:
Freetext Source:
Pathogens:
Start Date: 01/02/21 15:18
Fluid

Date Time	Tech	Task	Results
11/02/21 15:51	IIDAZVI	Final	The fluid culture is negative

Total accession selected: 1

Name: CCS BIOREACTOR, SEL
MRN/Age/Sex: SAP:735783768/5 months/Unspecified
Encounter Type: Quality Control
Provider: DR MARCUS WAGSTAFF
Location: SA PATHOLOGY/SA Pathology/RAH Lab
Admission Date: 09/06/21 00:00

Collected Date:	12/06/21 20:00	Received Date:	13/06/21 19:29	Start Date:	13/06/21 19:29
Procedure:	.CT C Fluid		Source:		CT Product
Accession Number:	21-163-09393		Body Site:		
Service Resource:	RAH Epicentre		Freetext Source:		
Antibiotics:			Pathogens:		

Date Time	Tech	Task	Results
23/06/21 20:00	ANGSERVE	Final	The fluid culture is negative

Day 3- Pooled spent media

Total accession selected: 1

********** END OF REPORT **********

Name: CCS BIOREACTOR, SEL
MRN/Age/Sex: SAP:735783768/5 months/Unspecified
Encounter Type: Quality Control
Provider: DR MARCUS WAGSTAFF
Location: SA PATHOLOGY/SA Pathology/RAH Lab
Admission Date: 09/06/21 00:00

Collected Date:	16/06/21 11:25	Received Date:	16/06/21 21:06	Start Date:	16/06/21 21:06
Procedure:	.CT C Fluid		Source:		CT Product
Accession Number:	21-167-11557		Body Site:		
Service Resource:	RAH Epicentre		Freetext Source:		
Antibiotics:			Pathogens:		

Date Time	Tech	Task	Results
27/06/21 09:01	ANGSERVE	Final	The fluid culture is negative

Day 7- Pooled spent media

Total accession selected: 1

********** END OF REPORT **********

Name: CCS BIOREACTOR, SEL
MRN/Age/Sex: SAP:735783768/5 months/Unspecified
Encounter Type: Quality Control
Provider: DR MARCUS WAGSTAFF
Location: SA PATHOLOGY/SA Pathology/RAH Lab
Admission Date: 09/06/21 00:00

Collected Date:	19/06/21 11:00	Received Date:	20/06/21 17:19	Start Date:	20/06/21 17:20
Procedure:	.CT C Fluid		Source:		CT Product
Accession Number:	21-170-09230		Body Site:		
Service Resource:	RAH Epicentre		Freetext Source:		
Antibiotics:			Pathogens:		

Date Time	Tech	Task	Results
30/06/21 18:00	ANGSERVE	Final	The fluid culture is negative

Day 10- Pooled spent media

Total accession selected: 1

********** END OF REPORT **********

Name: CCS BIOREACTOR, SEL
MRN/Age/Sex: SAP:735783768/5 months/Unspecified
Encounter Type: Quality Control
Provider: DR MARCUS WAGSTAFF
Location: SA PATHOLOGY/SA Pathology/RAH Lab
Admission Date: 09/06/21 00:00

Collected Date:	21/06/21 12:12	Received Date:	21/06/21 20:09	Start Date:	21/06/21 20:09
Procedure:	.CT C Fluid		Source:		CT Product
Accession Number:	21-172-11118		Body Site:		
Service Resource:	RAH Epicentre		Freetext Source:		
Antibiotics:			Pathogens:		

Date Time	Tech	Task	Results
01/07/21 21:00	ANGSERVE	Final	The fluid culture is negative

Day 12- Pooled spent media

Total accession selected: 1

********** END OF REPORT **********

Name: CCS BIOREACTOR, SEL
MRN/Age/Sex: SAP:735783768/5 months/Unspecified
Encounter Type: Quality Control
Provider: DR MARCUS WAGSTAFF
Location: SA PATHOLOGY/SA Pathology/RAH Lab
Admission Date: 09/06/21 00:00

Collected Date: 23/06/21 19:15
Procedure: .CT C Fluid
Accession Number: 21-174-16330
Service Resource: RAH Epicentre
Antibiotics:
Received Date: 24/06/21 12:48
Source:
Body Site:
Freetext Source:
Pathogens:
Start Date: 24/06/21 12:48
CT Product

Date Time	Tech	Task	Results
04/07/21 13:00	ANGSERVE	Final	The fluid culture is negative

Day 14- Pooled spent media

Total accession selected: 1

********** END OF REPORT **********

Name: CCS BIOREACTOR, SEL
MRN/Age/Sex: SAP:735783768/5 months/Unspecified
Encounter Type: Quality Control
Provider: DR MARCUS WAGSTAFF
Location: SA PATHOLOGY/SA Pathology/RAH Lab
Admission Date: 09/06/21 00:00

Collected Date: 23/06/21 19:30
Procedure: .CT C Fluid
Accession Number: 21-174-16331
Service Resource: RAH Epicentre
Antibiotics:
Received Date: 24/06/21 12:47
Source:
Body Site:
Freetext Source:
Pathogens:
Start Date: 24/06/21 12:47
CT Product

Date Time	Tech	Task	Results
04/07/21 13:00	ANGSERVE	Final	The fluid culture is negative

Day 14- Pooled purge media

Total accession selected: 1

********** END OF REPORT **********

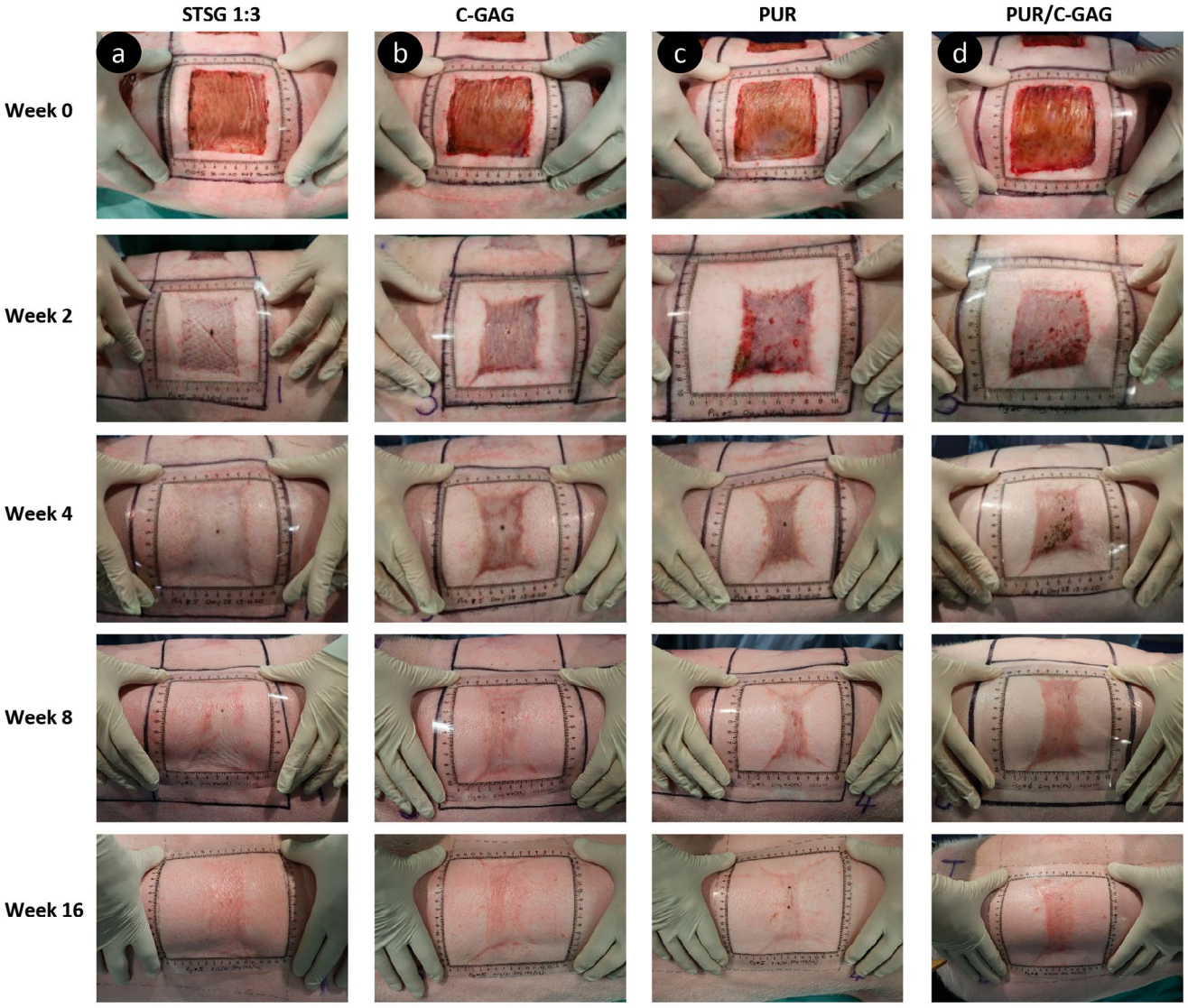

e Wound Contraction Day 0 – Day 112 Endpoint

STSG	C-GAG	PUR	PUR/C-GAG
44.17%	63.1%	67.87%	66.7%

Figure 1. Representative macroscopic images showing the progression of graft and skin substitute integration during weeks 0 – 16 post-transplant for each treatment condition. Meshed STSG (1:3) exhibited 44.2% contraction (column a), followed by the C-GAG substitute (63.1% column b), PUR/C-GAG 66.7% (column d) and the PUR substitute was on average the most contracted condition with 67.9% (column c). E, Percentage of contraction from day 0 after transplantation to day 112 endpoint.

Click to go back to original image

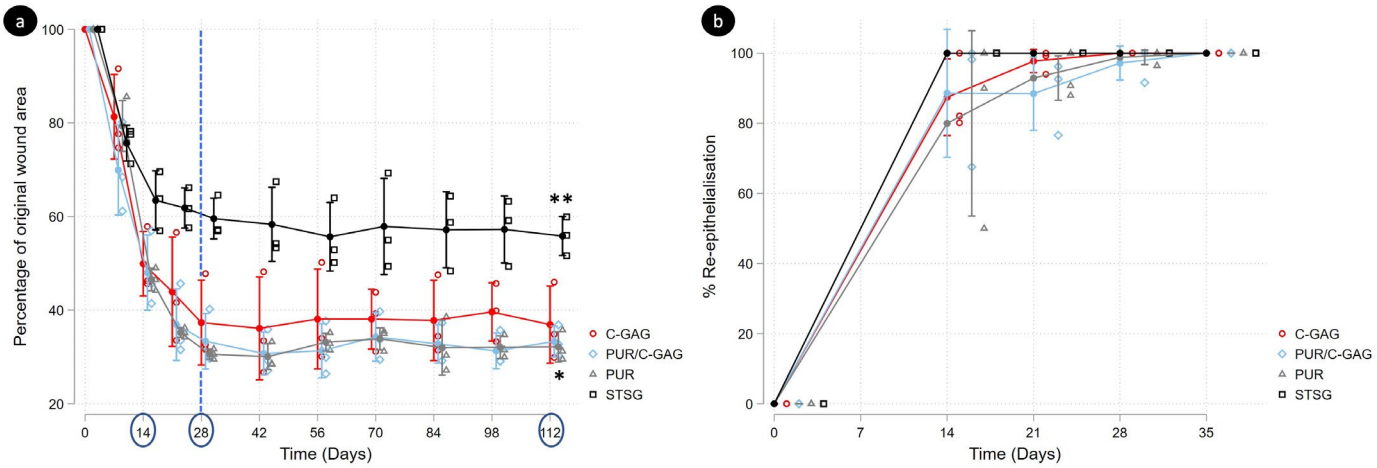

Figure 2. Wound percentage of original area and re-epithelialisation of the four test conditions over time shows the observed values and mean with standard deviation. (a) At 14 days post-transplant >80% of all wounds were re-epithelialised and by 28 days complete closure was obtained by secondary reepithelialisation. At 28 days (dotted line) to 112 days, wound areas stabilised, and significant differences (**$p < 0.05$) were noted for all three skin substitutes compared to the STSG site at day 112, however there were no differences within each skin substitute condition (*$p > 0.05$). (b) Mean percentage of reepithelialisation of test conditions over time until complete healing. No significant differences were found among the graft types after 14 days post-transplant ($p > 0.05$). Three biological replicates (n=3) for each condition were analysed using a linear mixed effects model with Bonferroni correction.

Click to go back to original image

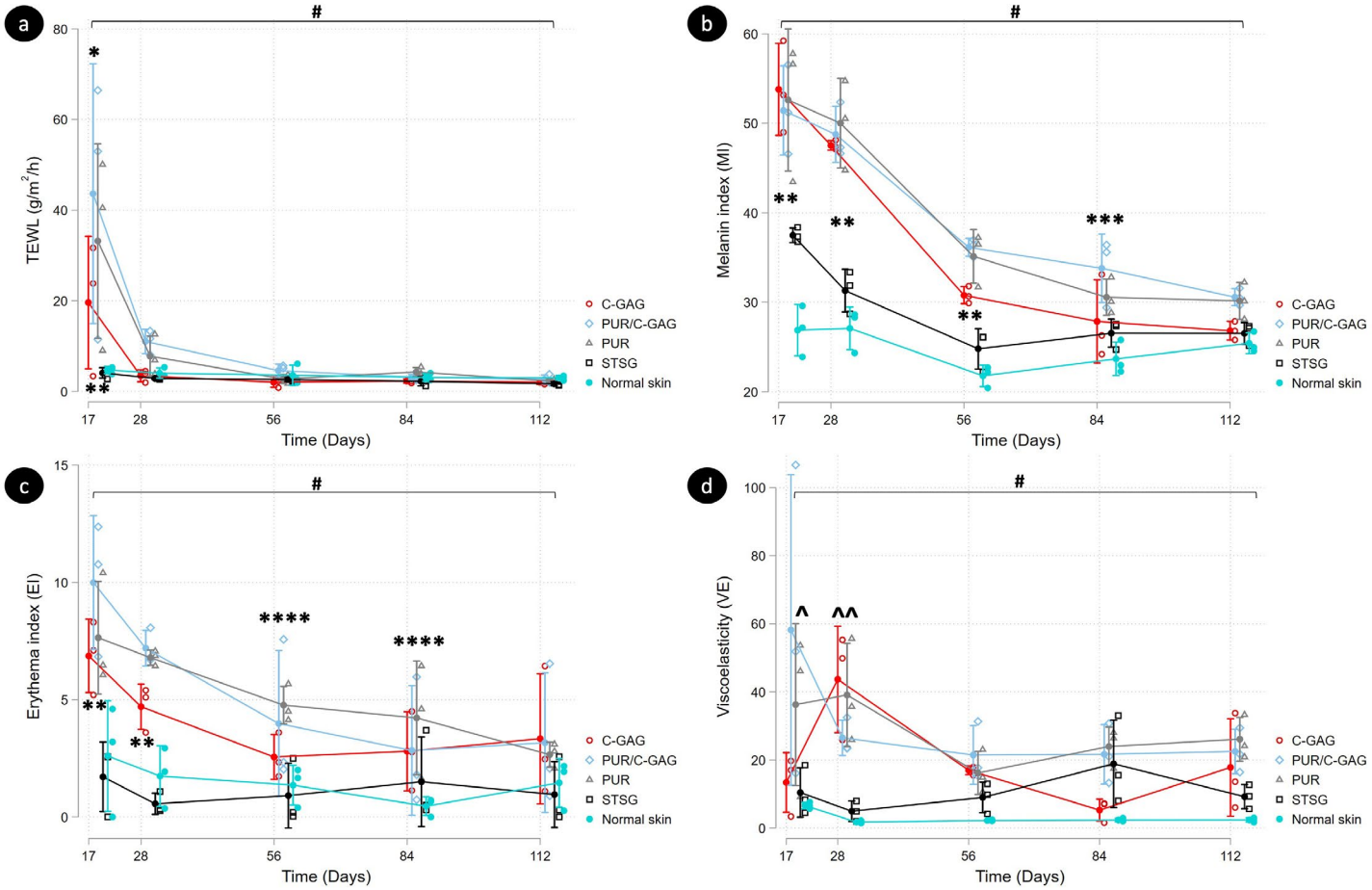

Figure 3. Results from the DermaLab with each biophysical wound assessment parameter graphed for all treatment conditions over time post-transplant. (a) Transepidermal water loss- TEWL (g/m2/h), (b) Melanin Index (MI), (c) Erythema Index (EI), and (d) Viscoelasticity (VE). The observed values represent the means and standard deviations at respective time points. The mean differences were compared among conditions and over time. *$p < 0.05$ for comparisons among PUR/C-GAG, PUR, and C-GAG **$p < 0.05$ Normal skin compared to all conditions including STSG. ***$p < 0.05$ for comparisons of PUR/C-GAG, and normal skin, STSG, C-GAG. ****$p <0.05$ PUR and normal skin. ^$p < 0.05$ Normal skin, STSG and both PUR-containing conditions. ^^$p < 0.05$ Normal skin, STSG and all test conditions. #$p < 0.05$ for comparisons among all test conditions at the indicated time points from day 17 to day 112. Three biological replicates (n=3) for each condition were analysed using a linear mixed effects model with Bonferroni correction.

Click to go back to original image

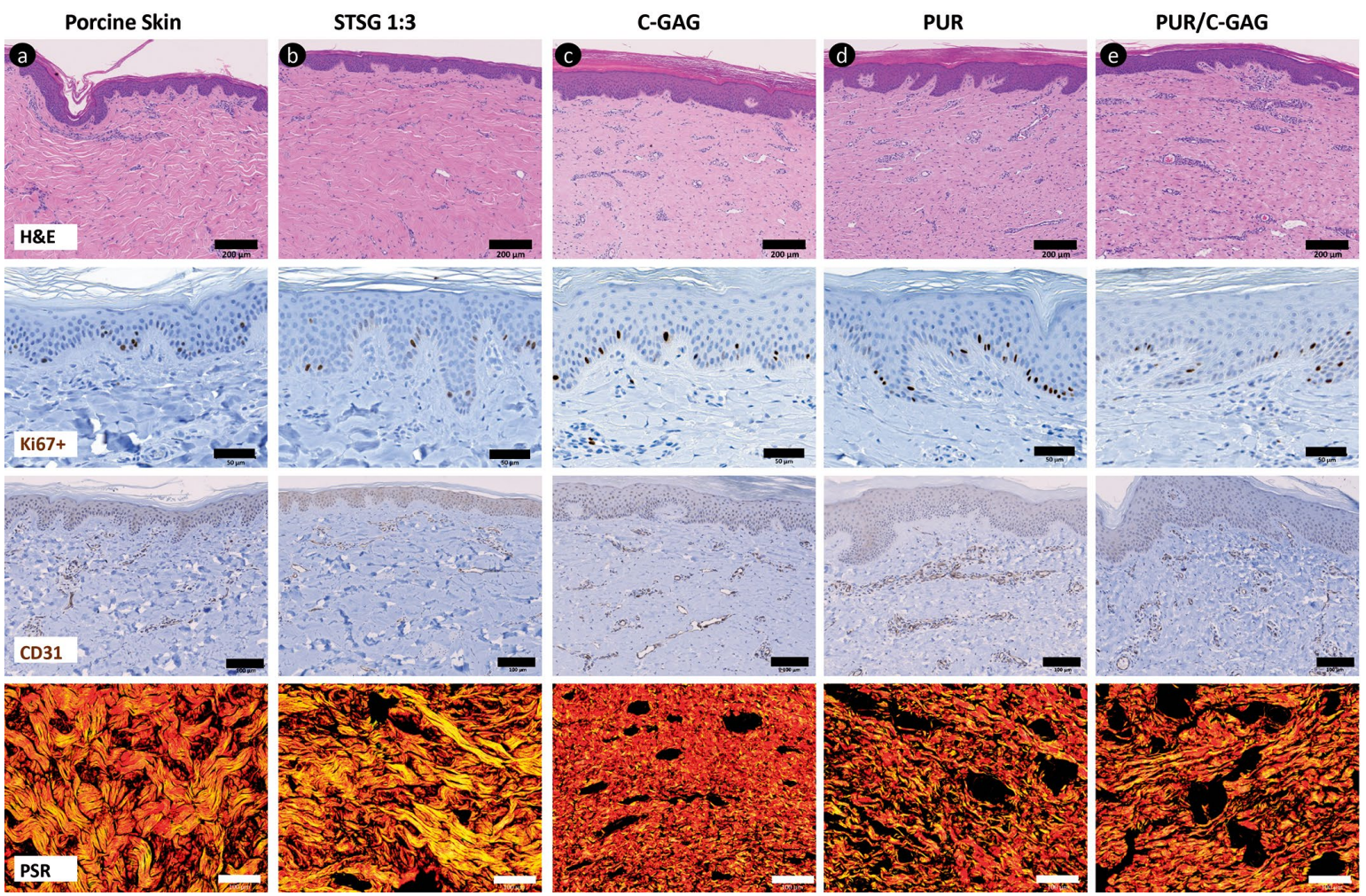

Figure 4. Representative histological images on day 112 post-transplantation. Haematoxylin and Eosin (H&E) row 1, Ki67-proliferative marker row 2, CD31- endothelial cell marker row 3 and Picrosirius red (PSR) stain row 4 for normal porcine skin (column a), and the four test conditions, skin graft (STSG-column b), C-GAG (column c), PUR (column d) and hybrid PUR/C-GAG (column e). The collagen structure was visualised using PSR under polarised light. Scale bar: 200µm row 1, 50µm row 2, 100µm row 3 and 4.

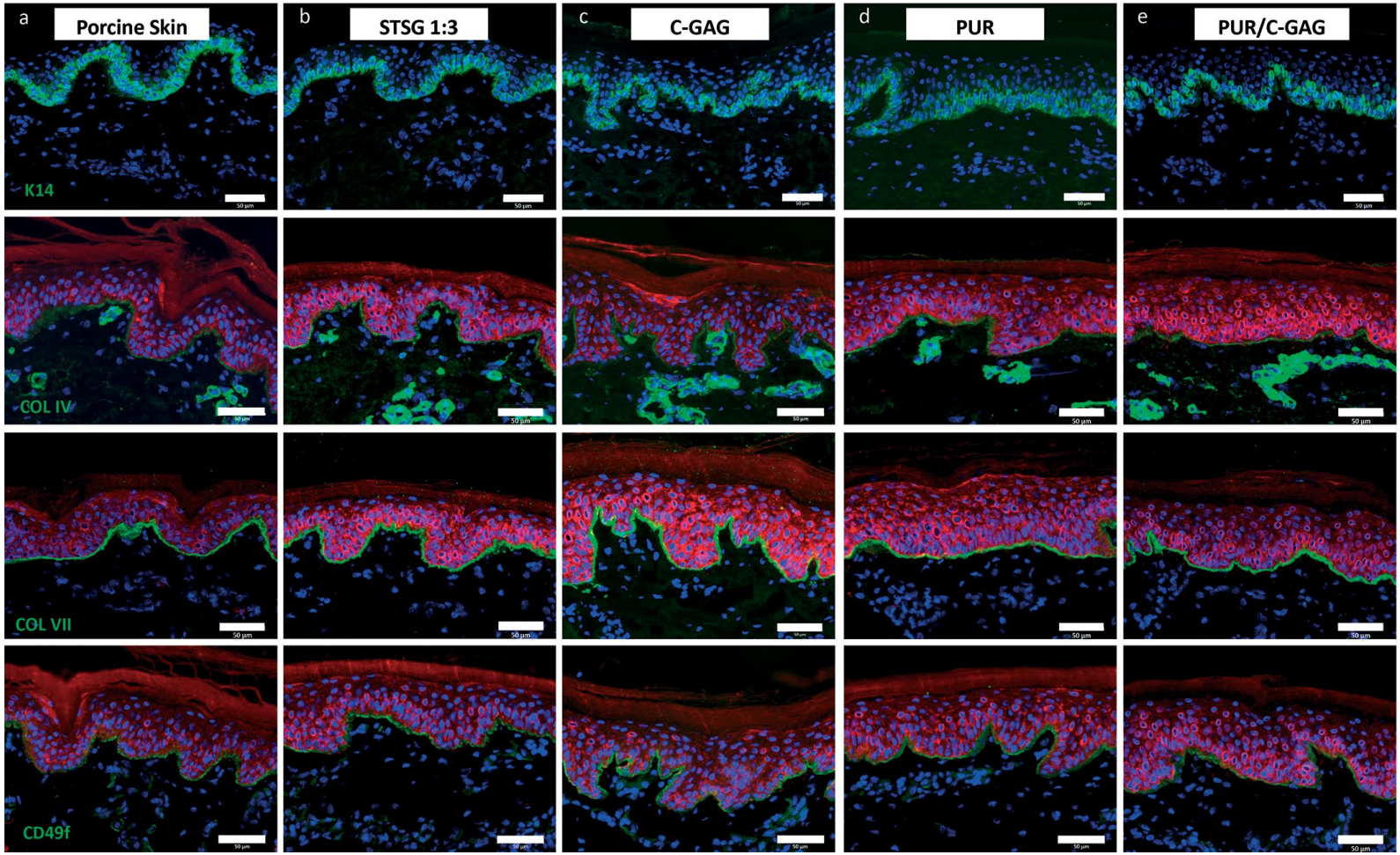

Figure 5. Representative histological images of normal porcine skin and test conditions at 112 days post-transplantation. Cytokeratin 14 row 1, Collagen IV row 2, Collagen VII row 3 and Integrin α6 (CD49f) row 4. Column a represents porcine normal skin, column b STSG, column c C-GAG, column d PUR and column e PUR/C-GAG. Red staining for wide spectrum cytokeratin, Green staining depicts relevant maker, DAPI nuclei stain. Scale bar: 50μm.

APPENDIX XI: Chapter 8 Figures

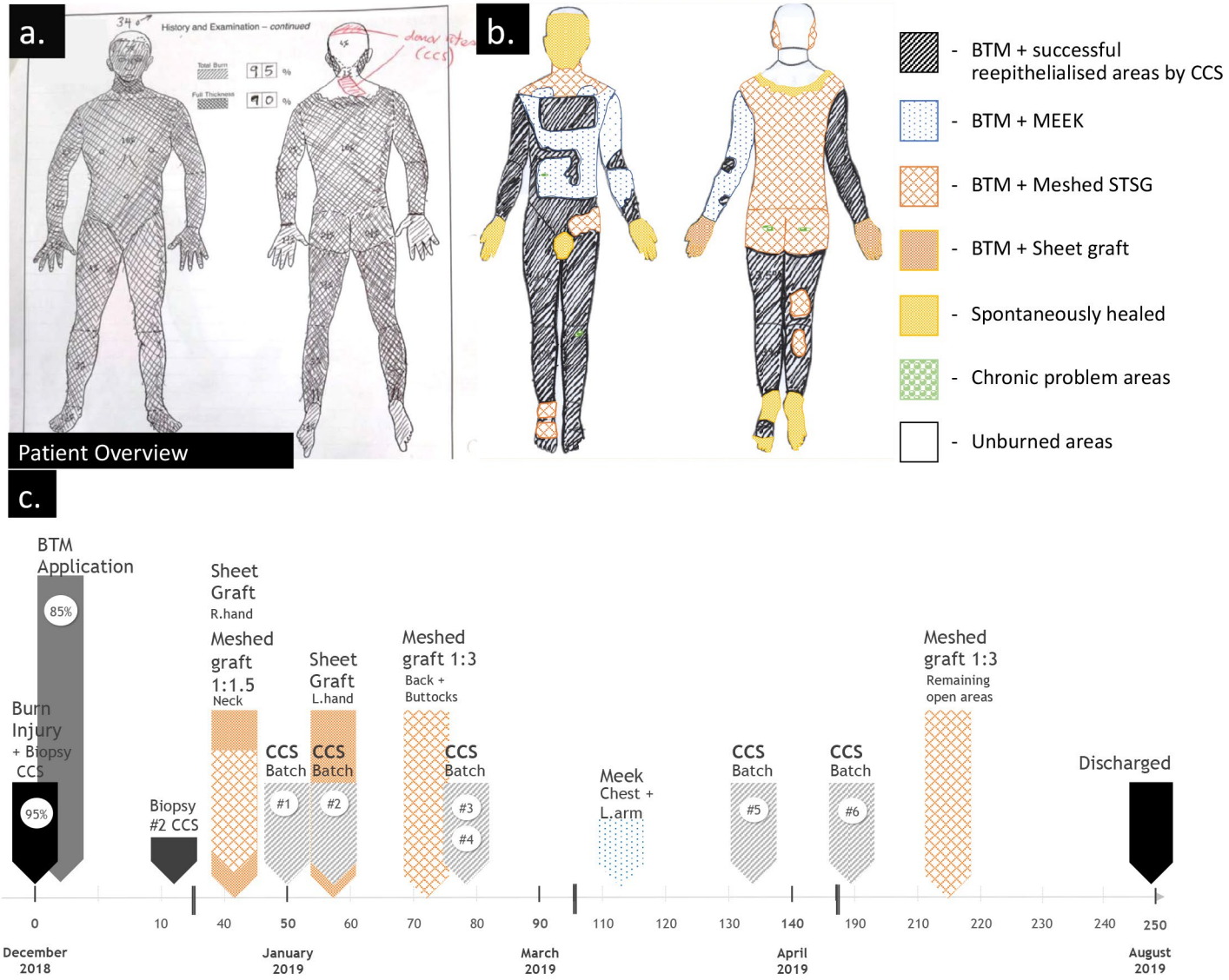

Figure. 1. Patient burn assessment and treatment modalities with timeline until discharge, a. Initial burn assessment was recorded using the Lund and Browder burn chart modified from Greenwood 2020, b. Schematic overview showing the alternative therapy treatments, and c. Outlines the treatment timeline from December 2018 to 8-months post burn injury with discharge to the rehabilitation centre.

Figure 2. Video of patient discharged and walking independently at 380 PBD (12.4 months)

Click on top image to watch video. If the video does not play within the thesis, separate video files are also listed with the PDF file.

Click to go back to original image

APPENDIX XI: Chapter 8 Figures

Figure 3. Photo images at 2.1 years PBD, a. Uninjured skin (marked), b. Donor site, c. Mesh 1:3 graft, d. Sheet graft, e. Meek (dotted area) with adjacent CCS and f. CCS, R arm, g. CCS, L leg (posterior), h. CCS L leg (anterior). R- right, L-Left.

APPENDIX XI: Chapter 8 Figures

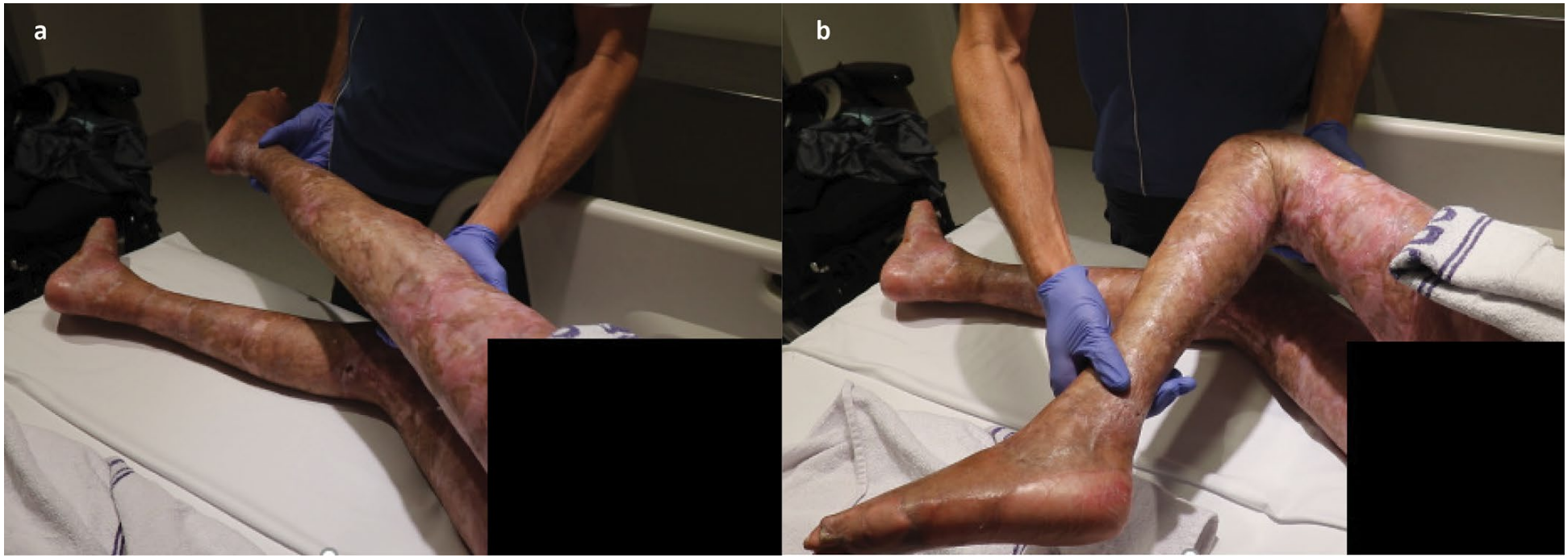

Figure 4. Extension (a) and flexion (b) of left knee joint showing range of motion at 13-months post-burn.

Figure 5. Photo images at 3.3 years PBD, a. Anterior full-body overview, b. Posterior fullbody overview.

Click to go back to original image

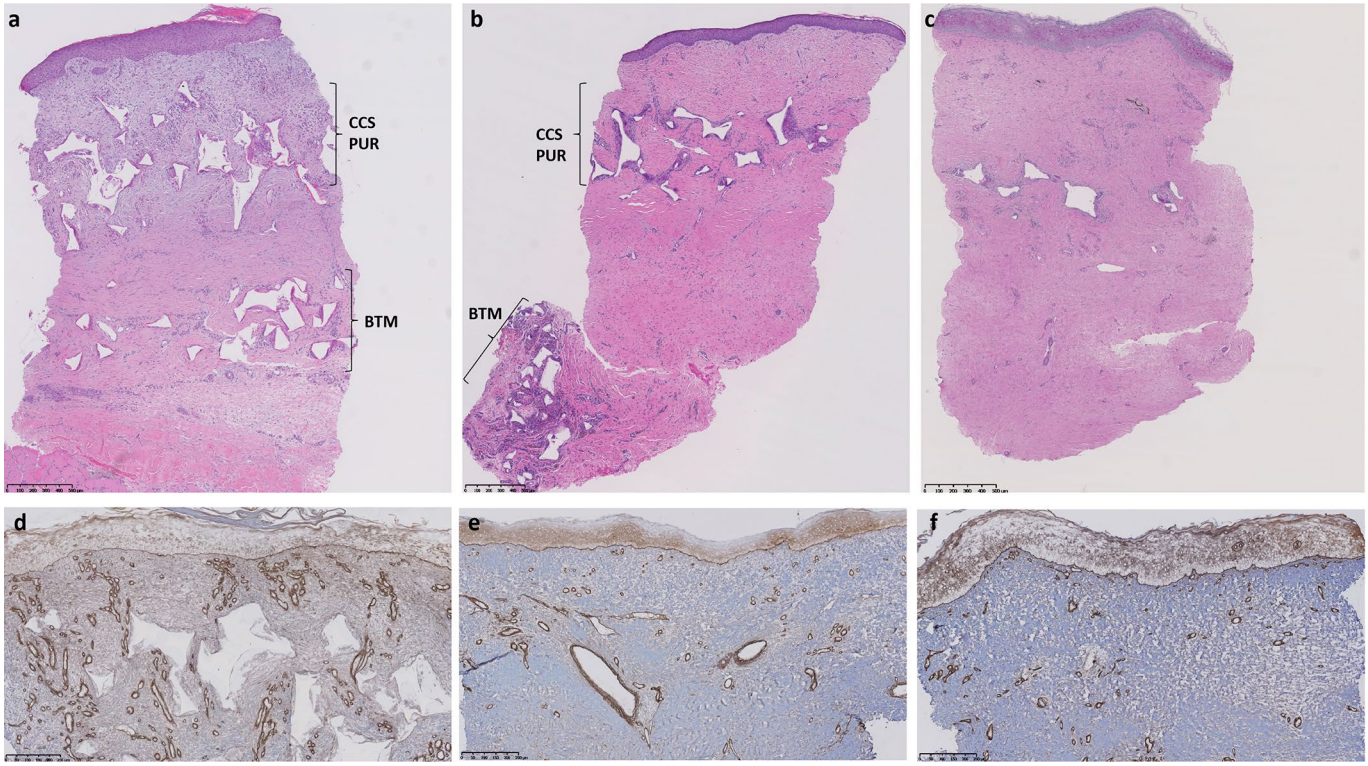

Figure 6. Histological sections stained with H&E (a-c) and Laminin (d-f). a, d - Day 21. b, e 3 - months, and c, f - 6 months. Note: The abundant laminin staining of the basement membrane of prominent blood vessels beneath the epidermis at Day 21, this vascularity decreased by 6-months. CCS PUR resides in the upper region of the section at 21 days and 3 months with the BTM layer present in the lower dermis. At 6-months minimal polymer remains in this section. Scale bar: a-c 500µm, d-f 250µm.

Click to go back to original image

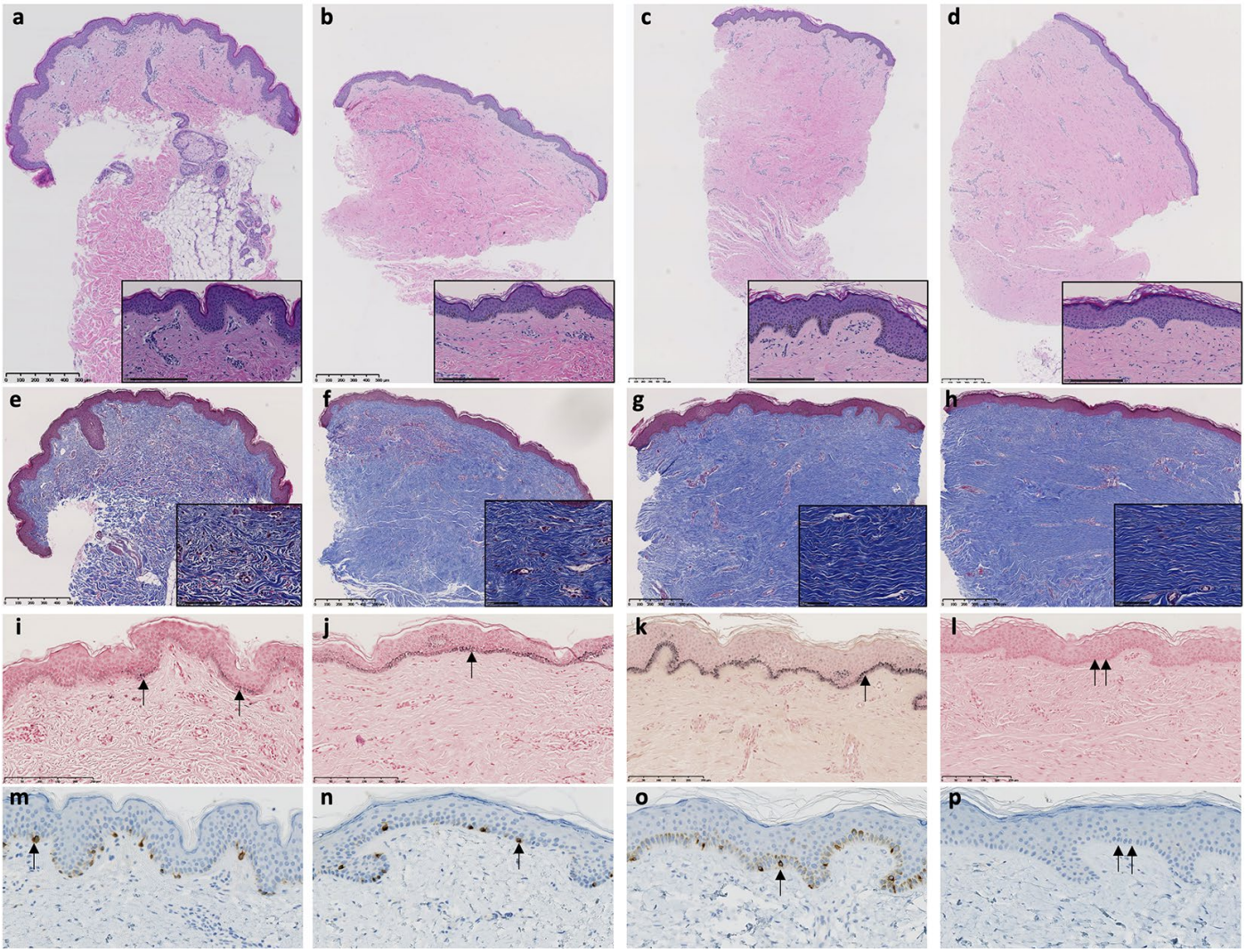

Figure 7. Representative histological sections and immunohistochemical staining (row 1H&E, row 2 Masson's trichrome, row 3 Masson's Fontana and row 4 Melan-A) at 582 PBD. a, e, i, m uninjured skin. b, f, j, n, Meek treated. c, g, k, o, CCS treated -Pigmented. d, h, l, p, CCS treated –non-pigmented site. Inset images, a-d show defined or lack of epidermal rete ridges of the uninjured skin to treated sites for the H&E sections and inset e-h show the varying collagen density in the MT sections. A single arrow indicates positive Melanin or Melan-A stained melanocytes in the pigmented sections and double arrows depict no staining along the basal layer in the non-pigmented section. Scale bar a-h 500 µm, i-l and a-d inset 250 µm, m-p and e-h inset 100 µm. H&E – Haematoxylin and eosin, MT – Masson's trichrome, MF – Masson's Fontana, PBD – post burn date.

Click to go back to original image

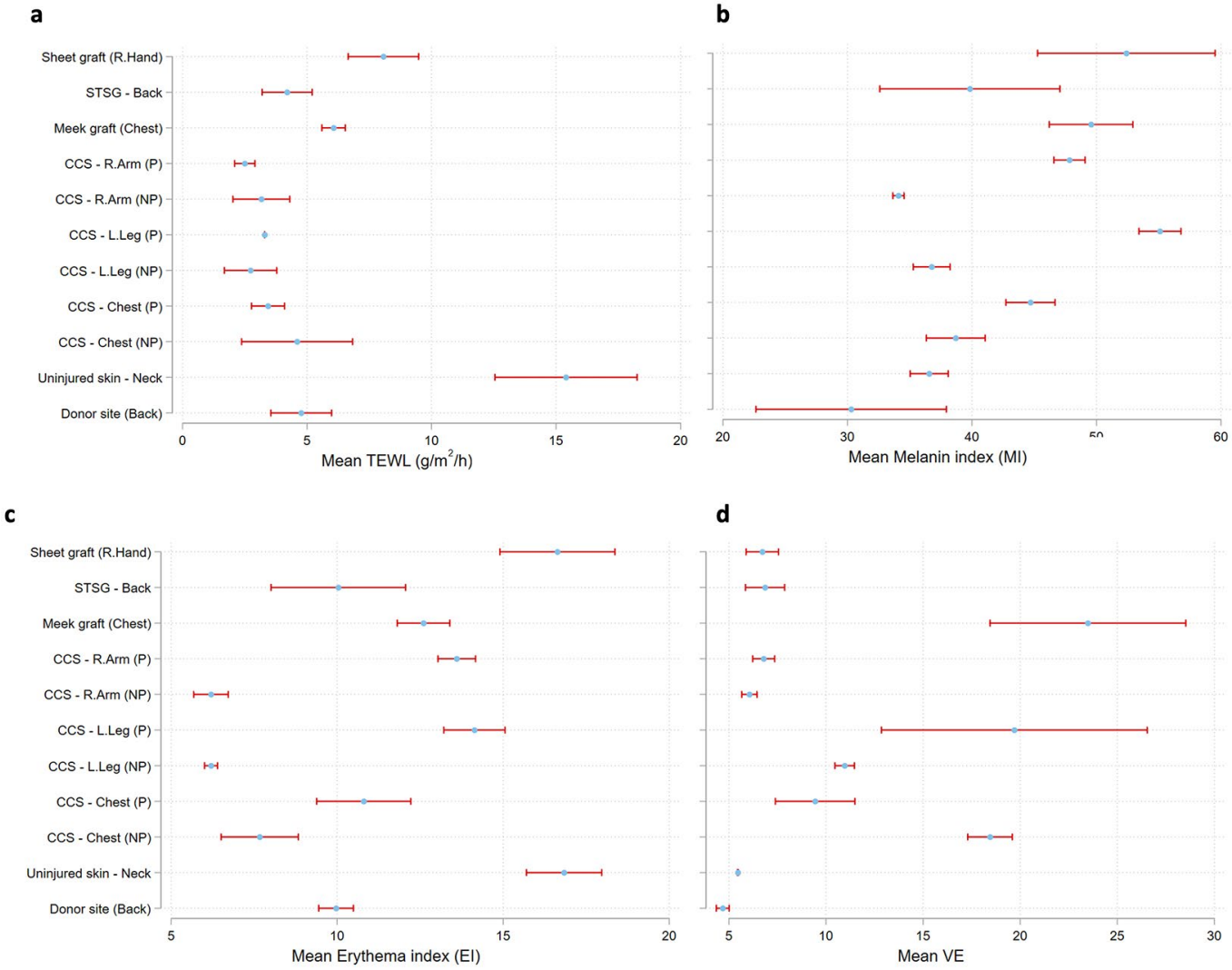

Figure 8. DermaLab Wound Parameters, at 2 years post-burn, a. Transepidermal water loss (TEWL), b. Melanin, c. Erythema, and d. ViscoElasticity (VE). Mean measurements are represented graphically for uninjured normal skin, meshed 1:3 autograft on the back, Meek graft on the chest, CCS on the arm, leg and chest and donor site on the back.

Click to go back to original image